Journal of Chemistry

Persistent Toxic Substances in the Environment and Humans

Lead Guest Editor: Yifeng Zhang
Guest Editors: Hangbiao Jin, Yuhe He, and Peng Zhang

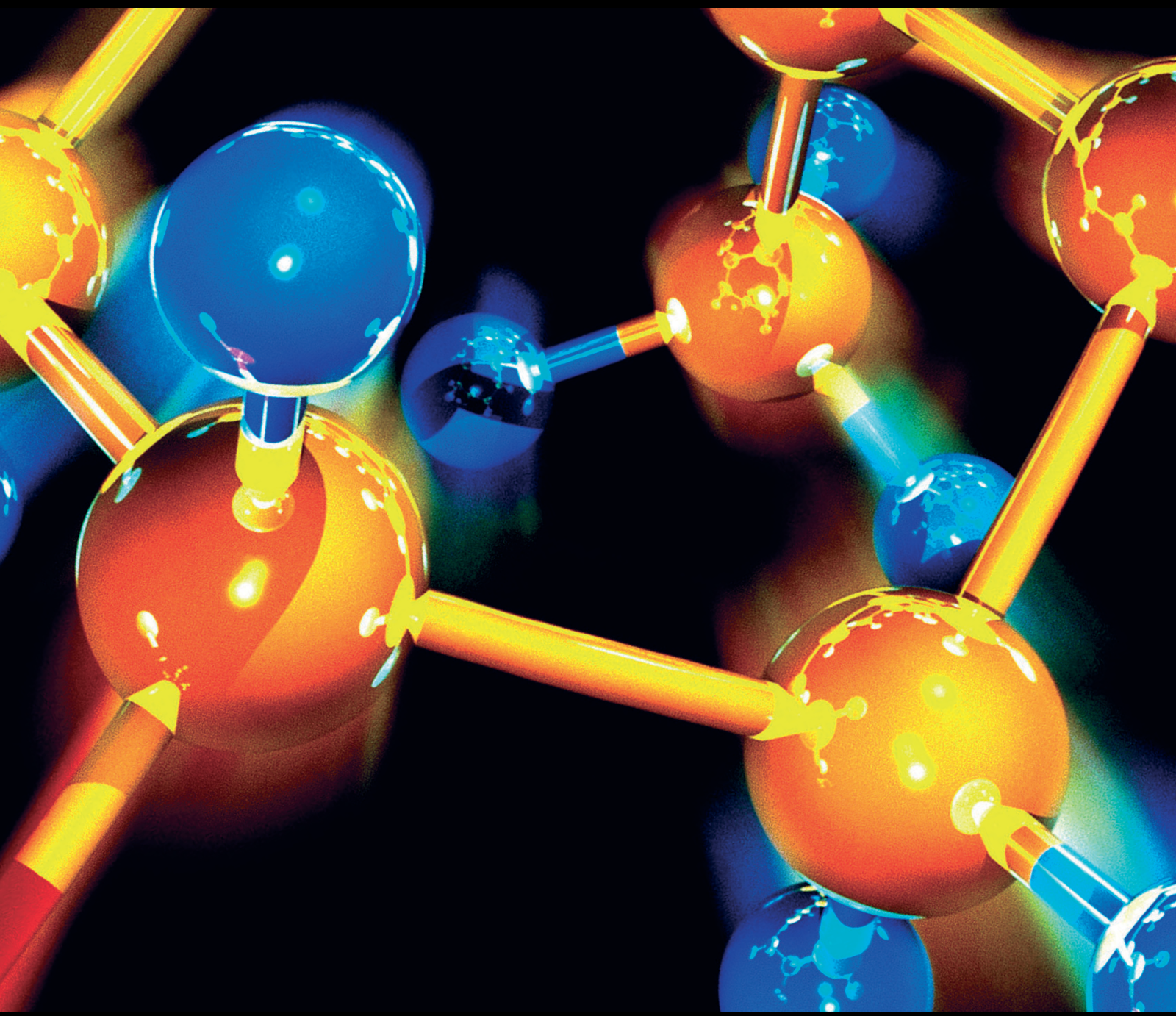

Persistent Toxic Substances in the Environment and Humans

Journal of Chemistry

Persistent Toxic Substances in the Environment and Humans

Lead Guest Editor: Yifeng Zhang
Guest Editors: Hangbiao Jin, Yuhe He, and Peng Zhang

Contents

Hindawi
Journal of Chemistry
Volume 2020, Article ID 9671871, 13 pages
https://doi.org/10.1155/2020/9671871

Research Article

Distinct Dispersion of As, Cd, Pb, and Zn in Farmland Soils near Abandoned Mine Tailings: Field Observation Results in South Korea

Sung-Wook Yun,[1] **Dong-Hyeon Kang**,[2] **Won-Hyun Ji**,[3] **Mun-Ho Jung**,[3] **and Chan Yu**[4]

[1]*Department of Agricultural Engineering, National Institute of Agricultural Sciences, RDA, Wanju, Jeonbuk 54875, Republic of Korea*
[2]*Department of General Education, Korea National College of Agricultural & Fisheries, Jeonju 54874, Republic of Korea*
[3]*Institute of Mine Reclamation Technology, Mine Reclamation Corp, 2 Segyero, Wonju 26464, Republic of Korea*
[4]*Department of Agricultural Engineering, Gyeongsang National University (Institute of Agriculture and Life Science), 900 Gazwa, Jinju, Gyeongnam 52828, Republic of Korea*

Correspondence should be addressed to Chan Yu; chanyu@gnu.ac.kr

Received 1 February 2020; Revised 1 May 2020; Accepted 20 May 2020; Published 8 August 2020

Guest Editor: Peng Zhang

We investigated the characteristics of metal(loid) transport and dispersion in agricultural soils near an abandoned metal mine. Topsoil samples were collected from 162 sampling sites in the study area, including 1 in the mine tailing dumps, to analyze the total concentrations of As, Pb, Cd, and Zn. Subsequently, the metal(loid) transport and dispersion characteristics were investigated using geographic information system (GIS) technology. The results of this study clearly demonstrated the variation in the dispersal of As, Cd, Pb, and Zn from the mine tailing dumps to nearby agricultural soils and the element-specific spatial variability in their respective transport and dispersion characteristics. These findings suggested that compared with the migration behavior of Cd, Pb, and Zn, that of As has a farther-reaching impact on agricultural soils owing to its geochemical cycling in the soil and groundwater environment. This impact differed significantly in magnitude from that of the other investigated metals. Therefore, special consideration must be given to the migration behavior of As.

1. Introduction

Globally, agricultural soil pollution caused by metal(loid)s from mining activities poses serious environmental concerns. Mine tailings, which are mine wastes derived from mining activities, contain several toxic metal(loid)s [1, 2]; thus, mine tailing dumps left untreated near abandoned metal mines are the primary sources of soil and water pollution in the surrounding areas [3–8]. Dispersal of metal(loid)s from mine tailing dumps into the ecosystems in the vicinity of such mining sites occurs primarily through two pathways: (1) dispersal of metal(loid)-bearing particles by the wind- and rainfall-driven erosion of mine tailings [2, 6, 9] and (2) infiltration of metal(loid)-bearing leachates into the soil below during rainfall–runoff processes and subsequent migration into nearby soils and groundwater [6, 7, 9, 10].

Recent studies on the transport and dispersion of metal(loid)s in contaminated soils near mining areas have suggested that the spatial distribution of such metal(loid)s is determined primarily by the erosion of mine tailings, particularly by wind-driven erosion [1, 2, 6, 11, 12]. Moreover, the closer the location of the site to the mine tailing dumps, the higher the concentration of the contaminants, and vice versa [1, 2, 5, 11, 12]. Studies on the transport of metal(loid)s in soils by the leaching of metal(loid)s from mine tailing dumps have focused on the depth-dependent distribution of metal(loid)s within the soil profile, i.e., the vertical migration of metal(loid)s [9, 13–15].

On the contrary, in countries such as Korea that experience monsoon-driven rainfall and distinctly different dry and rainy seasons [16], the transport and dispersion of metal(loid)s migrating from mine tailing dumps to nearby soils may show different distribution patterns through complex pathways of erosion and leaching. Metal(loid)s infiltrating into the soil through leachates during rainfall–runoff processes tend to migrate to the groundwater via the soil pore water [17–19]. This suggests that soil metal(loid)s, driven by the hydraulic gradient, migrate not only vertically within the soil profile but also along the horizontal plane. Moreover, variations in groundwater cycling, irrigation, and level can release metal(loid)s back into the surface environment. Metal(loid)s can also undergo mobility changes in the soil and groundwater environment owing to various factors, such as pH, oxidation–reduction (redox) potential, organic matter content, and adsorption reactions between various minerals [4]. Therefore, the range of spatial dispersal of metal(loid)s from mine tailings into nearby soils can vary significantly depending on the extent of erosion as well as the different migration behaviors of individual soil metal(loid)s. Thus, a proper understanding of this complex phenomenon is imperative to adequately monitor soil metal(loid)s in areas affected by mining activities.

The objective of this case study is to elucidate the distinctive dispersion and distribution pathways of different metal(loid)s from mine tailing dumps to the surrounding agricultural soils. To this end, the following approaches were adopted. The total concentrations of metal(loid)s (As, Cd, Pb, and Zn) in the agricultural soils were surveyed extensively on-site. Then, we examined the spatial distribution of the metal(loid)s by identifying their horizontal variation according to distance from the mine tailing dumps and created a distribution map using a geographical information system (GIS). The results of this study provide important input for developing efficient monitoring schemes for meta(loid)s in agricultural soils and strategies for soil remediation in areas affected by mining activities.

2. Materials and Methods

2.1. Description of the Study Site. The surveyed site lies in the village of Gwoni in Gyeongju City, Gyeongbuk Province, Republic of Korea (Figure 1). The village of Gwoni is spread over an area of 7.97 km^2 and comprises forests (7.09 km^2), paddy fields (0.48 km^2), and dry fields (0.25 km^2). According to the Korean Soil Information System [20], the soil types in the study site are classified as Inceptisols (7.56 km^2), Ultisols (0.13 km^2), Alfisols (0.10 km^2), and Mollisols (0.01 km^2), and the surface soil textures are loam (7.01 km^2) and sandy loam (0.79 km^2). The sandy loam occurs primarily in agricultural fields. The geology of the study site consists primarily of Cretaceous strata; Tertiary and Quaternary strata are unconformably distributed in the upper part (Figure 2) [21]. Hornblende-quartz-feldspar porphyry, hornblende-biotite granite, and granite, all belonging to the Bulguksa intrusive group of the Daedong supergroup, are distributed in the Cretaceous strata. In the upper part, andesite and tuff of the Tertiary Beomgockri group are unconformably distributed and are not visible in the presented geological map; the strata are unconformably covered at the top by Quaternary alluvium. At the study site, farmland is mostly distributed in the Quaternary alluvium (Figure 2).

Gwoni Reservoir, which is a fill-type dam built in 1964, is downstream of the study area (Figure 1). However, this reservoir is used for irrigating agricultural fields in its vicinity, and the groundwater pumping wells have traditionally been used for irrigation of the agricultural fields in the study area, which was confirmed during the field survey (Figure S1).

The study area is affected by a typical temperate monsoon climate, with an annual mean temperature of 14.1°C and extreme maximum and minimum temperatures of 38.6°C and −12.7°C, respectively [22]. The annual mean precipitation is 842.9 mm, and its temporal distribution throughout the year is strongly heterogeneous. More than 54% of the total annual precipitation is recorded between July and October [22]. During the dry winter seasons, winds from the northwesterly quadrant are predominant, whereas hot and humid summers are dominated by southerly winds [23].

The Sunyang Mine (Figure 1), situated in the study region, was initially developed during the Japanese occupying period (1910–1945). Details of this abandoned Au mine are presented in Table 1. In the vicinity of the buried mine shaft, mine tailings of more than 2,500 m^3, which is the main source of pollution, are piled together with waste rocks. The soil sampled near the mine tailing dumps, as indicated in Figure 1, has been reported to contain As, Cd, and Pb at concentrations far exceeding the prescribed thresholds [24]. During the field survey, we verified the presence of the mine tailing dumps and the collapsed stone wall piled up to contain the tailings (Figure S2).

2.2. Soil Sampling. An extensive investigation of the soil metal(loid) content was conducted in the study area in March 2014. Soil sampling was performed in the surrounding agricultural fields located downslope from the mine tailing dumps near the mine shaft of the Sunyang Mine to clearly determine the distribution patterns of metal(loid)s according to the distance from the mine tailing dumps (Figure 1). Soil samples were taken at depths of 0–30 cm from 162 agricultural fields, including 1 sample obtained from the mine tailing dumps (Figure 1). The sampling sites located in the forest areas shown in Figure 1 are currently used as agricultural fields, excluding the site located in the mine tailing dumps. Information about the locations of each sampling site is provided in Table S1. For each sample, five samples of surface soils were collected in a zig-zag pattern in each plot (<900 m^2) of the agricultural fields and were mixed thoroughly to obtain a representative composite sample in accordance with the standard Korean method prescribed for collecting soil samples [28]. The soil samples were collected using a stainless steel hand auger and stored in prelabeled polyethylene zip bags. Appropriate care was taken at the sampling sites to avoid the collection of any obvious contaminants as well as plant leaves, gravel, and other debris.

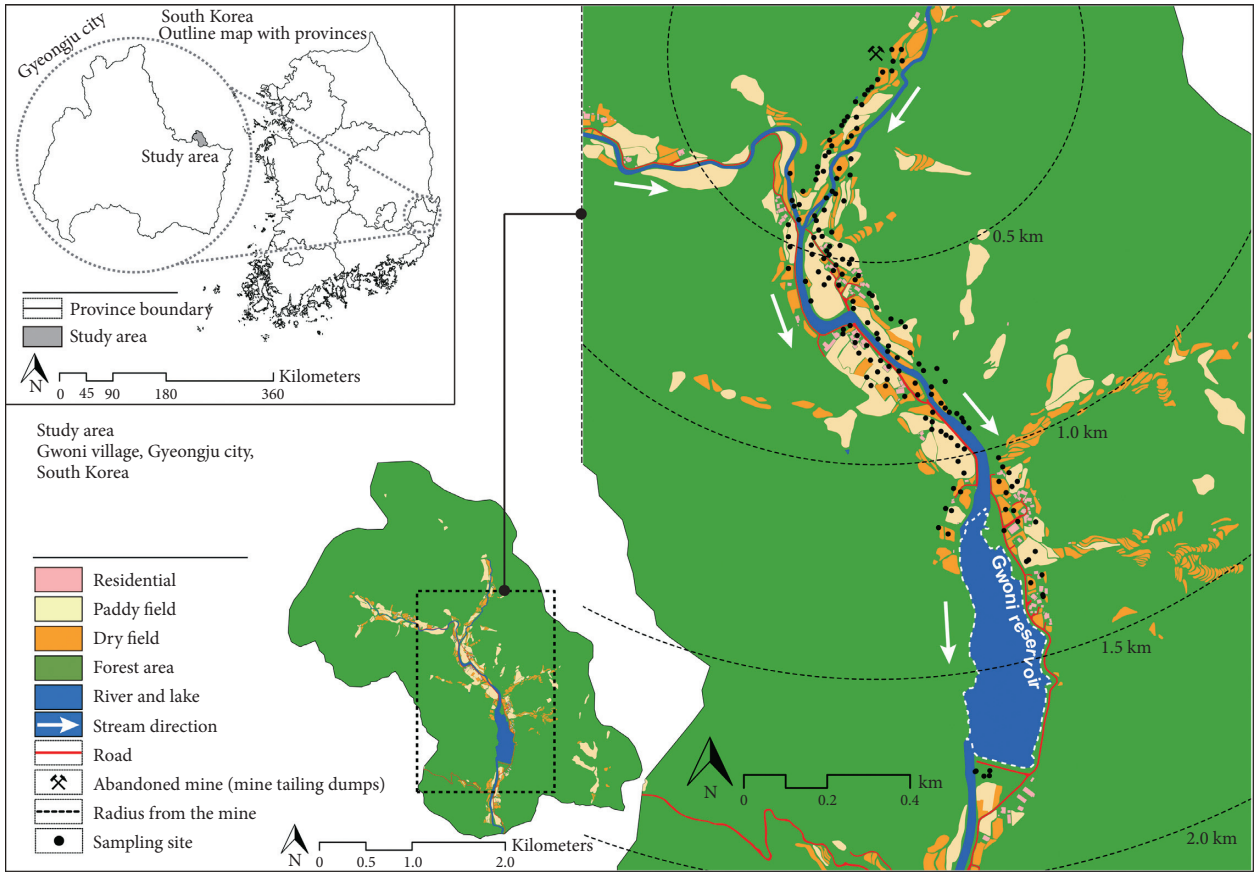

Figure 1: Sampling points in the study area, showing the distribution of land use types.

The sampled soils were spread on steel pans in one layer with uniform thickness. The samples were then air-dried for one week to eliminate moisture. Then, the soils were crushed, passed through a 2 mm stainless steel sieve, and stored in airtight polyethylene containers.

2.3. Chemical Analysis for Total Metal(loid) Content. All soil samples were analyzed at a nationally accredited professional analysis institute in South Korea, National Environment Lab (NAPAI), which tests for pollution in soil samples. The NAPAI's official website can be accessed at http://www.nelab.re.kr. For the analysis of metal(loid)s, the dried soils were pulverized and sieved to pass a 100 mesh (<0.15 mm), and a 3 g sample of the sieved soil was digested with 28 ml of aqua regia (3 : 1, v/v, $HCl + HNO_3$) for 1 h at 70°C. The digested solution was filtrated through 5B filter paper, and the total concentrations of As, Cd, Pb, and Zn were then determined using an Inductively Coupled Plasma Optical Emission Spectrometer (ICP–OES; Optima 7300DV, Perkin Elmer, USA) [28]. A reference soil (Environmental Resource Associates, USA) was used to measure the recovery and relative standard deviation (RSD) of the elements studied. The recovery in the reference soil was between 70% and 130%, and the RSD was less than 30%.

2.4. Spatial and Statistical Analyses. Statistical analyses were conducted using SPSS 20.0 (IBM, USA). The data were checked for normality via the Kolmogorov–Smirnov test with a confidence interval of 95% [29, 30]. A GIS tool (ArcGIS 10.2.2) was used to produce a land use map that indicates the soil sampling locations and distribution of the total concentrations of metal(loid)s in the agricultural fields in the study area. The GIS tool also enabled the analysis of the associated spatial data, such as the altitudes of the sampling locations and the distance from the mine. To investigate the transport and dispersion characteristics of the metal(loid)s released from the mine tailings, which is the primary anthropogenic pollution source in the study area, regression analyses were performed to determine the correlation between the spatial data and the total concentrations of the metal(loid)s. Graphs with curve fittings (regression models) were prepared using SigmaPlot 12.0 (Systat Software, Inc., USA).

3. Results

3.1. Total Concentrations of Metal(loid)s in Mine Tailings and Agricultural Soils. The total concentrations of the metal(loid)s in the sampled soil from the mine tailing dumps of the Sunyang Mine are presented in Table 2. The total concentrations of As, Cd, Pb, and Zn were measured to be 195, 11.9, 51,150, and 1,745 mg/kg, respectively, which significantly exceeded their respective upper national limits. In particular, the total concentration of Pb was found to be more than 250 times the national limit of 200 mg/kg.

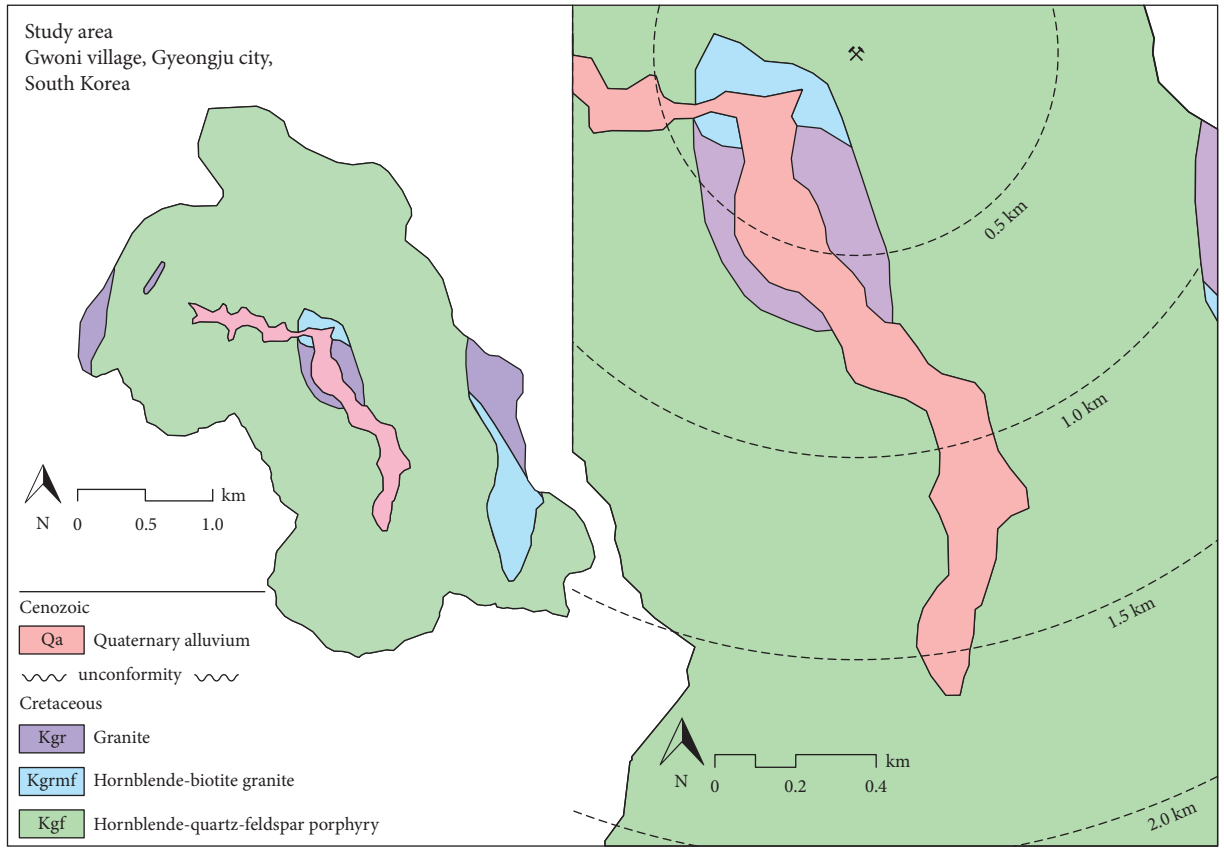

Figure 2: Geological map of the study area.

Table 1: Description of the abandoned mine in the study area.

Operation period	Main geology	Type of mineralization	Ore minerals	Grade of ore body	Ore mineral associations	Pollution source	Reference
Japanese colonial period, 1961–1972	Biotite granite, felsophyre, granite porphyry	Au-bearing quartz vein	Au, Ag	Au: 0.0–2.4 g/ton, Ag: 281–1,467 g/ton	Pyrite, galena, sphalerite	Tailings (>2,000 m^3)	[24–27]

Table 3 presents descriptive statistics for the raw data of the metal(loid)s contained in the agricultural soils. The table also presents the background metal concentrations (BMCs) in unpolluted agricultural soils of South Korea [32] and soils worldwide (WSs) [33]. The total concentrations of the metal(loid)s at each site are presented in Table S1. The concentration ranges of As, Cd, Pb, and Zn were 0.78–25.0, 0.10–5.50, 8.78–567.9, and 37.7–646.8 mg/kg, respectively (Table 3). The As, Cd, Pb, and Zn concentrations exceeded the national limits at 1, 2, 9, and 11 locations, respectively. The mean concentrations of these elements were 5.99, 0.88, 76.20, and 128.93 mg/kg, respectively, which, except for As, exceeded the values of both BMCs and WSs. The coefficients of variation (CVs) for As (62.9%), Cd (98.5%), Pb (108%), and Zn (78%) indicated high variations.

The application of the Kolmogorov–Smirnov test ($p > 0.05$) confirmed that the raw datasets for metal(loid)s in the sampled soils were not distributed normally (Table 3). The distributions for As, Cd, Pb, and Zn were all strongly positively skewed, with skewness values higher than 1.0, and their kurtoses were very sharp. Moreover, the distributions of these elements were still nonnormal after log- and square root-transformation.

3.2. Horizontal Variation of Metal(loid) Concentrations. To determine the characteristics of metal(loid) transport and dispersion from the mine to the surrounding agricultural soils, the distance to the mine was used as an ancillary predictor. Figure 3 illustrates the concentrations of metal(loid)s in soil with increasing distance from the mine as predicted by the regression analysis with curve fitting (regression models).

The concentrations of Cd, Pb, and Zn in the agricultural fields were highest in the vicinity of the mine tailing dumps, at 80 m and 415 m for Pb and Cd-Zn, respectively. The levels rapidly decreased with increasing distance from the mine tailing dumps and reached relatively stable levels 600 m from

Table 2: Total concentrations of metal(loid)s in the mine tailing soil and the corresponding spatial data.

Metal(loid)s (mg/kg)				Spatial data: Transverse mercator (Tokyo datum)		Altitude (m)
As	Cd	Pb	Zn	X	Y	
195.3	11.96	51,150	1,745	419,672	266,014	203

Note. The national limits for As, Cd, Pb, and Zn are 25, 4, 200, and 300 mg/kg, respectively [31].

Table 3: Statistical summary of metal(loid) concentrations (mg/kg) in agricultural soils of the study area.

	Mean ($N = 162$)	Median	Min	Max	SD	CV	Skew.	Kurto.	p (K–S test)	BMC	WS	NL	NL > BMC
As	5.99	5.14	0.78	25.00	3.77	62.9	2.871	10.194	0.00	6.24	6.00	25.00	1
Cd	0.88	0.66	0.10	5.50	0.87	98.5	2.627	8.946	0.00	0.14	0.35	4.00	2
Pb	76.20	49.44	8.78	567.95	82.85	108.7	3.678	15.405	0.00	20.07	35.00	200.00	9
Zn	128.93	93.73	37.67	646.78	100.60	78.0	2.593	8.083	0.00	71.07	90.00	300.00	11

SD: standard deviation; CV: coefficient of variation; Skew.: skewness; Kurto.: kurtosis; p (K–S test): p values of Kolmogorov–Smirnov test for normality of the raw data (for values higher than 0.05, the distribution is normal); BMC: background metal concentrations for unpolluted agricultural soils of South Korea [32]; WS: world soils unpolluted [33]; NL: national limits according to the soil quality standards of South Korea [31]; NL > BMC: number of samples with a concentration exceeding the national limit.

the mine (Figures 3(a)–3(c)). This spatial distribution pattern is in mathematical agreement with the exponential decay model ($y = y_0 + \alpha e^{-\beta x}$). In particular, the spatial distribution of Pb ($r = 0.626$) exhibited a relatively more pronounced exponential decay pattern as compared with Cd ($r = 0.367$) and Zn ($r = 0.362$). Zn and Cd showed similar distribution patterns in the agricultural soils (Figures 3(b) and 3(c), respectively), which were clearly distinguishable from that of Pb (Figure 3(a)).

The As content exhibited a distribution pattern (Figure 3(d)) that was distinct from those of Cd, Pb, and Zn. It showed the second-highest concentration, 24.78 mg/kg, at a point near the mine tailing dumps (46 m), which decreased until reaching a distance of 600 m from the mine. However, the As concentration began to increase continuously with an increase in the distance past that point. This behavior was in contrast to that of the other elements, which exhibited an exponential decay distribution and stabilized after 600 m onward. The highest As concentration, 25 mg/kg, appeared at the sampling site farthest from the mine, at 1,752 m. The distribution pattern of As showed the best fit with a quadratic model (convex down; $r = 0.724$), which suggests that the concentration of As in the study area decreased until reaching a specific distance from the mine and then increased steadily.

To further elucidate the distinct distribution patterns of As, Cd, Pb, and Zn past the 600 m mark, linear regression analyses of the distribution patterns were performed for the section between 600 m and the sampling site farthest from the mine. The results are presented in Figure S3. In the post-600 m section, Cd, Pb, and Zn showed stable distributions with no significant variability as compared with the results of the pre-600 m section, with concentrations showing high variability depending on the distance (Figures S3a–S3c). Contrary to this trend, the As concentrations clearly tended to increase linearly with an increase in distance past the 600 m mark (Figure S3d).

3.3. Relationships between Metal(loid)s. Figure 4 shows the relationships between As, Cd, Pb, and Zn based on linear regression models. Such relationships can indicate transport pathways or mechanisms from the metal(loid) sources [34, 35]. Among the four elements investigated, Cd and Zn showed a high linear correlation ($r = 0.890$; Figure 4(e)), which supports the finding that Cd and Zn had similar distribution patterns in the agricultural fields located downstream of the mine tailing dumps (Figure 3). No statistically significant correlations were present among the other investigated metal(loid)s.

3.4. Spatial Distribution of Metal(loid)s in the Study Site. Figure 5 illustrates the spatial distribution of the total concentrations of As, Cd, Pb, and Zn in the soil samples collected from the study area. The sampling site and metal(loid) distribution maps given in the figure help to visualize the distance-dependent distribution patterns of the metal(loid)s shown in Figure 3. Pb occurs in hotspots characterized by high concentrations in a dense distribution at points that differ slightly from those of Cd and Zn, at about 80 m and 400 m distance, respectively. However, these three elements all occurred in hotspots at points located within 500 m from the mine tailing dumps, showing lower concentrations with increasing distance from the mine. On the contrary, higher As concentrations were observed at significantly farther points, past the 1,000 m mark from the mine tailing dumps, which occurred in hotspots at points farthest from the mine tailing dumps, past the 1,500 m mark. This distribution pattern differed distinctly from those of Cd, Pb, and Zn.

4. Discussion

The dispersion of metal-bearing mine tailings into nearby agricultural soils can be attributed to the elevated levels of

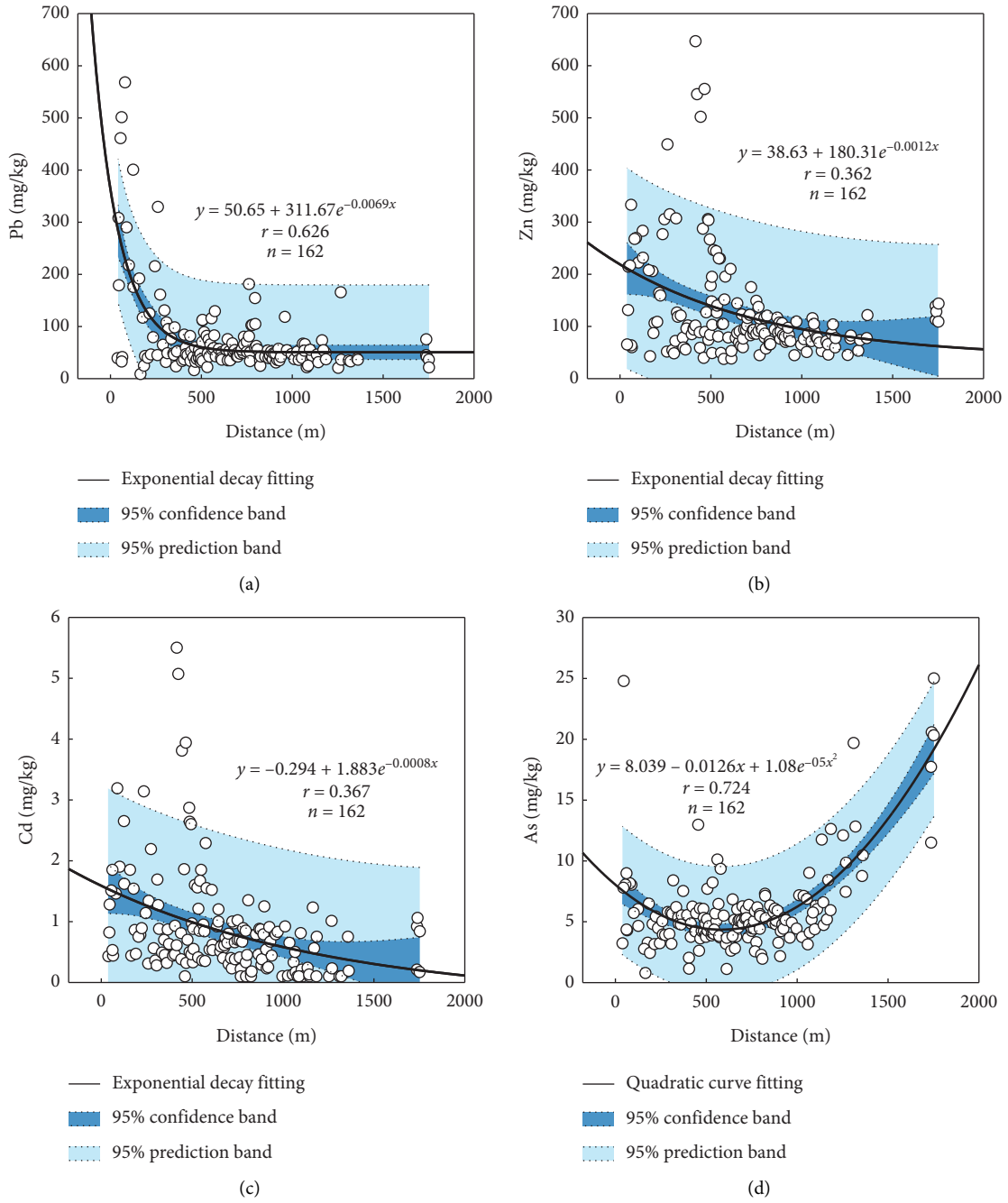

FIGURE 3: Scatter plots of metal(loid) concentrations in agricultural soils ($n = 162$) corresponding to an increasing distance from the mine tailing dumps for (a) Pb, (b) Zn, (c) Cd, and (d) As. The trend lines and 95% confidence (blue) and prediction (sky blue) bands are shown for the regressions. All p values (<0.0001) for the F-test in ANOVA were less than the specified significance level (0.005).

toxic metals observed in and around abandoned metalliferous mines [1, 2, 12, 36, 37]. Moreover, it should be noted that the primary ore body of the Sunyang Mine is a quartz vein containing Au and Ag that includes sulfide minerals, such as pyrite, galena, and sphalerite (Table 1). In addition, this quartz vein is commonly accompanied by arsenopyrite (FeAsS) [38–40], which is the most common As-bearing mineral [41, 42]. In general, the mine tailings generated by mining activities at Au or Ag mines in Korea contain high amounts of arsenopyrite [38]. Oxidation of the residual sulfides releases Fe and other metal(loid)s from the mine tailings, such as Pb, Cd, and Zn [43, 44]. The wide variations of their concentrations in the agricultural soils of the study area can be attributed to the dispersion of the mine tailings (CVs in Table 3) because high CVs (>50%) are often reliable indicators of anthropogenic activity [34, 35, 45–47]. Moreover, the hotspots of As, Cd, Pb, and Zn formed in the agricultural fields located downstream of the mine tailing dumps offer clear evidence for the dispersion of the mine tailings (Figure 5).

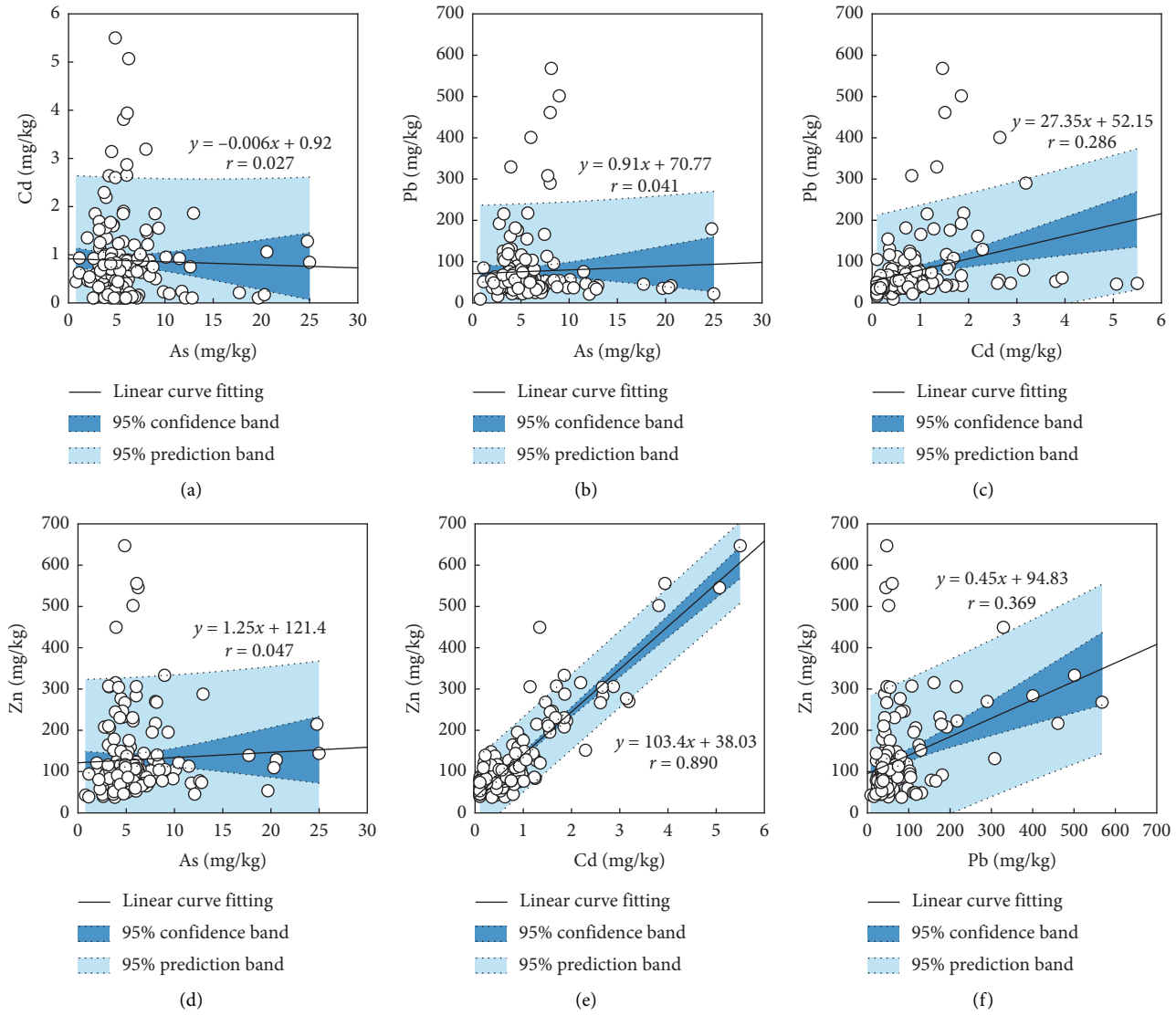

Figure 4: Relationships between (a) As and Cd, (b) As and Pb, (c) Cd and Pb, (d) As and Zn, (e) Cd and Zn, and (f) Pb and Zn concentrations in the agricultural soils ($n = 162$) of the study area.

To explain the characteristics of transport and dispersion of As, Cd, Pb, and Zn in the investigated agricultural soils, the primary mechanisms by which the metal(loid) migrate from the mine tailing dumps were examined. The migration of metal(loid)s from mine tailing dumps to the surrounding soils largely occurs via two pathways. The first and direct migration pathway of metal(loid)-bearing particles is the erosion of the mine tailings. Improperly disposed mine tailings are exposed to two types of erosion: water erosion with transport during heavy rainfall events and wind erosion, which induces fine-particle dispersion [3, 6, 9, 12, 36]. Such erosion of mine tailings can be ascribed to natural factors, which significantly influence the spatial distribution of metal(loid)s in the surrounding regions [1, 2]. The second migration pathway involves the infiltration of metal(loid)s dissolved in mine tailing leachates. The dissolved metal(loid)s infiltrate into the nearby soils with mine tailing leachates during rainfall-runoff processes and migrate with the soil pore water, thus, degrading the adjacent soil and groundwater environment [7, 10].

A common distribution pattern was observed for Cd, Pb, and Zn, which is characterized by an exponential decay in concentration with increasing distance from the mine tailing dumps (Figure 3). This spatial distribution is associated with the direct dispersion of metal(loid)s from anthropogenic sources. Typical examples of the exponential decay-type distribution pattern occur in areas near abandoned mines due to wind- and rainfall-driven erosion of mine tailings

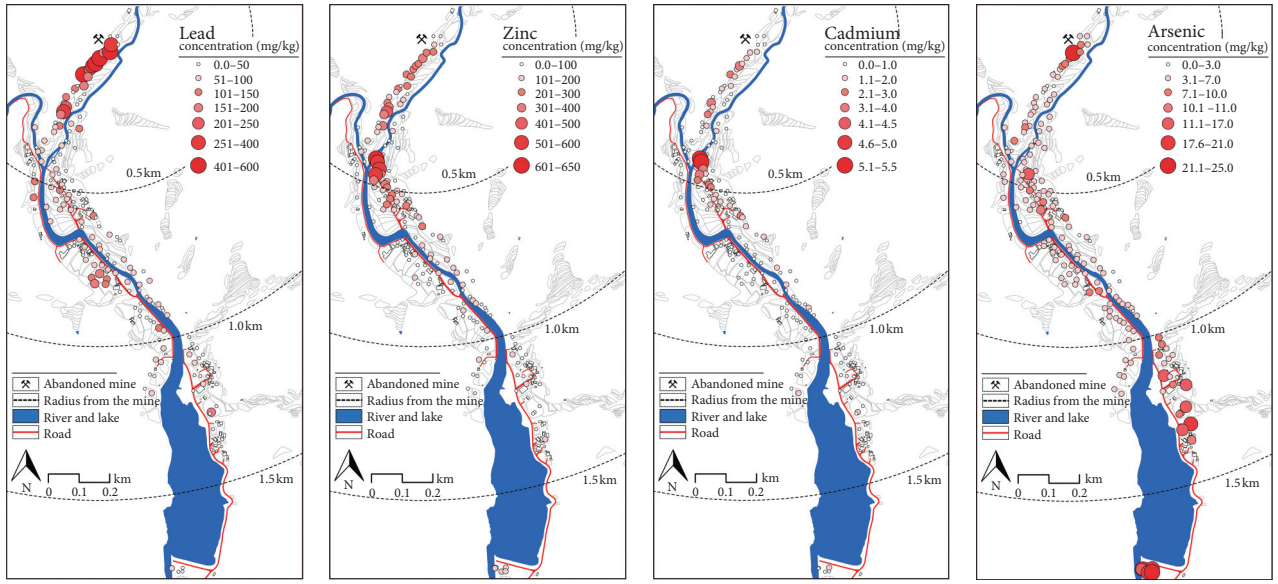

Figure 5: Distribution maps of (a) Pb, (b) Zn, (c) Cd, and (d) As in the agricultural soils of the study area. The circle size indicates the relative degree of metal(loid) concentrations.

[35, 48, 49] and the anthropogenic metal(loid)s in the soils near industrial complexes or smelters/refineries by the deposition of airborne particles released from them [50–54]. Thus, the observed distribution pattern clearly indicates the presence of an anthropogenic contamination source. Similarly, the distribution patterns of Cd, Pb, and Zn in the soils of the agricultural fields suggest that they are closely associated with wind- and rainfall-driven erosion of the mine tailings. However, two slightly different tendencies were observed: Cd and Zn showed almost identical patterns that were distinguishable from that of Pb (Figure 3). Moreover, their hotspots were formed at sampling sites located farther from the mine tailing dumps than those of Pb, at 400 m versus 80 m, respectively (Figure 5). The high linear correlation between Cd and Zn, as illustrated in Figure 4, indicates that these elements have the same migration pathways. In nature, Cd occurs mainly in association with Zn ores, among which sphalerite (ZnS), the dominant mineral in the Sunyang Mine, is the primary geologic source of Zn and Cd (Table 1) [55]. Given that Cd, Pb, and Zn are anthropogenic inputs from the same contamination source (mine tailing dumps), the results shown in Figures 3–5 suggest that the migration mechanism of Cd and Zn is different from that of Pb and that As migration involves a mechanism different from those of Cd, Pb, and Zn.

In addition to the erosion of mine tailings, another pathway for metal(loid) dispersal from the mine tailings is through the migration of soil pore water by downward percolating rainwater and readjustment of the groundwater table. Metals may also move upwards to the topsoil through evaporation and osmotic suction [56]. Given that soil metal(loid)s migrate only with the soil pore water, their mobility can be strongly influenced by the adsorption preferences between different types of soil minerals and the dissolved metal(loid)s [57–60]. In general, the adsorption preferences of soil minerals for metal(loid)s are known in the order of $Cr \geq Pb \geq Cu > Co > Zn > Ni \geq Cd$ [61]. Because mobility and adsorption preference are inversely related, Pb has a lower mobility than Zn and Cd, which explains why Pb hotspots occurred much closer to the mine than Zn and Cd hotspots. This finding is consistent with the results of column leaching tests performed in other studies, which suggest that the Pb concentration in leaching solutions is very low, even in mining-impacted soil containing high concentrations of Pb [62–64].

Considering these behaviors, the dispersal of metal(loid)s from mine tailings to nearby agricultural soils can be attributed to two mechanisms with some varying details. The primary pathway of Pb, Cd, and Zn migration is the direct dispersion of metal(loid)-bearing particles through erosion of the mine tailings. Moreover, given its extremely low mobility in soil, Pb mainly migrates via erosion, which is in good agreement with the Pb distribution pattern observed in this study, which also showed the best fit with the exponential decay model. In contrast, Cd and Zn have higher mobility in soil, which may explain their farther migration as compared to Pb, along with the leachates of mine tailings and the soil pore water in which they are dissolved. Therefore, the dispersal mechanisms for Cd and Zn are much more complex than a simple erosion-induced dispersion. A similar

distribution pattern between Cd and Zn suggests that the soil in the study site was clearly affected by tailing dumps (Figures 3–5). The similarity in the distribution patterns of Cd and Zn in the soil during the metal(loid) dispersal processes also validates the distribution patterns of Pb and As observed in this study (Figure 3).

On the contrary, the spatial distribution of the As concentration cannot be explained by the erosion of mine tailings alone. As previously mentioned, another metal(loid) migration pathway involves the infiltration of metal(loid)s dissolved in the mine tailing leachates into the soil during rainfall-runoff processes and migration to the surrounding soils with the soil pore water. To examine the As transport and dispersion characteristics, we investigated the geochemical behaviors of As in the soil and groundwater environment.

The geochemical behavior of As differs completely from that of other metal(loid)s because it undergoes various geochemical processes, such as adsorption/desorption, precipitation or coprecipitation, and oxidation/reduction [65–68]. These processes change the forms of As, which further changes its behavior in the environment and affects its fixation or migration [68, 69]. In nature, As exists mainly in the forms of arsenate [As(V)] and arsenite [As(III)]. Although the major factors responsible for its states have not been clearly identified [68] thus far, the redox potential is considered to be a key factor influencing the form and migration of As [70]. Under oxidizing conditions, As exists predominantly as As(V); however, under reducing conditions with a low redox potential, arsenate is reduced to As(III), which has higher toxicity and mobility [70–72].

Moreover, the mobility of As is enhanced by the reductive dissolution of Fe/Mn (hydr)oxides under reducing conditions [73, 74]. This phenomenon can be attributed to the fact that Fe/Mn (hydr)oxides in soil, which are present in aerobic environments, absorb various trace elements containing metal(loid)s in high concentrations [75, 76]. This is corroborated by the fact that the ore body of the abandoned mine in the study area is a quartz vein containing Au and Ag, including the sulfide mineral pyrite (Table 1); the mine tailing dumps near the mine can be closely associated with this sulfide mineral. Its main components are Fe and S, which are regarded as the primary sink for As [77–79].

Metals with a constant valence under reducing conditions, such as Cd, Pb, and Zn, are likely to have lower mobility because they are immediately readsorbed by soil oxides (e.g., aluminum (hydr)oxides and remaining Fe (hydr)oxides), even under the reductive dissolution of Fe/Mn (hydr)oxides [80]. Pinto et al. [81] reported that under oxidizing conditions, Cd, Pb, and Zn in mine tailing soils have much higher mobility as compared with reducing conditions. In contrast, the valence of As is dependent on the redox potential; therefore, it can be continuously released into the soil pore water through reduction from As(V) to As(III) and reductive dissolution of Fe/Mn (hydr)oxides. Moreover, several studies have reported that the primary As migration mechanism in soil and groundwater is associated with the reductive dissolution of Fe(III) (hydr)oxides and a consequent release of adsorbed and coprecipitated As [82–87].

In the soil environment, the reduced state is developed in a saturated soil layer beneath the groundwater table [70]. The As concentration in groundwater may vary depending on the depth of the groundwater table and alterations to the flooding cycle [87]. More specifically, the groundwater level rises closer to the surface through the rise of the groundwater table, thereby facilitating the contact of groundwater with the mine tailing dumps. If the groundwater table rises up to the topsoil, the soil environment alters to a reduced state, making it easier for As to be released into the pore water through the processes of reduction from As(V) to As(III) and reductive dissolution of Fe(III) (hydr)oxides. Given that Korea experiences concentrated rainfall during a specific period, the groundwater table may rise up to the surface. In addition, most of the agricultural fields in the study area are paddy fields (Figure 1), which are periodically flooded and drained during the rice-growing season. Yun et al. [34, 35] noted that As transported to paddy soil can affect a wider area owing to the reducing conditions of the paddy soil and the hydraulic characteristics. Moreover, in this area, the traditional irrigation method is groundwater pumping, which has been maintained even after the construction of the reservoir in 1964 (Figure S1). The As released from the mine tailing dumps to the soil and groundwater environment migrates vertically and horizontally by vertical and horizontal hydraulic gradients. Its concentration is likely to increase in groundwater that flows longer and to a wider area under reducing conditions, in which the As mobility increases. Polizzotto et al. [88] reported that the concentrations of As released from near-surface wetland sediments to the groundwater tended to increase in proportion to the period of time and distance traveled by the groundwater. The As input into agricultural fields through groundwater pumping tends to remain in the topsoil due to oxidation, adsorption, and coprecipitation under oxidizing conditions in the topsoil layer [89].

Considering the geochemical behaviors of soil As and the role of soil as the major sink for released metal(loid)s, the groundwater circulation in the study area provides clues for the observed characteristics in the As distribution.

As indicated in Figure 6, As, Cd, Pb, and Zn released to the soil environment by processes other than the dispersion pathways common to all metal(loid)s, i.e., by the wind- and rainfall-driven erosion of mine tailings, are likely to have different mobilities depending on the redox state. However, As, driven by a substantially increased mobility owing to reduction from As(V) to As(III) and reductive dissolution of Fe(III) (hydr)oxides, can migrate to a wider area and, thus, has a stronger impact on agricultural soils than Cd, Pb, and Zn through groundwater cycling.

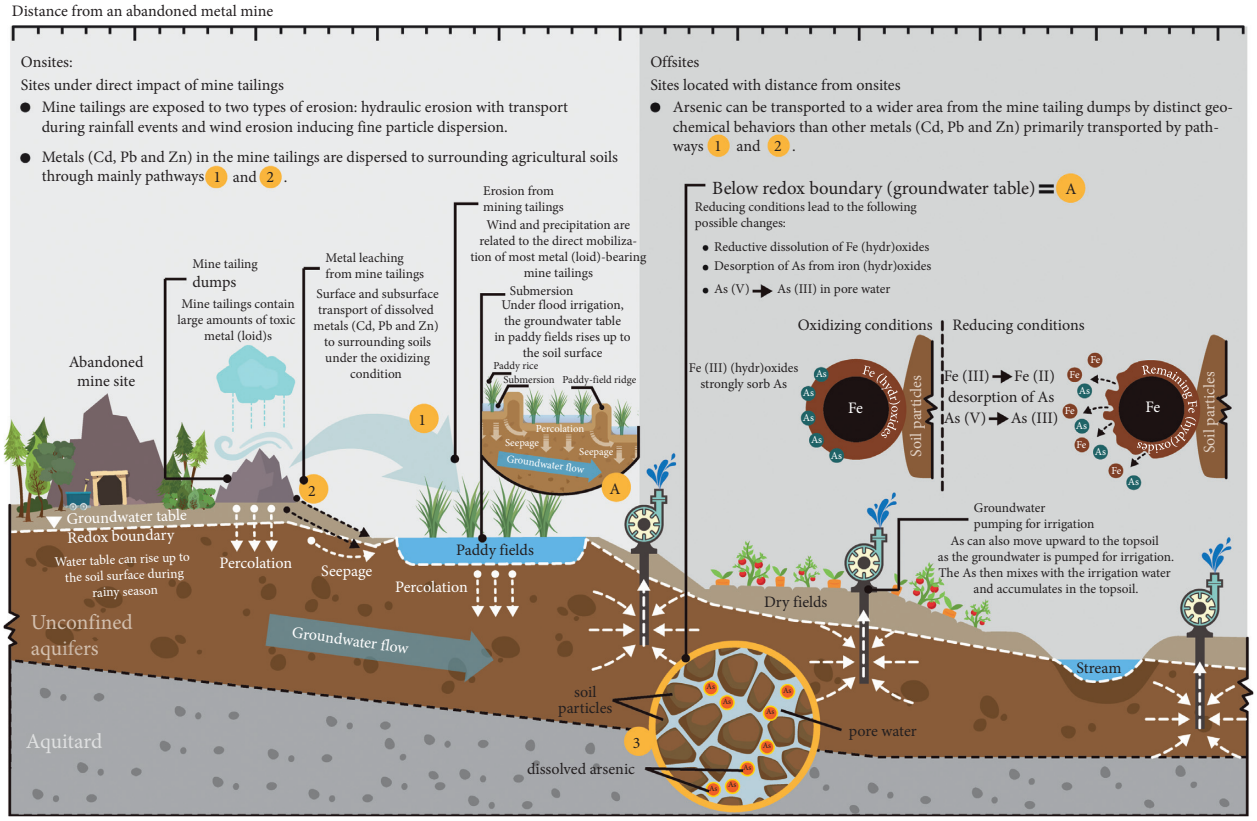

Figure 6: Conceptual diagram illustrating the transport processes of metal(loid)s from the mine tailing dumps to the surrounding agricultural soils in the study area.

5. Conclusions

In this study, we used field surveys and GIS mapping to identify the distinct transport and dispersion characteristics of different metal(loid)s by tracing the migration pathways of As, Cd, Pb, and Zn from the mine tailing dumps of an abandoned mine to nearby agricultural fields. The results of this study show a common migration pathway for As, Cd, Pb, and Zn: direct dispersion of metal(loid)-bearing particles in the tailings through the wind- and rainfall-driven erosion. In addition, As, Cd, Pb, and Zn released to the soil environment from the mine tailing dumps during rainfall-runoff processes adopt different migration patterns. The dispersion and spatial distribution characteristics of these patterns are dependent on the soil and groundwater environment as well as the adsorption preferences of various soil minerals for individual metal(loid)s. In particular, As can influence a larger geographical area than do other metals owing to its distinct geochemical behavior.

To efficiently manage and remediate the surrounding agricultural fields that have been polluted by anthropogenic sources, such as abandoned metal mines, the area of influence must first be accurately set for the environment surrounding the anthropogenic source. However, in Korea, pollution management and remediation activities are generally only conducted in agricultural fields that are within a 1-2 km radius of an abandoned mine. The results of this research clearly show that the existing distance, especially for the area of influence of As, may be underestimated. Therefore, special consideration should be given to the migration behavior of As during the development of appropriate soil remediation activities, such as soil management, for agricultural soils contaminated by anthropogenic metal(loid)s as a result of mining activities.

Data Availability

The data used to support the findings of this study are included within the paper and Supplementary Materials.

Conflicts of Interest

The authors declare that there are no conflicts of interest regarding the publication of this paper.

Acknowledgments

This work was conducted with the support of the "Cooperative Research Program for Agriculture Science & Technology Development (Project no. PJ014190)", Rural Development Administration, Republic of Korea.

Supplementary Materials

Figure S1: overview of the pumping well for irrigation in the study area. Figure S2: overview of the mine tailing dumps

located in the study area. Figure S3: scatter diagrams of metal(loid) concentrations in the agricultural soils ($n = 162$) and increasing distance from the mine tailing dumps. Table S1: total concentrations of metal(loid)s in the studied samples of agricultural soils and their corresponding spatial data. (*Supplementary Materials*)

References

[1] C. S. Kim, T. L. Anthony, D. Goldstein, and J. J. Rytuba, "Windborne transport and surface enrichment of arsenic in semi-arid mining regions: examples from the Mojave Desert, California," *Aeolian Research*, vol. 14, pp. 85–96, 2014.

[2] X. Li, H. Yang, C. Zhang et al., "Spatial distribution and transport characteristics of heavy metals around an antimony mine area in central China," *Chemosphere*, vol. 170, pp. 17–24, 2017.

[3] M. C. Jung, "Heavy metal contamination of soils and waters in and around the Imcheon Au-Ag mine, Korea," *Applied Geochemistry*, vol. 16, no. 11-12, pp. 1369–1375, 2001.

[4] L. Rodríguez, E. Ruiz, J. Alonso-Azcárate, and J. Rincón, "Heavy metal distribution and chemical speciation in tailings and soils around a Pb-Zn mine in Spain," *Journal of Environmental Management*, vol. 90, no. 2, pp. 1106–1116, 2009.

[5] M. N. Rashed, "Monitoring of contaminated toxic and heavy metals, from mine tailings through age accumulation, in soil and some wild plants at Southeast Egypt," *Journal of Hazardous Materials*, vol. 178, no. 1-3, pp. 739–746, 2010.

[6] M. Mileusnić, B. S. Mapani, A. F. Kamona, S. Ružičić, I. Mapaure, and P. M. Chimwamurombe, "Assessment of agricultural soil contamination by potentially toxic metals dispersed from improperly disposed tailings, Kombat mine, Namibia," *Journal of Geochemical Exploration*, vol. 144, pp. 409–420, 2014.

[7] W. Zhang, L. Alakangas, Z. Wei, and J. Long, "Geochemical evaluation of heavy metal migration in Pb-Zn tailings covered by different topsoils," *Journal of Geochemical Exploration*, vol. 165, pp. 134–142, 2016.

[8] M. Gabarrón, A. Faz, S. Martínez-Martínez, and J. A. Acosta, "Change in metals and arsenic distribution in soil and their bioavailability beside old tailing ponds," *Journal of Environmental Management*, vol. 212, pp. 292–300, 2018.

[9] S. Boussen, A. Sebei, M. Soubrand-Colin, H. Bril, F. Chaabani, and S. Abdeljaouad, "Mobilization of lead-zinc rich particles from mine tailings in northern Tunisia by aeolian and run-off processes," *Bulletin de la Société Géologique de France*, vol. 181, no. 5, pp. 459–471, 2010.

[10] V. M. Ngole-Jeme and P. Fantke, "Ecological and human health risks associated with abandoned gold mine tailings contamination soil," *PloS One*, vol. 12, no. 2, Article ID e0172517, 2017.

[11] B. D. Tembo, K. Sichilongo, and J. Cernak, "Distribution of copper, lead, cadmium and zinc concentrations in soils around Kabwe town in Zambia," *Chemosphere*, vol. 63, no. 3, pp. 497–501, 2006.

[12] D. Meza-Figueroa, R. M. Maier, M. de la O- Villanueva et al., "The impact of unconfined mine tailings in residential areas from a mining town in a semi-arid environment: Nacozari, Sonora, Mexico," *Chemosphere*, vol. 77, no. 1, pp. 140–147, 2009.

[13] U. Kraus and J. Wiegand, "Long-term effects of the Aznalcóllar mine spill-heavy metal content and mobility in soils and sediments of the Guadiamar river valley (SW Spain)," *Science of the Total Environment*, vol. 367, no. 2-3, pp. 855–871, 2006.

[14] D. Ciszewski, U. Kubsik, and U. Aleksander-Kwaterczak, "Long-term dispersal of heavy metals in a catchment affected by historic lead and zinc mining," *Journal of Soils and Sediments*, vol. 12, no. 9, pp. 1445–1462, 2012.

[15] K. Pi, Y. Wang, X. Xie, Y. Liu, T. Ma, and C. Su, "Multilevel hydrogeochemical monitoring of spatial distribution of arsenic: a case study at Datong Basin, northern China," *Journal of Geochemical Exploration*, vol. 161, pp. 16–26, 2016.

[16] S. S. Lee, P. N. Vinayachandran, K. J. Ha, and J. G. Jhun, "Shift of peak in summer monsoon rainfall over Korea and its association with El Niño–Southern Oscillation," *Journal of Geophysical Research*, vol. 115, no. D2, Article ID D02111, 2010.

[17] H. Tutu, T. S. McCarthy, and E. Cukrowska, "The chemical characteristics of acid mine drainage with particular reference to sources, distribution and remediation: the Witwatersrand Basin, South Africa as a case study," *Applied Geochemistry*, vol. 23, no. 12, pp. 3666–3684, 2008.

[18] A. N. Roychoudhury and J. Petersen, "Geochemical evaluation of soils and groundwater affected by infiltrating effluent from evaporation ponds of a heavy mineral processing facility, West Coast, South Africa," *Journal of Geochemical Exploration*, vol. 144, pp. 478–491, 2014.

[19] W. Gitari, R. Thobakgale, and S. Akinyemi, "Mobility and attenuation dynamics of potentially toxic chemical species at an abandoned copper mine tailings dump," *Minerals*, vol. 8, no. 2, p. 64, 2018.

[20] KSIS, *Korean Soil Information System*, Rural Development Administration (RDA), Jeonju, Korea, 2019, http://soil.rda.go.kr.

[21] KMGEO, *The Korean Multiplatform GEOscience Information System*, Korea Institute of Geoscience and Mineral Resource (KIGMR), Daejeon, Korea, 2019, http://mgeo.kigam.re.kr.

[22] KOSIS, *Statistics Yearbook of Gyeongju City, 2013*, Korean Statistical Information Service, Daejeon, Korea, 2014.

[23] KMA, *Annual Climatological Report, 2013*, Korea Meteorological Administration, Seoul, Korea, 2014.

[24] KMoE, *Detailed Soil Survey on the Current Status of Soil Contamination near Abandoned Mines, 2007*, Korea Ministry of Environment, Sejong, Korea, 2008.

[25] KMoE, *Exploratory Soil Survey on the Current Status of Soil Contamination near Abandoned Mines in Gyeongsang Province*, Korea Ministry of Environment, Sejong, Korea, 2005.

[26] KORES, *Prospecting and Exploration of Mineral Deposits No. 6*, Korea Resources Corporation, Wonju, Korea, 1983.

[27] KORES, *Mineral Deposits in Korea No. 10*, Korea Resources Corporation, Wonju, Korea, 1987.

[28] KMoE, *Standard Methods of Soil Sampling and Analysis*, Korea Ministry of Environment, Sejong, Korea, 2013.

[29] K. Zhao, W. Fu, Q. Qiu et al., "Spatial patterns of potentially hazardous metals in paddy soils in a typical electrical waste dismantling area and their pollution characteristics," *Geoderma*, vol. 337, pp. 453–462, 2019.

[30] K. Zhao, L. Zhang, J. Dong et al., "Risk assessment, spatial patterns and source apportionment of soil heavy metals in a typical Chinese hickory plantation region of southeastern China," *Geoderma*, vol. 360, p. 114011, 2020.

[31] KMoE, *Soil Environment Conservation Act*, Korea Ministry of Environment, Sejong, Korea, 2015.

[32] KMoE, *Result of Soil Pollution Investigation by Soil Quality Monitoring Network in Korea, 2013*, Korea Ministry of Environment, Sejong, Korea, 2014.

[33] D. C. Adriano, *Trace Elements in Terrestrial Environments: Biogeochemistry, Bioavailability and Risks of Metals*, Springer-Verlag, New York, NY, USA, 2001.

[34] S.-W. Yun, P. C. Baveye, K.-B. Kim et al., "Effect of post-mining land use on the spatial distribution of metal(loid)s and their transport in agricultural soils: analysis of a case study of Chungyang, South Korea," *Journal of Geochemical Exploration*, vol. 170, pp. 157–166, 2016.

[35] S.-W. Yun, D.-H. Kim, D.-H. Kang et al., "Effect of farmland type on the transport and spatial distribution of metal(loid)s in agricultural lands near an abandoned gold mine site: confirmation of previous observations," *Journal of Geochemical Exploration*, vol. 181, pp. 129–137, 2017.

[36] A. Boularbah, C. Schwartz, G. Bitton, and J. L. Morel, "Heavy metal contamination from mining sites in South Morocco: 1. Use of a biotest to assess metal toxicity of tailings and soils," *Chemosphere*, vol. 63, no. 5, pp. 802–810, 2006.

[37] M. C. Navarro, C. Pérez-Sirvent, M. J. Martínez-Sánchez, J. Vidal, P. J. Tovar, and J. Bech, "Abandoned mine sites as a source of contamination by heavy metals: a case study in a semi-arid zone," *Journal of Geochemical Exploration*, vol. 96, no. 2-3, pp. 183–193, 2008.

[38] J. S. Ahn, J. Y. Kim, C. M. Chon, and H. S. Moon, "Mineralogical and chemical characterization of arsenic solid phases in weathered mine tailings and their leaching potential," *Economic and Environmental Geology*, vol. 36, pp. 27–38, 2003.

[39] J. U. Kim, H. S. Moon, Y. Song, and J. H. Yoo, "Chemical forms of heavy metal elements in mine wastes, stream sediments and surrounding soils from the Gubong mine, Korea," *Economic and Environmental Geology*, vol. 32, pp. 261–271, 1999.

[40] H. O. Son and M. C. Jung, "Relative extraction ratio (RER) for arsenic and heavy metals in soils and tailings from various metal mines, Korea," *Environmental Geochemistry and Health*, vol. 33, no. S1, pp. 121–132, 2001.

[41] R. W. Boyle and I. R. Jonasson, "The geochemistry of arsenic and its use as an indicator element in geochemical prospecting," *Journal of Geochemical Exploration*, vol. 2, no. 3, pp. 251–296, 1973.

[42] A. H. Welch, M. S. Lico, and J. L. Hughes, "Arsenic in ground water of the western United States," *Ground Water*, vol. 26, no. 3, pp. 333–347, 1988.

[43] O. Talavera-Mendoza, J. Ruiz, G. E. Gehrels, V. A. Valencia, and E. Centeno-García, "Detrital zircon U/Pb geochronology of southern Guerrero and western Mixteca arc successions (southern Mexico): new insights for the tectonic evolution of southwestern North America during the late Mesozoic," *Geological Society of America Bulletin*, vol. 119, no. 9-10, pp. 1052–1065, 2007.

[44] A. Dótor-Almazán, M. A. Armienta-Hernández, O. Talavera-Mendoza, and J. Talavera-Mendoza, "Geochemical behavior of Cu and sulfur isotopes in the tropical mining region of Taxco, Guerrero (southern Mexico)," *Chemical Geology*, vol. 471, pp. 1–12, 2017.

[45] A. Mihailović, L. Budinski-Petković, S. Popov et al., "Spatial distribution of metals in urban soil of Novi Sad, Serbia: GIS based approach," *Journal of Geochemical Exploration*, vol. 150, pp. 104–114, 2015.

[46] T. Chen, X. Liu, M. Zhu et al., "Identification of trace element sources and associated risk assessment in vegetable soils of the urban-rural transitional area of Hangzhou, China," *Environmental Pollution*, vol. 151, no. 1, pp. 67–78, 2008.

[47] G. Guo, F. Wu, F. Xie, and R. Zhang, "Spatial distribution and pollution assessment of heavy metals in urban soils from southwest China," *Journal of Environmental Sciences*, vol. 24, no. 3, pp. 410–418, 2012.

[48] R. D. Roberts and M. S. Johnson, "Dispersal of heavy metals from abandoned mine workings and their transference through terrestrial food chains," *Environmental Pollution (1970)*, vol. 16, no. 4, pp. 293–310, 1978.

[49] M. C. Jung and I. Thornton, "Heavy metal contamination of soils and plants in the vicinity of a lead-zinc mine, Korea," *Applied Geochemistry*, vol. 11, no. 1-2, pp. 53–59, 1996.

[50] X. Bi, X. Feng, Y. Yang et al., "Environmental contamination of heavy metals from zinc smelting areas in Hezhang County, western Guizhou, China," *Environment International*, vol. 32, no. 7, pp. 883–890, 2006.

[51] S. Wu, S. Zhou, and X. Li, "Determining the anthropogenic contribution of heavy metal accumulations around a typical industrial town: Xushe, China," *Journal of Geochemical Exploration*, vol. 110, no. 2, pp. 92–97, 2011.

[52] P. Li, C. Lin, H. Cheng, X. Duan, and K. Lei, "Contamination and health risks of soil heavy metals around a lead/zinc smelter in southwestern China," *Ecotoxicology and Environmental Safety*, vol. 113, pp. 391–399, 2015.

[53] M. Ghayoraneh and A. Qishlaqi, "Concentration, distribution and speciation of toxic metals in soils along a transect around a Zn/Pb smelter in the northwest of Iran," *Journal of Geochemical Exploration*, vol. 180, pp. 1–14, 2017.

[54] S.-W. Yun, P. C. Baveye, D.-H. Kim et al., "Analysis of metal(loid)s contamination and their continuous input in soils around a zinc smelter: development of methodology and a case study in South Korea," *Environmental Pollution*, vol. 238, pp. 140–149, 2018.

[55] T. C. Robson, C. B. Braungardt, J. Rieuwerts, and P. Worsfold, "Cadmium contamination of agricultural soils and crops resulting from sphalerite weathering," *Environmental Pollution*, vol. 184, pp. 283–289, 2014.

[56] B. Dold and L. Fontboté, "A mineralogical and geochemical study of element mobility in sulfide mine tailings of Fe oxide Cu-Au deposits from the Punta del Cobre belt, northern Chile," *Chemical Geology*, vol. 189, no. 3-4, pp. 135–163, 2002.

[57] J. C. Echeverría, M. T. Morera, C. Mazkiarán, and J. J. Garrido, "Competitive sorption of heavy metal by soils. Isotherms and fractional factorial experiments," *Environmental Pollution*, vol. 101, no. 2, pp. 275–284, 1998.

[58] M. P. F. Fontes and P. C. Gomes, "Simultaneous competitive adsorption of heavy metals by the mineral matrix of tropical soils," *Applied Geochemistry*, vol. 18, no. 6, pp. 795–804, 2003.

[59] H. B. Bradl, "Adsorption of heavy metal ions on soils and soils constituents," *Journal of Colloid and Interface Science*, vol. 277, no. 1, pp. 1–18, 2004.

[60] S. Chotpantarat, S. K. Ong, C. Sutthirat, and K. Osathaphan, "Competitive sorption and transport of Pb^{2+}, Ni^{2+}, Mn^{2+}, and Zn^{2+} in lateritic soil columns," *Journal of Hazardous Materials*, vol. 190, no. 1-3, pp. 391–396, 2011.

[61] M. F. Schultz, M. M. Benjamin, and J. F. Ferguson, "Adsorption and desorption of metals on ferrihydrite: reversibility of the reaction and sorption properties of the regenerated solid," *Environmental Science & Technology*, vol. 21, no. 9, pp. 863–869, 1987.

[62] S. W. Yun and C. Yu, "Immobilization of Cd, Zn, and Pb from soil treated by limestone with variation of pH using a column test," *Journal of Chemistry*, vol. 2015, Article ID 641415, 8 pages, 2015.

[63] A. P. Puga, L. C. A. Melo, C. A. De Abreu, A. R. Coscione, and J. Paz-Ferreiro, "Leaching and fractionation of heavy metals in mining soils amended with biochar," *Soil and Tillage Research*, vol. 164, pp. 25–33, 2016.

[64] H. Arabyarmohammadi, A. K. Darban, S. E. A. T. M. Van der Zee, M. Abdollahy, and B. Ayati, "Fractionation and leaching of heavy metals in soils amended with a new biochar nanocomposite," *Environmental Science and Pollution Research*, vol. 25, no. 7, pp. 6826–6837, 2018.

[65] P. L. Smedley and D. G. Kinniburgh, "A review of the source, behaviour and distribution of arsenic in natural waters," *Applied Geochemistry*, vol. 17, no. 5, pp. 517–568, 2002.

[66] L. Xu, Z. Zhao, S. Wang, R. Pan, and Y. Jia, "Transformation of arsenic in offshore sediment under the impact of anaerobic microbial activities," *Water Research*, vol. 45, no. 20, pp. 6781–6788, 2011.

[67] D. Panagiotaras, G. Panagopoulos, D. Popoulis, and P. Avramidis, "Arsenic geochemistry in groundwater system," in *Geochemistry—Earth's System Processes*, D. Panagiotaras, Ed., pp. 27–38, InTech Europe, University Campus STeP Ri, Rijeka, Croartia, 2012.

[68] C. Yang, S. Li, R. Liu, P. Sun, and K. Liu, "Effect of reductive dissolution of iron (hydr)oxides on arsenic behavior in a water-sediment system: first release, then adsorption," *Ecological Engineering*, vol. 83, pp. 176–183, 2015.

[69] E. D. Burton, S. G. Johnston, and R. T. Bush, "Microbial sulfidogenesis in ferrihydrite-rich environments: effects on iron mineralogy and arsenic mobility," *Geochimica et Cosmochimica Acta*, vol. 75, no. 11, pp. 3072–3087, 2011.

[70] Y. N. Vodyanitskii and I. O. Plekhanova, "Biogeochemistry of heavy metals in contaminated excessively moistened soils (analytical review)," *Eurasian Soil Science*, vol. 47, no. 3, pp. 153–161, 2014.

[71] D. Moon, D. Dermatas, and N. Menounou, "Arsenic immobilization by calcium-arsenic precipitates in lime treated soils," *Science of the Total Environment*, vol. 330, no. 1-3, pp. 171–185, 2004.

[72] R. S. Oremland and J. F. Stolz, "The ecology of arsenic," *Science*, vol. 300, no. 5621, pp. 939–944, 2003.

[73] I. Hindersmann and T. Mansfeldt, "Trace element solubility in a multimetal contaminated soil as affected by redox conditions," *Water, Air, & Soil Pollution*, vol. 225, no. 10, pp. 1–20, 2014.

[74] S.-W. Yun and C. Yu, "The leaching characteristics of Cd, Zn, and as from submerged paddy soil and the effect of limestone treatment," *Paddy and Water Environment*, vol. 13, no. 1, pp. 61–69, 2015.

[75] G. E. M. Hall, G. Gauthier, J.-C. Pelchat, P. Pelchat, and J. E. Vaive, "Application of a sequential extraction scheme to ten geological certified reference materials for the determination of 20 elements," *Journal of Analytical Atomic Spectrometry*, vol. 11, no. 9, pp. 787–796, 1996.

[76] A. Suda and T. Makino, "Functional effects of manganese and iron oxides on the dynamics of trace elements in soils with a special focus on arsenic and cadmium: a review," *Geoderma*, vol. 270, pp. 68–75, 2016.

[77] D. Gregory, S. Meffre, and R. Large, "Comparison of metal enrichment in pyrite framboids from a metal-enriched and metal-poor estuary," *American Mineralogist*, vol. 99, no. 4, pp. 633–644, 2014.

[78] P. Le Pape, M. Blanchard, J. Brest et al., "Arsenic incorporation in pyrite at ambient temperature at both tetrahedral S-I and octahedral Fe(II) sites: evidence from EXAFS-DFT analysis," *Environmental Science & Technology*, vol. 51, no. 1, pp. 150–158, 2017.

[79] M. Keith, D. J. Smith, G. R. T. Jenkin, D. A. Holwell, and M. D. Dye, "A review of Te and Se systematics in hydrothermal pyrite from precious metal deposits: insights into ore-forming processes," *Ore Geology Reviews*, vol. 96, pp. 269–282, 2018.

[80] Y. Takahashi, R. Minamikawa, K. H. Hattori, K. Kurishima, N. Kihou, and K. Yuita, "Arsenic behavior in paddy fields during the cycle of flooded and non-flooded periods," *Environmental Science & Technology*, vol. 38, no. 4, pp. 1038–1044, 2004.

[81] P. X. Pinto, S. R. Al-Abed, C. Holder, and D. J. Reisman, "Evaluation of metal partitioning and mobility in a sulfidic mine tailing pile under oxic and anoxic conditions," *Journal of Environmental Management*, vol. 140, pp. 135–144, 2014.

[82] J. M. McArthur, P. Ravenscroft, S. Safiulla, and M. F. Thirlwall, "Arsenic in groundwater: testing pollution mechanisms for sedimentary aquifers in Bangladesh," *Water Resources Research*, vol. 37, no. 1, pp. 109–117, 2001.

[83] C. B. Dowling, R. J. Poreda, A. R. Basu, S. L. Peters, and P. K. Aggarwal, "Geochemical study of arsenic release mechanisms in the Bengal Basin groundwater," *Water Resources Research*, vol. 38, no. 9, pp. 12–18, 2002.

[84] A. Van Geen, Y. Zheng, Z. Cheng et al., "Transect of groundwater and sediment properties in Araihazar, Bangladesh: further evidence of decoupling between as and Fe mobilization," *Chemical Geology*, vol. 228, no. 1–3, pp. 85–96, 2006.

[85] V. S. Chauhan, R. T. Nickson, D. Chauhan, L. Iyengar, and N. Sankararamakrishnan, "Ground water geochemistry of Ballia district, Uttar Pradesh, India and mechanism of arsenic release," *Chemosphere*, vol. 75, no. 1, pp. 83–91, 2009.

[86] A. H. M. S. Reza, J.-S. Jean, M.-K. Lee, H.-J. Yang, and C.-C. Liu, "Arsenic enrichment and mobilization in the Holocene alluvial aquifers of the Chapai-Nawabganj district, Bangladesh: a geochemical and statistical study," *Applied Geochemistry*, vol. 25, no. 8, pp. 1280–1289, 2010.

[87] I. C. Yadav, N. L. Devi, and S. Singh, "Reductive dissolution of iron-oxyhydroxides directs groundwater arsenic mobilization in the upstream of Ganges River basin, Nepal," *Journal of Geochemical Exploration*, vol. 148, pp. 150–160, 2015.

[88] M. L. Polizzotto, B. D. Kocar, S. G. Benner, M. Sampson, and S. Fendorf, "Near-surface wetland sediments as a source of arsenic release to ground water in Asia," *Nature*, vol. 454, no. 7203, pp. 505–508, 2008.

[89] P. Kumarathilaka, S. Seneweera, A. Meharg, and J. Bundschuh, "Arsenic speciation dynamics in paddy rice soil-water environment: source, physico-chemical, and biological factor—a review," *Water Research*, vol. 140, pp. 403–414, 2018.

Hindawi
Journal of Chemistry
Volume 2020, Article ID 5497952, 7 pages
https://doi.org/10.1155/2020/5497952

Research Article

Assessment of Health Risk due to Pesticide Residues in Fruits, Vegetables, Soil, and Water

Nikhat Khan, Ghazala Yaqub, Tahreem Hafeez, and Madiha Tariq

Department of Environmental Sciences, Kinnaird College for Women, Lahore 54000, Pakistan

Correspondence should be addressed to Ghazala Yaqub; ghazala_yaqub@yahoo.com

Received 10 January 2020; Revised 10 April 2020; Accepted 12 May 2020; Published 24 June 2020

Guest Editor: Yifeng Zhang

The present study was conducted to assess the contamination and health risk due to the presence of pesticides in fruits and vegetables. A total of six vegetable samples, 3 fruit samples, 7 soil samples, and 6 water samples were collected from three different sampling points. High-performance liquid chromatography using acetonitrile and water solvent system was employed for the quantitative and qualitative analysis. The pesticides having the highest health risk in vegetables were Bifenthrin and Difenoconazole as their health risk index was found to be exceeding the cut off value of 1. Imidacloprid was found in all vegetable samples but had no associated health risk, as all the health risk indices for imidacloprid were below the cut off value of 1. The pesticide Glyphosate detected in only one sample had no health risk associated with it. Health risks in fruits were the highest for Amamectin, Bifenthrin, and Difenoconazole and were crossing the threshold limit of 1. The results reveal the health risk indices of Bifenthrin and Difenoconazole range from 7.8 to 12.46 in vegetables and from 2.704 to 30.454 in fruits, hence, posing a serious threat to human health. Amamectin, although detected in only fruit and water samples, had the highest health risk of 30.454. Imidacloprid and Glyphosate found in every fruit sample had no associated health risk. The results revealed the presence of pesticides in water, soil, fruit, and vegetable samples. Consumers utilizing these vegetables and fruits are under potential health risks due to the presence of pesticides in soil and water. *Practical Applications*. In this study, an analytical method for detecting pesticides in a variety of environmental matrices including fruits, vegetables, water, and the soil is presented and the health risk associated with the presence of pesticides in a wide range of fruits and vegetables is assessed. It is highly significant because in developing countries agricultural activities contribute majorly toward the total gross domestic product and pesticides are extensively used to control, prevent, devastate, and diminish any harmful pest that destroys crops.

1. Introduction

Economic growth and development is largely dependent upon agriculture. It is the main source of living and income in rural areas and it also ensures the availability of food in rural and urban populations. Being the dominant sector of the economy in Pakistan, its GDP contribution in Pakistan for the year 2019 is 18.53% [1]. Agrochemicals are intensively used globally. Developing countries have been using 108 kinds of insecticides, 30 kinds of fungicides, 39 kinds of weedicides, 5 kinds of acaricides, and 6 different kinds of rodenticides [2]. Food is the main route of exposure through which pesticide contamination can be caused. Exposure to pesticides through consumption of food is considered to be five times higher in magnitude as compared to other exposures like air and water [3]. According to the World Health Organization, fruits and vegetables are the most commonly consumed food group, and on average, 30% of food consumption is based on fruits and vegetables. Moreover, because fruit and vegetables are primarily consumed raw or semiprocessed, it is expected that they contain higher amounts of pesticide residue levels in comparison to other food groups of plant origin, such as bread and other foodstuffs based on cereal processing [4].

Pesticides due to their persistent nature, toxic properties, bioaccumulation, lipophilicity, and adverse impacts on human health are of greater concern. These pesticides can enter the human body through the consumption of contaminated fruits and vegetables. The major health impacts associated with pesticides include cancers, birth defects,

neurological disorders, endocrine disruptors, and reproductive effects. The effect of a pesticide is determined by the duration of exposure and toxicity of a particular pesticide. The effects which can be caused are either acute or chronic. Acute effects can result in rashes, diarrhea, dizziness, rashes, and blindness. Chronic health impacts include cancers, reproductive effects, thyroid, and endocrine disruption [5]. Due to the potential health risks associated with pesticide consumption, continuous monitoring of fruits and vegetables is required. After their use on vegetables and fruits, there is no proper preharvest time frame followed because of their high market demand and less knowledge about toxic effects of pesticides which can be caused on human health after the consumption of these contaminated foods.

The residual level of pesticides is examined through the maximum residual limit which is based on the analysis of pesticide residues left behind on the food products [6]. The Maximum Residue Limit (MRL) is the maximum amount of pesticide which can be present in the food at the time of its sale. These limits are expressed as mg/kg. These pesticide limits are established by the national governments which ensure that good agricultural practices are being pursued to standardize international trade [7]. These limits are used as indicators of health risks and assure food safety to consumers. Health safety limits for human health are usually expressed as acceptable daily intake ADI. The standard method to calculate human exposure with pesticides is based on the average consumption per person per day, average adult weight, and pesticide residue data [8]. The objective of the study is to provide an analytical method for detecting pesticides in a variety of environmental matrices including fruits, vegetables, water, and soil and also to assess the health risk associated with the presence of pesticides in a wide range of fruits and vegetables.

2. Materials and Methods

2.1. Primary Data Collection. Initially, primary data was collected, studied, and revised from selected agricultural areas of Lahore. After the extraction of relevant information, detailed visits were planned. The information gathered from field visits was about the types of fruits and vegetables grown, pesticides used in that area, and reasons and frequency of pesticides used in that area.

2.2. Collection of Samples. Three types of samples were collected from the agricultural areas of Lahore. Fresh fruits and vegetables were acquired from agricultural fields before sending them to the markets. Samples of vegetables, fruits, and soil were obtained in labeled polythene bags and were quickly transported to the laboratory for analysis. The water samples used for irrigation purposes were collected from market Raiwind, badian, and market area in autoclaved bottles. Controlled samples for each vegetable, fruit, soil sample, and wastewater were also collected for the comparative analysis (t was taken from the farm where no pesticides are used). All samples were kept at room temperature and transported to Kinnaird College's Environmental Science Laboratory for experimentation. Table 1 shows the sample type and sampling location of different samples.

2.3. Selection of Pesticides. On the basis of primary data, field surveys and interviews with farmers concerning the type, amount, and frequency of pesticides that are sprayed on the sites were conducted. The farmers were found spraying pesticides in selected agricultural sampling areas. The pesticides selected were Glyphosate, Bifenthrin, Amamectin, Imidacloprid, Difenoconazole, Dichlorvos, and Lambda.

2.4. Experimental Chemical, Apparatus, and Instrumentation. HPLC grade chemicals, i.e., ethyl acetate, dichloromethane, methanol, sodium chloride, sodium anhydrous sulphate, acetonitrile, and distilled water, were used in the experiment. The main apparatus and equipment used in the experiment were magnetic stirrer, rotary evaporator, and high-performance liquid chromatography (UV-Visible).

2.4.1. Sample Preparation and Pretreatment. The samples of fruits, vegetables, and soil were prepared for the determination of pesticides. The samples were pretreated for running before being analyzed by high-performance liquid chromatography. Fruit and vegetable samples were chopped, air-dried for 4–5 days, and then ground into a fine powder form prior to extraction. Soil samples were also air-dried and crushed into a fine powder.

2.4.2. Preparation of Vegetable and Fruit Samples. 2 g of air-dried and finely ground fruit and vegetable sample was taken in a beaker and mixed with 40 ml of ethyl acetate, 40 ml of dichloromethane (DCM), 150 ml of distilled water, and 5 g of NaCI on a magnetic stirrer. This mixture was then transferred to separating funnel and allowed to stand for 30 minutes until two layers were formed. The lower layer (organic layer) was collected in a beaker. 40 ml of ethyl acetate: DCM (1 : 1) was added additionally in the upper layer. The lower organic layer when formed was collected and mixed with the previous organic layer. The same extraction process was repeated for all fruit and vegetable samples.

2.4.3. Preparation of Soil Sample. 5 g of air-dried and finely ground soil sample was taken in a beaker and followed by the addition of 40 ml of dichloromethane (DCM), 40 ml ethyl acetate, and 200 ml of distilled water. The mixture was placed on a magnetic stirrer for 15 minutes to get a homogenous mixture. Then, it was shifted into a separating funnel to allow the separation of the organic layer from the aqueous layer. When both layers got separated, the organic layer was collected in a beaker. 20 ml of ehty1 acetate and dichloromethane each was added again into the aqueous layer. After 10 minutes, both organic layers were mixed. This extraction procedure was repeated for all soil samples.

Table 1: Mean concentration of detected pesticides.

Samples	Samples names	Sample location	Amamectin (ppm)	Bifenthrin (ppm)	Dichlorvos (ppm)	Glyphosate (ppm)	Imidacloprid (ppm)	Lambda (ppm)
Fruits	Grape fruit	Market	—	—	—	0.7451	—	—
		Badian	—	—	—	6.1576	—	—
	Guava	Market	2.1247	1.3527	2.0926	0.5082	—	—
		Badian	—	—	—	—	—	—
		Raiwind	—	—	—	0.2576	0.0091	—
	Orange	Market	—	2.2250	—	0.5705	—	—
		Badian		—	—	1.4352	—	—
		Raiwind	—	—	—	1.1016	—	—
Soil samples	Carrot	Badian	—	0.7289	—	—	—	—
	Grape fruit	Badian	—	0.2324	—	—	—	—
	Guava	Badian	—	28.1500	—	—	—	—
		Raiwind	—	—	—	—	—	—
	Orange	Badian	—	0.2057	—	—	—	—
		Raiwind	—	—	—	—	—	—
	Spinach	Badian	—	0.2443	—	—	—	—
	Turnip	Badian	—	—	—	—	—	—
Vegetables	Carrot	Market	—	—	—	0.2892	—	—
		Badian	—	13.5772	—	—	—	—
	Spinach	Market	—	—	—	—	—	—
		Badian	—	21.6753	—	—	—	—
	Turnip	Market	—	—	—	0.9306	—	—
		Badian	—	—	—	—	0.0063	—
Water samples	Carrot	Badian	0.5495	—	0.5412	0.4593	—	—
	Grape fruit	Badian	0.4541	—	0.4472	—	0.0054	—
	Guava	Badian	0.3304	—	0.3254	—	—	—
		Raiwind	—	—	—	—	—	—
	Orange	Badian	14.2435	—	14.0286	—	—	—
		Raiwind	—	—	—	—	—	—
	Spinach	Badian	—	—	—	—	—	—
	Turnip	Badian	—	0.4185	—	—	—	—

2.4.4. Preparation of Water Samples. 200 ml of water sample along with 40 ml of ethy1 acetate and 40 ml of dichloromethane was taken in a beaker and allowed to mix for 15 minutes on a magnetic stirrer. The mixture of wastewater and organic solvents was then transferred into a separating funnel for 30 minutes and was allowed to separate. The organic layer was taken in a beaker after 30 minutes so that organic layers separate from the aqueous layer. The lower layer which is the organic layer was collected and the upper layer was followed by the addition of 20 ml of ethy1 acetate and 20 ml of DCM again. After 10 minutes of stay, the organic layer was again collected and mixed with the previous organic layer. The same process was repeated for all wastewater samples.

2.4.5. Dehydration. To ensure the removal of any water vapors from the organic layer, 20 gm of sodium sulphate was added in each sample. The mixture was then filtered through Whitman filter paper. The solvent from the mixture was evaporated in a rotary evaporator at 40°C, and leftover residues were collected by adding 20 ml of methanol. For fruit samples, 10 gm of sodium sulphate was used (Figure 1).

2.4.6. Preparation of Standards. Seven pesticides, i.e., Amamectin, Bifenthrin, Dichlorvos, Glyphosate, Imidacloprid, Difenoconazole, and Lambda standard stock solution, were prepared by perusing the same procedure as for sample preparation with the only difference in the amount of sample and solvent. For all the standards, 1 mg of the compound was mixed with 30 ml of distilled water and 30 ml of solvents with no addition of NaCl. Then, 5 ml of methanol of HPLC grade was added.

2.4.7. High-Performance Liquid Chromatography (HPLC) Analysis. In the prepared samples and standard vials, 15 ml of methanol was added to completely fill the vials. We wash the HPLC vials with distilled water and methanol and fill the prepared samples and standards in HPLC Agilent 1260, Quaternary Gradient System, set at chromatographic conditions.

The solution obtained after extraction and cleanup was diluted by adding 5 ml to 7 ml of methanol in 0.5 ml of sample based on the consistency of the sample and desired color acquired. For dark colored samples, 7 ml of methanol was added, and for light-colored samples, 5 ml of methanol was added; each dilution was injected in the HPLC system equipped with Diode UV/V is detector set at 254 nm. C18 Licospher column was used with an acetonitrile: water (40 : 60) mobile phase at a flow rate of 1.0 ml/min at 25°C column temperature. The injection volume was 5.000 μl.

Figure 1: Map of the study area.

2.5. Quality Assurance and Method Validation. Each sample and standard was run in triplicate for quality assurance following the European commission guidelines. For method validation, optimization studies were performed in triplicate on each HPLC parameter like solvent ratio, pH, column temperature, sample/injection volume, flow rate, wavelength and post time, etc. System sensitivity, linearity, and peak area reproducibility were also evaluated. For precision in optimization, only one parameter was changed once keeping all other parameters constant. The recovery of pesticides was determined by spiking with a standard pesticide aqueous solution. For accuracy measurement, the actual spiked values of samples were compared with the samples with known concentrations of respective pesticides. Calibration experiments were tested for linearity, accuracy, and precision. The limit of detection and the limit of quantification were considered as "an individual analytical procedure is the lowest amount of analyte in a sample which can be detected but not necessarily quantified as an exact value" and "an individual analytical procedure is the lowest amount of analyte in a sample which can be quantitatively determined with suitable precision and accuracy." The limit of detection (3 : 1) and limit of quantification (10 : 1) were calculated as a signal-to-noise ratio. In the current study, LOD was 0.01 while LOQ was 0.03 mg/L, respectively, for the selected pesticides.

2.6. Qualitative and Quantitative Analysis. After the qualitative assessment of the presence of pesticides in each sample, quantitative analysis was carried out to calculate the quantity of detected pesticides. For this purpose, the following formulas formulated by CHROMacademy were used:

$$\textbf{response factor} = \frac{\text{peak area of standard}}{\text{standard amount}}. \tag{1}$$

The concentration of the analyte in each sample will be calculated by

$$\textbf{amount of analyte} = \frac{\text{peak area of sample}}{\text{response factor}}. \tag{2}$$

2.7. Health Risk Assessment. The degree of risk associated with the consumption of each pesticide detected was monitored by evaluating the results of pesticide residues detected in samples. The health risk index was found by using EDI and ADI. ADI was used from literature studies. The EDI was calculated by multiplying the average consumption of a person per day (kg/day) and residual concentration of pesticide (mg/kg) and dividing by the average weight of an Asian (60 kg). The average consumption of fruit and vegetables for adults was considered 0.43 and 0.345 kg/person/day according to the field survey. The health risk index for each pesticide was calculated using the following formula [9]:

$$\text{health risk index} = \frac{\text{estimated daily intake}}{\text{acceptable daily intake}},$$
$$\text{EDI} = \frac{\text{concentration of detected pesticide } x \text{ food consumption}}{\text{body weight of an adult}}. \tag{3}$$

3. Results and Discussion

The presence of pesticides in samples was confirmed by comparing the standard chromatogram with the sample chromatogram. According to the results obtained, six pesticides were detected in different samples of fruits, vegetables, soil, and water. Detected pesticides were Amamectin, Bifenthrin, Dichlorvos, Glyphosate, Imidacloprid, and Difenoconazole. One of the pesticides Lambda was not detected in any sample.

Amamectin was present in guava samples. The general practice of farmers is to spray the fruit or vegetable with pesticides before sending them to the market to increase its shelf life. However, the pesticides are also absorbed from the soil and water as they were found to be present in samples. The peak of the sample chromatogram is in accordance with the peak of the standard chromatogram. The analysis has also revealed the presence of Amamectin in water samples of orange, guava, grapefruit, and carrot. Among all these, the water which is used for orange contained the maximum amount of Amamectin as compared to all other samples. The reason behind this could be that the water was standing and it also absorbs the pesticides from the soil and its environment. Another possibility is that the water used for irrigation was already toxic and mixed with the pollutants. However, only fruit and water samples had Amamectin but it was not present in vegetable or soil samples. It is dangerous for human health because it can damage the nerve cells of our human body and also affects the muscle cells, so the farmers should be very careful while the application of this pesticide. Glyphosate commonly used as a fungicide and is used to control weeds and/or herbs in agricultural fields. Glyphosate was detected in orange samples. Both samples of grapefruit obtained contained Glyphosate. Two samples of guava also contained the residues of Glyphosate. In vegetable samples, carrot and turnip had the residues. In water samples, only carrot water had the residue of Glyphosate. It was not present in any soil sample. Human health is affected if too much pesticide is used as pesticides are not good for health at all and can cause cancer [10]. Imidacloprid is commonly used as an insecticide to control pests in agricultural fields. The peak was used as the diagnostic peak of Glyphosate in fruit, vegetable, and soil samples. The concentration of Imidacloprid was detected in spinach, bitter gourd, mustard plant, beetroot, guava, and soil samples. The concentration of Imidacloprid in samples was 6.667, 3.374, 1.9643, 1.2902, 2.392, and 8.3090 mg/kg, respectively. The permissible limit of Imidacloprid for beetroot is 0.5 mg/kg. This pesticide was also present in one water sample of grapefruit. It is known as persistent in nature and persists in soil. Health effects associated with its consumption include neurotoxicity, reproductive, and mutagenic health effects [11].

Another pesticide whose concentration was detected in samples was Difenoconazole. It is used as a fungicide for disease control in fruits, vegetables, and crops. It is a broad-spectrum nitrogen-containing fungicide that belongs to the group of triazole [12]. Difenoconazole was detected in two fruit samples, i.e., orange and guava, and one vegetable sample, mustard plant. The concentration of Difenoconazole in oranges, guavas, and lemons was 3.4680 mg/kg, 12.264 mg/kg, and 433.162 mg/kg, respectively. The permissible limits prescribed by the MRLs for orange and guava and lemon are 0.6 mg/kg, 0.8 mg/kg, and 0.8 mg/kg, respectively. The residual concentration of Difenoconazole in oranges and guavas was 578 and 1533 times higher than the permissible limit. The concentration of Difenoconazole in the mustard plant was 15.2899 mg/kg. The permissible limit for the mustard plant according to MRLs was 2 mg/kg. The residual amount of Difenoconazole in the mustard plant was 794 times higher than the permissible limits. The concentration of Difenoconazole in soil was 23.0855 mg/kg. However, the MRLs for the concentration of Difenoconazole in soil samples are not available. Difenoconazole is known for its high persistence in the soil. Hence, the residual amount of Difenoconazole in fruit and vegetable samples is associated with their high persistence in soil. Consumption of foods containing Difenoconazole above the permissible limits can cause serious health implications including carcinogenicity, decreased human fertility, and neurotoxicity, reproductive, developmental, and acute toxicity [13] Bifenthrin is a pyrethroid compound used as an effective pesticide used for agricultural fields, fruits, and vegetable pest control. However, the peaks of a few samples of fruits, vegetables, soil, and water were similar to those of standard peaks of Bifenthrin. The results reveal that fruits like oranges and guavas contained Bifenthrin. The concentrations in oranges and guavas collected from different areas were 2.225 mg/kg, 1.452 mg/kg, 4.475 mg/kg, and 3.37749 mg/kg, respectively. The standard limits of this insecticide according to MRLs in oranges and guavas are 0.05 and 0.03 mg/kg, respectively. The concentration of Bifenthrin in both fruit samples was higher in comparison with WTO and MRLS. Vegetables especially carrots, mustard plants, and spinach collected from different sources had the highest levels of Bifenthrin as it was 13.57 mg/kg, 1.7612 mg/kg, and 21.67 mg/kg, respectively. In soil samples, orange and guava soil samples did not have any residue of Bifenthrin. Both samples of guavas and oranges were exceeding the Maximum Residue Limits (MRLs). They were much higher than the permissible level. However, the soil samples of grapefruits, oranges, guavas, carrots, and spinach all contained the residues of Bifenthrin. Among all guavas, the soil had the maximum residue up to 28.15 mg/kg which is very high. Only one sample of water of turnip had some residue of Bifenthrin. The reason for its presence in fruits, vegetables, and the soil is due to its ability of bioaccumulation and high persistence in environmental matrices. Long persistency of Bifenthrin under aerobic and anaerobic conditions has been observed by many researchers. The degradation rate of Bifenthrin in the soil is very much slower due to its half-life which varies from 8 to 17 months at 20°C [14]. It is transported to fruits and vegetables through contaminated soil; due to its high toxicity and adverse health impacts, it is banned in various countries. It is dangerous for human health as it belongs to the pyrethroid family. Health implications linked with the exposure to Bifenthrin include irritation, headache, dizziness, nausea, allergies, asthma,

Table 2: Health risk assessment of pesticide residues in sample fruits and vegetables.

Sample type	Type of pesticides	ADI (mg/kg/d)	EDI (mg/kg/d)	Sample name	HRI	Health risk
Vegetable samples	Bifenthrin	0.01	0.45	Spinach 1	7.8	Yes
				Carrot	12.46	Yes
				Spinach 2	1.01269	Yes
	Imidacloprid	0.06	0.45	Mustard plant	0.1881	No
				Spinach 1	0.6389	No
				Beet root	0.1236	No
				Bitter gourd	0.3233	No
				Turnip	0.891	No
	Difenoconazole	0.01	0.45	Mustard plant	8.7916	Yes
	Glyphosate	0.3	0.45	Carrot	0.0055	No
Fruit samples	Bifenthrin	0.01	0.43	Orange 1	1.594	Yes
				Guava 1	0.96	No
				Orange 2	3.2	Yes
				Guava 2	2.704	Yes
	Imidacloprid	0.06	0.43	Guava 1	0.001	No
				Guava 2	0.285	No
	Difenoconazole	0.01	0.43	Orange	2.485	Yes
				Guava	8.789	Yes
	Amamectin	0.0005	0.43	Guava	30.454	Yes
				Grapefruit	0.0177	No
	Glyphosate	0.3	0.43	Guava 1	0.0121	No
				Orange 1	0.0136	No
				Orange 2	0.0342	No
				Orange 3	0.2427	No

nasal discharge, bronchitis, sinusitis, and sneezing. It affects the nervous system of a human being. It is also carcinogenic in the long run [15]. Dichlorvos belongs to the organophosphate group; it was detected only in one sample of fruit, i.e., guavas. Other than that, it was present in most of the water samples, i.e., orange, guava, grapefruit, and carrot water. Canal water is used for irrigation and there is a possibility that it is contaminated with the industrial effluents. It also affects the nervous system and inhibits the choline esterase enzymes in the nervous system. Long-term exposure can cause endocrine disruption and weaken the immune system. Short-term exposure will cause headaches, fatigue, loss of memory, and convulsions.

3.1. Risk Assessment. To estimate the degree of risk which can be caused by the detected pesticide residues in samples, an exposure analysis was carried out by monitoring the results. Risk assessment was calculated by using EDI and ADI. EDI was calculated by average consumption per person per day and pesticide residue data. The percent EDI to ADI ratio was calculated by multiplying it with the average body weight of 60 kg [8]. The EDI for vegetables and fruits was 0.45 and 0.43, respectively. Hazard index for Difenoconazole in mustard plants, oranges, and guavas was 8.7916, 2.485, and 8.789, respectively. Hazard index for Bifenthrin in spinach, carrots, oranges, and guavas was 7.8, 12.46, 3.2, and 2.704, respectively. The hazard index for Amamectin in guavas was 30.454. In all of the above three pesticides (Difenoconazole, Bifenthrin, and Glyphosate), health risk was high. Results exceeding the cut-off value of 1 indicate the potential health risk. Pesticides like Imidacloprid and Glyphosate had no potential health risk due to the values below the cut-off limit of 1. The results indicate that even in some samples the pesticide residual concentration was exceeding the maximum residual levels but had no associated health risks (Table 2).

4. Conclusions and Recommendations

The use of pesticides has greatly enhanced agricultural production. But this is only one side of the coin; the other side showed that the presence of these pesticides has resulted in serious threats to human health and the environment. This study reveals the presence of pesticides in fruits and vegetables exceeding the MRLs. Pesticides such as Bifenthrin, Amamectin, and Difenoconazole pose significant health risk toward consumers as their health risk indices were above the cut-off value of 1. The results reveal the health risk indices of Bifenthrin and Difenoconazole ranging from 7.8 to 12.46 in vegetables and from 2.704 to 30.454 in fruits, hence, posing a serious threat to human health. In developing countries like Pakistan, some legal measures should be taken in order to monitor the pesticide residues in fruits and vegetables because of potential health risks and to accomplish the standards and to make the products safely consumable by the consumers. It is also recommended that in future studies the risk for child and expecting mothers can be calculated.

Data Availability

The data used to support the findings of this study are available from the corresponding author upon request.

Conflicts of Interest

The authors declare that they have no conflicts of interest.

References

[1] Pakistan Bureau of Statistics, 2019, http://www.pbs.gov.pk/sites/default/files//tables/Table-7_0.pdf.

[2] J. L. F. Moreno, F. J. A. Libanas, A. G. Frenich, and J. L. M. Vidal, "Evaluation of different sample treatments for determining pesticide residues in fat vegetable matrices like avocado by low pressure gas chromatography–tandem mass spectrometry," *Journal of Chromatography A*, vol. 1111, no. 1, pp. 97–105, 2006.

[3] W. L. Claeys, J.-F. Schmit, C. Bragard, G. Maghuin-Rogister, L. Pussemier, and B. Schiffers, "Exposure of several Belgian consumer groups to pesticide residues through fresh fruit and vegetable consumption," *Food Control*, vol. 22, no. 3-4, pp. 508–516, 2011.

[4] C. K. Schiffers, A. B. Kwofie, D. Denutsui, J. Asomaning, and A. O. Tutu, "Monitoring of pesticide residues in fruits and vegetables and related health risk assessment in kumasi metropolis, Ghana," *Research Journal of Environmental and Earth Sciences*, vol. 3, no. 6, pp. 761–771, 2011.

[5] J. Gan, S. J. Lee, W. P. Liu, D. L. Haver, and J. N. Kabashima, "Distribution and persistence of pyrethroids in runoff sediments," *Journal of Environmental Quality*, vol. 34, no. 3, pp. 836–841, 2005.

[6] A. Sana, Y. Ghazala, H. Almas, A. Zainab, and A. Sidra, "Determination of pesticide residues in selected vegetables and fruits from a local market of Lahore," *Current World Environment*, vol. 13, no. 2, pp. 242–250, 2018.

[7] A. Z. Chowdhury, M. Hasan, N. Karim et al., "Contamination and health risk assessment of pesticide residues in vegetables from agricultural fields of gazipur district, Bangladesh," *Journal of Agriculture & Environmental Science*, vol. 14, no. 5, pp. 421–427, 2014.

[8] Y.-H. Seo, T.-H. Cho, C.-K. Hong et al., "Monitoring and risk assessment of pesticide residues in commercially dried vegetables," *Prevention Nutrition and Food Science*, vol. 18, no. 2, pp. 145–149, 2013.

[9] M. S. Hossain, A. N. M. Fakhruddin, A. Z. M. Chowdhury, M. A. Rahman, and A. M. Khorshed, "Health risk assessment of selected pesticide residues in locally produced vegetables of Bangladesh," *International Food Research Journal*, vol. 22, no. 1, pp. 110–115, 2015.

[10] Y. Latif, S. T. H. Sherazi, and M. I. Bhanger, "Monitoring of pesticide residues in commonly used fruits in hyderabad region, Pakistan," *American Journal of Analytical Chemistry*, vol. 2, no. 8, pp. 46–52, 2011.

[11] L. Chensheng, K. Toepel, R. Irish, R. A. Fenske, D. B. Barr, and R. Bravo, "Organic diets significantly lower children's dietry exposure to organophosphorus pesticides," *Environmental Health Perspectives*, vol. 114, no. 2, pp. 260–263, 2006.

[12] Y.-F. Jiang, X.-T. Wang, Y. Jia et al., "Occurrence, distribution and possible sources of organochlorine pesticides in agricultural soil of Shanghai, China," *Journal of Hazardous Materials*, vol. 170, no. 2-3, pp. 989–997, 2009.

[13] S. Tao, W. Liu, Y. Li et al., "Organochlorine pesticides contaminated surface soil as reemission source in the haihe plain, China," *Journal of Environmental Science and Technology*, vol. 42, no. 22, pp. 8395–8400, 2004.

[14] H.-Y. Zhang, R.-T. Gao, Y.-F. Huang, X.-H. Jia, and S.-R. Jiang, "Spatial variability of organochlorine pesticides (DDTs and HCHs) in surface soils from the alluvial region of Beijing, China," *Journal of Environmental Sciences*, vol. 19, no. 2, pp. 194–199, 2007.

[15] Z. R. Parveen, S. Iqbal, B. M. Abbas, and M. Ahmed, "Monitoring of multiple pesticides residues in some fruits in Karachi, Pakistan," *Pakistan Journal of Botany*, vol. 43, no. 4, pp. 1915–1918, 2011.

Hindawi
Journal of Chemistry
Volume 2020, Article ID 8758432, 6 pages
https://doi.org/10.1155/2020/8758432

Research Article

Al_2O_3 Nanoparticles Promote the Removal of Carbamazepine in Water by *Chlorella vulgaris* Immobilized in Sodium Alginate Gel Beads

Wu Yi-cheng,[1] Yang Ai-li,[1] Gao Wei,[1] Fu Hai-yan,[1] and Wang Ze-jie[2]

[1]*Fujian Engineering and Research Center of Rural Sewage Treatment and Water Safety, Xiamen University of Technology, Xiamen 361024, China*
[2]*College of Environmental Science and Engineering, Qilu University of Technology (Shandong Academy of Sciences), Jinan 250353, China*

Correspondence should be addressed to Wang Ze-jie; wangzejie@qlu.edu.cn

Received 17 October 2019; Accepted 11 December 2019; Published 26 May 2020

Guest Editor: Peng Zhang

The roles of Al_2O_3 nanoparticles on the removal of carbamazepine (CBZ) by *Chlorella vulgaris* immobilized in sodium alginate gel beads were for the first time investigated. The optimum conditions to prepare immobilized *C. vulgaris* beads with addition of Al_2O_3 nanoparticles were determined as follows: *C. vulgaris* density was 3.0×10^6 cells for 1 mL sodium alginate solution, Al_2O_3 nanoparticle concentration was 0.5 g/L, and concentrations of sodium alginate and $CaCl_2$ were 1.6% and 1%, respectively. The results showed that the proposed algae beads achieved the highest CBZ removal rate of 89.6% after 4 days of treatment, relative to 68.84%, 48.56%, and 17.76% in sodium alginate-immobilized *C. vulgaris*, free microalgae, and Al_2O_3 nanoparticle alginate beads, respectively. The results also showed that the CBZ removal rate increased with more proposed algae beads, while decreased with increased bead diameter. The algae beads exhibited excellent CBZ removal ability even after three recycles. This work provided an economical and effective approach to remove CBZ from water.

1. Introduction

The presence of pharmaceutical and personal care products (PPCPs) in surface water has been well documented in recent years [1–4]. Carbamazepine (CBZ) as an important species of PPCPs is widely used for the treatment of epilepsy and neuralgia. As early as in 1997, the consumption of CBZ had reached 6.33 tons per year in Austria [4]. After being consumed, CBZ is predominantly metabolized in the liver, and 2-3% of the given dose would be excreted via urine in its original form [5]. The excreted CBZ was suspected to enter rivers, streams, and surface waters through the effluent of waste water treatment plants due to its low removal efficiency [6–8]. The accumulation of CBZ in surface wasters was found to pose a great threat for aquatic environment and human health [9–11].

Owing to high photosynthesis efficiency and removal efficiency towards CBZ, microalgae are considered to be one of the most promising ways to polish CBZ-contaminated water [12–14]. It was revealed that immobilized microalgae demonstrated higher resistance to hazardous materials and faster reaction kinetics relative to free microalgae because of the higher cell density [15,16]. However, immobilization with traditional carriers such as sodium alginate has the disadvantage of poor mass transfer process [17–19]. Because of the large specific surface area and perfect biocompatibility, addition of nanoparticles to a sodium alginate-immobilized microalgae system demonstrated promising advantage to promote the contact between immobilized microorganisms and pollutants [20–22].

Al_2O_3 nanoparticles possess high specific surface area and surface energy, which provided sufficient space for the immobilized microorganism and promoted the contact of the microorganism and the pollutant and thus enhanced the removal efficiency of pollutants [23]. In the current study,

Al_2O_3 nanoparticles were adopted as additives into sodium alginate-immobilized *C. vulgaris* (termed as ANFICV) for the purpose of promoting the removal of CBZ.

2. Materials and Methods

2.1. Chemicals and Reagents. CBZ (purity ≥ 98%) and Al_2O_3 nanoparticles (purity ≥ 99.99%) were purchased from Aladdin Industrial Corporation (California, USA), and methanol (HPLC grade) was provided by Fisher Chemical (USA). All the other chemicals used in this study were of analytical grade.

2.2. Microalgae Cultures. The *C. vulgaris* was purchased from the Institute of Hydrobiology, Chinese Academy of Sciences. The microalga was cultivated with the autoclaved BG11 medium in an Erlenmeyer flask under illumination at 28°C and with a light/dark period of 18 h/6 h [24]. Fluorescent lamps (36 W; Lifemax Super 80, Philips, Shanghai, China) were employed as the light source.

2.3. Immobilization of C. vulgaris. ANFICV was prepared according to previous studies [25, 26]. *C. vulgaris* in the logarithmic growth phase was harvested by centrifuging at 4500 rpm for 5 min. The cell residues were washed with distilled water and then resuspended in the BG11 medium to form a microalgae solution with high cell density. Both Al_2O_3 nanoparticles and the resuspended *C. vulgaris* were added to the sodium alginate solution and then mixed evenly in 100 ml Erlenmeyer flasks, resulting in a volume of 30 mL. After that, the BG11 medium was added to the resulted mixture. The mixture was then added to the $CaCl_2$ solution drop by drop with a syringe to form immobilized beads. Beads without *C. vulgaris* cells or Al_2O_3 nanoparticles were prepared to carry out control experiments. The prepared beads were washed with sterile distilled water and stored at 4°C for further experiments.

To gain optimal immobilization condition, the microalgae density and concentration of Al_2O_3 nanoparticles, $CaCl_2$, and sodium alginate were adopted as factors to design a four-factor and three-level orthogonal experiment $L_9(3^4)$ (Table 1).

2.4. Determination of Cell Density in ANFICV. The cell density of suspended *C. vulgaris* was determined at the wavelength of 680 nm by an F-4600 spectrophotometer (Hitachi, Japan). Optical density was converted to cell density using a previously prepared calibration curve. Cell density in ANFICV was measured as follows: ANFICV beads were dissolved in 50 g/L sodium citrate solution and then centrifuged at 4500 rpm for 10 min, and the cell residues were resuspended in BG11 for the subsequent optical density determination [27].

2.5. Determination of CBZ. The concentration of CBZ was determined by high pressure liquid chromatography (HPLC) equipped with a UV-VIS detector (LC-20, Shimadzu, Japan) [28, 29]. Prior to analysis, the samples were filtrated through a 0.22 μm membrane filter (Bandao, China) and then injected into a C18 column (250 mm × 4.6 mm, 5 μm, Shimadzu, Japan), maintaining a column temperature of 30°C and a pressure of 25 MPa. The mobile phase was the mixture of HPLC grade methanol and water (65 : 35 v/v) and was introduced into the C18 column at a flow rate of 1 mL/min. The CBZ in the column effluent was detected at 285 nm.

2.6. Statistical Analysis. The experiments were carried out in triplicates, and data were processed by OriginPro8.0 and the statistical software package of SPSS (Ver.19.0). One-way analysis of variance was performed to determine the significant difference between means ($n = 3$) at a significant level of $P < 0.05$.

3. Results and Discussion

3.1. Optimization of ANFICV Preparation. An orthogonal experiment was carried out in order to determine the optimal factors to prepare ANFICV (Table 2). It was demonstrated that $A_3B_2C_3D_1$ achieved the best results towards CBZ removal, for which Al_2O_3 nanoparticle concentration was determined as 0.5 g/L, sodium alginate concentration as 1.6%, the density of microalga cell as 3.0×10^6 cell/mL, and the $CaCl_2$ concentration as 1%. Under such conditions, the removal efficiency of CBZ reached 94.68 ± 0.81% after 5 days; meanwhile, the mechanical strength of the ANFICV bead was the best. According to the range value (R), the concentration of $CaCl_2$ was the most important factor for the removal of CBZ, followed by microalgae density, the concentration of Al_2O_3 nanoparticles, and sodium alginate concentration.

3.2. Al_2O_3 Nanoparticles Promoted the Growth of Immobilized Microalgae. The specific surface area was measured by an automatic specific surface area and porosity analyzer (ASAP2020, Micromeritics Instrument Corporation, USA). The results showed that the specific surface area of the beads prepared by the sodium alginate alone was 2.64 m^2/g, which was increased to 3.57 m^2/g with the addition of Al_2O_3 nanoparticles. The effect of addition of Al_2O_3 nanoparticles into sodium alginate-immobilized beads on the growth of microalgae was evaluated through determining the cell density of the microalgae. It was demonstrated that the difference in cell density was enlarged over inoculation time ($P < 0.05$). After 5 days inoculation, the cell density with Al_2O_3 nanoparticles was determined as 4.80×10^6 cells/mL, larger than 4.21×10^6 cells/mL with no addition of Al_2O_3 nanoparticles (Figure 1). The results confirmed that Al_2O_3 nanoparticles could effectively promote the metabolism of *C. vulgaris*.

3.3. ANFICV Enhanced the Removal Efficiency of CBZ. The removal of CBZ from water by ANFICV and three control treatments (sodium alginate-immobilized *C. vulgaris*, free algae, and Al_2O_3 nanoparticles alginate bead) was

Table 1: Factors and levels of the orthogonal experiment design.

Levels	Factor A Al_2O_3 nanoparticles (g/L)	Factor B Sodium alginate concentration (%)	Factor C Microalgae density (cell/ml)	Factor D $CaCl_2$ concentration (%)
1	0.5	1	1×10^6	1
2	1.0	1.6	2×10^6	2
3	1.5	2.4	3×10^6	3

Table 2: Orthogonal experimental results.

Group number	Factor level				Removal efficiency (%)	Strength
	A	B	C	D		
1	0.5	1.0	1	1	82.43 ± 1.49	+
2	0.5	1.6	2	2	82.66 ± 2.99	++
3	0.5	2.4	3	3	78.53 ± 0.80	+++
4	1.0	1.0	3	2	90.28 ± 0.51	+
5	1.0	1.6	1	3	80.97 ± 0.28	++
6	1.0	2.4	2	1	89.78 ± 5.18	+++
7	1.5	1.0	2	3	76.36 ± 0.78	+
8	1.5	1.6	3	13	94.68 ± 0.81	+++
9	1.5	2.4	1	2	78.58 ± 0.93	++
K_1	78.79	89.29	89.92	90.92		
K_2	79.45	81.63	77.35	80.39		
K_3	86.34	83.28	69.41	65.31		
R	5.800	3.806	7.168	9.215		

The number of "+" indicates the level of mechanical strength of the prepared microalgae beads. More "+" means higher level. K_1, K_2, and K_3 represent the value of CBZ removal under different factors at leve1, 2, and 3, respectively. R represents the range of CBZ removal under different factors.

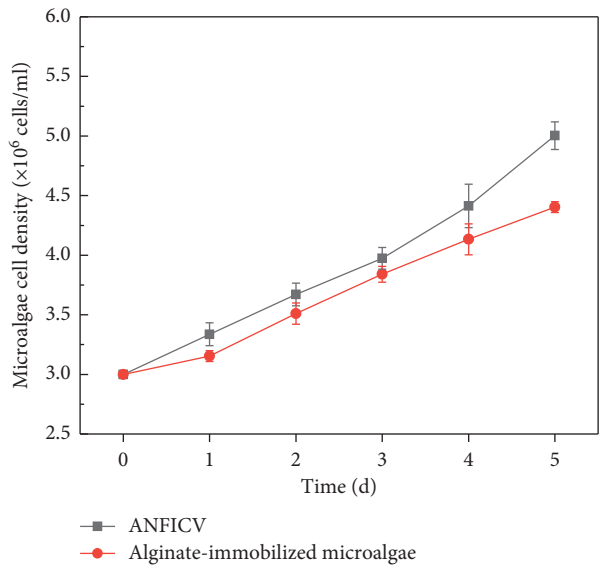

Figure 1: The growth curves of *C. vulgaris* immobilized in beads with and without Al_2O_3 nanoparticles.

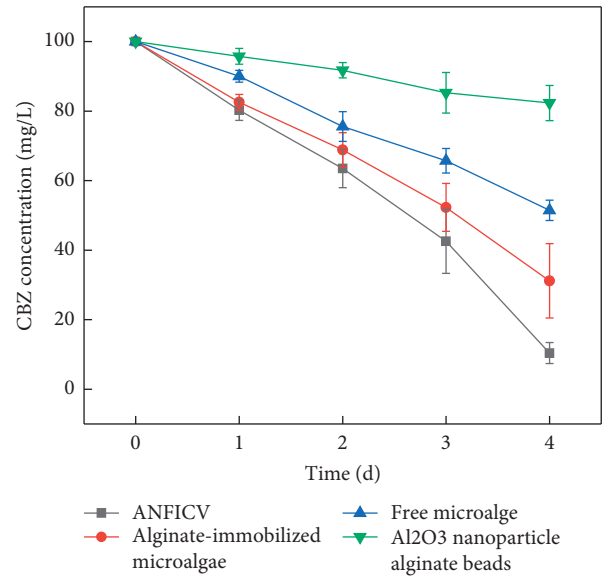

Figure 2: The concentration of CBZ with time under different treatment proposals.

compared. It was illustrated that the concentration of CBZ decreased rapidly on the first day for ANFICV and sodium alginate-immobilized microalgae beads, followed by free microalgae and Al_2O_3 nanoparticle alginate beads (Figure 2). It might be related to the strong adsorption of CBZ by the alginate bead and *C. vulgaris*. The concentration of CBZ in water decreased slightly in Al_2O_3 nanoparticle alginate beads over time probably due to the saturated adsorption of CZB.

With prolonged treatment, the concentration of CBZ decreased continuously and the treatment efficiency for ANFICV, sodium alginate-immobilized *C. vulgaris*, and free *C. vulgaris* became larger and larger ($P < 0.05$). After 4 days of treatment, the CBZ concentration decreased from 100 to 10.40 ± 3.01 mg/L treated by ANFICV, followed by 31.16 ± 10.69 mg/L and 51.44 ± 2.91 mg/L for sodium alginate-immobilized *C. vulgaris* and free algae, respectively,

while it was decreased to 82.34 ± 5.08 mg/L for Al_2O_3 nanoparticle alginate beads. The largest removal efficiency of CBZ by ANFICV might be because of the promoted metabolism of *C. vulgaris* caused by the addition of Al_2O_3 nanoparticles, as well as the adsorption of CBZ by Al_2O_3 nanoparticles.

3.4. Effect of Initial Concentration on CBZ Removal. The effect of initial concentration of CBZ on the removal efficiency by ANFICV was evaluated. It was observed that the removal efficiency of CBZ decreased with increased CBZ concentration (Figure 3). The removal efficiency of CBZ for 4 days of treatment by ANFICV reached $86.73 \pm 3.06\%$ for an initial concentration of 40 mg/L, which was reduced to $72.83 \pm 3.46\%$, $65.29 \pm 3.57\%$, and $65.25 \pm 2.75\%$ for 80, 120, and 160 mg/L CBZ, respectively. The result showed the removal efficiency of CBZ decreases with the increase in initial concentration ($P < 0.05$). The reason might be that the increase in CBZ concentration inhibited the growth and the physiological characteristics of C. *vulgaris*, especially when the concentration of CBZ was increased to 160 mg/L.

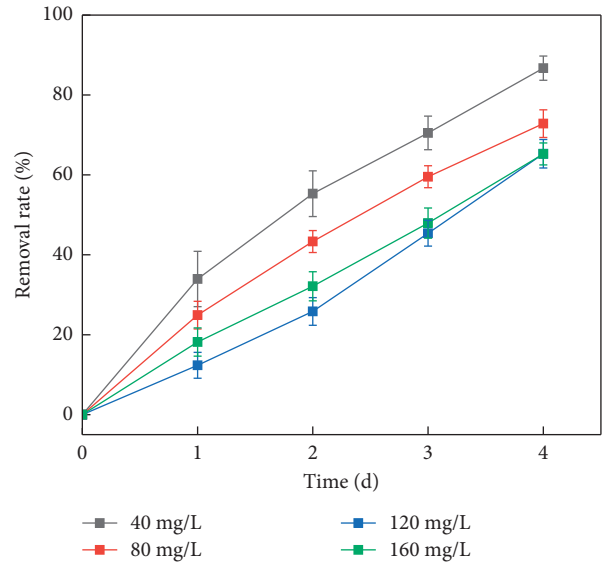

Figure 3: Removal efficiency of CBZ with different initial concentrations by ANFICV.

3.5. Effect of ANFICV Bead Diameter on CBZ Removal. Bead diameter could affect the mass transfer performance of the bead, which in turn affects pollutant absorption by the microorganism immobilized within the bead [30]. In order to investigate the effect of bead size on CBZ removal by ANFICV, three bead diameters of 6 mm (big bead), 4 mm (middle bead), and 2 mm (small bead) were prepared with the same Al_2O_3 nanoparticles concentration, C. *vulgaris* cell density, and sodium alginate. It was shown that the bead diameter significantly affected the removal of CBZ, and its effects were enlarged over time ($P < 0.05$). After 4 days of inoculation, the concentration of CBZ reduced from 100 to 60.02 ± 7.93 mg/L with big beads, which was 16.89 mg/L higher than that for middle beads and was 5.91 times of that for small beads (Figure 4). The larger removal efficiency of CBZ by the smaller bead might be because the smaller bead could result in a larger surface/volume ratio, which was beneficial for microalgae to obtain light and pollutant.

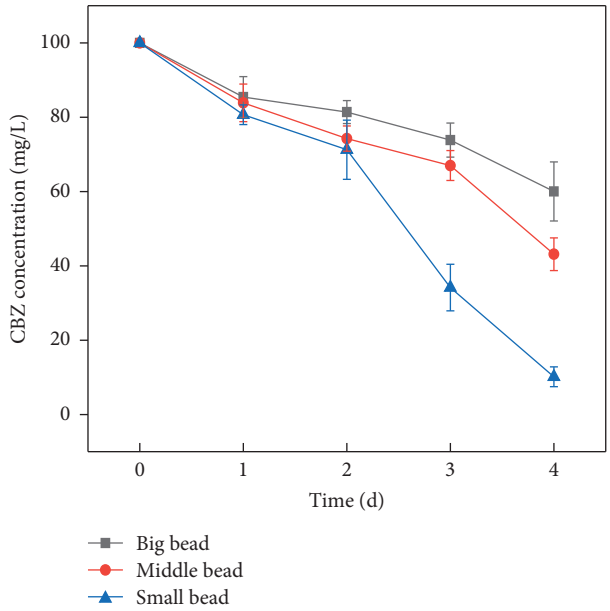

Figure 4: The effect of bead size of ANFICV on CBZ removal.

3.6. Effect of ANFICV Bead Dosage on CBZ Removal. Moreover, the present research evaluated the effects of the ANFICV bead dosage on the removal of CBZ. The results showed that the concentration of CBZ was reduced from 100 mg/L to 50.14 ± 3.54 mg/L when 100 ANFICV beads were adopted (Figure 5). It was further decreased to 38.77 ± 4.40 mg/L, 21.71 ± 5.43 mg/L, and 7.44 ± 2.42 mg/L when the dosage of ANFICV bead was increased to 300, 500, and 700, respectively. The promoted removal performance of CBZ with increased ANFICV dosage might be mainly because more ANFICV beads could increase the number of microalgae cells to remove CBZ, and it could also increase the quantity of ANFICV to absorb CBZ.

3.7. Effect of Recycling Times on the Performance of CBZ Removal. The recycling of ANFICV bead can significantly reduce the cost and promote its practical application. The effect of recycling times of the ANFICV bead on the removal efficiency of CBZ was evaluated. As shown in Figure 6, the removal efficiency of CBZ was 87.67% for the first cycle, while decreased to 52.86% for the third cycle. The removal efficiency of CBZ decreased with the increased recycling

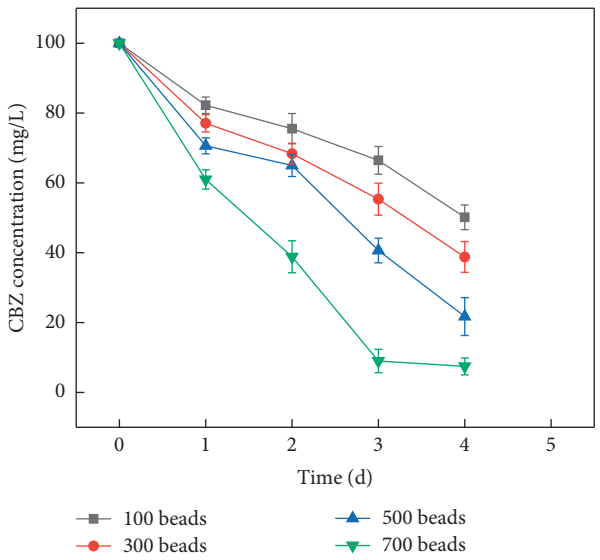

Figure 5: Effect of the dosage of the ANFICV bead on the removal of CBZ.

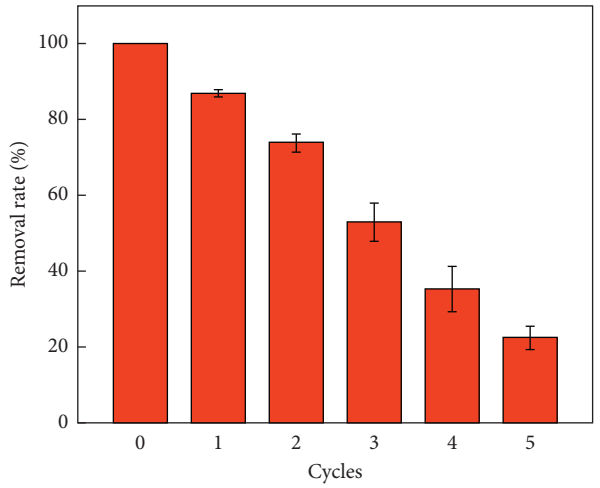

Figure 6: Effect of recycling times on the performance of CBZ removal.

times, which was mainly due to the expansion and pyrolysis of partial ANFICV beads during operation.

4. Conclusions

The present research confirmed that ANFICV with Al_2O_3 nanoparticles as additives significantly promoted the growth of immobilized *C. vulgaris* and improved the performance of CBZ removal by immobilized *C. vulgaris*. The $CaCl_2$ concentration was revealed with the most significant impact on ANFICV preparation for CBZ removal. The results demonstrated that both dosage and diameter of the ANFICV bead could affect the removal efficiency of CBZ. Relative smaller ANFICV beads benefited CBZ removal, and CBZ removal efficiency was increased with the increased dosage of ANFICV beads. This study provided a low-cost and efficient method for the treatment of CBZ-contaminated water.

Data Availability

The data used to support the findings of this study are available from the corresponding author upon request.

Conflicts of Interest

The authors declare that they have no conflicts of interest.

Acknowledgments

This work was supported by the Natural Science Foundation of Fujian Province (2019J01848), Xiamen Science and Technology Plan Guidance Project (3502Z20179029), and Scientific Climbing Plan of Xiamen University of Technology (XPDKQ18032).

References

[1] C. Vannini, G. Domingo, M. Marsoni et al., "Effects of a complex mixture of therapeutic drugs on unicellular algae *Pseudokirchneriella subcapitata*," *Aquatic Toxicology*, vol. 101, no. 2, pp. 459–465, 2011.

[2] M.-K. Ji, A. N. Kabra, J. Choi et al., "Biodegradation of bisphenol a by the freshwater microalgae chlamydomonas mexicana and *Chlorella vulgaris*," *Ecological Engineering*, vol. 73, pp. 260–269, 2014.

[3] C. I. Nannou, C. I. Kosma, and T. A. Albanis, "Occurrence of pharmaceuticals in surface waters: analytical method development and environmental risk assessment," *International Journal of Environmental Analytical Chemistry*, vol. 95, no. 13, pp. 1242–1262, 2015.

[4] G. F. Rooyen, D. Badenhorst, K. J. Swart, H. K. L. Hundt, T. Scanes, and A. F. Hundt, "Determination of carbamazepine and carbamazepine 10,11-epoxide in human plasma by tandem liquid chromatography–mass spectrometry with electrospray ionisation," *Journal of chromatography. B, Analytical Technologies in the Biomedical and Life Sciences*, vol. 769, no. 1, pp. 1–7, 2002.

[5] M. Clara, B. Strenn, and N. Kreuzinger, "Carbamazepine as a possible anthropogenic marker in the aquatic environment: investigations on the behaviour of carbamazepine in wastewater treatment and during groundwater infiltration," *Water Research*, vol. 38, no. 4, pp. 950–954, 2004.

[6] C. Lacey, S. Basha, A. Morrissey, and J. M. Tobin, "Occurrence of pharmaceutical compounds in wastewater process streams in dublin, Ireland," *Environmental Monitoring and Assessment*, vol. 184, no. 2, pp. 1049–1062, 2011.

[7] T. Heberer, "Occurrence, fate, and removal of pharmaceutical residues in the aquatic environment: a review of recent research data," *Toxicology Letters (Shannon)*, vol. 131, no. 1-2, pp. 5–17, 2002.

[8] C. I. Kosma, D. A. Lambropoulou, and T. A. Albanis, "Occurrence and removal of PPCPs in municipal and hospital wastewaters in Greece," *Journal of Hazardous Materials*, vol. 179, no. 1–3, pp. 804–817, 2010.

[9] B. Ferrari, N. Paxéus, R. L. Giudice, A. Pollio, and J. Garric, "Ecotoxicological impact of pharmaceuticals found in treated wastewaters: study of carbamazepine, clofibric acid, and

diclofenac," *Ecotoxicology and Environmental Safety*, vol. 55, no. 3, pp. 359–370, 2003.

[10] M. M. Painter, M. A. Buerkley, M. L. Julius et al., "Antidepressants at environmentally relevant concentrations affect predator avoidance behavior of larval fathead minnows (Pimephales promelas)," *Environmental Toxicology and Chemistry*, vol. 28, no. 12, pp. 2677–2684, 2009.

[11] P. Tsiaka, V. Tsarpali, I. Ntaikou, M. N. Kostopoulou, G. Lyberatos, and S. Dailianis, "Carbamazepine-mediated pro-oxidant effects on the unicellular marine algal species *Dunaliella tertiolecta* and the hemocytes of mussel *Mytilus galloprovincialis*," *Ecotoxicology*, vol. 22, no. 8, pp. 1208–1220, 2013.

[12] J.-Q. Xiong, M. B. Kurade, R. A. I. Abou-Shanab et al., "Biodegradation of carbamazepine using freshwater microalgae *Chlamydomonas mexicana* and *Scenedesmus obliquus* and the determination of its metabolic fate," *Bioresource Technology*, vol. 205, pp. 183–190, 2016.

[13] V. Matamoros, E. Uggetti, J. García, and J. M. Bayona, "Assessment of the mechanisms involved in the removal of emerging contaminants by microalgae from wastewater: a laboratory scale study," *Journal of Hazardous Materials*, vol. 301, pp. 197–205, 2016.

[14] X. Bai and K. Acharya, "Algae-mediated removal of selected pharmaceutical and personal care products (PPCPs) from Lake Mead water," *Science of The Total Environment*, vol. 581-582, pp. 734–740, 2017.

[15] G. Mujtaba and K. Lee, "Treatment of real wastewater using co-culture of immobilized Chlorella vulgaris and suspended activated sludge," *Water Research*, vol. 120, pp. 174–184, 2017.

[16] J. Jin, L. Yang, S. M. N. Chan, T. Luan, Y. Li, and N. F. Y. Tam, "Effect of nutrients on the biodegradation of tributyltin (tbt) by alginate immobilized microalga, *Chlorella vulgaris*, in natural river water," *Journal of Hazardous Materials*, vol. 185, no. 2-3, pp. 1582–1586, 2011.

[17] H. Zamani, R. Rakhshaee, and S. R. Garakoui, "Two contrary roles of Fe3O4 nanoparticles on kinetic and thermodynamic of Paclitaxel degradation by Citrobacter amalonaticus Rashtia immobilized on sodium alginate gel beads," *Journal of Hazardous Materials*, vol. 344, pp. 566–575, 2018.

[18] S. Rui and X. Qiang, "Release mechanism of lipid nanoparticles immobilized within alginate beads influenced by nanoparticle size and alginate concentration," *Colloid and Polymer Science*, vol. 297, pp. 1183–1198, 2019.

[19] M. Zhao, Z. Tang, and P. Liu, "Removal of methylene blue from aqueous solution with silica nano-sheets derived from vermiculite," *Journal of Hazardous Materials*, vol. 158, no. 1, pp. 43–51, 2008.

[20] G. Absalan, M. Asadi, S. Kamran, L. Sheikhian, and D. M. Goltz, "Removal of reactive red-120 and 4-(2-pyridylazo) resorcinol from aqueous samples by Fe_3O_4 magnetic nanoparticles using ionic liquid as modifier," *Journal of Hazardous Materials*, vol. 192, no. 2, pp. 476–484, 2011.

[21] H. Guo, Q. Lai, W. Wang et al., "Functional alginate nanoparticles for efficient intracellular release of doxorubicin and hepatoma carcinoma cell targeting therapy," *International Journal of Pharmaceutics*, vol. 451, no. 1-2, pp. 1–11, 2013.

[22] P. Zhang, C. Jin, Z. Sun, G. Huang, and Z. She, "Assessment of acid enhancement schemes for electrokinetic remediation of Cd/Pb contaminated soil," *Water, Air, & Soil Pollution*, vol. 227, p. 217, 2016.

[23] Y. Li, W. Zhou, B. Hu, M. Min, P. Chen, and R. R. Ruan, "Integration of algae cultivation as biodiesel production feedstock with municipal wastewater treatment: strains screening and significance evaluation of environmental factors," *Bioresource Technology*, vol. 102, no. 23, pp. 10861–10867, 2011.

[24] M. Lin, Y. Liu, W. Chen, H. Wang, and X. Hu, "Use of bacteria-immobilized cotton fibers to absorb and degrade crude oilfibers to absorb and degrade crude oil," *International Biodeterioration & Biodegradation*, vol. 88, pp. 8–12, 2014.

[25] N. Massalha, A. Brenner, C. Sheindorf, and I. Sabbah, "Application of immobilized and granular dried anaerobic biomass for stabilizing and increasing anaerobic bio-systems tolerance for high organic loads and phenol shocks," *Bioresource Technology*, vol. 197, pp. 106–112, 2015.

[26] M. Zhou, H. He, T. Jin, and H. Wang, "Power generation enhancement in novel microbial carbon capture cells with immobilized chlorella vulgaris," *Journal of Power Sources*, vol. 214, pp. 216–219, 2012.

[27] Y. Zhang, S.-U. Geißen, and C. Gal, "Carbamazepine and diclofenac: removal in wastewater treatment plants and occurrence in water bodies," *Chemosphere*, vol. 73, no. 8, pp. 1151–1161, 2008.

[28] G. W. Dong, R. Kaul, and B. Mattiasson, "Evaluation of alginate immobilized *Lactobacillus casei* for lactate production," *Applied Microbiology and Biotechnology*, vol. 36, pp. 309–314, 1991.

[29] P. Zhang, G. Huang, C. An et al., "An integrated gravity-driven ecological bed for wastewater treatment in subtropical regions: process design, performance analysis, and greenhouse gas emissions assessment," *Journal of Cleaner Production*, vol. 212, pp. 1143–1153, 2019.

[30] A. Idris and W. Suzana, "Effect of sodium alginate concentration, bead diameter, initial pH and temperature on lactic acid production from pineapple waste using immobilized *Lactobacillus delbrueckii*," *Process Biochemistry*, vol. 41, no. 5, pp. 1117–1123, 2006.

Hindawi
Journal of Chemistry
Volume 2020, Article ID 6956402, 8 pages
https://doi.org/10.1155/2020/6956402

Research Article

Biomonitoring of Workers Exposed to Volatile Organic Compounds Associated with Different Occupations by Headspace GC-FID

Ghazala Yaqub, Almas Hamid, Nikhat Khan, Sunaina Ishfaq, Asha Banzir, and Tayyaba Javed

Department of Environmental Sciences, Kinnaird College for Women, Lahore 54000, Pakistan

Correspondence should be addressed to Ghazala Yaqub; ghazala_yaqub@yahoo.com

Received 10 January 2020; Accepted 23 April 2020; Published 8 May 2020

Guest Editor: Yifeng Zhang

The present study has been undertaken to analyze the total accumulated burden of volatile organic compounds (VOCs) in blood of occupationally exposed workers. The headspace technique combined with gas chromatography with flame ionization detector was used for the quantitative analysis of the different volatile organic compounds (isopropyl alcohol, phenol, benzene, dichloromethane, ethanol, ethyl acetate, and toluene) in 80 blood samples from the workers belonging to different occupations i.e., shoe polish workers, thinner handlers, paint workers, furniture polish workers, petrol station attendants, textile dyeing workers, printing press workers, and dry port workers as biomonitoring is one of the most promising methods for analyzing the individual burden of VOCs. Another purpose of this study was to investigate the correlation between detected concentrations of VOCs and associated health issues reported by the workers of these professions. Results of the study revealed the presence of different VOCs in blood samples of approximately 70 workers out of 80, and statistical analysis proved a strong relationship between the reported work experience, working hours, and diseases and the detected concentrations of respective volatile organic compounds.

1. Introduction

Organic solvents, isopropyl alcohol, phenol, benzene, dichloromethane, ethanol, ethyl acetate, and toluene, are present in a wide range of commercially available products and have been widely used in different workplaces and industrial sectors (e.g., in manufacturing of paints, adhesives, thinners, glues, plastic, pitch, bitumen, and some pharmaceutical products; in shoe polish industries; in printing presses; and in petroleum industries) and as intermediate in the formation of other chemical substances according to their requirements. They are direct or indirect source of volatile organic compounds (VOCs) at workplaces.

Solvents use in different workplaces has rapidly increased in recent era. Individuals living or working in such conditions are commonly exposed to pollutants released from solvents. Most of these organic solvents are considered as environmental contaminants because of their high volatility and hazardous nature, even when they are present in low concentrations. VOCs are also considered as environmental contaminants because they persist in the air [1]. In recent years VOCs in the atmosphere has gained much attention due to their direct and indirect effects. Many VOCs are very toxic and others are supposed to be carcinogenic. The direct effects of these toxic compounds are their potential to cause serious health effects [2]. On the other hand, indirect effects of VOCs are related to their typical reactions in troposphere. Different species of VOCs behave differently while taking part in the formation of tropospheric ozone [3]. VOCs can enter our body through several routes. Inhalation is usually the most common and known route of entry of VOCs into our body, but they may enter the body also by absorption through skin which further leads to irritation of skin, eyes, nose, and throat. The common characteristic of all VOCs is that "they are lipid-soluble." The key target of all VOCs is brain and causes dizziness, loss of concentration, headache, and memory loss after their accumulation in blood and urine. Health effects due to occupational exposure of VOCs include kidney and liver damage and effects on central nervous system

(CNS) including memory loss, balance and gait disturbances, diminished cognition, and hand-eye and foot-eye coordination. Common symptoms are depressions, irritability, mood disorders, and fatigue. VOCs can also trigger exacerbation of asthma in very severe cases [2].

The extent to which and the complete details on how VOCs affect human health are still unknown. Several studies have observed that the VOCs exposure is more in occupational settings compared to environmental settings. Biomonitoring is a most promising method to analyze individual burden of these contaminants. It provides useful information on toxic build-up of chemicals in body mainly in fatty tissues [4]. Biomonitoring also allowed the determination of the individual health risk and the measurement of the target analytes concentration in the environment [5, 6]. Volatile organic compounds like benzene, phenols, alcohols, and toluene have been a great concern, as they pose serious health concern, when inhaled [4]. Solvent inhalation is usually occupational and not intentional, requiring serious preventive control of solvent use in industrial or commercial sites. Several researches works on the monitoring of exposure to such compounds [7–9], and their effects on human health have been reported [10]. One way to measure the human contamination with volatile organic compounds is to test urine or blood samples [11]. Different methods have been developed for the determination of solvents and VOCs in blood and/or urine. However, most of the promising and successful studies reported the biomonitoring of such compounds in urine and blood samples by gas chromatography or GC-MS. There are many techniques which can be used to analyze VOCs in blood. These techniques are gas chromatography-mass spectrometer (GC-MS), headspace gas chromatography along with mass spectrometer (HS-GC-MS), and gas chromatography with flame ionization detector (GC-FID).

Due to the severity of VOCs effects on environment and human health, the present study was designed to analyze total burden of VOCs in exposed workers blood. In future, this research may be helpful for suggesting major priorities in the light of its outcomes, in order to minimize occupational related health issues and to ensure complete safety of worker at their workplaces. This study thus focused on the headspace technique combined with GC-FID for the qualitative and quantitative determination of VOCs in blood of occupationally exposed workers and for the investigation of the correlation between the detected concentration of VOCs and associated health issues reported by the workers of these occupations [12].

2. Study Population

For the purpose of biomonitoring of VOCs, workers belonging to following industrial/occupational sectors have voluntarily participated in the study.

(i) Shoe polish workers
(ii) Thinner handlers
(iii) Paint workers
(iv) Furniture polish workers
(v) Petrol station attendants
(vi) Textile dyeing and printing press workers
(vii) Petroleum products handlers at dry port

The main components involved in the manufacturing of paint are pigments (including titanium dioxide) solvents, resins, and additives.

3. Materials and Methods

The current study was carried out to determine the concentrations of VOC level in blood of occupationally exposed workers by gas chromatography with flame ionization detector. Analytical grade chemicals, i.e., methanol, isopropyl alcohol, phenol, benzene, dichloromethane, ethanol, ethyl acetate, and sodium chloride, were used for present research.

3.1. Data Collection. Secondary data were gathered to develop questionnaire and methodology and to review literature. For primary data collection, series of meetings with each workplace manager were planned and necessary information was gathered. Walkthrough survey was conducted in order to check the type of solvents being used by industries/workplaces and to analyze the environmental/working conditions of workers. Interviews were held with workers of the associated professions, and a questionnaire was filled to get information regarding their work experience, working hours, smoking habits, exposure time, and diseases they suffer like headache, fatigue, skin problems/allergies, irritation to eyes, irritation to nose/breathing problem/nausea, irritation to throat, weakness, dizziness, diabetes, migraine, cancer, obesity, and others if any.

3.2. Consent Form. Ethical guidelines and protocols were completely followed/adopted during the whole research. According to the international ethical guidelines for biomedical research, consent should be obtained from those workers who are voluntarily participating in the research [13]. In the present research, participation of all workers was voluntary. Their blood samples used in the present research were taken after 8-hour work shift and were stored with private code numbers. After the workers' verbal commitment to participate in the present research, they were asked to sign a consent form.

3.3. Selection of Exposed Workers. Exposed workers were selected on the basis of primary data. The workers fall in the age range of 18–45 years and have the average working experience of 3–12 years. Workers of all the selected industries work averagely for 8–10 hours per day. All the workers when asked said that they have the habit of smoking. Although they were being provided with personal protective equipment (PPE), i.e., gloves and face masks, they were not using them, because according to them wearing the PPE decreases their work efficiency. Table 1 shows workplaces/industrial sectors and the number of selected workers.

Table 1: Industries and their selected workers.

Sr. no.	Industries/workplaces	Workers' duty section/department	Selected no. of workers
1	Textile industry	Dyeing	9
		Printing	10
2	Electrical industry	Painting	5
		Thinner handling	2
2	Petrol station	Petrol filling	7
3	Furniture workshops	Furniture polish	5
4	Dry port workers		10
5	Small-sized printing press	Printing	10
	Medium-sized printing press		10
	Large-sized printing press		10
6	Others	Shoe polish	2
			2
7	Control (general population)		Total workers = 80 Control samples = 2

3.4. Selection of VOCs for Blood Analysis. VOCs such as isopropyl alcohol, phenol, benzene, dichloromethane, ethanol, and ethyl acetate were selected to be analyzed in blood of workers based on literature and information gathered during primary data collection.

3.5. Blood Collection Method. For the collection of blood samples from workers, a trained paramedical staff member was hired. Samples were collected after 15–20 minutes of 8-hour work shift. For VOCs analysis in blood, gray top Vacutainer tubes of 5 mL were selected depending on the need of samples. These Vacutainer tubes already contained sodium fluoride and potassium oxalate as preservative and anticoagulant. The blood samples of workers were obtained by venipuncture (using BD 5 ml syringe) as described by Cardinali et al. and Ashley et al. [14, 15]. After blood collection, the vial was shaken well 2-3 times to prevent blood from clotting. Blood samples were then immediately placed in a container of ice cubes. Finally the samples were transferred to laboratory and were stored at 4°C. The collected blood samples were analyzed within the same day.

3.6. Preparation of Blood Samples and Standards. After collection, blood samples were quickly transferred to laboratory and were analyzed by headspace method for gas chromatography. 2 ml of blood sample was transferred from Vacutainer tube to 16 ml headspace vial which already contains 1 ml of sodium chloride, and it was sealed immediately with a silicone/PTFE septum. Blood sample was gently stirred for 5–10 min and was then incubated at 60°C for about 35–40 min. After partial pressure has been achieved, 0.5 ml of headspace air was injected into the gas chromatograph for further analysis. This technique was previously used for identification of variety of solvents and was also successfully employed in our laboratory. A discard box was prepared to put all the used syringes, Vacutainer tubes, microfilters, gloves, vials, and other hazardous waste. Every time after sample preparation, the discard box was immediately sent to the nearest hospital waste bin with great care. For preparation of standards of selected volatile organic compounds, method quoted by EI-Haj et al. was followed with few modifications according to laboratory conditions [16]. The chromatographic coelution of selected VOCs was also evaluated by direct injection of these compounds into the GC [17].

3.7. Analytical Analysis. Gas chromatography with flame ionization detector (GC-FID) was used for qualitative and quantitative determination of VOCs in blood samples. GC was equipped with both split and splitless capillary injectors. Temperature of both detector and injection was kept at 200°C while column temperature was programmed between 50 and 100°C. N2 flow and H2 flow were both kept at 40 μL/min while air flow was 400 μL/min. Total run time was 15 min.

3.8. Method Development and Quality Control. A rapid and sensitive gas chromatographic method was developed and validated to determine different VOCs in blood samples. For method development, studies were performed on each GC parameter, and for optimization, one parameter was changed at one time while all others were kept constant. In order to ensure method precision, each sample was analyzed in triplicate to record the variation (if any), and mean value was considered. Calibration experiments were tested for linearity, accuracy, and precision. Limit of detection (3 : 1) and limit of quantification (10 : 1) were calculated as signal-noise ratio.

3.9. Qualitative and Quantitative Analysis. Qualitative analysis on the basis of peak height and retention time was done to determine the presence of different VOCs in the prepared blood samples.

Quantitative analysis of results was done by calculating response factor and relative response factor (RRF) by formulas given below.

3.10. Response Factors. From results of analytes, peak area and concentration were taken to calculate response factor. Equations (1) and (2) were used to calculate response factor of samples and standards [18]:

$$\text{responce factor} = \frac{\text{peak area of standard}}{\text{concentration}}, \quad (1)$$

$$\text{response factors} = \frac{\text{peak area of sample}}{\text{concentration}}. \quad (2)$$

The calculated response factors of standard (1) and sample (2) were then used to calculate relative response factor (RRF) between two analytes. The following equation was used to calculate relative response factor [17]:

$$\text{relative response factor (RRF)} = \frac{\text{response factor B}}{\text{response factor A}}. \quad (3)$$

Relative response factor was further used in order to calculate the unknown concentration of analyte (VOC selected):

$$\text{concentration of analyte} = \frac{\text{peak area of } A}{\text{peak area of } B} \times \frac{1}{\text{RRF}} \times \text{concentration of standard}. \quad (4)$$

3.11. Statistical Analysis. Statistical analysis was done with Microsoft Excel version 4.0 on personal computer. Primary data were collected from the workers of all occupations, and the questions asked were related to work experience, working hour, workplace conditions (status of work), and diseases such as headache, fatigue, skin problems/allergies, irritation to eyes, irritation to nose/breathing problem/nausea, irritation to throat, weakness, dizziness, diabetes, migraine, cancer, and obesity; all these data were statistically analyzed with the detected concentrations of different VOCs. Statistical test, i.e., "phi coefficient," was selected for analysis as phi is interpretable as a nonparametric correlation coefficient and means just the same thing as the Pearson r in terms of the strength and direction of the relationship between two variables.

4. Results and Discussion

Occupational exposure to solvents may often lead to serious illnesses and injuries through absorption of irritants via skin and/or inhalation of toxic vapors. The risk may become worse while working in confined areas. Several studies have reported various adverse effects of solvent intoxication such as neuropathological effects, nephrotoxic effects, hepatotoxic effects, and cognitive impairment [19, 20].

The purpose of the present study was to analyze total burden of VOCs in blood of occupationally exposed workers by using GC-FID. Total collected blood samples of workers were 80, i.e., two shoe polish workers, two thinner handlers, five paint workers, five furniture polish workers, seven petrol station attendants, nine textile dyeing workers, ten textile printing workers, ten dry port workers, and thirty printing press workers. All of the participating workers were male. Two control samples were also taken from the general population people (who do not have any previous or current record of occupational exposure to solvents) (Table 2).

A detailed questionnaire was designed to obtain information of participants regarding age, BMI, work experience, exposure period, health issues, and present working environments (as mentioned earlier in Section 3).

Blood samples were analyzed for presence of VOCs both qualitatively and quantitatively. All samples were run in triplicate for quality assurance, and mean value was considered. Analysis showed the presence of isopropyl alcohol in almost all blood samples which were collected from shoe polish workers, paint workers, furniture polish workers, one thinner handler, and three printing press workers. All these workers were apparently underweight and normal. The detected concentration of isopropyl alcohol in shoe polish workers was 15.2 ppm and 20.3 ppm. The concentration of isopropyl alcohol detected in thinner handlers was 30.0 ppm. In paint workers, it was detected in concentration of 22.54 ppm, 35.9 ppm, 351.38 ppm, 23.6 ppm, and 33.85 ppm, respectively. In blood of furniture polish workers isopropyl alcohol was present in concentration of 21.0 ppm, 25.9 ppm, 22.9 ppm, 226.75 ppm, and 18.49 ppm, while its determined concentration in blood of printing press workers was 28.44 ppm, 80.64 ppm, and 82.64 ppm, respectively. The samples taken from petrol station attendants, textile dyeing workers, textile printing workers, and dry port workers did not show its presence in their blood. During primary data collection, the health effects reported by affected workers were irritation to skin, eyes, throat, headache, fatigue, and sometimes weakness during duty. Furthermore, furniture and shoe polish workers and some textile dyeing workers had also complained about nose irritation. Their response is also supported by hazardous fact sheet prepared by New Jersey Department of Health which highlighted the fact that contact to isopropyl alcohol can cause irritation to skin and eyes, while inhaling it can cause nose and throat irritation. Overexposure can cause unconsciousness, confusion, headache, and loss of coordination [21]. Among all samples, phenol was detected and quantified in blood samples of one petrol station attendant in concentration of 2.39 ppm, five textile dyeing workers (3.52 ppm, 3.18 ppm, 3.02 ppm, 2.69 ppm, and 3.13 ppm), and five printing press workers (4.82 ppm, 3.24 ppm, 3.2 ppm, 16.36 ppm, and 16.00). Phenol was not detected in any other sample. Workers (with phenols detected in blood) also reported problems like irritation to skin, eye, and throat; headache; fatigue; and sometimes weakness which is also supported by hazardous fact sheet prepared by New Jersey Department of Health indicating that exposure to phenol can cause throat, skin, and eye irritation and sometimes lead to skin burns and eye damage. Its high exposure may reduce the blood ability to transport oxygen, causing fatigue, headache, dizziness, and blue color to lips and skin [22].

Benzene, a solvent for paints, inks, and plastics, is used in manufacturing of dyes, rubbers, drugs, lubricants, pesticides, and detergents and was found in one blood sample of a

Table 2: Quantitative analysis of VOCs in blood samples.

Sr. no.	Participants	Sample code	Isopropyl alcohol (ppm)	Phenol (ppm)	Benzene (ppm)	Dichloromethane (ppm)	Ethanol (ppm)	Ethyl acetate (ppm)	Toluene (ppm)
1	Shoe polish workers	68635	15.2	0	0	0	0	0	0
		68183	20.3	0	0	0	0	0	0
2	Thinner handlers	68189	30.0	0	0	0	0	0	0
		68458	0	0	0	0	0	17.51	0
3	Paint workers	671	22.54	0	0	0	0	35.95	0
		67425	35.9	0	0	0	0	373.70	0
		68503	351.83	0	0	0	0	25.12	0
		68202	23.6	0	0	0	0	0	0
		67435	33.85	0	0	0	0	31.84	0
4	Furniture polish workers	68205	21.0	0	0	0	0	0	0
		68453	25.9	0	0	0	0	0	0
		68249	22.9	0	0	0	0	0	0
		68147	226.75	0	0	0	0	0	0
		68203	18.49	0	0	0	0	0	0
5	Petrol station attendants	69189	0	2.39	0	0	0	0	0
		68259	0	0	0	0	9.73	0	0
6	Textile dyeing workers	215394	0	3.52	0	0	0	0	0
		215477	0	3.18	0	0	0	0	0
		68235	0	0	0	0	1.31	0	0
		683615	0	0	0	6.49	0	0	0
		1046747	0	3.02	0	0	0	0	0
		68361	0	0	81.62	6.40	0	0	0
		1046456	0	2.69	0	0	0	0	0
		68387	0	0	0	5.05	0	0	0
		215654	0	3.13	0	0	0	0	0
7	Textile printing workers	1022195	0	0	0	5.01	0	0	0
		215636	0	0	0	7.85	0	0	0
		215377	0	0	0	6.64	0	0	0
		215478	0	0	0	6.64	0	0	0
		1047332	0	0	0	5.34	0	0	0
		215491	0	0	0	6.86	0	0	0
		215330	0	0	0	5.48	0	0	0
		1022687	0	0	0	5.67	0	0	0
		10464567	0	0	0	4.53	0	0	0
		68234	0	0	0	7.85	0	0	0
6	Dry port workers	00215357	0	0	199.89	0	0	0	0
		00214411	0	0	0.776	0	95.89	0	0
		00216744	0	0	0.06	0	49.72	0	0
		00215616	0	0	0.97	0	141.63	0	0
		00213477	0	0	0	0	88.80	0	0.000001
		00217018	0	0	0	0	24.74	0.016	0.006
		00216755	0	0	0	0	88.80	0.0012	0
		00215616	0	0	0	0	0	0.01	0
		00215590	0	0	0	0	110.89	1.06	0
		00216676	0	0	0	0	133.76	0	0
7	Small-sized printing press	68360	0	0	0	0	15.61	0	0
		68303	28.44	0	0	0	0	0	0
		68392	0	4.82	0	0	0	0	0
		68366	0	0	0	10.94	0	0	0
		68213	0	3.24	0	0	0	0	0
		68241	0	0	5.16	0.41	0	0	0

Table 2: Continued.

Sr. no.	Participants	Sample code	Isopropyl alcohol (ppm)	Phenol (ppm)	Benzene (ppm)	Dichloromethane (ppm)	Ethanol (ppm)	Ethyl acetate (ppm)	Toluene (ppm)
8	Medium-sized printing press	E31986	0	0	0	6.6	0	0	0
		E47334	0	0	0	319.28	0	0	0
		E68353	0	3.2	0	0	0	0	0
		E68387	0	0	0	7.24	0	0	0
		E68352	0	0	0	0	16.7	0	0
		E35231	0	0	0	8.07	0	0	0
		E46452	0	0	0	7.42	0	0	0
		E31987	0	0	0	6.6	0	0	0
		E31999	0	0	0	15.61	0	0	0
9	Large-sized printing press	215328	0	0	0	5.85	0	0	0
		215335	0	0	0	6.81	0	0	0
		215455	80.64	16.36	0	0	0	0	0
		215656	82.64	16.00	0	0	0	0	0

textile dyeing worker in concentration of 81.62 ppm, one blood sample of a textile printing worker (5.16 ppm), four blood samples of dry port workers (199.89 ppm, 0.776 ppm, 0.06 ppm, and 0.97 ppm), and one sample of a printing press worker (5.16). During survey the prominent reported health effects of the exposed worker were again irritation to skin, eye, and throat; headache; weakness; and fatigue during their working hours which are also supported by literature; according to a report prepared by Agency for Toxic Substances and Disease Registry (ATSDR), very small exposure (5 to 10 minutes) to a very high level of benzene in air (10,000 to 20,000 ppm) can result in death. Lower levels (700 to 3,000 ppm) can cause headache, unconsciousness, dizziness, drowsiness, and confusion [23]. It is also a moderate skin and eye irritant [24]. Dichloromethane (DCM), also known as methylene chloride, is widely used as a solvent in adhesives, paint strippers and removers, textile printing, and printing presses. In the current study, DCM was found in only three blood samples of textile dyeing workers (6.49 ppm, 5.05 ppm, and 6.40 ppm), all blood samples collected from textile printing workers (5.01 ppm, 7.85 ppm, 6.64 ppm, 6.64 ppm, 5.34 ppm, 6.86 ppm, 5.48 ppm, 5.67 ppm, 4.53 ppm, and 7.85 ppm), and eleven blood samples of printing press workers (10.94 ppm, 0.41 ppm, 6.6 ppm, 319.28 ppm, 7.24 ppm, 8.07 ppm, 7.42 ppm, 6.6 ppm, 15.61 ppm, 5.85 ppm, and 6.81 ppm). According to hazardous fact sheet by New Jersey Department of Health dichloromethane can cause skin and eye irritation, sometimes lead to eye damage and breathing its high level can cause nose and throat irritation [25]. Ethyl Acetate, as a solvent used in making of dyes and perfumes [26], was found in blood samples of one thinner handler (was 17.51 ppm), four paint workers (35.95 ppm, 373.70 ppm, 25.12 ppm, and 38.14 ppm), and four dry port workers (0.016 ppm, 0.0012 ppm, 0.01 ppm, and 1.06 ppm). Exposed workers have also reported problems like headache, fatigue, and sometimes weakness during their duty time. This is also supported by previous studies which reported that inhalation of 400 ppm of ethyl acetate for 3–5 min can cause irritation to nose and throat. Its high concentration can lead to headache and also congestion in upper respiratory tract [27]. Ethanol has many applications as a solvent (in manufacturing of paint, ink, varnishes, perfumes), as a fuel, and as raw material for making of chemicals (such as production of ethyl acetate, acetic acid, ethylene, and ethyl acrylate) [28]. It was detected and quantified in only one blood sample of a petrol station attendant (8.17 ppm), one blood specimen of a textile dyeing worker (1.31 ppm), eight samples of dry port workers (95. 89 ppm, 49.72 ppm, 141.63 ppm, 88.80 ppm, 24.74 ppm 88.80 ppm, 110.89 ppm, and 133.76 ppm), and two blood samples of printing press workers (15.61 ppm and 16.7 ppm). According to hazardous fact sheet prepared by New Jersey Department of Health, exposure to ethanol is moderately irritating to eye and skin. It can cause nose and throat irritation and sometimes shortness of breath. Headache, nausea, vomiting, and unconsciousness are also associated with its exposure [29].

Results of statistical analysis also showed positive relationship between the detected concentrations of different VOCs in blood of workers and their work experience, working hours, and workplace conditions. For example, the phi values (0.853, 0.710, 0.514, 0 1.145, 0.359, and 0.389) show that there is strong positive relationship between work experience and solvents used in that workplace and indicate that the greater the number of years spent at the workplace, the higher the quantity of solvents in the blood of the respective workers. The case with other parameters is the same (Table 3).

Results of statistical analysis for determining the correlation between the presence of VOCs in blood samples and the diseases reported by the workers working in that environment also depicted strong correlation between these variables. For example, in case of isopropyl alcohol case, phi =0.359, which shows a positive relationship between the two variables (isopropyl alcohol and headache).This indicates that the person who is exposed to the workplace conditions having isopropyl and with its concentration detected in blood as bioindicator of this pollutant will be a possible victim of headache. As there is strong positive correlation between the two, the greater the quantity of

Table 3: Correlation between the detected concentrations of different VOCs in blood of workers and their work experience, working hours, and workplace conditions.

	Isopropyl alcohol	Phenol	Benzene	DCM	Ethanol	Ethyl acetate
Work experience	0.853	0.710	0.514	1.145	0.359	0.389
Working hour	0.756	0.599	0.202	0.751	0.594	0.339
Workplace conditions (status of work)	0.620	0.613	0.144	0.789	0.329	0.345

Table 4: Correlation between the presence of VOCs in blood samples and the diseases reported by the workers.

Diseases reported	Isopropyl alcohol	Phenol	Benzene	DCM	Ethanol	Ethyl acetate
Headache	0.359	0.308	0.101	0.425	0.145	0.163
Fatigue	0.260	0.311	0.082	0.403	0.269	0.132
Skin problems/allergies	0.403	0.377	0.124	0.541	0.265	0.200
Irritation to eyes	0.209	0.344	0.066	0.579	0.322	0.107
Irritation to nose/breathing problem/nausea	0.398	0.398	0.169	0.602	0.239	0.270
Irritation to throat	0.479	0.389	0.173	0.641	0.263	0.265
Weakness	0.478	0.385	0.171	0.530	0.242	0.293
Dizziness	0.531	0.382	0.116	0.574	0.226	0.370
Diabetes	0.496	0.316	0.377	0.579	0.112	0.469
Migraine	0.134	0.106	0.490	0.702	0.061	0.068
Cancer	0.066	1.000	0.021	0.087	0.030	0.033
Obesity	0.556	0.353	0.204	0.559	0.230	0.348

isopropyl alcohol in blood, the greater the chance of headache problem among victims (Table 4).

5. Conclusion

Workers' safety and surveillance setup is an important subject worldwide. However, in developing countries like Pakistan, it is most neglected one, as workers' safety has never been given a major priority. There are thousands of workers who are routinely exposed to many solvents and chemicals at their workplaces. The present study was thus conducted to quantify working conditions of exposed workers at their workplaces, the major health issues faced by these workers, and the correlation between these two parameters. The efforts made towards this study will be very fruitful in future in light of its outcomes, and it may be very helpful to minimize major health risks in order to ensure complete safety of workers at their workplaces. Different VOCs were detected in above 70 blood samples of the workers belonging to different professions out of a total of 80 samples. Statistical analysis showed a strong relationship between the reported work experience, working hours, and diseases and the detected concentrations of respective volatile organic compounds. Selective and sensitive method of GC-FID was used for the analysis.

Data Availability

All related data provided in this article are included in the article, and spectrum and charts may be obtained from the corresponding author on request at ghazala_yaqub@yahoo.com.

Conflicts of Interest

The authors declare that they have no conflicts of interest.

Acknowledgments

The authors would like to thank Higher Education Commission, Pakistan, for funding and Ms. Adila Kokab for assistance during statistical analysis.

References

[1] P. Wilford, *VOC Detection and Measurement Techniques*, AWE International, San Diego, CA, USA, 2006.

[2] R. J. Delfino, H. Gong, W. S. Linn, Y. Hu, and E. D. Pellizzari, "Respiratory symptoms and peak expiratory flow in children with asthma in relation to volatile organic compounds in exhaled breath and ambient air," *Journal of Exposure Science & Environmental Epidemiology*, vol. 13, no. 5, pp. 348–363, 2003.

[3] C. Cai, F. Geng, X. Tie, Q. Yu, and J. An, "Characteristics and source apportionment of VOCs measured in Shanghai, China," *Atmospheric Environment*, vol. 44, no. 38, pp. 5005–5014, 2010.

[4] H. K. Wilson, "Breath analysis. Physiological basis and sampling techniques," *Scandinavian Journal of Work, Environment & Health*, vol. 12, no. 3, pp. 174–192, 1986.

[5] M. Vitali, F. Ensabella, D. Stella, and M. Guidotti, "Exposure to organic solvents among handicraft car painters: a pilot study in Italy," *Industrial Health*, vol. 44, no. 2, pp. 310–317, 2006.

[6] F.-K. Chang, M.-L. Chen, S.-F. Cheng, T.-S. Shih, and I.-F. Mao, "Evaluation of dermal absorption and protective effectiveness of respirators for xylene in spray painters," *International Archives of Occupational & Environmental Health*, vol. 81, no. 2, pp. 145–150, 2007.

[7] K. Demeestere, J. Dewulf, B. De Witte, and H. Van Langenhove, "Sample preparation for the analysis of volatile organic compounds in air and water matrices," *Journal of Chromatography A*, vol. 1153, no. 1-2, pp. 130–144, 2007.

[8] A. Talapatra and A. Srivastava, "Ambient air non-methane volatile organic compound (NMVOC) study initiatives in

India-A review," *Journal of Environmental Protection*, vol. 2, no. 1, pp. 21–36, 2011.

[9] L. H. Van, *Volatile Organic Compounds (VOCs). Environmental Chemistry Course Notes*, University of Ghent, Ghent, Belgium, 2010.

[10] Hazardous Substances Data Bank (HSDB), *Benzene*, National Library of Medicine, Bethesda, MD, USA, 2007.

[11] T. K. Alkalde, M. d. C. R. Peralba, C. A. Zini, and E. B. Caramão, "Quantitative analysis of benzene, toluene and xylenes in urine by means of headspace solid phase microexraction," *Journal of Chromatography A*, vol. 1027, no. 1-2, pp. 37–40, 2004.

[12] P. C. F. D. L Gomes, E. D. D. Andrea, C. B. Mendes, and M. E. P. B. siqueira, "Determination of benzene, toluene and N-hexane in urine and blood by headspace solid-hase microextraction/gas-chromatograpy for the biomonitoring of occupational exposure," *Journal of the Brazilian Chemical Society*, vol. 21, no. 1, pp. 119–126, 2010.

[13] WHO, *International Ethical Guidelines for Biomedical Research Involving Human Subjects Prepared by the Council for International Organizations of Medical Sciences (CIOMS) in Collaboration with the World Health Organization*, (WHO), Geneva, Switzerland, 2002.

[14] F. L. Cardinali, J. M. McCraw, D. L. Ashley, M. Bonin, and J. Wooten, "Treatment of Vacutainers for use in the analysis of volatile organic compounds in human blood at the low parts-per-tri11ion level," *Journal of Chromatographic Science*, vol. 33, no. 10, pp. 557–560, 1995.

[15] D. L. Ashley, M. A. Bonin, F. L. Cardinali et al., "Determining volatile organic compounds in human blood from a large sample population by using purge and trap gas chromatography/mass spectrometry," *Analytical Chemistry*, vol. 64, no. 9, pp. 1021–1029, 1992.

[16] B. M. El-Haj, A. M. Al-Amri, M. H. Hassan, R. K. Bin-Khadm, and A. A. Al-Hadi, "A GC-MS method for the detection of toluene and ethylbenzene in volatile substance Abuse," *Journal of Analytical Toxicology*, vol. 24, no. 6, pp. 390–394, 2000.

[17] S. A. Fatima, A. Hamid, G. Yaqub, A. Javed, and H. Akram, "Detection of volatile organic compounds in blood of farmers and their general health and safety profile," *Nature Environment and Pollution Technology*, vol. 17, pp. 657–660, 2018.

[18] K. Rome and A. McIntyre, "Intelligent use of relative response factors in gas chromatography-flame ionization detection," *Chromatography Today*, pp. 52–57, Elsevier, Amsterdam, Netherlands, 2012.

[19] ICH Q2 R1, *Validation of Analytical Procedures: Text and Methodology*, ICH, Geneva, Switzerland, 1995.

[20] F. Tomei, P. Giuntoli, M. Biagi, T. P. Baccolo, E. Tomao, and M. V. Rosati, "Liver damage among shoe repairers," *American Journal of Industrial Medicine*, vol. 36, no. 5, pp. 541–547, 1999.

[21] New Jersey Department of Health, "Hazardous substance fact sheet-isopropyl alcohol," 2011, http://nj.gov/health/eoh/rtkweb/documents/fs/1076.pdf.

[22] New Jersey Department of Health, "Hazardous substance fact sheet–phenol," 2010, http://nj.gov/health/eoh/rtkweb/document/fs/1487.pdf.

[23] Agency for Toxic Substances and Disease Registry (ATSDR), *Toxicological Profile for Benzene*, U.S. Department of Health and Human Services. Public Health Service, Washington, DC, USA, 2007.

[24] International Programme on Chemical Safety (IPCS), *Environmental Health Criteria 150-Benzene*, World Health Organization, Geneva, Switzerland, 1993.

[25] New Jersey Department of Health and Senior Services, "Hazardous substance fact sheet-methylene chloride," 2008, http://nj.gov/health/eoh/rtkweb/documents/fs/1255.pdf.

[26] New Jersey Department of Health and Senior Services, "Hazardous substance fact sheet-ethyl acetate," 2002, http://nj.gov/health/eoh/rtkweb/documents/fs/0841.pdf.

[27] Royal Society of Chemistry, *Chemical Safety Data Sheets*, Vol. 1, Royal Society of Chemistry, London, UK, 1992.

[28] ANSES—French Agency for Food, Environmental and Occupational Health & Safety, "Assessing the risks of ethanol," 2013, https://www.anses.fr/en/content/assessing-risks-ethanol.

[29] New Jersey Department of Health, "Hazardous substance fact sheet-ethanol," 2011, http://nj.gov/health/eoh/rtkweb/documents/fs/0844.pdf.

Hindawi
Journal of Chemistry
Volume 2020, Article ID 4217294, 18 pages
https://doi.org/10.1155/2020/4217294

Research Article

Characteristics, Distribution, and Source Analysis of the Main Persistent Toxic Substances in Karst Groundwater at Jinan in North China

Hao Shang,[1] **Xiaofan Qi**,[2] **Mengnan Zhang**,[2] **Hu Li**,[3] **Gang Li**,[3] **and Lizhi Yang**[1]

[1]*Shandong Institute of Geological Survey, Jinan, China*
[2]*Center for Hydrogeology and Environmental Geology Survey, China Geological Survey, Baoding, China*
[3]*Jinan Rail Transit Group Co., Ltd., Jinan, China*

Correspondence should be addressed to Xiaofan Qi; xf-q@163.com

Received 12 October 2019; Revised 13 December 2019; Accepted 11 January 2020; Published 28 February 2020

Guest Editor: Yifeng Zhang

Karst water in northern China is an important water source for economic and social development in its distribution area and water source for ecological function guarantee. With the enhancement of human activities, the water quality of karst water in the north has deteriorated and the bearing capacity of economic activities and social and ecological environment has weakened. The study on the distribution characteristics and source analysis of toxic substances in typical karst springs in northern China is of great practical significance for the sustainable development of karst areas in northern China. Based on the abundant karst water samples, the concentration, detection, and spatial distribution of toxic heavy metals and typical organic substances in karst waters were analyzed, the quality was evaluated, and the source of substances was analyzed. The results show that the toxic substances in karst water in Jinan are mainly distributed in the northern part of the Jinan urban karst water subsystem and Baiquan karst water subsystem in Jinan city, and the detection rate is low in other areas. The main distribution areas of toxic substances in karst water are the northeast and southwest parts of Jinan city. In the recharge area and runoff area of the karst spring area, the contribution rate of toxic substances to the comprehensive quality evaluation of karst water is relatively low and relatively high in the drainage area of the spring area. The organic index contributes more to the comprehensive quality evaluation of karst water. The distribution of toxic substances is related to the historical and current industrial layouts, and industrial discharge or leakage is the primary source of pollutants in karst water. The concentration of toxic substances in karst water has persistence and inheritance. This study enriches the research results on the distribution and sources of toxic substances in typical karst springs in northern China and provides essential data support for scientific understanding of the changes in karst water quality and optimization of water resource management in northern China.

1. Introduction

There are 6.85×10^5 km^2 carbonate rock distribution areas in northern China [1] and 1.09×10^{10} m^3/a of karst water resources [2]. Karst water is an important water source for water supply and ecological function guarantee in northern China [3]. The unique geological and topographic conditions make most karst water in northern China discharged in the form of springs or spring samples [4]. In the past 40 years, a variety of environmental problems have arisen in the karst water system in northern China, such as deterioration of water quality, water cutoff of springs, and water level drop [4]. The development and change of these environmental problems have brought challenges to the management of karst water resources, and scientific research is needed to serve the management, protection, and sustainable utilization of water resources.

Jinan is a typical karst water distribution area in northern China. It is known as "city of springs." There are numerous springs in Jinan, and it has "72 famous springs." Karst groundwater is an indispensable and important resource for industrial and agricultural production and social development

in Jinan [5]. Over the past decades, with the industrialization and urbanization of Jinan, the water resource conditions of Jinan karst water system have changed [6–9], and the water quality has changed significantly [6, 10]. The concentration of toxic substances in karst water, including toxic heavy metals and persistent organic compounds, has increased [11, 12], causing negative effects or potential threats to the ecological environment, economic activities and human health [13]. Therefore, it is of great significance for the development and utilization of karst water resources and ecological environmental protection to analyze the concentration and distribution status of persistent toxic substances in underground water in Jinan karst spring area and find out their pollution sources and influencing factors.

The unique hydrogeological conditions make the groundwater quality in the karst area more sensitive to human activities [14, 15]. Persistent toxic substances have caused different degrees of karst water pollution in the karst distribution areas of the world, such as toxic heavy metals in the karst area of southern China [16–19] and persistent organic substances in Italy [20], Turkey [21], China [22, 23], etc. Liu et al. [18] analyzed the hydrochemistry and distribution characteristics of heavy metals in four typical karst underground rivers in southwest China, including As, Cr^{6+}, and other heavy metals and analyzed the influence of human activities. Dong et al. [24] summarized that polycyclic aromatic hydrocarbons (PAHs) and organochloride pesticides (OCPs) are the main toxic organic compounds detected in groundwater of karst spring area in China, and the toxic organic compounds concentration in karst water is relatively low. In the karst spring area of Jinan area, Gao et al. [11] discussed the trace element concentration and distribution change characteristics of Jinan karst water in high and low water periods, including the analysis of toxic heavy metals like Cr^{6+}. Yang et al. [12] summarized the detection of toxic organic compounds in Jinan urban subsystem of karst spring area in Jinan, pointing out that the detection rate of trichloromethane is high. Xu et al. [23] analyzed the distribution rule of toxic organic compounds in karst water in Jinan, pointing out that the detection rate of toxic organic compounds is high and the concentration is low, and its distribution is controlled by the distribution of industrial enterprises and groundwater field. The above results show that there are still few studies on persistent toxic substances in karst water in northern China, and the scattered results mostly describe the distribution or source of toxic substances from one aspect or one side, and the data used are relatively early, and no systematic research results have been seen at present. In this paper, Jinan spring area, a typical karst spring area in northern China, is selected to study the distribution characteristics and source analysis of persistent toxic substances in groundwater, which can supplement relevant research results and provide data support for scientific understanding of the changes in karst water quality in northern China.

2. Materials and Methods

2.1. Overview of the Study Area. Jinan is located in the mid-latitude inland zone and belongs to the warm temperate continental monsoon climate zone. It has the climatic characteristics of drought-prone spring, hot and rainy summer, and cold and dry winter. The annual average temperature is 14.3°C, the annual average precipitation is 641.68 mm (1956–2012), and the annual average evaporation is 1500–1900 mm [13]. The annual distribution of precipitation in the region is uneven, with the rainy season concentrated in June to September, and the precipitation accounts for more than 70% of the annual precipitation.

Jinan geotectonic division is the Luzhong uplift in the Luxi uplift area of the north China plate, which is generally a northdip monoclinic structure with the Neoarchaean Taishan group as the base and the Paleozoic carbonate rock strata as the main body. In monoclinic structure, several groups of northwest-oriented faults are developed, forming relatively independent monoclinic blocks, and each monoclinic block forms a relatively independent karst water system. This specific geological structure condition in Jinan area controls the spatial distribution of regional aquifers, groundwater movement, water circulation conditions, and water-rich conditions.

The study area includes the Jinan-Changqing karst water system and Mingshui karst water system, in which the former is divided into Changqing-Xiaolipu karst water subsystem, Jinan urban karst water subsystem, and Baiquan karst water subsystem (Figure 1). There is basically no hydraulic connection between Jinan-Changqing karst water system and Mingshui karst water system; there are different degrees of hydraulic connection within Jinan-Changqing karst water system, in which the Changqing-Xiaolipu subsystem and the northern boundary of Jinan urban subsystem present weak permeability, and the northern boundary of Jinan urban subsystem and Baiquan subsystem are closely linked.

The carbonate rock fissure karst aquifer system in the study area is composed of the Sup-Zhangxia Formation ($\epsilon_2 z$) and Upper Cambrian Fengshan Formation and Ordovician ($\epsilon_3 f$-O), and the lithology is dominated by carbonate rocks such as limestone, dolomitic limestone, limestone dolomite, and argillaceous limestone. The karst fissures in each karst water system are developed with good connectivity, which is conducive to the recharge, runoff, and enrichment of groundwater. Groundwater recharge is mainly infiltration recharge of atmospheric precipitation, followed by surface water leakage recharge. The underground runoff generally moves from south to north, northwest, and west along the stratum tendency. In the north, it is blocked by gabbro rock and carboniferous and Permian strata, rises to form springs for drainage, or is discharged by artificial mining.

2.2. Layout of Sampling Points. In order to study the distribution characteristics of toxic substances in karst groundwater in Jinan and to facilitate the analysis of pollutant sources, two principles should be grasped in the layout of sampling sites: one is to cover the surface and grasp the macroscopic distribution of toxic substances; the other is to properly encrypt the layout in key areas and study the

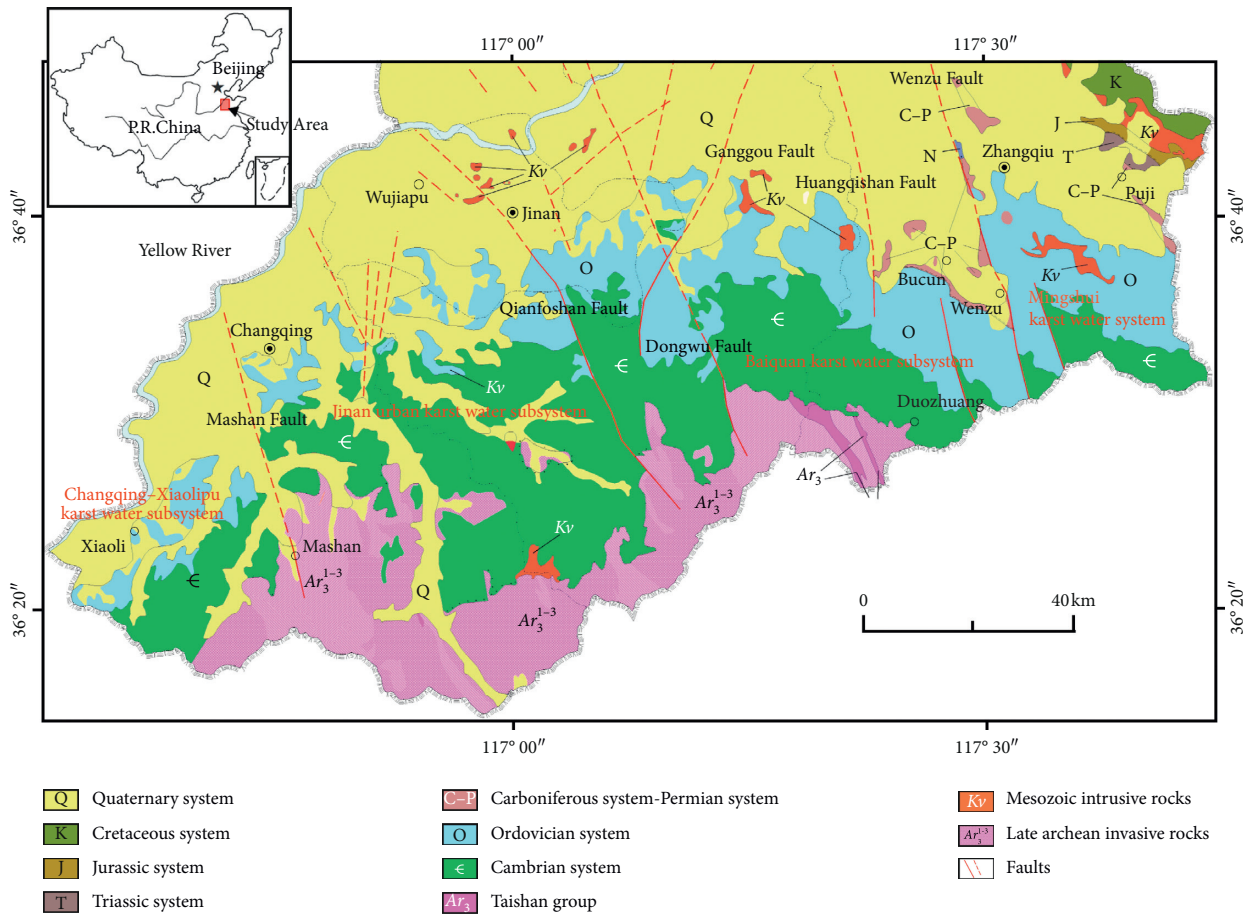

Figure 1: General map of the study area and the division of karst water systems.

distribution characteristics of toxic substances in key areas. A total of 194 sampling points were set up.

2.3. Sample Processing and Determination. Karst water samples were collected at 8.25 on 2011/8/15 and 12.23 on 2012/10/9. Samples were collected and tested in strict accordance with relevant requirements of groundwater quality standard (GB/T 14848-2017). From the recharge area to the drainage area in Jinan karst spring area, samples of karst groundwater were collected along the flow direction of groundwater, and their inorganic hydrochemical and organic components were tested. Groundwater samples are collected directly from the wellhead, the wells are cleaned before collection, and the stored water is discharged from the wellhead. A portable tester was used to test temperature, water temperature, pH value, conductivity, dissolved oxygen, redox potential, and turbidity. When collecting organic samples, the water inflow rate are control without air bubbles and gas flow. Special VOA sample bottles and SVOA sample bottles are sealed and stored and transported in a special refrigerator at 4°C.

2.4. Quality Control and Assurance. Sample determination is controlled by blank method, matrix addition and a parallel sample of matrix addition. The final quantitative results of target test indexes are deducted by blank and corrected by the recovery rate. During the sampling process, 5% parallel samples and 5% outbound samples were collected and standard samples and blank samples were set to track and monitor the sampling and test quality. All organic samples (including experimental samples, blank samples, and spiked samples) were added with recovery indicators to control the efficiency in the sample pretreatment process, and the recovery met the quality control standards as specified in *Technical Requirements for Quality Control of Groundwater Pollution Investigation and Evaluation Sample Analysis* (DD2014-15) by the China Geological Survey. The recovery rates of volatile organic compounds (VOCs) are controlled at 80%~120%, while the recovery rates of semivolatile organic compounds (SVOCs) are controlled at 65%~130%.

2.5. Data Analysis Compounds and Methods. Two-hundred and thirteen samples from all 194 sampling sites were tested for inorganic compounds, including toxic heavy metals, general chemical parameters, and toxic inorganic parameters, and 163 samples from 149 sampling sites were selected for organic component testing. The toxic heavy metals selected in this paper include arsenic, cadmium, hexavalent chromium, lead, and mercury. The general chemical

parameters and the toxic inorganic parameters are determined by traditional analysis methods suitable for karst groundwater [13]. The organic analytes include persistent organic compounds, such as dichlorodiphenyltrichloroethane (DDT). In addition, several typical organic compounds were selected for analysis. The organic compounds include 21 volatile organic compounds, namely, trichloromethane, carbon tetrachloride, 1,1,1-trichloroethane, trichloroethylene, tetrachloroethylene, dichloromethane, 1,2-dichloroethane, 1,1,2-trichloroethane, 1,2-dichloropropane, bromoform, vinyl chloride, 1,1-dichloroethylene, *cis*-1,2-dichloroethylene, chlorobenzene, p-dichlorobenzene, toluene, ethylbenzene, xylene and styrene, 5 semivolatile organic compounds, total benzenehexachloride (BHC), γ-BHC (lindane), total DDT, hexachlorobenzene, and benzo(a) pyrene. The detection limits of the toxic heavy metals and the organic compounds are listed in Tables 1 and 2.

In this paper, the material concentration analysis is carried out by the simple statistical method. The karst water quality evaluation is carried out according to the national groundwater quality standard GB/T 14848-2017, and the spatial distribution characteristics and material sources are analyzed. The substance distribution maps are drawn by the MapGIS software, and the contoured maps are drawn using the method of the inverse distance weighted (IDW). The IDW method mainly depends on the power parameter, and the power parameter used in the paper is 2. The IDW method is a widely used the interpolation method, and its specific calculation processes are no longer repeated in the paper. After the IDW interpolation, the contours are modified manually according to specific hydrogeological conditions to make them more precise.

Table 1: Detection limits of the toxic heavy metals.

No.	Toxic heavy metals	Detection limits (mg/L)
1	Arsenic	0.005
2	Cadmium	0.0002
3	Hexavalent chromium	0.006
4	Lead	0.002
5	Mercury	0.0001

Table 2: Detection limits of the organic compounds.

No.	Organic compounds	Detection limits (μg/L)
1	Trichloromethane	0.1
2	Carbon tetrachloride	0.1
3	1,1,1-Trichloroethane	0.1
4	Trichloroethylene	0.1
5	Tetrachloroethylene	0.1
6	Dichloromethane	0.2
7	1,2-Dichloroethane	0.2
8	1,1,2-Trichloroethane	0.1
9	1,2-Dichloropropane	0.2
10	Bromoform	0.2
11	Vinyl chloride	0.1
12	1,1-Dichloroethylene	0.1
13	*cis*-1,2-Dichloroethylene	0.1
14	Chlorine benzene	0.1
15	Phthalates	0.1
16	Dichlorobenzene	0.1
17	Benzene	0.2
18	Toluene	0.1
19	Ethylbenzene	0.1
20	Ditoluene	0.2
21	Styrene	0.1
22	Total BHC	0.01
23	γ-BHC (lindane)	0.01
24	Total DDT	0.002
25	Hexachlorobenzene	0.01
26	Benzo(a) pyrene	0.002

3. Results

3.1. Concentration and Distribution of Substances

3.1.1. Toxic Heavy Metals. Among the toxic heavy metals, cadmium was detected in 86 samples, the detection rate was 44.3%, and the concentration was 0.0002 mg/L~0.002 mg/L, which were distributed in the whole study area (Figure 2). Lead was detected in 28 samples, the detection rate was 14.4%, and the concentration ranged from 0.002 mg/L~0.007 mg/L, which were distributed in the whole study area too (Figure 3). Hexavalent chromium was detected in 21 samples with a detection rate of 10.8%. Except for the one group located in the south of Jinan spring area with a concentration of 0.48 mg/L, the detection concentration of hexavalent chromium in other samples ranged from 0.006 mg/L to 0.09 mg/L. A group of arsenic was detected with the concentration of 0.0134 mg/L, which was located in the recharge area of the karst water subsystem in Jinan city. Mercury was not detected in all samples.

Overall, the concentration and detection rate of heavy metals in the northwest of the study area along the yellow river and the eastern suburbs of Jinan are relatively low. There are certain detections in a wide area in the south-central and east of the spring area. Samples with a high concentration of heavy metals are scattered around the urban area of Jinan.

3.1.2. Organic Compounds. Among the 149 karst water samples, one or more of the 26 organic compounds were detected in 75 samples and the total detection rate was 50.34%. From the spatial distribution, toxic organic compounds are mainly detected in the karst water subsystem of Jinan urban area and in the north of Baiquan karst water subsystem. Samples with 1 to 3 toxic organic compounds detected were mainly distributed in the southwest of Jinan city and the area from Guodian to Ganggou in the east; samples with 4 or more toxic organic compounds detected were mainly distributed in the area from south industrial road in the eastern suburbs to Wangsheren town, which is the area with the most serious organic pollution of fissure karst water in Jinan city (Figure 4).

The highest detection rate of individual organic compounds was trichloromethane, with a detection rate of

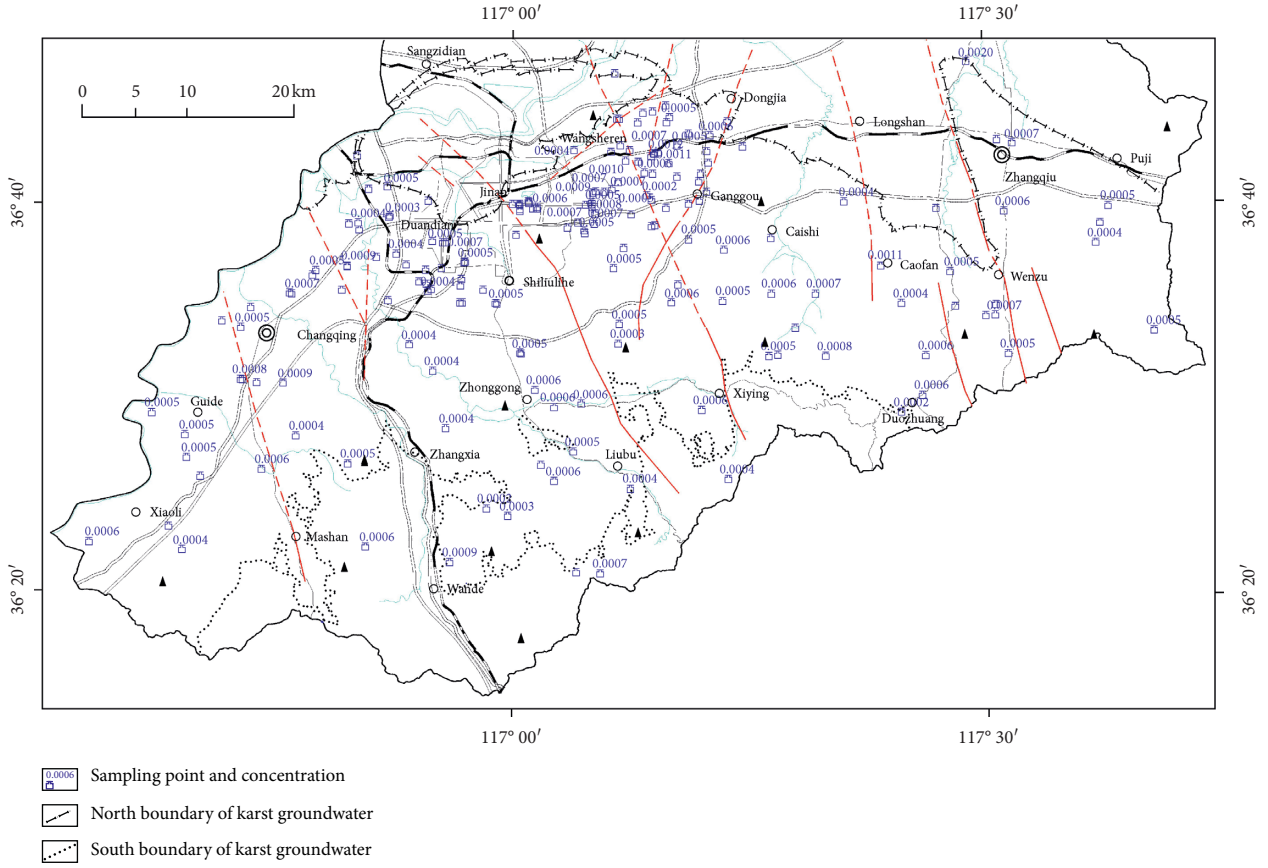

Figure 2: Distribution of Cd concentrations in fractured karst water.

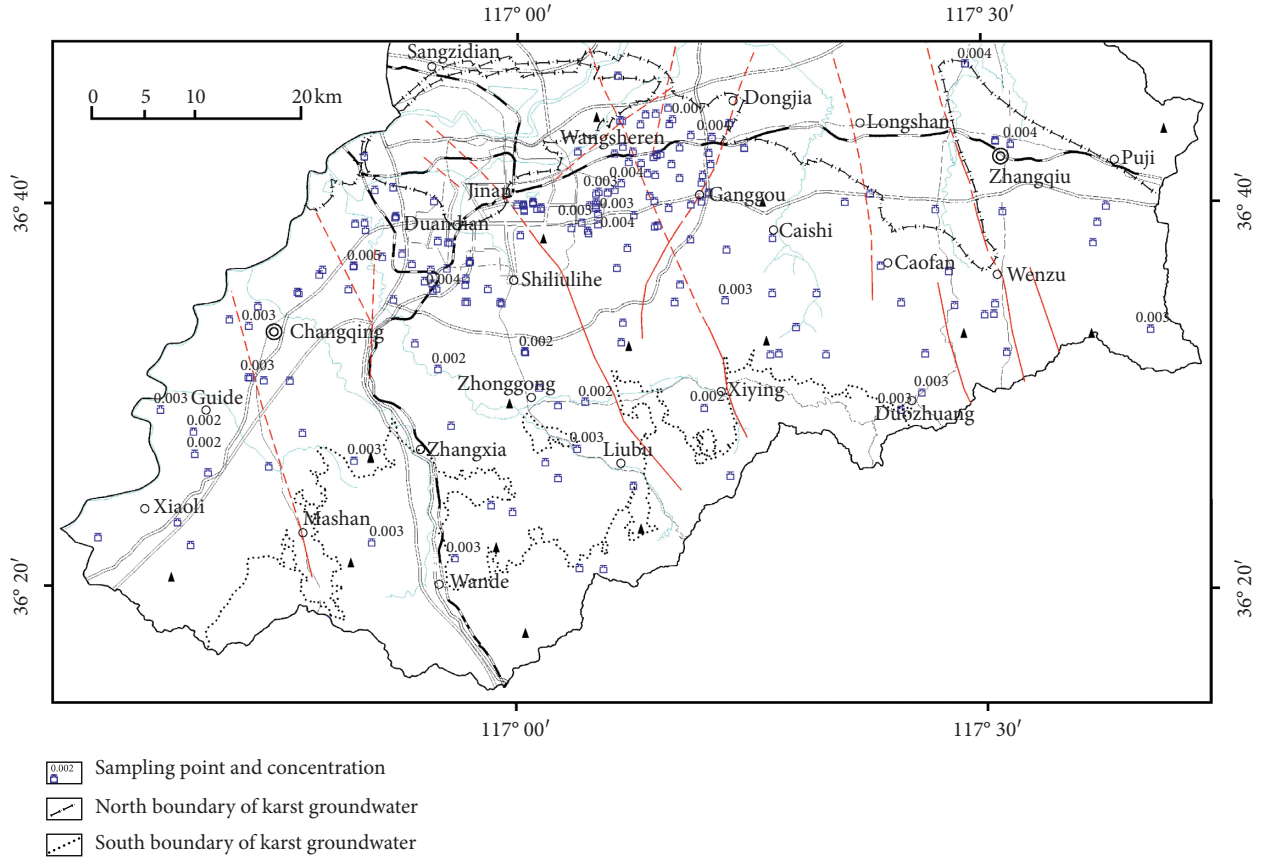

Figure 3: Distribution of Pb concentrations in fractured karst water.

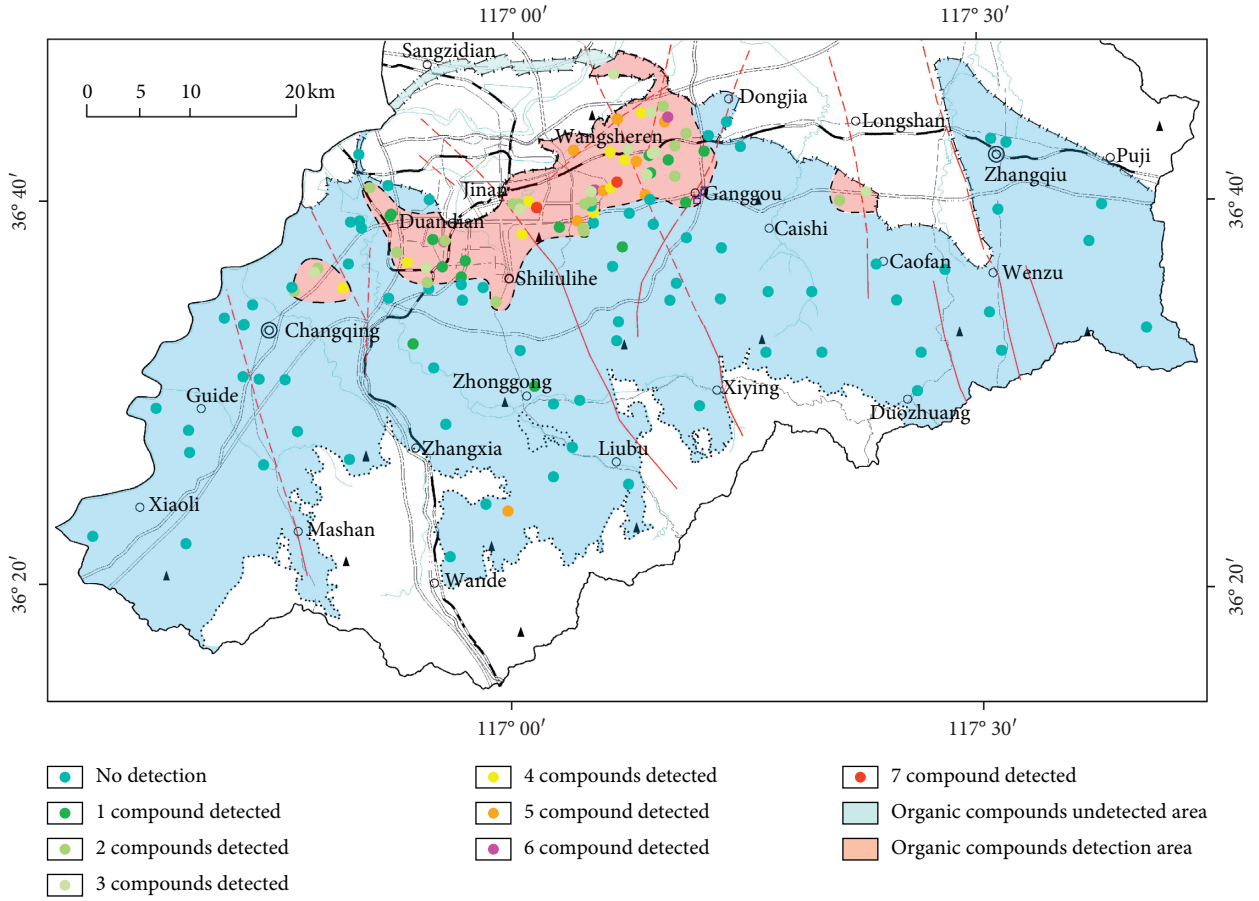

Figure 4: Distribution of the number of toxic organic compounds in fractured karst water.

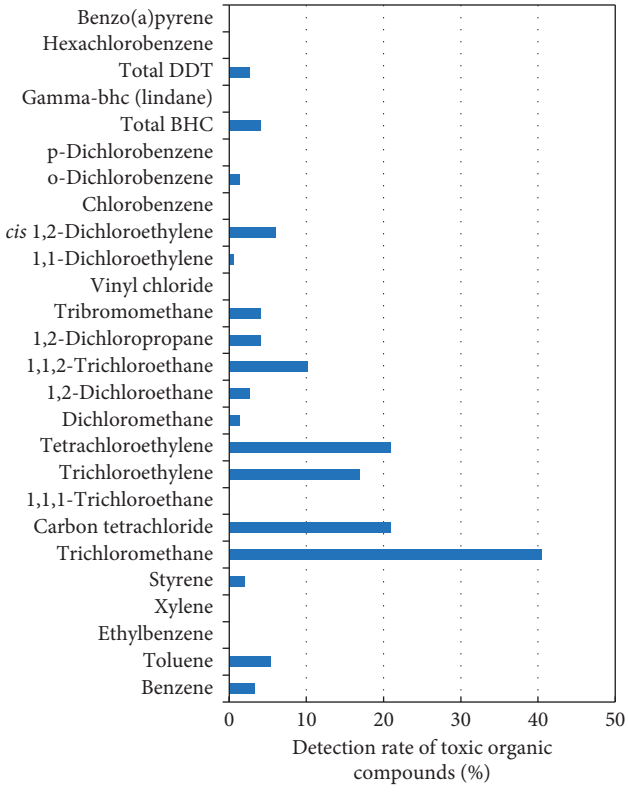

Figure 5: Distribution of toxic organic compound detection rate.

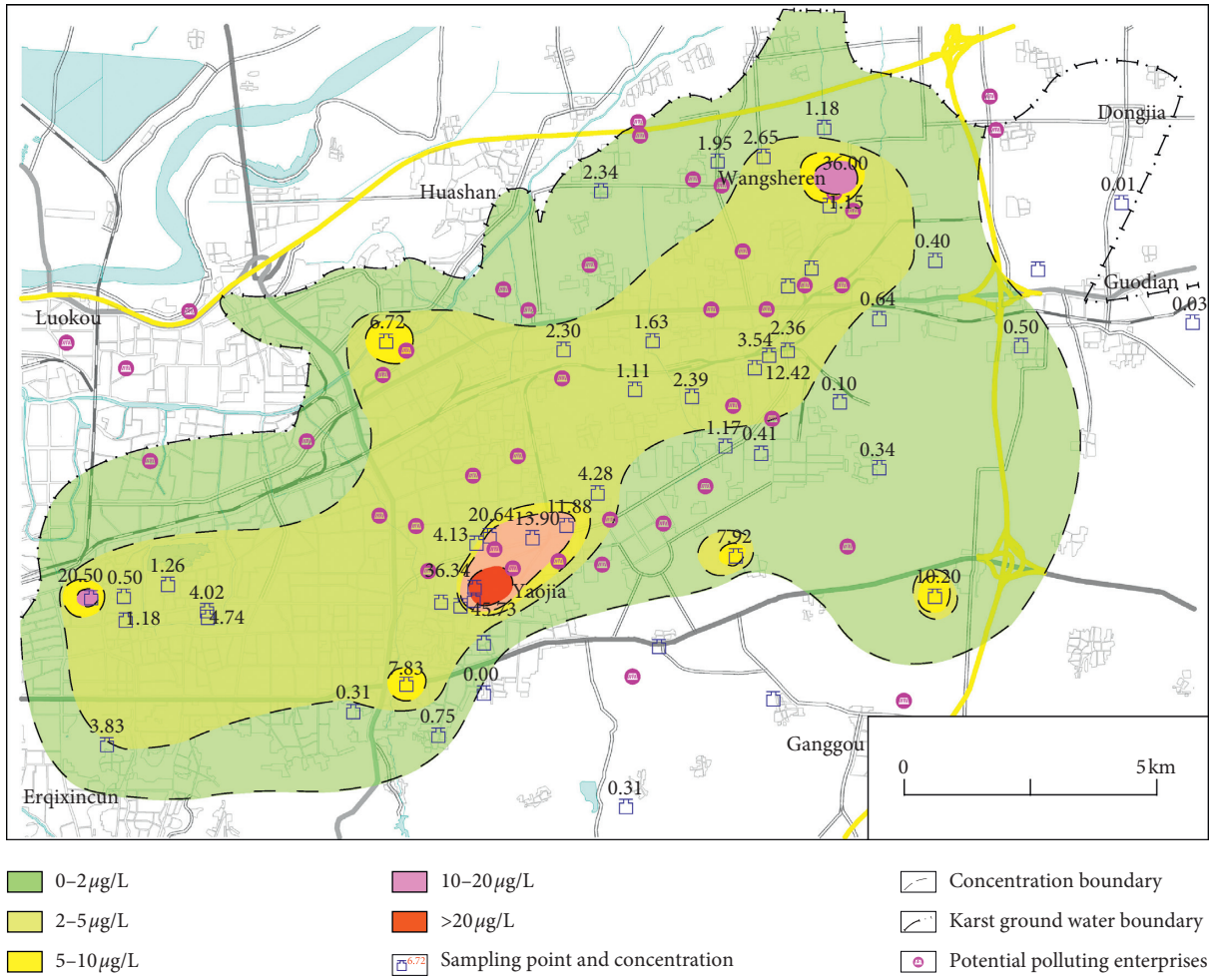

Figure 6: Distribution of total toxic organic compounds in fractured karst water in northeast spring area.

40.54%, followed by carbon tetrachloride and tetrachloroethylene, with a detection rate of 20.95% and trichloroethylene with a higher detection rate, with a detection rate of 16.89% (Figure 5).

The eastern outskirts of Jinan city are the key areas of organic pollution. There are many kinds of toxic organic compounds detected and the total amount is high, forming a relatively obvious pollution halo (Figure 6).

The spatial distribution of trichloromethane and carbon tetrachloride was analyzed. The karst water subsystem and the north part of Baiquan karst water subsystem in Jinan urban area are the main distribution areas of the two (Figures 7 and 8), which have obvious correlation with the intensive distribution of industrial enterprises in the northeast of the urban area.

3.2. Quality Evaluation and Classification

3.2.1. Toxic Heavy Metals. Quality evaluation was carried out according to the groundwater quality standard GB/T 14848-2017 in which groundwaters meet standards I, II, III, IV, and V. Groundwater which meets standards I and II is suitable for all kinds of uses, while groundwater which meets standard III is mainly applicable to centralized drinking water sources and industrial and agricultural water. Groundwater which meets standard IV is suitable for agriculture and some industrial water, and with proper treatment, the water can be used for drinking water, while groundwater which meets standard V is not suitable as a drinking water source and can only be selected to use according to certain other purposes. For 194 fissure karst water samples, the concentrations of each toxic metal in each sample are compared against the standards (Table 3), and then the comprehensive quality evaluation of heavy metal was carried out (Table 4). Among all the samples, the number of heavy metal comprehensive quality exceeding class III standard samples accounted for 3.09%, indicating that the heavy metal index have little influence on the comprehensive quality of fissure karst water. The main impact compounds exceeding class III criteria were Cr^{6+} (2.58%) and As (0.52%).

Samples that contain toxic heavy metals in class III, class IV, and class V are mainly distributed in the northern part of the karst water subsystem and Baiquan karst water

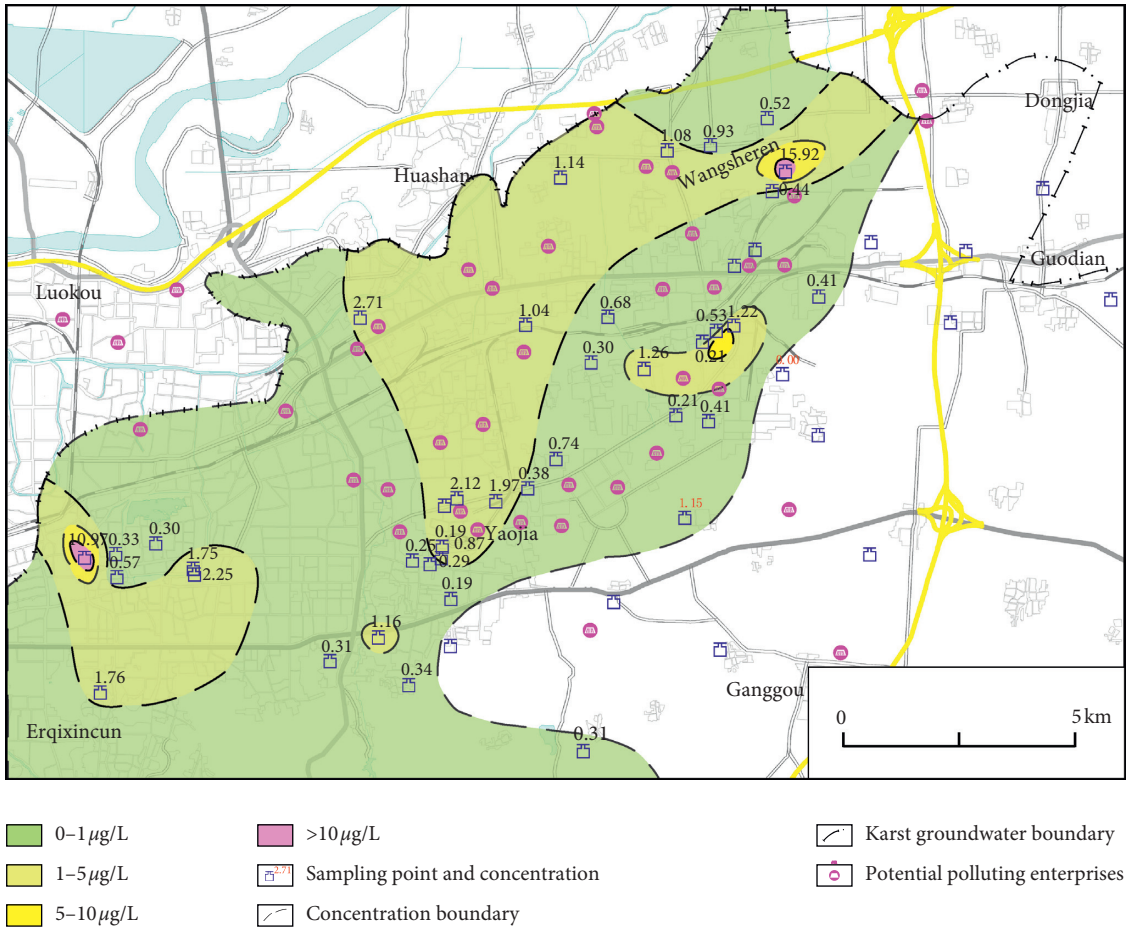

Figure 7: Distribution of the trichloromethane concentration in fractured karst water in northeast spring area.

subsystem in Jinan city, which are related to the production of industrial enterprises in this area, while the quality of the other areas is dominated by class I and class II (Figure 9).

3.2.2. Organic Compounds. Quality evaluation was carried out according to the groundwater quality standard GB/T 14848-2017. For 149 fissure karst water samples, the concentrations of each organic compound in each sample are compared against the standards (Table 5), and then the comprehensive quality evaluation was carried out (Table 6).

The quality evaluation of organic compounds shows that, among all samples, the number of classes IV and V standard samples was 14 samples, accounting for 9.40% of the total, indicating that toxic organic compounds have affected the comprehensive quality of fissure karst water in spring area.

In terms of spatial distribution (Figure 10), class I samples are widely distributed in the study area, while other class II and above samples are mainly distributed in the northern part of the karst water subsystem in Jinan urban area and the karst water subsystem in Baiquan, which is affected by human production and life. The main impact compounds exceeding class III standard were as follows: 12 samples of carbon tetrachloride (8.07%), including 11 samples of class IV water, 1 sample of class V water, and 2 samples of 1,1,2-trichloroethane (1.34%).

3.2.3. Influence of Toxic Substances on Comprehensive Quality Classification. In addition to the above toxic heavy metals and organic substances, 12 general chemical parameters, including pH, iron, manganese, zinc, aluminum, chloride ions, sulfate ions, total hardness, soluble total solids, total oxygen demand, ammonium ions, and sodium and 4 toxic inorganic parameters, including selenium, fluoride ions, nitrate ions, and nitrite, were selected for geochemical quality evaluation.

Quality evaluation was carried out according to the groundwater quality standard GB/T 14848-2017. For 149 fissure karst water samples, the concentrations of each general geochemical compound and each inorganic toxicology compound in each sample are compared against the standards (Tables 7 and 8), and then the comprehensive quality evaluation was carried out (Table 9, Figure 11).

Through comparative analysis, in the recharge area and runoff area of karst spring area, the groundwater impacted with toxic heavy metals are mainly classified as classes I or

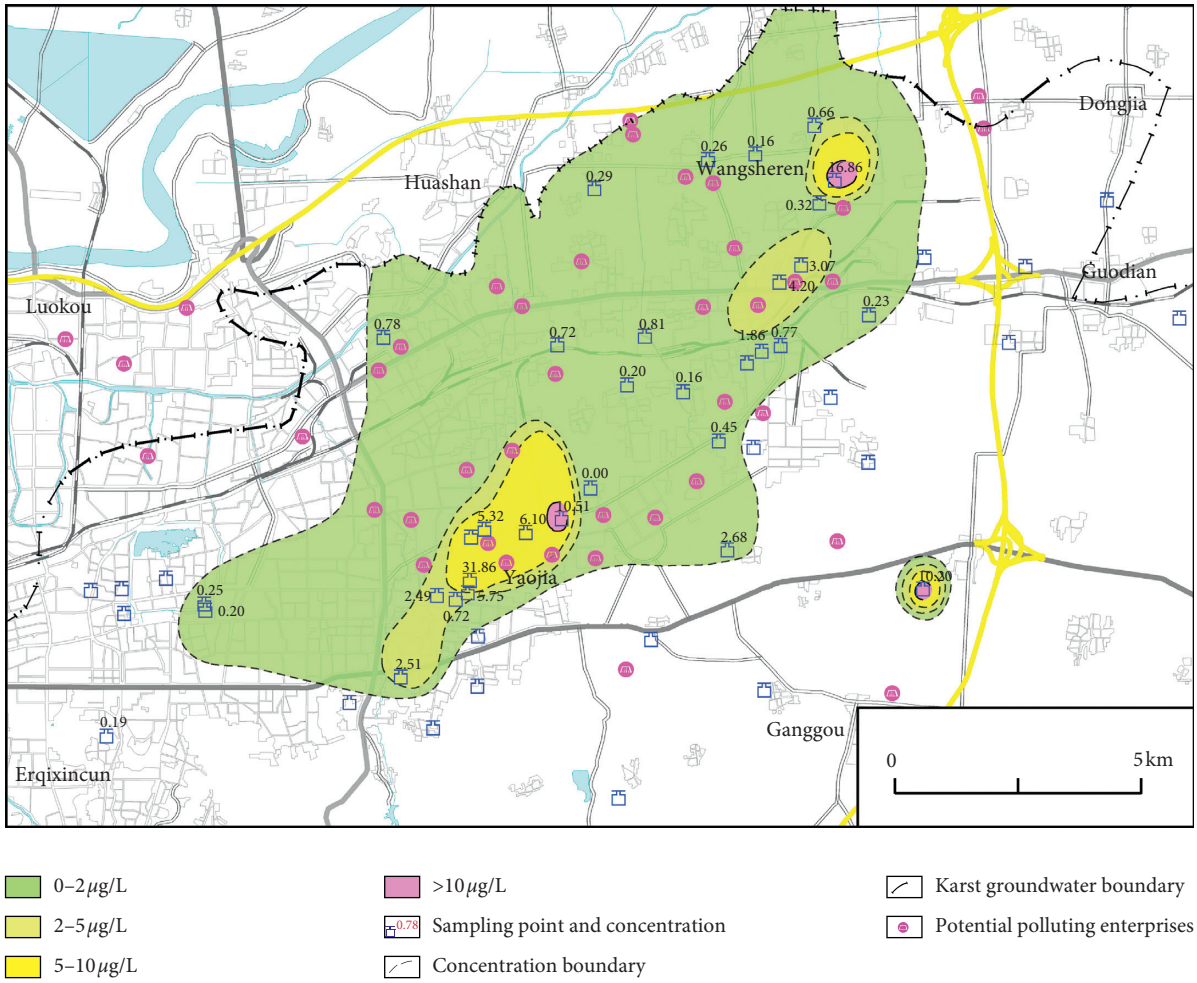

Figure 8: Distribution of the carbon tetrachloride concentration in fractured karst water in northeast spring area.

II and the groundwater impacted with toxic organic compounds are basically classified as class I, while groundwater impacted by the geochemical indicators are classified as classes III or IV, so the impact of the toxic heavy metals or toxic organic compounds is low compared with the impact of the geochemical indicators. In the drainage area of spring area, especially the southwest and northeast of Jinan urban area, the evaluation results of toxic heavy metals and toxic organic compounds are relatively consistent with the comprehensive quality evaluation results, which are classes IV or V, so the contribution rate is relatively high.

3.3. Source Analysis. Distribution of toxic substances has obvious correlation with historical and current industrial layout, and its concentration has persistence and inheritance. In terms of spatial distribution, according to incomplete statistics, there are 835 potential pollution enterprises in the current study area, mainly in the electromechanical, chemical, and steel smelting categories (Figure 12). Its distribution has obvious regional characteristics, mainly distributed in urban built-up areas, economic development zones, and near traffic trunk lines. Historically, the advantageous industries in Jinan urban areas include machinery, textile, steel, chemical light industry, food, and building materials. In recent years, machinery (high-performance, high-added value mechanical products, and metallurgical products), vehicles (advanced heavy vehicles, modified automobiles, and motorcycles), electricity (emerging industries electronic products and high-grade household appliances), chemical (modern biomedical chemical, fine chemical, and chemical fibers) have been developed and have become the city's four leading industries. The new enterprises may cause pollution to both soil and groundwater, which brings new challenges to contaminated soil remediation [25] and wastewater treatment [26]. Analyzing history and current situation, we concluded that the production activities of industrial enterprises should be the main reasons for the detection of toxic substances in karst water in Jinan. Toxic heavy metals may mainly originate from Jinan iron and steel plant, Jinan Huangtai power plant, and other smelting and thermal enterprises, while organic substances may mainly originate

Table 3: Quality evaluation of toxic heavy metals in fractured karst water.

Evaluating compounds	I		II		III		IV		V	
	Groundwater quality standard (mg/L)	Fraction of samples meeting the standard (%)	Groundwater quality standard (mg/L)	Fraction of samples meeting the standard (%)	Groundwater quality standard (mg/L)	Fraction of samples meeting the standard (%)	Groundwater quality standard (mg/L)	Fraction of samples meeting the standard (%)	Groundwater quality standard (mg/L)	Fraction of samples meeting the standard (%)
As	≤0.001	99.48	≤0.001	0	≤0.01	0	≤0.05	0.52	>0.05	0
Cd	≤0.0001	56.19	≤0.001	41.75	≤0.005	2.06	≤0.01	0	>0.01	0
Cr^{6+}	≤0.005	89.18	≤0.01	4.64	≤0.05	3.61	≤0.10	1.55	>0.10	1.03
Pb	≤0.005	99.48	≤0.005	0	≤0.01	0.52	≤0.10	0	>0.10	0
Hg	≤0.0001	100	≤0.0001	0	≤0.001	0	≤0.002	0	>0.002	0

Table 4: Comprehensive quality evaluation of toxic heavy metals in fractured karst water.

Quality classification of toxic heavy metals in karst water	Number of samples	Percentage (%)
I	99	51.03
II	77	39.69
III	12	6.19
IV	4	2.06
V	2	1.03
Total	194	100

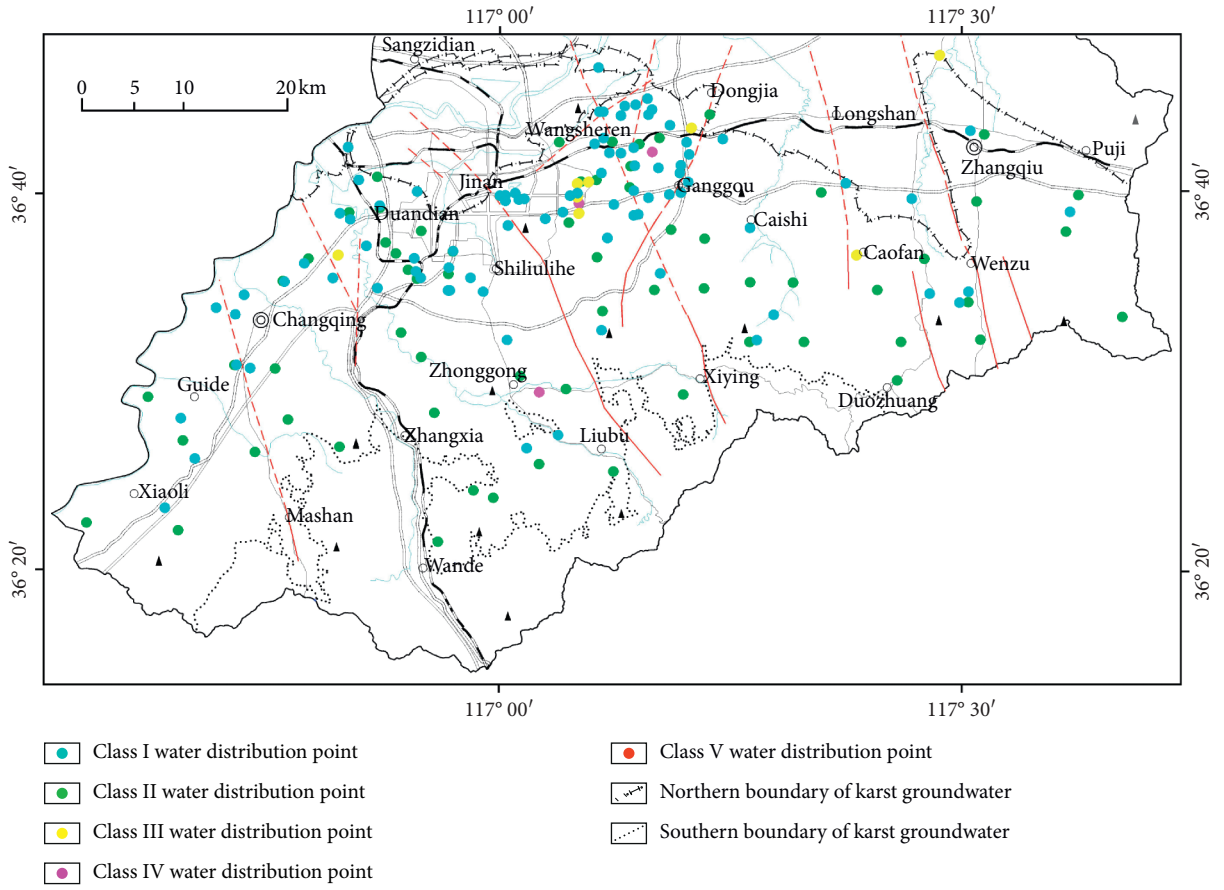

Figure 9: Comprehensive quality evaluation of toxic heavy metals in fractured karst water.

from Jinan refinery, Qilu pharmaceutical enterprise, Jinan yuxing chemical plant, and other chemical and pharmaceutical enterprises.

The long-term persistence of toxic substance concentration in the study area is further illustrated by the test results in the 1980s. In terms of toxic heavy metals, 212 fractured karst water samples were collected in Jinan urban area and eastern and western suburbs for two consecutive years in the early 1980s. The detection rates of hexavalent chromium, mercury, and arsenic were 41.51%, 8.02%, and 1.89%, respectively. Hexavalent chromium samples were mainly distributed in three regions, two of which were located in the northeast of Jinan urban area, with Wangsheren town and Qilihe, Huangtai as the distribution centers, Jinan iron and steel plant and Huangtai power plant, and Jinan second iron and steel plant as the main pollution sources; the other was located in the southwest of Jinan city, Baima mountain to Duandian area. The above areas are also the main distribution areas of current industrial enterprises. The distribution of toxic heavy metal elements in the 1980s is consistent with this result, which indicates that heavy metals mainly originate from industrial production and have a long-term nature. On the one hand, groundwater pollution itself is not easy to eliminate; on the other hand, it is also related to the long-term existence of enterprise production activities.

In terms of toxic organic compounds, the detection rate of volatile phenol was 4.25% in the 1980s, and its

Table 5: Quality evaluation of organic compounds in fractured karst water.

Evaluating compounds	I		II		III		IV		V	
	Groundwater quality standard (μg/L)	Fraction of samples meeting the standard (%)	Groundwater quality standard (μg/L)	Fraction of samples meeting the standard (%)	Groundwater quality standard (μg/L)	Fraction of samples meeting the standard (%)	Groundwater quality standard (μg/L)	Fraction of samples meeting the standard (%)	Groundwater quality standard (μg/L)	Fraction of samples meeting the standard (%)
Trichloromethane	≤0.5	77.85	≤6	20.13	≤60	2.01	≤300	0	>300	0
Carbon tetrachloride	≤0.5	87.25	≤0.5	0	≤2.0	4.70	≤50.0	7.38	>50.0	0.67
1,1,1-Trichloroethane	≤0.5	100	≤400	0	≤2000	0	≤4000	0	>4000	0
Trichloroethylene	≤0.5	91.95	≤7.0	7.38	≤70.0	0.67	≤210	0	>210	0
Tetrachloroethylene	≤0.5	92.62	≤4.0	7.38	≤40.0	0	≤300	0	>300	0
Dichloromethane	≤1	100	≤2.0	0	≤20.0	0	≤500	0	>500	0
1,2-Dichloroethane	≤0.5	100	≤3.0	0	≤30.0	0	≤40.0	0	>40.0	0
1,1,2-Trichloroethane	≤0.5	98.66	≤0.5	0	≤5.0	0	≤60.0	0	>60.0	1.34
1,2-Dichloropropane	≤0.5	98.66	≤0.5	0	≤5.0	1.34	≤60.0	0	>60.0	0
Bromoform	≤0.5	95.97	≤10.0	4.03	≤100	0	≤800	0	>800	0
Vinyl chloride	≤0.5	100	≤0.5	0	≤5.0	0	≤90.0	0	>90.0	0
1,1-Dichloroethylene	≤0.5	100	≤3.0	0	≤30.0	0	≤60.0	0	>60.0	0
cis-1,2-Dichloroethylene	≤0.5	95.3	≤5.0	3.36	≤50.0	1.34	≤60.0	0	>60.0	0
Chlorobenzene	≤0.5	100	≤60.0	0	≤300	0	≤600	0	>600	0
Phthalates	≤0.5	100	≤200	0	≤1000	0	≤2000	0	>2000	0
Dichlorobenzene	≤0.5	100	≤30.0	0	≤300	0	≤600	0	>600	0
Benzene	≤0.5	100	≤1.0	0	≤10.0	0	≤120	0	>120	0
Toluene	≤0.5	100	≤140	0	≤700	0	≤1400	0	>1400	0
Ethylbenzene	≤0.5	100	≤30.0	0	≤300	0	≤600	0	>600	0
Ditoluene	≤0.5	100	≤100	0	≤500	0	≤1000	0	>1000	0
Styrene	≤0.5	100	≤2.0	0	≤20.0	0	≤40.0	0	>40.0	0
Total BHC	≤0.01	95.97	≤0.50	4.03	≤5.00	0	≤300	0	>300	0
γ-BHC (lindane)	≤0.01	100	≤0.20	0	≤2.00	0	≤150	0	>150	0
Total DDT	≤0.01	100	≤0.10	0	≤1.00	0	≤2.00	0	>2.00	0
Hexachlorobenzene	≤0.01	100	≤0.10	0	≤1.00	0	≤2.00	0	>2.00	0
Benzo(a) pyrene	≤0.002	100	≤0.002	0	≤0.01	0	≤0.50	0	>0.50	0

Table 6: Comprehensive quality evaluation of organic compounds of fractured karst water.

Quality classification of organic index of fractured karst water	Number of samples	Percentage
I	105	70.47
II	21	14.09
III	9	6.04
IV	11	7.38
V	3	2.02
Total	149	100

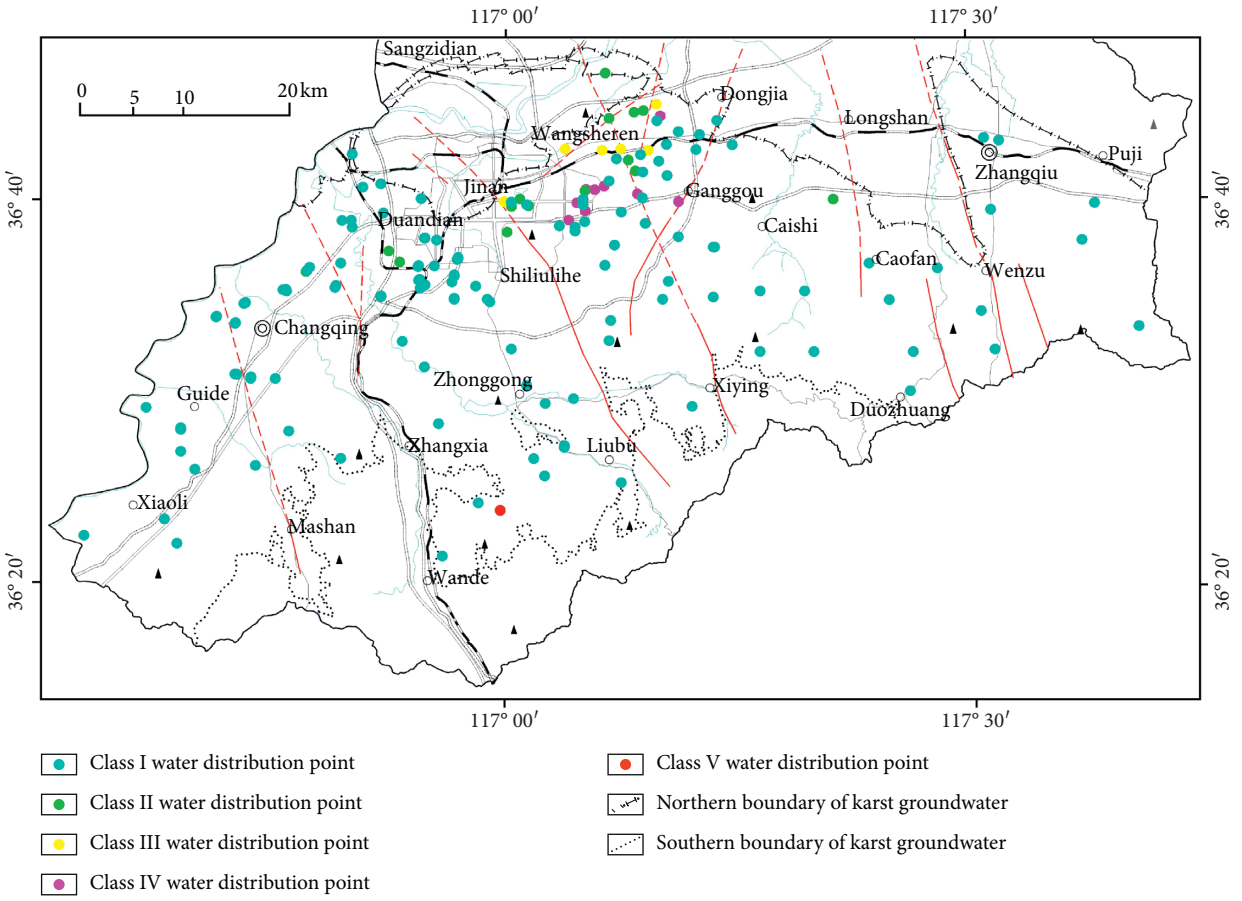

Figure 10: Quality evaluation of organic compounds of fractured karst water.

samples were mainly located near Licheng pesticide factory and Jinan light industry chemical factory at that time. Fifteen samples of fractured karst water were collected to test HCH and DDT in organochlorine pesticides. The detection rates of HCH and DDT were 100% and 93%, respectively, showing a general distribution. Organochlorine pesticides have been discontinued in Jinan for nearly 30 years. Organochlorine pesticides were still detected in 10 of 148 samples collected this time, indicating the persistence of karst water pollution.

The source of trichloromethane and carbon tetrachloride with the highest detection rate of toxic organic compounds was analyzed. Trichloromethane is an important raw material for organic synthesis, which is used to make lipids, rubber, paints, synthetic fibers, plastics, etc. Enterprises producing methane-based chlorinated hydrocarbons are a frequent source of pollution for trichloromethane entering the environment. Carbon tetrachloride is mainly used in the production of chlorofluorocarbon (CFC) refrigerants, foaming agents, and solvents, as well as in the manufacture of paints and plastics, as well as in metal cleaning, fumigants, and other solvents. Accidents in the above industries may cause the contamination of karst water by both substances. The detected water samples of trichloromethane and carbon tetrachloride are mainly distributed in the eastern part of the urban area, which has obvious correlation with the industrial

Table 7: Quality evaluation of general geochemical compounds in fractured karst water.

Evaluating compounds	I		II		III		IV		V	
	Groundwater quality standard (mg/L)	Fraction of samples meeting the standard (%)	Groundwater quality standard (mg/L)	Fraction of samples meeting the standard (%)	Groundwater quality standard (mg/L)	Fraction of samples meeting the standard (%)	Groundwater quality standard (mg/L)	Fraction of samples meeting the standard (%)	Groundwater quality standard (mg/L)	Fraction of samples meeting the standard (%)
pH	pH 6.5 to 8.5	100	pH 6.5 to 8.5	0	pH 6.5 to 8.5	0	pH 5.5 to 6.5 or 8.5 to 9.0	0	pH <5.5 or >9.0	0
Fe	≤0.1	81.21	≤0.2	8.05	≤0.3	3.36	≤2.0	6.71	>2.0	0.67
Mn	≤0.05	97.99	≤0.05	0	≤0.10	2.01	≤1.50	0	>1.50	0
Zn	≤0.05	91.28	≤0.5	8.05	≤1.00	0	≤5.00	0.67	>5.00	0
Al	≤0.01	63.09	≤0.05	20.81	≤0.20	14.77	≤0.50	0.67	>0.5	0.67
Cl^-	≤50	69.8	≤150	28.86	≤250	1.34	≤350	0	>350	0
SO_4^{2-}	≤50	15.44	≤150	69.8	≤250	11.41	≤350	3.36	>350	0
Total hardness	≤150	0	≤300	19.46	≤450	57.72	≤650	22.15	>650	0.67
TDS	≤300	12.08	≤500	56.38	≤1000	30.87	≤2000	0.67	>2000	0
DO	≤1.0	97.32	≤2.0	1.34	≤3.0	1.34	≤10.0	0	>10.0	0
NH_4^+ (In N)	≤0.02	99.33	≤0.10	0	≤0.50	0.67	≤1.50	0	>1.50	0
Na^+	≤100	100	≤150	0	≤200	0	≤400	0	>400	0

Table 8: Quality evaluation of inorganic toxicology compounds in fractured karst water.

Evaluating compounds	I		II		III		IV		V	
	Groundwater quality standard (mg/L)	Fraction of samples meeting the standard (%)	Groundwater quality standard (mg/L)	Fraction of samples meeting the standard (%)	Groundwater quality standard (mg/L)	Fraction of samples meeting the standard (%)	Groundwater quality standard (mg/L)	Fraction of samples meeting the standard (%)	Groundwater quality standard (mg/L)	Fraction of samples meeting the standard (%)
Se	≤0.01	100	≤0.01	0	≤0.01	0	≤0.1	0	>0.1	0
F^-	≤1.0	20.81	≤1.0	51.68	≤1.0	26.17	≤2.0	0.67	>2.0	0.67
NO_3^- (In N)	≤2.0	3.36	≤5.0	16.11	≤20.0	67.79	≤30.0	8.05	>30.0	4.7
NO_2^- (In N)	≤0.01	90.6	≤0.1	5.37	≤1.00	2.01	≤4.8	1.34	>4.8	0.67

Table 9: Comprehensive quality evaluation of fractured karst water.

Comprehensive quality classification of fractured karst water	Number of samples	Percentage (%)	Distribution area (km^2)	Percentage (%)
II	12	8.05	152.49	5.56
III	82	55.03	2414.32	88.04
IV	40	26.85	151.75	5.54
V	15	10.07	23.72	0.86
Total	149	100	2742.28	100

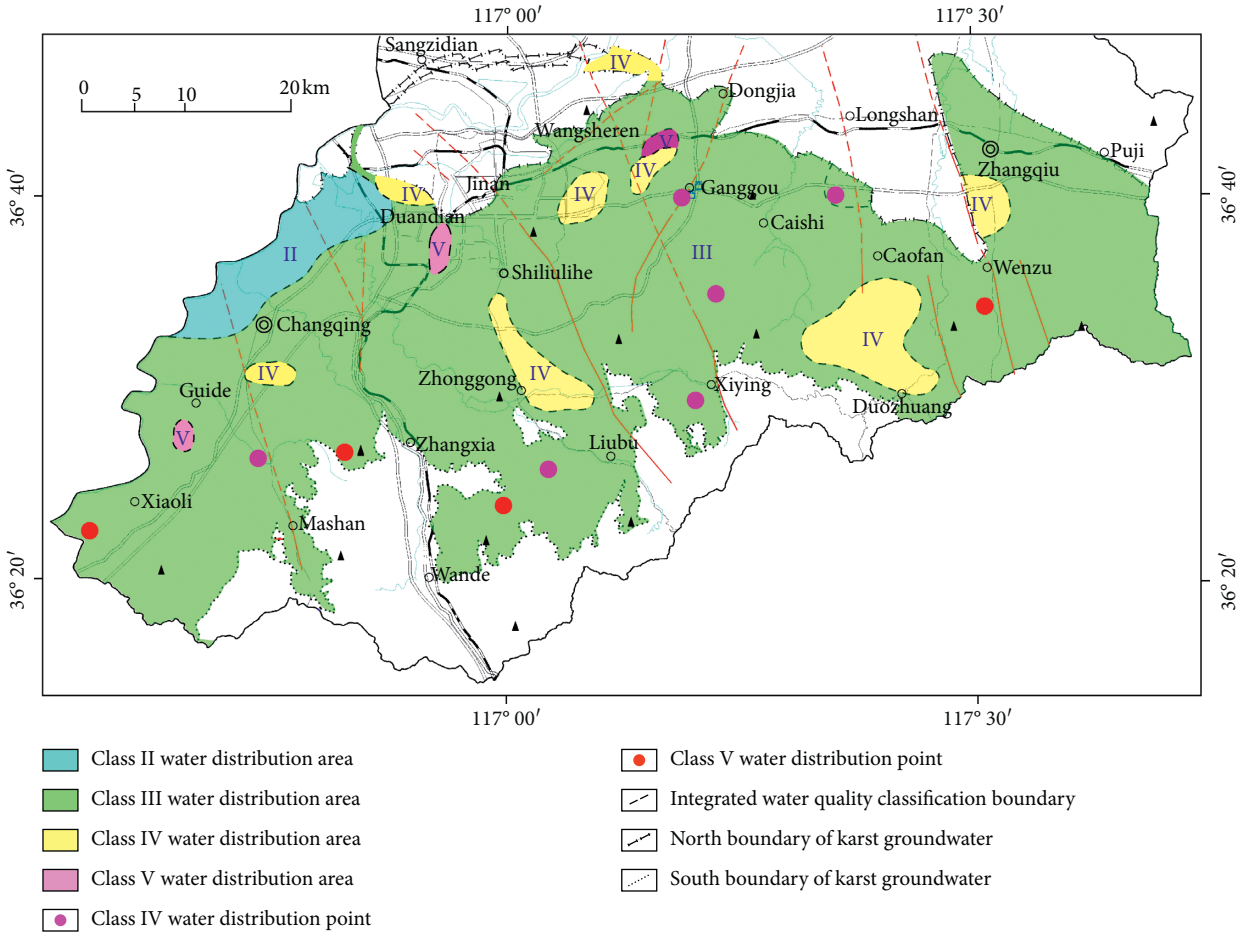

Figure 11: Comprehensive quality distribution of fractured karst water.

enterprises such as petrochemical, paint, plastics, and steel which have been gathered for a long time in the eastern part of the urban area.

Carbon tetrachloride was taken as an example to analyze the persistence of toxic substance concentration. Because of the barrier of gabbro in the north of the spring area in Jinan area, it is difficult for surface carbon tetrachloride to enter the karst water directly by leaching, and at the same time, carbon tetrachloride is rarely used by enterprises nowadays, which can basically exclude the possibility that the existing pollution sources cause carbon tetrachloride exceeding the standard in karst water. In the previous studies, carbon tetrachloride in Xuzhou, China, can cause continuous pollution of groundwater for more than 12 years [13], and it takes a long time to eliminate the impact of carbon tetrachloride on water quality. According to investigation, Jinan chemical plant has been using carbon tetrachloride to produce freon refrigerant from 1974 to 1996, with annual consumption of up to 5000 tons; among them, the plant directly produced carbon tetrachloride from 1989 to 1992, with annual production of up to 500 tons. In addition, companies such as Bluestar petroleum have used or produced carbon tetrachloride in small quantities. Therefore, it is considered that the serious pollution of carbon tetrachloride in fissure karst water in northeastern Jinan is caused by the emission or leakage of carbon tetrachloride produced or used in the history of the above enterprises.

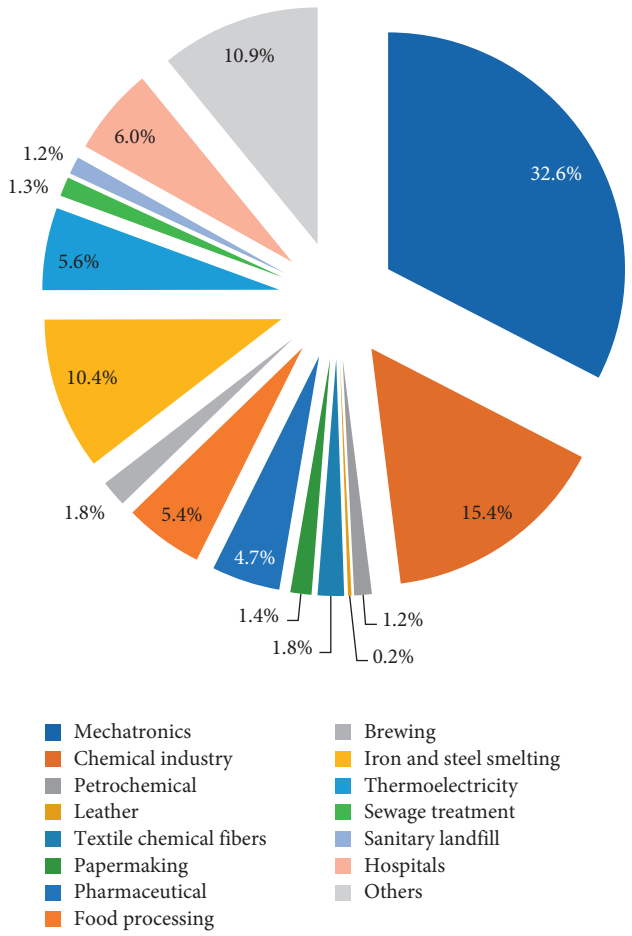

Figure 12: Classification of potential pollution enterprises in Jinan area.

4. Conclusion

The comprehensive evaluation of groundwater in a karst aquifer system that provide groundwater to an industrial area with more than six million people is of great significance for understanding the main toxic substances and the water quality. The study provides scientific understanding which is beneficial to the improvements of groundwater quality and the sustainable development of Jinan's economy, society, and ecology. The toxic substances of karst water in Jinan are mainly distributed in the northern part of the Jinan karst water subsystem and the Baiquan karst water subsystem, while in other areas, the toxic substances have comparatively low detection rates and low concentrations. The distribution of karst water quality is determined by the concentration of evaluation indexes, and the northeast and southwest parts of Jinan urban area are the main distribution areas exceeding class III standard. In the recharge area and the runoff area of the karst spring area, the influence of toxic substances on the comprehensive quality classification is relatively low, and in the drainage area, the influence is relatively high. Compared with toxic heavy metals, organic compounds contribute more to the comprehensive quality of karst water.

Toxic substances have been widely distributed in Jinan karst water. Among the toxic heavy metals, the detection rates of cadmium, lead, hexavalent chromium, arsenic, and mercury were in order from high to low. The detection rates of organic compounds from high to low are trichloromethane, carbon tetrachloride, tetrachloroethylene, trichloroethylene, etc. The above compounds are important compounds to control the comprehensive quality of karst groundwater.

The distribution of toxic substances has an obvious correlation with the historical and current industrial layout, and its concentration has persistence and inheritance. The production activities of industrial enterprises are the main reasons for the detection of toxic substances in karst water in Jinan. On the one hand, the long-term persistence of toxic substances is related to its own difficulty to eliminate, that is, once they enter the groundwater, it is difficult to degrade or lose; on the other hand, it is also related to the long-term nature of the production activities of enterprises, that is, there may be persistent toxic substances entering the groundwater.

Effective measures should be taken to improve the quality of karst groundwater in Jinan to serve the needs of environmental restoration and ecological civilization construction. One is to strengthen the supervision and improve the process to minimize the leakage of new toxic substances; the other is to treat and repair existing pollution by appropriate engineering and technical means; the third is to strengthen the monitoring to provide data support for scientific evaluation of the evolution of karst water quality, government consultation, and decision-making and the implementation of rehabilitation projects.

Data Availability

The data used to support the findings of this study are available from the corresponding author upon request.

Disclosure

Hao Shang and Xiaofan Qi are co-first authors.

Conflicts of Interest

The authors declare that they have no conflicts of interest.

Authors' Contributions

Hao Shang and Xiaofan Qi have contributed equally to this work.

Acknowledgments

This work was jointly supported by the Geological Survey Project of Shandong Province (Lu Kanzi (2011)46, Lu Kanzi (2018)5), the Project of Jinan Rail Transit Group Co., Ltd. (2018GDCG01Z0301), and the Key Research and Developmental Program of Shandong Province (Major Scientific and Technological Innovation Project) (2019JZZY020105).

References

[1] Y. P. Liang and X. R. Han, *Environmental Problems and Protection of Karst Groundwater in Northern China*, Geology Publishing House, Beijing, China, 2013, in Chinese.

[2] G. C. Hou, M. S. Zhang, and F. Liu, *Groundwater Investigations and Research of Ordos Basin*, Geological Publishing House, Beijing, China, 2008, in Chinese.

[3] Z. X. Zhang, Y. X. Xu, Y. B. Zhang, and J. H. Cao, "Review: karst springs in Shanxi, China," *Carbonates and Evaporites*, vol. 34, no. 4, pp. 1213–1240, 2019.

[4] Y. Liang, X. Gao, C. Zhao et al., "Review: characterization, evolution, and environmental issues of karst water systems in Northern China," *Hydrogeology Journal*, vol. 26, no. 5, pp. 1371–1385, 2018.

[5] J. Y. Wang, J. L. Wang, and M. G. Jin, "Hydrochemical characteristics and formation causes of karst water in Jinan spring catchment," *Earth Science*, vol. 42, no. 5, pp. 821–631, 2017, in Chinese.

[6] J. Wang, M. Jin, G. Lu, D. Zhang, F. Kang, and B. Jia, "Investigation of discharge-area groundwaters for recharge source characterization on different scales: the case of Jinan in Northern China," *Hydrogeology Journal*, vol. 24, no. 7, pp. 1723–1737, 2016.

[7] K. Q. He, W. Du, S. Q. Zhang, and Y. R. Lu, "Analysis on the rational exploitation and regulatory storage of karst water resources in the central-south region of Shandong Province, China," *Water Resources Management*, vol. 24, pp. 349–362, 2010.

[8] J. Qian, H. Zhan, Y. Wu, F. Li, and J. Wang, "Fractured-karst spring-flow protections: a case study in Jinan, China," *Hydrogeology Journal*, vol. 14, no. 7, pp. 1192–1205, 2006.

[9] C. L. Wen, W. H. Dong, Y. Meng, C. S. Li, and Q. C. Zhang, "Application of a loose coupling model for assessing the impact of land-cover changes on groundwater recharge in the Jinan spring area, China," *Environmental Earth Sciences*, vol. 78, p. 382, 2019.

[10] F. Kang, M. Jin, and P. Qin, "Sustainable yield of a karst aquifer system: a case study of Jinan springs in Northern China," *Hydrogeology Journal*, vol. 19, no. 4, pp. 851–863, 2011.

[11] Z. J. Gao, J. X. Xu, S. C. Wang et al., "The distribution characteristics and hydrogeological significance of trace elements in karst water, Jinan, China," *Earth Science Frontiers*, vol. 21, no. 4, pp. 135–146, 2014, in Chinese.

[12] L. Z. Yang, C. H. Liu, and X. F. Qi, "Study on characteristic variation of hydro-chemistry of Jinan spring," *Journal of Water Resources & Water Engineering*, vol. 27, no. 1, pp. 59–64, 2016, in Chinese.

[13] L. Z. Yang, Z. Li, Z. R. Wei et al., *Report on Jinan Urban Geological Survey*, Shandong Institute of Geological Survey, Jinan, China, 2014, in Chinese.

[14] Y. Jiang, M. Cao, D. Yuan, Y. Zhang, and Q. He, "Hydrogeological characterization and environmental effects of the deteriorating urban karst groundwater in a karst trough valley: Nanshan, SW China," *Hydrogeology Journal*, vol. 26, no. 5, pp. 1487–1497, 2018.

[15] K. Kalhor, R. Ghasemizadeh, L. Rajic, and A. Alshawabkeh, "Assessment of groundwater quality and remediation in karst aquifers: a review," *Groundwater for Sustainable Development*, vol. 8, pp. 104–121, 2019.

[16] F. Liao, G. Wang, Z. Shi et al., "Distributions, sources, and species of heavy metals/trace elements in shallow groundwater around the Poyang lake, east China," *Exposure and Health*, vol. 10, no. 4, pp. 211–227, 2018.

[17] F. Liu, C.-q. Liu, Y. Zhao, and Z. Li, "Changes of hydrochemical composition and heavy metals concentration in shallow groundwater from karst hilly areas in Guiyang region, China," *Journal of Central South University of Technology*, vol. 17, no. 6, pp. 1216–1222, 2010.

[18] S. Liu, C. Liang, L. Yang et al., "Distribution characteristics of chemicals and heavy metals in typical karst subterranean rivers in South China," *Carbonates and Evaporites*, vol. 34, no. 4, pp. 1867–1875, 2019.

[19] L. Zhang, X. Qin, J. Tang, W. Liu, and H. Yang, "Review of arsenic geochemical characteristics and its significance on arsenic pollution studies in karst groundwater, Southwest China," *Applied Geochemistry*, vol. 77, pp. 80–88, 2017.

[20] S. Indelicato, S. Orecchio, G. Avellone et al., "Effect of solid waste landfill organic pollutants on groundwater in three areas of Sicily (Italy) characterized by different vulnerability," *Environmental Science and Pollution Research*, vol. 24, no. 20, pp. 16869–16882, 2017.

[21] M. Ekmekci, "Pesticide and nutrient contamination in the Kestel polje-Kirkgoz karst springs, Southern Turkey," *Environmental Geology*, vol. 49, no. 1, pp. 19–29, 2005.

[22] Y. R. Lu, "Karst water resources and geo-ecology in typical regions of China," *Environmental Geology*, vol. 51, pp. 695–699, 2007.

[23] J. G. Xu, H. H. Zhu, H. Xu, C. H. Liu, and Z. Zhang, "Study on organic pollution of karst underground water in Jinan spring area," *Carsologica Sinica*, vol. 28, no. 3, pp. 249–254, 2009, in Chinese.

[24] W. Dong, W. Xie, X. Su, C. Wen, Z. Cao, and Y. Wan, "Review: micro-organic contaminants in groundwater in China," *Hydrogeology Journal*, vol. 26, no. 5, pp. 1351–1369, 2018.

[25] P. Zhang, C. J. Jin, Z. F. Sun, G. H. Huang, and Z. L. She, "Assessment of acid enhancement schemes for electrokinetic remediation of Cd/Pb contaminated soil," *Water Air and Soil Pollution*, vol. 227, pp. 1–28, 2016.

[26] P. Zhang, G. Huang, C. An et al., "An integrated gravity-driven ecological bed for wastewater treatment in subtropical regions: process design, performance analysis, and greenhouse gas emissions assessment," *Journal of Cleaner Production*, vol. 212, pp. 1143–1153, 2019.

Hindawi
Journal of Chemistry
Volume 2020, Article ID 5101936, 8 pages
https://doi.org/10.1155/2020/5101936

Research Article

Organochlorine Pesticides in Surface Water of Jiuxi Valley, China: Distribution, Source Analysis, and Risk Evaluation

Zheng Liu,[1,2,3] Guanlin Zheng ,[4] and Zhen Liu[1,2,3]

[1]*School of Environmental Science and Engineering, Xiamen University of Technology, Xiamen, China*
[2]*Fujian Engineering and Research Center of Rural Sewage Treatment and Water Safety, Xiamen, China*
[3]*Key Laboratory of Environmental Biotechnology (XMUT), Fujian Province University, Fuzhou, Fujian, China*
[4]*College of Environment and Ecology, Xiamen University, Xiamen, China*

Correspondence should be addressed to Guanlin Zheng; golin_zheng@xmu.edu.cn

Received 11 October 2019; Accepted 2 January 2020; Published 27 February 2020

Guest Editor: Hangbiao Jin

Residual levels of 11 organochlorine pesticides (OCPs) in surface water of Jiuxi Valley were determined during spring and autumn at nine sampling points to assess their contamination and potential risks. The water samples were extracted by solid-phase extraction (SPE), and OCPs were analyzed by gas chromatograph equipped with a ^{63}Ni-ECD detector. The investigation results indicated that the concentration of total OCPs varied from 4.07 to 13.5 ng·L^{-1} with an average value of 7.15 ng·L^{-1} in spring, and from 12.5 to 30.1 ng·L^{-1} with an average value of 19.9 ng·L^{-1} in autumn. Jiuxi Valley was slightly contaminated by OCPs, and the concentrations of ΣHCHs and ΣDDTs in the river were at relatively low levels. HCHs were the main pollutant in spring, and also in autumn, and α-HCH was the main component of the HCH isomers at most sampling points. Source analysis indicated that local use of lindane or input of fresh γ-HCH contributed to the presence of HCHs. New inputs were the major sources of DDTs, aldrin, heptachlor, and endrin. The OCP levels of this investigation were within the standard limits set by a majority of the water quality standards and guidelines of China, WHO, European Union, and Canada. However, although the γ-HCH concentrations at all sampling sites, endrin concentrations at all sampling sites, and β-HCH concentrations at most sampling sites were below the human health water quality standard, and the levels of other tested OCPs (α-HCH, p,p′-DDD, p,p′-DDE, p,p′-DDT, aldrin, and heptachlor) exceeded the value of EPA-recommended water quality criteria for human health, which indicated potential risks to human health around the region.

1. Introduction

As common persistent organic pollutants (POPs), organochlorine pesticides (OCPs) have received great attention worldwide due to their high toxicity, chemical durability, and biological concentration [1]. These chemicals were once widely used in agricultural production and pest control universally. Researchers had found OCPs caused great threats to ecosystems and human health [2, 3]. Despite the prohibition of production and use of these pesticides by many countries in the 1970s and 1980s, some OCPs, including hexachlorocyclohexanes (HCHs), dichlorodiphenyltrichloroethanes (DDTs), aldrin, heptachlor, and endrin, were still widely distributed everywhere because of their persistence. China produced a large number of OCPs using for broad spectrum pesticides, medical, and industrial purposes from the late 1940s to the 1980s. From the 1950s to 1983, millions of tons of technical-grade HCHs and DDTs were yielded, accounting for the world output of 33% and 20%, respectively [4]. Even though production and use of OCPs had been forbidden since 1983, the comparatively high concentrations of residue OCPs were still detected in water and other environmental media.

As an important environmental medium, water bodies play a vital part in the migration and transformation of OCPs. OCPs can enter rivers or lakes via agricultural nonpoint source pollution, industrial wastewater discharge, atmospheric sedimentation, and other ways [5–7]. Although

most OCPs are difficult to dissolve in water, they are easy to be enriched in organisms by reason of their relatively high octanol-water partition coefficient and have the probability to bioaccumulate through the food chain, causing health risks [8, 9]. After being discharged into water bodies, they are mainly adsorbed on suspended particles. Under certain circumstances, it will be resuspended after disturbance and become a secondary pollution source [10, 11]. In addition, OCPs may be involved in atmospheric circulation and migrated to remote places from the source, causing environmental issues at regional and global scale [12].

Jiuxi Valley is located in the east of Xiang'an District, Xiamen City. Xiamen is a beautiful tourist city in southeast China. Jiuxi Valley is 21 km long and has a drainage area of 101 km^2. The nine main branches form a tree-like water system, which flows into the Dadeng sea area in Xindian Town. Jiuxi is called the mother river of Xiang'an District. It flows across the basic farmland protection area of Xiamen. It is a source of farmland irrigation and livestock drinking water. There are also a large number of egrets perched every winter. The government has viewed the Jiuxi Valley as a beautiful ecological green stream. After comprehensive treatment, the water quality of the Jiuxi Valley has been improved, but more information is needed to evaluate the pollution situation and identify the potential risk to human health and ecological risk to aquatic life. As far as we know, this work first reported on the concentrations of OCPs contaminants in Jiuxi Valley.

The major aims of this research work were (1) to investigate the concentrations, spatial distribution, and composition of 11 OCPs (α-HCH, β-HCH, γ-HCH, δ-HCH, p,p′-DDD, p,p′-DDE, o,p′-DDT, p,p′-DDT, aldrin, heptachlor, and endrin) in surface water of Jiuxi Valley and (2) to investigate the pollution profiles to identify seasonal pollution characteristics, and source apportionment and to evaluate potential risks to human health around the region, thus offering scientific information for efficient strategical environmental management.

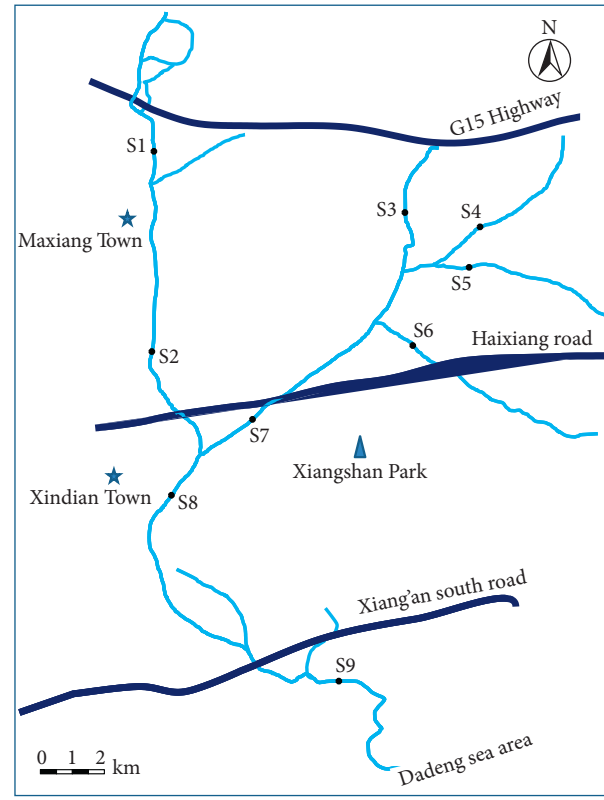

Figure 1: Sampling points of the Jiuxi Valley, Xiamen.

2. Methodology

2.1. Sampling. Nine sampling points (namely, S1 to S9) along the river were selected, as shown in Figure 1. The collection of water samples at 0.15 m below the surface of water was carried out in autumn (October 8 to November 8, 2018) and spring (March 12 to April 12, 2019), and they were stored in precleaned 1 L brown glass bottles. The suspended matter and impurities in water samples were removed by using 0.45 μm fiber glass filters. The extraction was completed within 7 days, and the analysis was completed within 30 days.

2.2. Extraction. The water samples were extracted by solid-phase extraction (SPE). In brief, the Florisil SPE cartridges (1000 mg/6 ml) were rinsed successively with 5 ml of ethyl acetate, 5 ml of methanol, and 10 ml of ultrapure water. Using vacuum pumping, water samples flowed via the SPE columns at a flow velocity of 10 ml/min. When the extraction was completed, the OCPs captured in SPE columns were eluted twice with 10 ml of ethyl acetate. Then, anhydrous sodium sulfate (roasted at 300°C) was used to dehydrate the extracts, and then the extracts were concentrated to roughly 0.5 ml with high purity nitrogen streaming. The extracts were spiked with 5.0 μl of TCmX (2,4,5,6-tetrachloro-m-xylene) as internal standard and redissolved to 1 ml with *n*-hexane [13]. Finally, the extracts were transferred into vials and kept sealed at −20°C until analysis.

2.3. Chemical Analysis. The OCPs residues were analyzed by using gas chromatograph (Agilent 7890B; 30 m × 0.25 mm i.d. ×0.25 μm film thickness, HP-5 capillary column) equipped with a ^{63}Ni-ECD detector. Samples (2 μl) were injected in the splitless injection mode with high purity nitrogen as both carrier gas (1 ml·min^{-1}) and makeup gas (60 ml·min^{-1}). The temperature of the column oven was first set at 100°C (with an equilibration time of 2 min), raised to 200°C (6°C·min^{-1}), then to 230°C (1°C·min^{-1}), and finally reached to 280°C (10°C·min^{-1}) and retained for 10 min. The injection port and detector temperatures were kept at 280°C and 300°C, respectively. The target OCPs were identified by the retention times matched to each standard. The concentrations of OCPs were acquired using peak area based on a six-point standard curve. In this study, the OCPs analyzed were HCHs (including α-HCH, β-HCH, γ-HCH, and δ-HCH), DDTs (including p,p′-DDD, p,p′-DDE, o,p′-DDT, and p,p′-DDT), aldrin, heptachlor, and endrin.

Table 1: OCPs concentration in surface water from Jiuxi Valley ($ng \cdot L^{-1}$).

Compounds	Spring, 12.03.2019–12.04.2019 ($n = 32$)			Autumn, 08.10.2018–08.11.2018 ($n = 32$)		
	Mean	S. D.[a]	Range	Mean	S. D.	Range
α–HCH	1.45	1.63	0.120–5.24	7.17	3.05	4.31–13.0
β–HCH	0.968	0.798	0.509–2.98	3.84	2.95	2.25–11.5
γ–HCH	1.08	0.327	0.844–1.84	3.16	0.854	2.42–5.02
δ–HCH	0.198	0.0589	0.142–0.312	0.598	0.0939	0.485–0.756
ΣHCHs	3.69	2.10	1.71–8.12	14.8	4.99	9.94–23.5
p,p′–DDT	1.11	0.332	0.715–1.84	1.48	0.403	0.849–2.12
o,p′–DDT	0.904	0.421	0.247–1.86	1.45	0.120	0.708–4.13
p,p′–DDD	0.0612	0.0318	<0.04–0.128	0.120	0.109	<0.04–0.316
p,p′–DDE	0.161	0.0680	<0.05–0.246	0.283	0.165	0.0724–0.622
ΣDDTs	2.23	0.615	1.19–3.31	3.34	1.31	1.90–6.23
Aldrin	0.736	0.524	<0.05–1.62	1.28	1.63	0.213–2.45
Heptachlor	0.426	0.554	<0.04–1.75	0.316	0.371	0.0634–1.23
Endrin	0.063	0.0312	<0.04–0.110	0.126	0.0980	<0.04–0.196
ΣOCPs	7.15	3.08	4.07–13.5	19.8	6.65	12.5–30.1

Note. Levels below the LOD were assumed to be half the LOD during the data analysis. [a]S. D. means standard deviation.

2.4. Quality Control. The analytical quality control scheme included procedural blanks, spiked recovery tests, duplicates, and comparison of standards [3, 6]. A procedural blank and a standard sample were carried out to check any cross-contamination and repeatability in every set of 9 samples. All blanks were below the limits of detection (LOD). The LOD were set to be triple the standard deviation of the blank. The LOD of target OCPs ranged from 0.04 to 0.3 $ng \cdot L^{-1}$. The mean recoveries for surrogates (TCmX) were 79.5 ± 12.2%. Spiked recovery tests of the OCPs using 20 ng of composite standards showed acceptable recoveries ranging from 72.4% to 105%, with the relative standard deviation less than ±14.1%. The calibration curves had acceptable degree of linearity ($R^2 > 0.997$) for all the compounds.

3. Results and Discussion

3.1. Temporal Characteristics of OCPs. The seasonal concentrations of the target analytes in the surface water from Jiuxi Valley are presented in Table 1. In the investigation, the total OCPs concentration in spring was different from that in autumn. During the wet season in spring, the total OCPs concentration varied from 4.07 to 13.5 $ng \cdot L^{-1}$ (mean: 7.15 $ng \cdot L^{-1}$). During the dry season in autumn, the total OCPs concentration varied from 12.5 to 30.1 $ng \cdot L^{-1}$(mean: 19.8 $ng \cdot L^{-1}$). The difference indicated that the total OCPs concentration in surface water of Jiuxi Valley had seasonal characteristics.

Generally, when the rainfall is relatively high, the land runoff of the farmland will increase the erosion by stream, and some OCPs can be released to water from the soil, resulting in an increase in OCPs [10]. Moreover, turbulence caused by rainfall drainage can also lead to the rerelease of OCPs in suspended sediments [11]. The higher level of OCPs found during autumn might be partially attributed to less water flowing. While in spring, the concentration of OCPs was diluted by the stream owing to rich rainfall, and the soil was not easily eroded because of the large vegetation coverage near the valley and the solidification of asphalt or concrete pavement, which resulted in the relatively lower level of OCPs.

The highest concentrations of OCPs in samples were detected at S5 (30.1 $ng \cdot L^{-1}$ in autumn) and S6 (13.5 $ng \cdot L^{-1}$ in spring), and the lowest was at S9 (4.07 $ng \cdot L^{-1}$ in spring and 12.5 $ng \cdot L^{-1}$ in autumn). Sampling point S9 was connected with a wetland park. Meanwhile, the OCPs were diluted with large amounts of water flowed through S9. While the sampling points S5 and S6 were situated upstream, the vegetation coverage was relatively large, and the water environment was relatively stable. Therefore, the levels of OCPs in Jiuxi Valley were mainly affected by the convergence of stream current and the external environment.

In the upper reaches of the river, the levels of OCPs at S1 and S2 were relatively low in spring and autumn compared to S3, S4, S5, and S6. S1 and S2 were situated in the neighborhoods, where the soil was rarely exposed and the use of OCPs was limited. S3, S4, S5, and S6 were situated in agricultural areas, and the OCPs were used in agriculture pest control for decades, resulting in high residual levels.

In recent years, many OCPs contaminations in surface waters had been reported around the world (Table 2). The investigation showed that Jiuxi Valley was slightly contaminated by OCPs. The concentrations of ΣHCHs and ΣDDTs in the river were at relatively low levels. It was difficult to assess large-scale temporal changes in water quality of Jiuxi Valley due to lack of previous studies.

3.2. Seasonal Compositions of OCPs. Changes in the concentrations and compositions of isomers and derivatives of OCPs in the environment keep ongoing, which are connected with the physicochemical properties of the environmental medium and the duration of compounds' exposure [18]. The concentration changes of HCHs and DDTs were studied to identify the seasonal pollution characteristics.

For the individual compounds, four types of HCHs and aldrin were detected at different sampling sites. Four types of DDTs, heptachlor, and endrin were detected at multiple sampling sites.

Table 2: Comparison of ΣHCHs and ΣDDTs in surface waters (ng·L^{-1}).

Location	ΣHCHs	ΣDDTs	Reference
Yongding river	<0.08–13.87 (spring), <0.08–19.53 (summer)	<0.12–194.34 (spring), <0.12–88.68 (summer)	[10]
Honghu lake	0.95–7.04 (dry season), 0.79–4.00 (wet season)	0.06–0.49 (dry season), 0.15–0.82 (wet season)	[11]
River Ravi	2.15–12.73 (postmonsoon), 2.53–6.90 (premonsoon)	4.09–33.28 (postmonsoon), 3.36–93.15 (premonsoon)	[13]
Lake Small Baiyangdian	0.53–6.81	N.D.	[14]
Poyang Lake	4.38–59.65	2.31–33.4	[15]
River Hooghly	8–114	N.D.–26	[16]
River Chenab	3.6–200 (summer), <6.7–330 (winter)	0.55–550 (summer), 0.63–580 (winter)	[17]
Jiuxi Valley	1.71–8.12 (spring), 9.94–23.5 (autumn)	1.19–3.31 (spring), 1.90–6.23 (autumn)	This study

Figures 2, 3(a), and 3(b) showed the seasonal compositions of OCPs. In the spring, HCHs were the dominant compounds, contributing 51.6% to the total OCPs, whereas DDTs contributed 31.2% to the total OCPs. Of all HCH isomers investigated, α-HCH was the dominant chemical with the highest level at S6 (5.24 ng·L^{-1}). Among all DDT isomers surveyed, p,p′-DDT was detected with the highest level at S8 (1.84 ng·L^{-1}). In the autumn, HCHs were also the main pollutant, contributing 72.7% to the total OCPs, whereas DDTs contributed 16.4% to the total OCPs. Also, α-HCH and p,p′-DDT were still in large quantities: α-HCH made up 48.6% of the total HCHs, and the maximum concentration was found at S5 (13.0 ng·L^{-1}), whereas p,p′-DDT made up 44.4% of the total DDTs, and the maximum concentration was detected at S6 (2.12 ng·L^{-1}). p,p′-DDE and p,p′-DDD were observed at relatively low levels in most locations.

At most sampling points in the Jiuxi Valley, α-HCH was the main component of the HCH isomers, which was mainly because of the composition of the technical-grade HCHs. Technical-grade HCH typical contained 55%–80% α-HCH [19–21], and technical-grade HCH and DDT were extensively used in the late 60s and 70s in China [11]. Compared to the other three HCH isomers, β-HCH was nonvolatile and more persistent [10]; therefore, it was more likely to accumulate in the environment and accounted for a relatively large proportion of HCHs in Jiuxi Valley. p,p′-DDT was the main pollutant of DDTs mainly because the technical-grade DDT contained approximately 75% p,p′-DDT [22–24]. In addition, o,p′-DDT also contributed a relatively large proportion of DDTs. Although DDTs were restricted in 1983, China was still producing DDTs due to the production of dicofol. o,p′-DDT and other DDTs remained in the dicofol product as impurities, and o,p′-DDT was the most abundant in these impurities [25]. Dicofol was one of the commonly used insecticides in agriculture, and the sale and use of dicofol in China were not completely banned until 2018.

3.3. Sources Identification of OCPs. OCPs participated in various physical and chemical processes after entering the environment. Sources of HCHs and DDTs in surface water might be identified by differences in composition between HCHs or DDTs.

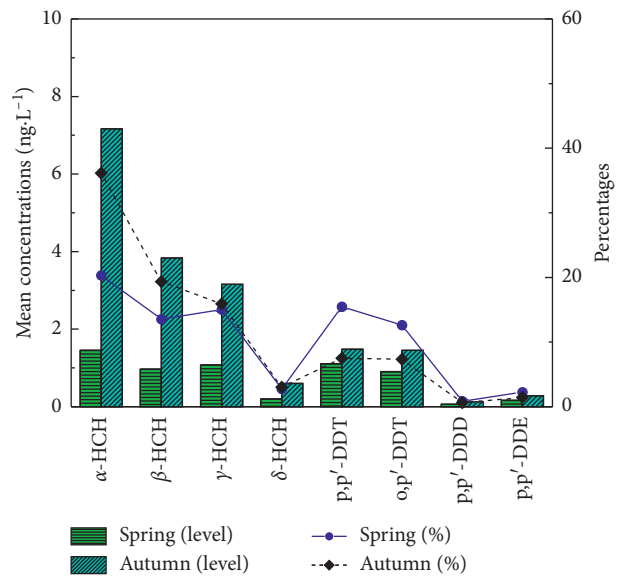

Figure 2: Concentrations and percentages of HCHs and DDTs in surface water from Jiuxi Valley.

HCHs in the environment were mainly derived from historical pesticide residues. The main sources of HCHs included technical-grade HCH and lindane. Technical-grade HCH typically contained 10–15% γ-HCH, while lindane was mainly compounded of γ-HCH (>99%) [26]. The concentration ratio of α-HCH/γ-HCH was often applied to estimating the source of HCHs. In general, this ratio was in the range of 3–7 for technical-grade HCH. The ratios less than 3 indicated the use of lindane was the main source, and ratios above 7 suggested great distances migration or recirculation of technical-grade HCH in the environment [26, 27]. Furthermore, γ-HCH could be isomerized into α-HCH under ultraviolet radiation during long-distance migration, which might make the ratio exceed 7 [28, 29]. In this survey, the ratios of α-HCH/γ-HCH in the surface water of Jiuxi Valley were less than 3, which revealed that the HCHs of Jiuxi Valley were primarily derived from local use of lindane or input of fresh γ-HCH. Actually, the production, use, import, and export of lindane were not banned until March, 2019 [30].

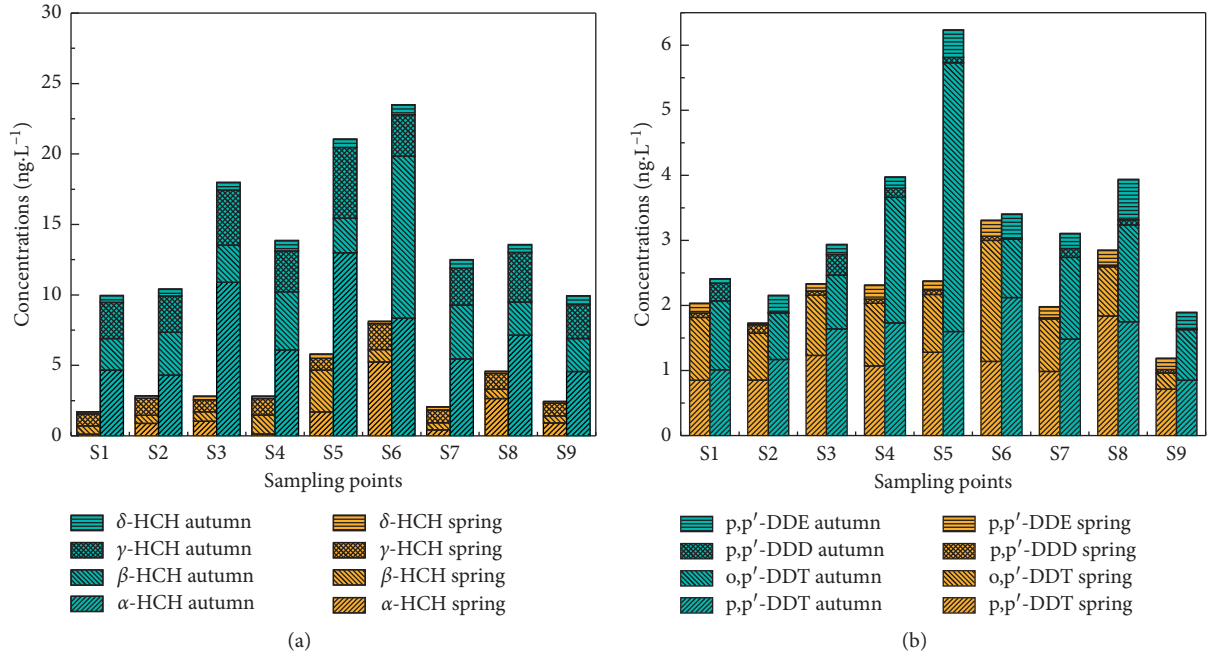

Figure 3: Seasonal compositions and of HCHs (a) and DDTs (b) of sampling points.

Table 3: Surface water OCPs concentration standards ($\mu g \cdot L^{-1}$).

Country/Organization	γ-HCH	DDTs	Heptachlor	Aldrin	Dieldrin	Endrin	Isodrin
China	2.0	1.0	–	–	–	–	–
United States	0.95	1.1	0.52	3.0	0.24	0.086	–
European union	–	0.025	–	0.01[a]			
Canada	0.01	–	–	–	–	–	–

Note. "–" denotes "no data"; "a" means the sum of aldrin, dieldrin, endrin, and isodrin.

p,p′-DDT can be degraded to p,p′-DDE and p,p′-DDD under aerobic conditions and anaerobic conditions, respectively [31, 32]. The concentration ratio of p,p′-(DDE + DDD)/DDT can be applied to estimating the source of DDTs [33, 34]. p,p′-(DDE + DDD)/DDT > 1 indicated that local DDT residues were the primary source, and less than 1 indicated a new DDT input source [35, 36]. In this survey, the ratio of p,p′-(DDE + DDD)/DDT in the surface water of Jiuxi Valley was less than 1 at all sampling points, which suggested that Jiuxi Valley has a new input source for DDT contamination.

Other OCPs (including aldrin, heptachlor, and endrin) had been detected in most water samples of Jiuxi Valley, although they had never been used extensively in the region. These compounds might come from other regions and entered the Jiuxi Valley through atmosphere flow. Although many of these chemicals were forbidden in most areas of the Northern Hemisphere, they are still used in Southeast Asia [37, 38]. In addition, probably 45–80% of OCPs migrated to the rest of the earth [39, 40].

3.4. Potential Ecological Risk Evaluation. Water quality criteria are critical guidelines on ecological risk evaluation and water environment management. Some water quality standards and guidelines (as shown in Table 3) were applied for the evaluation of OCPs contamination and potential risks of surface water from Jiuxi Valley.

Chinese standards of surface water (GB 3838–2002) specify the limits of γ-HCH and DDT [41]. The results of this investigation indicated that the levels of OCPs in all tested samples were much lower than this standard.

Based on the World Health Organization (WHO) regulations, the limits for the concentration of selected pollutants γ-HCH, δ-HCH, p,p′-DDT, p, p′-DDE, heptachlor, and aldrin are 2, 2, 2, 2 0.03, 0.03 $\mu g \cdot L^{-1}$, respectively [42]. The OCPs levels of this investigation were also within the standard limits set by the WHO.

The European Union Directive 2008/105/EC specifies the DDTs concentration limits and the total concentration limits for aldrin, dieldrin, endrin, and isodrin [43]. The residual concentrations of DDTs in the spring and autumn of Jiuxi Valley surface water were below the standard limits. Due to the lack of concentrations of dieldrin and isodrin, it was difficult to ascertain whether the total concentration of the sum of aldrin, endrin, dieldrin, and isodrin exceeded the limits of the instruction.

The Canadian CCME specifies the γ-HCH concentration limit [44]. The γ-HCH residual concentrations in the spring and autumn of Jiuxi Valley surface water were also below the standard limits.

Table 4: National recommended water quality standards for OCPs ($\mu g \cdot L^{-1}$).

OCPs	For human health			For aquatic organisms (freshwater)		
	Consumption water and organism	Consumption organism only	Publication year	Acute toxicity	Chronic toxicity	Publication year
α-HCH	0.00036	0.00039	2015	—	—	
β-HCH	0.0080	0.014	2015	—	—	
γ-HCH	4.2	4.4	2015	0.95	—	1995
p,p′-DDD	0.00012	0.00012	2015	—	—	
p,p′-DDE	0.000018	0.000018	2015	—	—	
p,p′-DDT	0.000030	0.000030	2015	1.1	0.001	1980
Aldrin	0.00000077	0.00000077	2015	3.0	—	1980
Heptachlor	0.0000059	0.0000059	2015	0.52	0.0038	1980
Endrin	0.03	0.03	2015	0.086	0.036	1995

Note. "—" denotes "no data."

As shown in Table 4, EPA developed OCPs criteria of ambient water quality for the environment and human health on the basis of toxicological information [45]. Human health ambient water quality standards represent specific concentration of particular chemicals in water that are not expected to adversely affect human health. Aquatic organism standards represent the highest concentration of particular contaminants in water that are not expected to cause major risks to most aquatic organisms. In this investigation, except for the p,p′-DDT concentration of individual sampling points, the levels of OCPs in Jiuxi Valley were lower than the standard values of chronic toxicity water quality of freshwater aquatic organisms. However, although the γ-HCH at all sampling sites, endrin concentrations at all sampling sites, and β-HCH concentrations at most sampling sites were below the human health water quality standard, and the levels of other tested OCPs (α-HCH, p,p′-DDD, p,p′-DDE, p,p′-DDT, aldrin, and heptachlor) exceeded the value of EPA recommended water quality criteria for human health. In particular, the aldrin concentration in the autumn at sampling site S6 was 3,822 times the standard value. With these in mind, OCPs pollution might pose ecological risks to physical health in the district and have limited impact on freshwater aquatic organisms.

4. Conclusions

In present work, the contamination profiles of 11 OCPs in surface water of Jiuxi Valley were determined. The results showed Jiuxi Valley was slightly contaminated by OCPs, and the level of total OCPs in autumn was higher than that in spring. HCHs were the main pollutant in spring, also in autumn, and α-HCH was the main component of the HCH isomers at most sampling points. The HCHs of Jiuxi Valley were mainly derived from the local use of lindane or input of fresh γ-HCH. New inputs were the major sources of DDTs, aldrin, heptachlor, and endrin. The OCP levels of this investigation were within the standard limits set by most of the water quality standards and guidelines. However, although the γ-HCH concentrations at all sampling sites, endrin concentrations at all sampling sites, and β-HCH concentrations at most sampling sites were below the human health water quality standard, the levels of other tested OCPs (α-HCH, p,p′-DDD, p,p′-DDE, p,p′-DDT, aldrin, and heptachlor) exceeded the value of EPA-recommended water quality criteria for human health, indicating potential risks to human health in the region. In future work, more effort should be directed towards OCPs in sediments to explore migration and transformation of OCPs between water and the sediment.

Data Availability

The data used to support the findings of this study are available from the corresponding author upon request.

Conflicts of Interest

The authors declare that they have no conflicts of interest.

Acknowledgments

This work was supported by the Open Research Fund Program from Fujian Engineering and Research Center of Rural Sewage Treatment and Water Safety (RST201805), Research Climbing Program of Xiamen University of Technology (XPDKQ19015), and Innovation Program of XMUT University Students (201811062190).

References

[1] W. Wang, J. Bai, G. Zhang et al., "Depth-distribution, possible sources, and toxic risk assessment of organochlorine pesticides (OCPs) in different river sediment cores affected by urbanization and reclamation in a Chinese delta," *Environmental Pollution*, vol. 230, pp. 1062–1072, 2017.

[2] K. E. Zimmer, M. Montaño, I. Olsaker et al., "In vitro steroidogenic effects of mixtures of persistent organic pollutants (POPs) extracted from burbot (Lota lota) caught in two Norwegian lakes," *Science of the Total Environment*, vol. 409, no. 11, pp. 2040–2048, 2011.

[3] C. Zhao, H. Xie, J. Zhang, J. Xu, and S. Liang, "Spatial distribution of organochlorine pesticides (OCPs) and effect of soil characters: a case study of a pesticide producing factory," *Chemosphere*, vol. 90, no. 9, pp. 2381–2387, 2013.

[4] J. Fu, B. Mai, G. Sheng et al., "Persistent organic pollutants in environment of the Pearl River Delta, China: an overview," *Chemosphere*, vol. 52, no. 9, pp. 1411–1422, 2003.

[5] D. Pimentel, "Amounts of pesticides reaching target pests: environmental impacts and ethics," *Journal of Agricultural and Environmental Ethics*, vol. 8, no. 1, pp. 17–29, 1995.

[6] J. Feng, M. Zhai, Q. Liu, J. Sun, and J. Guo, "Residues of organochlorine pesticides (OCPs) in upper reach of the Huaihe River, East China," *Ecotoxicology and Environmental Safety*, vol. 74, no. 8, pp. 2252–2259, 2011.

[7] U. Ali, J. H. Syed, R. N. Malik et al., "Organochlorine pesticides (OCPs) in South Asian region: a review," *Science of the Total Environment*, vol. 476-477, pp. 705–717, 2014.

[8] M. Miclean, O. Cadar, E. A. Levei, and D. A. Todea, "Human health risk assessment of organochlorine compounds associated with raw milk consumption in a Romanian industrial area," *Italian Journal of Food Science*, vol. 30, pp. 116–127, 2018.

[9] M. Miclean, O. Cadar, C. Tanaselia, A. Gog, M. Senila, and I. S. Groza, "Levels of metals and organochlorine compounds in seafood consumed in Cluj-Napoca, Romania," *Environmental Engineering and Management Journal*, vol. 11, no. 1, pp. 133–140, 2012.

[10] Y. Wang, S. Zhang, W. Cui, X. Meng, and X. Tang, "Polycyclic aromatic hydrocarbons and organochlorine pesticides in surface water from the Yongding River basin, China: seasonal distribution, source apportionment, and potential risk assessment," *Science of the Total Environment*, vol. 618, pp. 419–429, 2018.

[11] L. Yuan, S. Qi, X. Wu, C. Wu, X. Xing, and X. Gong, "Spatial and temporal variations of organochlorine pesticides (OCPs) in water and sediments from Honghu Lake, China," *Journal of Geochemical Exploration*, vol. 132, pp. 181–187, 2013.

[12] J. Sheng, X. Wang, P. Gong et al., "Monsoon-driven transport of organochlorine pesticides and polychlorinated biphenyls to the Tibetan Plateau: three year atmospheric monitoring study," *Environmental Science & Technology*, vol. 47, no. 7, pp. 3199–3208, 2013.

[13] M. Baqar, Y. Sadef, S. R. Ahmad, A. Mahmood, J. Li, and G. Zhang, "Organochlorine pesticides across the tributaries of River Ravi, Pakistan: human health risk assessment through dermal exposure, ecological risks, source fingerprints and spatio-temporal distribution," *Science of the Total Environment*, vol. 618, pp. 291–305, 2018.

[14] Y. Wang, W.-J. Wu, W. He, N. Qin, Q.-S. He, and F.-L. Xu, "Residues and ecological risks of organochlorine pesticides in lake small baiyangdian, north China," *Environmental Monitoring and Assessment*, vol. 185, no. 1, pp. 917–929, 2013.

[15] H. Zhi, Z. Zhao, and L. Zhang, "The fate of polycyclic aromatic hydrocarbons (PAHs) and organochlorine pesticides (OCPs) in water from Poyang Lake, the largest freshwater lake in China," *Chemosphere*, vol. 119, pp. 1134–1140, 2015.

[16] P. Chakraborty, S. N. Khuman, S. Selvaraj et al., "Polychlorinated biphenyls and organochlorine pesticides in river brahmaputra from the outer himalayan range and river hooghly emptying into the bay of bengal: occurrence, sources and ecotoxicological risk assessment," *Environmental Pollution*, vol. 219, pp. 998–1006, 2016.

[17] S. A.-M.-A.-S. Eqani, R. N. Malik, A. Katsoyiannis et al., "Distribution and risk assessment of organochlorine contaminants in surface water from River Chenab, Pakistan," *Journal of Environmental Monitoring*, vol. 14, no. 6, pp. 1645–1654, 2012.

[18] V. Y. Tsygankov, "Organochlorine pesticides in marine ecosystems of the far eastern seas of Russia (2000–2017)," *Water Research*, vol. 161, pp. 43–53, 2019.

[19] J. A. Placencia and S. Contreras, "Organochlorine pesticides in surface waters from Reloncaví Fjord and the inner sea of Chiloé (~ 39.5°S–43°S), Chilean Patagonia," *Marine Pollution Bulletin*, vol. 126, pp. 389–395, 2018.

[20] X. Qiu, T. Zhu, J. Li et al., "Organochlorine pesticides in the air around the Taihu Lake, China," *Environmental Science & Technology*, vol. 38, no. 5, pp. 1368–1374, 2004.

[21] A. Mahmood, R. N. Malik, J. Li, and G. Zhang, "Levels, distribution pattern and ecological risk assessment of organochlorines pesticides (OCPs) in water and sediments from two tributaries of the Chenab River, Pakistan," *Ecotoxicology*, vol. 23, no. 9, pp. 1713–1721, 2014.

[22] R. F. Bopp, H. J. Simpson, C. R. Olsen, R. M. Trier, and N. Kostyk, "Chlorinated hydrocarbons and radionuclide chronologies in sediments of the Hudson River and estuary, New York," *Environmental Science & Technology*, vol. 16, no. 10, pp. 666–676, 1982.

[23] Y. Zhu, H. Liu, Z. Xi, H. Cheng, and X. Xu, "Organochlorine pesticides (DDTs and HCHs) in soils from the outskirts of Beijing, China," *Chemosphere*, vol. 60, no. 6, pp. 770–778, 2005.

[24] Y. Yu, Y. Li, Z. Shen et al., "Occurrence and possible sources of organochlorine pesticides (OCPs) and polychlorinated biphenyls (PCBs) along the Chao River, China," *Chemosphere*, vol. 114, pp. 136–143, 2014.

[25] X. Qiu, T. Zhu, B. Yao, J. Hu, and S. Hu, "Contribution of dicofol to the current DDT pollution in China," *Environmental Science & Technology*, vol. 39, no. 12, pp. 4385–4390, 2005.

[26] J. Gao, H. Zhou, G. Pan, J. Wang, and B. Chen, "Factors influencing the persistence of organochlorine pesticides in surface soil from the region around the hongze lake, China," *Science of the Total Environment*, vol. 443, pp. 7–13, 2013.

[27] Y. F. Li, D. J. Cai, and A. Singh, "Technical hexachlorocyclohexane use trends in China and their impact on the environment," *Archives of Environmental Contamination and Toxicology*, vol. 35, no. 4, pp. 688–697, 1998.

[28] L. A. Barrie, D. Gregor, B. Hargrave et al., "Arctic contaminants—sources, occurrence and pathways," *Science of the Total Environment*, vol. 122, no. 1-2, pp. 1–74, 1992.

[29] K. L. Willett, E. M. Ulrich, and R. A. Hites, "Differential toxicity and environmental fates of hexachlorocyclohexane isomers," *Environmental Science & Technology*, vol. 32, no. 15, pp. 2197–2207, 1998.

[30] Ministry of Ecology and Environment of the People's Republic of China (MEE), *Notice on the Prohibition of the Production, Circulation, Use and Import and Export of Persistent Organic Pollutants*, MEE Web, Beijing, China, 2019, http://www.mee.gov.cn/xxgk2018/xxgk/xxgk01/201903/t20190312_695462.html.

[31] R. Bossi, B. Larsen, and G. Premazzi, "Polychlorinated biphenyl congeners and other chlorinated hydrocarbons in bottom sediment cores of Lake Garda (Italy)," *The Science of The Total Environment*, vol. 121, pp. 77–93, 1992.

[32] T. Heberer and U. Dünnbier, "DDT metabolite bis(chlorophenyl)acetic acid: the neglected environmental contaminant," *Environmental Science & Technology*, vol. 33, no. 14, pp. 2346–2351, 1999.

[33] T. F. Bidleman, "Atmospheric transport and air-surface exchange of pesticides," *Fate of Pesticides in the Atmosphere: Implications for Environmental Risk Assessment*, vol. 115, no. 1-4, pp. 115–166, 1999.

[34] K. T. Lee, S. Tanabe, and C. H. Koh, "Distribution of organochlorine pesticides in sediments from Kyeonggi Bay and nearby areas, Korea," *Environmental Pollution*, vol. 114, no. 2, pp. 207–213, 2001.

[35] K. Jaga and C. Dharmani, "Global surveillance of DDT and DDE levels in human tissues," *International Journal of Occupational Medicine and Environmental Health*, vol. 16, no. 1, pp. 7–20, 2003.

[36] X. Wang, N. Ren, H. Qi, W. Ma, and Y. Li, "Levels, distributions, and source identification of organochlorine pesticides in the topsoils in Northeastern China," *Journal of Environmental Sciences*, vol. 21, no. 10, pp. 1386–1392, 2009.

[37] M. Grung, Y. Lin, H. Zhang et al., "Pesticide levels and environmental risk in aquatic environments in China—a review," *Environment International*, vol. 81, pp. 87–97, 2015.

[38] P. I. Devi, J. Thomas, and R. K. Raju, "Pesticide consumption in India: a spatiotemporal analysis," *Agricultural Economics Research Review*, vol. 30, no. 1, pp. 163–172, 2017.

[39] F. Wania, J. Axelman, and D. Broman, "A review of processes involved in the exchange of persistent organic pollutants across the air-sea interface," *Environmental Pollution*, vol. 102, no. 1, pp. 3–23, 1998.

[40] K. Breivik, R. Alcock, Y. F. Li, R. E. Bailey, H. Fiedler, and J. M. Pacyna, "Primary sources of selected POPs: regional and global scale emission inventories," *Environmental Pollution*, vol. 128, no. 1-2, pp. 3–16, 2004.

[41] Ministry of Ecology and Environment of the People's Republic of China, *Environmental Quality Standards for Surface Water (GB 3838–2002)*, MEE Web, Beijing, China, 2002, http://kjs.mee.gov.cn/hjbhbz/bzwb/shjbh/shjzlbz/200206/t20020601_66497.shtml.

[42] D. J. Hamilton, Á. Ambrus, R. M. Dieterle et al., "Regulatory limits for pesticide residues in water (IUPAC technical report)," *Pure and Applied Chemistry*, vol. 75, no. 8, pp. 1123–1155, 2003.

[43] European Union, *Directive 2008/105/EC of the European Parliament and of the Council of 16 December 2008*, EU Publications Web, Brussels, Belgium, 2008, https://eur-lex.europa.eu/legal-content/EN/TXT/?uri=CELEX%3A32008L0105.

[44] Canadian Council of Ministers of the Environment (CCME), *Canadian Environmental Quality Guidelines*, CCME Web, Winnipeg, Canada, 2015, http://st-ts.ccme.ca/en/index.html.

[45] United States Environmental Protection Agency (USEPA), *Current Water Quality Criteria Tables*, USEPA Web, Washington, DC, USA, 2015, https://www.epa.gov/wqc.

Hindawi
Journal of Chemistry
Volume 2020, Article ID 7971294, 13 pages
https://doi.org/10.1155/2020/7971294

Research Article

Spatial Variations and Potential Risks of Heavy Metals in Seawater, Sediments, and Living Organisms in Jiuzhen Bay, China

Xia Sun,[1] Bao-Shi Li,[1] Xuan-Li Liu,[1] and Cheng-Xuan Li[2,3]

[1]*Marine Ecology Research Center, The First Institute of Oceanography, Ministry of Natural Resources of China, Qingdao 266061, China*
[2]*Laboratory for Marine Ecology and Environmental Science, Qingdao National Laboratory for Marine Science and Technology, Qingdao 266237, China*
[3]*Key Laboratory of Science and Technology of Marine Ecological Environment, The First Institute of Oceanography, Ministry of Natural Resources of China, Qingdao 266061, China*

Correspondence should be addressed to Cheng-Xuan Li; cxli@fio.org.cn

Received 18 October 2019; Revised 23 December 2019; Accepted 9 January 2020; Published 3 February 2020

Guest Editor: Yuhe He

Coastal waters are polluted by heavy metals to varying degrees, posing potential risks to marine ecology and human health. In May 2006, the pollution levels, sources, and ecological risks of heavy metals (Cu, Pb, Zn, Cd, Hg, and As) in seawater, surface sediments, and living organisms were studied in Jiuzhen Bay in Fujian, China. This study identified Hg (0.26–0.72 μg/L) and As (20.3–31.5 μg/L) pollution in the seawater of Jiuzhen Bay. In sediments, heavy Pb pollution (946 μg/g dw) was only detected at one station at a level posing very serious potential risk, while Hg pollution (0.052–0.087 μg/g dw) was observed at three stations at a level posing serious potential risk. No heavy metal pollution was detected in sediments at other stations. The concentrations of five heavy metals (Cu, Zn, As, Cd, and Pb) exceeded the corresponding National Quality Standards for oysters, indicating heavy pollution, based on an ecological risk assessment. In clams, two heavy metals (Pb and As) exceeded the standards, indicating light pollution, based on an ecological risk assessment. No heavy metal pollution was found in fish or shrimps. The heavy metals in the seawater and sediments of Jiuzhen Bay are mainly derived from the river discharges of Luxi and Wujiang Rivers although sewage discharge along the coast of Jiuzhen Bay is another source of heavy metal pollution at some stations. Given the pollution of Pb, Hg, and As in seawater and sediments at some stations within the bay, the potential risks of Pb, Hg, and As in living organisms to both the marine ecology and human health deserve increased attention.

1. Introduction

Over the past 40 years, because of rapid industrialization and economic development in China, the problem of soil contamination by heavy metals has become increasingly serious [1], with large amounts of these soil pollutants being discharged into coastal and estuarine environments by rivers and other pathways [2, 3]. Compared with other pollutants, heavy metals are persistent and have toxic as well as bioaccumulation effects, which severely damage marine environments [4]. Therefore, heavy metal contamination has attracted much attention and become the focus of global concern in recent years. Estuaries and coastal regions (such as bays) are important components of coastal systems, receiving large amounts of heavy metals via riverine input [5–7].

Estuaries are zone of complex interaction between fluvial and marine ecosystems in which many critical environmental processes including sediment deposition, fresh water-salt water interaction, delta accretion, pollutant retention, and material-energy exchanges occur. Particularly, the mixing of continental river water and marine salt water usually leads to flocculation and accumulation processes of heavy metals [8]. Although metal-aquo chemistry is the main factor affecting the removal and transformation of heavy metals, sediment type also has a major effect on transport and accumulation of heavy metals. Therefore, the spatial patterns of heavy metals are

closely related to sediment types [9]. The spatial distributions of heavy metals are often consistent with those of fine-grained sediments [10]. Most heavy metals become part of the sediment through different biogeochemical processes, which trigger precipitation and deposition [11]. Heavy metals do not behave conservatively, and they are also affected by changing physicochemical conditions, such as salinity, pH, and redox conditions [12]. When sedimentary environments change, the heavy metals in the sediment may be released back into the water body through various processes of remobilization, producing secondary pollution within the environment [13]. Therefore, marine sediments are considered an important sink of heavy metals, especially in coastal areas.

Heavy metals in seawater and marine sediments can be directly absorbed by organisms and then accumulated and transformed within their bodies. Accumulation may be magnified via the food chain, thereby threatening the marine ecosystem and human health [14–16]. Zhao et al. [17] reported that some seafood from Xiangshan Bay might pose noncarcinogenic risks to both adults and children. Although consumption of most common types of seafood from Xiamen markets does not pose a noncarcinogenic risk, some types, such as yellowfin bream (*Sparus latus*), oyster, and the Red alga (nori; *Porphyra tenera*), could form a carcinogenic risk [18]. The levels of five metals in marine fish and shellfish from China are generally low, based on published data. However, some findings suggest that there are health risks from exposure to Cd and As in some shellfish [19]. Considering the pollution of heavy metals in seawater and sediments in coastal areas, the risk of heavy metal pollution in seafood deserves greater attention.

Jiuzhen Bay is located on the southern coast of Fujian, between Gulei and Liu'ao Peninsulas. It is a concave, semienclosed shallow bay, forming an estuary. Its coastline is 45.97 km in length, with a total embayed area of 69.64 km^2. The entire bay is occupied by an intertidal shoal, except for its tidal channel. The intertidal area accounts for about 80% of the bay area. The tidal inlet runs from the bay's mouth to the Luxi River outlet [20]. Jiuzhen Bay has rich marine biological resources and is an important marine aquaculture base in Fujian. The main aquaculture species are shellfish. Along the coast of Jiuzhen Bay, there are multiple industries, such as wind power generation, shipbuilding, placer mining, seafood processing, and shipping. In addition, the nearby Gulei Port Economic Development Zone is one of the seven petrochemical bases in China. The pollutant discharges from these various industrial enterprises may be causing serious environmental impacts on Jiuzhen Bay.

Given the environmental and sedimentation characteristics of Jiuzhen Bay, most of the heavy metals entering Jiuzhen Bay accumulate within the bay. To date, there has been no research on the distribution and ecological risk of heavy metals in seawater, sediments, or seafood of Jiuzhen Bay. The purpose of this study was to (1) determine the contents and distributions of various heavy metals in seawater, sediments, and living organisms within the bay; (2) analyze the sources of these heavy metals; and (3) evaluate the degree of heavy metal pollution, using the single-factor pollution index, comprehensive index evaluation, and potential ecological risk index.

The data provided here will assist the local government to monitor the change in the heavy metal pollution status of this area and implement targeted control measures.

2. Materials and Methods

2.1. Sample Collection. A total of nine stations were investigated during the survey of May 2006, as shown in Figure 1. A GO-FLO water sampler (General Oceanics, Inc., Miami, FL, USA) was used for sample collection. Water only within the surface layer was collected at stations, where water depths were less than 5 m (A1, B1, and B2), while water samples from surface (Sur) and bottom (Bot) layers were collected at stations with water depths of 5–20 m (B3, C1, C2, and E1–E3). Water samples were preserved at −20°C for later analysis. Sediment samples were collected using a grab bucket-type bottom sampler; sediments from the 0–2 cm surface layer were placed in a polyethylene sealing bag and preserved at −20°C for later analysis.

Biological samples were collected by trawling, and strict criteria were used to select adults of local representative biological species for the study. Specimens were preserved at −20°C for later analysis.

2.2. Laboratory Analysis. Six heavy metals—Cu, Pb, Zn, Cd, Hg, and As—in seawater, sediments, and living organisms were analyzed in this study.

All water samples were filtered using a hybrid cellulose ester Millipore filter, which was dipped before filtering in acid. The filtrate was acidified to $pH < 2$ with HNO_3 and stored in a Teflon bottle.

Before analysis of the sediment samples, they were freeze-dried. All large debris was removed, followed by grinding and sieving. Dry sediment samples were dissolved in an equimolar mixture of HF, HNO_3, and $HClO_4$, having a volumetric ratio of 3 : 1 : 0.5, and then evaporated to dryness. The samples were redissolved with aqua regia, and three parts of this metal solution were diluted with HNO_3.

Edible parts of living organisms were removed using biomedical stainless-steel implements, smashed using a stamping machine, blended, and dried in an oven, allowing moisture content to be calculated. Dried biological samples were digested like sediments.

Cu, Pb, Zn, and Cd were analyzed using an Agilent 7500a inductively coupled plasma source mass spectrometer (Agilent Technologies, Inc., Santa Clara, CA, USA), while Hg and As were analyzed using an atomic fluorescent photometer AFS200T (Skyray Instrument, Inc., Stoughton, MA, USA).

Total nitrogen (TN), total phosphorus (TP), dissolved inorganic nitrogen (DIN), dissolved inorganic silicon (DSi), and PO_4 were measured using a spectrophotometric method, while total organic carbon (TOC), redox potential (Eh), and pH were analyzed using $K_2Cr_2O_7$ oxidation-reduction volumetric method and potentiometer and acid meter method, respectively. DIN is the sum of NO_3^-, NO_2^-,

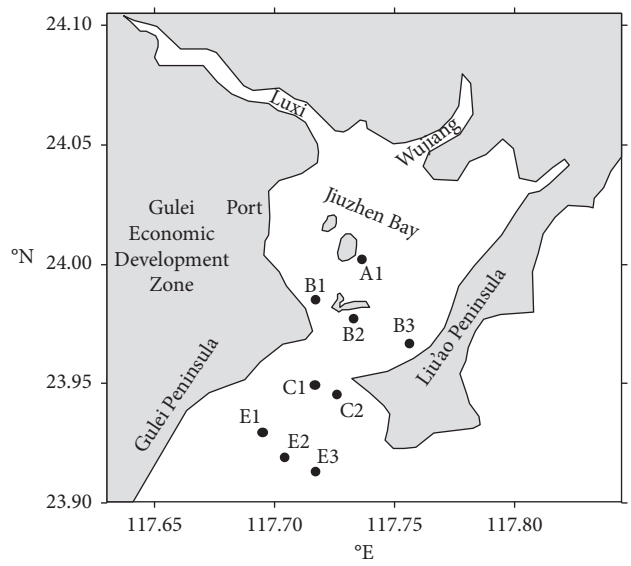

Figure 1: Location of the Jiuzhen Bay study area and all sampling stations.

and NH_4^+. TN, TP, DIN, DSi, and PO_4 were analyzed using a flow injection analyzer (model: Lachat-QC8000). Redox potential (Eh) and pH were determined using an acid meter (model: pHS-3C).

2.3. Quality Control and Quality Assurance. Laboratory quality assurance and quality control methods were practiced, involving standard operating procedures, calibration using standards, and analysis of reagent blanks. All samples were analyzed in parallel at proportions of 10%. Quality control was ensured by measuring nationally certified standard reference materials (GBW07314, GBW080042, GBW080230, GBW080040, and GBW 10050). The differences in the concentrations between the certified and measured values were <5%. The recoveries of all metals were within the range of 85%–99%. The relative measurement error was less than 10%.

2.4. Data Analysis and Evaluation Methods. Pearson correlation analysis was used to quantify relationships among heavy metals. Data calculation and statistics were performed with SPSS 17.0 statistical software (IBM, Armonk, NY, USA) and Microsoft Excel (Microsoft Corp., Albuquerque, NM, USA). The figures in this paper were drawn with Surfer 8 (Scientific Software Group, Salt Lake City, UT, USA).

The single-factor index method was used to evaluate heavy metals in seawater, using the formula below:

$$P_i = C_i \times S_{ij}, \tag{1}$$

where P_i is the heavy metal pollution index, C_i is the concentration value of a given heavy metal, and S_{ij} is the standard value of a given heavy metal. The Type I Standard of the National Seawater Quality Standard (China) was used to obtain standard values of heavy metals in seawater, yielding values for Cu (5 μg/L), Zn (20 μg/L), As (20 μg/L), Cd (1 μg/L), Hg (0.05 μg/L), and Pb (1 μg/L).

Biotoxicity or biological risks of heavy metals in sediments were evaluated using the potential ecological risk index proposed by the Swedish scholar Hakanson [21], using the formula below:

$$E_r^i = T_r^i \times C_r^i = T_r^i \times \frac{C_i}{C_n^i},$$
$$RI = \sum_{i=1}^{n} E_r^i, \tag{2}$$

where T_r^i is the toxicity response coefficient of a heavy metal and those of Hg, Cd, As, Cu, Pb, and Zn are, respectively, set as 40, 30, 10, 5, 5, and 1 [22, 23]; C_r^i is the pollution index of a given heavy metal, also called its enrichment coefficient; C_i is the measured concentration of the given heavy metal in sediments; C_n^i is the background value of the given heavy metal; E_r^i is the potential ecological risk index of the given heavy metal; and RI is the total potential ecological risk index related to multiple heavy metals. The degrees of ecological risk corresponding to E_r^i and RI values are given in Table 1.

The single-factor evaluation method and comprehensive index evaluation method were combined to evaluate heavy metals in living organisms. In this case, the National Quality Standard was a bivalve, referred to as the Type I Standard in *Marine Biological Quality (China) (GB18421-2001)*. Standard values for crustacea and fish are taken from previously determined values from monitoring and evaluation of heavy metal pollution elements in offshore areas [24].

The formula for the comprehensive index evaluation method is given below:

$$P_{ij} = \sqrt{\frac{(\max P_i)^2 + (\text{ave}P_i)^2}{2}}, \tag{3}$$

where P_{ij} is the comprehensive quality index, P_i is the single-factor pollution index, $\max P_i$ is the maximum value of the single-factor pollution index for a given living organism, and $\text{ave}P_i$ is the average value of the single-factor pollution index of a given living organism.

The degree of heavy metal pollution in marine living organisms that correspond to values obtained from the comprehensive index method are given in Table 2.

In this paper, the bioconcentration factors (BCFs) and biota-sediment accumulation factors (BSAFs) were calculated to analyze the bioaccumulation of heavy metals from seawater and sediments in living organisms. The BCFs indicate the status of organisms enriched in heavy metals from the surrounding waters, while the BSAFs evaluate the equilibrium relationship of heavy metal contents in benthic organisms and sediments, i.e., the indirect absorption of heavy metals by benthic organisms from their living environments [25, 26].

The calculations are defined as follows:

Table 1: Degrees of potential risks corresponding to various values of the potential risk index (E_r^i) and total potential ecological risk index (RI).

Range of potential ecological risk index E_r^i of a single heavy metal	Range of total potential comprehensive ecological risk index RI	Degree of potential ecological risk
$E_r^i < 40$	$RI < 150$	Low potential ecological risk
$40 \le E_r^i < 80$	$150 \le RI < 300$	Moderate potential ecological risk
$80 \le E_r^i < 160$	$300 < RI < 600$	Relatively severe potential ecological risk
$160 \le E_r^i < 20$	$RI \ge 600$	Severe potential ecological risk
$E_r^i \ge 320$	—	Very heavy potential ecological risk

Table 2: Grades for the comprehensive quality index (P_{ij}) evaluation of heavy metals in marine living organisms.

Grade	Comprehensive quality index, P_{ij}	Pollution degree
Grade I	$P_{ij} > 3$	Heavy pollution
Grade II	$2 < P_{ij} \le 3$	Medium pollution
Grade III	$1 < P_{ij} \le 2$	Light pollution
Grade IV	$P_{ij} \le 1$	No pollution

$$\mathrm{BCF} = \frac{C_x}{C_{\mathrm{sw}}}, \qquad \mathrm{BSAF} = \frac{C_x}{C_{\mathrm{s}}}, \tag{4}$$

where C_x and C_{sw} are the mean concentrations of a given metal in the organism and in seawater, respectively, while C_{s} is the mean concentration of the metal in the sediment.

3. Results and Discussion

3.1. Distribution Characteristics and Evaluation of Heavy Metal Pollution in Seawater

3.1.1. Distribution Characteristics of Heavy Metals in Seawater. Heavy metal contents in seawater were measured in samples from all stations within Jiuzhen Bay, as shown in Table 3. Analysis of their vertical distributions show that the average values of heavy metals—Cd and Pb—in seawater from the surface layer were higher than those in the bottom layer, while other heavy metal contents (Cu, Zn, As, and Hg) in the surface layer were lower than those in the bottom layer. Zn concentrations in the bottom layer were twice those in the surface layer.

The overall horizontal distribution characteristics were as follows. The distribution of heavy metals (Cu, As, and Hg) in the surface and bottom seawater layers were relatively consistent, both layers showing a decrease from the outer to inner parts of the bay, with highest values within the bay's mouth and outer areas. There was a distinct difference in the distribution of Pb in the surface and bottom seawater layers. An area having a low Pb content occurred on the inner side of the mouth. The Pb content gradually increased in surrounding areas, resulting in a high value at station B1 on the west side of the bay. In the bottom seawater layer, high levels of Pb were detected at stations B3 and C2, while Pb gradually decreased from east to west. An overall decrease from the bay's mouth to outer areas was observed for Cd in both the surface and bottom seawater layers, with the highest values within the mouth area. The distribution of Zn varied greatly in the surface and bottom seawater layers. Although Zn displayed a consistent trend, like those of Cu, As, and Hg in surface seawater, its concentration at station C2 in the bottom seawater layer was 123 μg/L, which was seven times that of surrounding stations. Distributions of all six heavy metals within Jiuzhen Bay are shown in Figure 2.

The contents of heavy metals in seawater measured in the present study were compared with historical data and studies of other regions in China (Table 4). In comparison with historical data [20], the contents of Cu and Cd have increased markedly. Except for the much higher contents of Hg and As, the heavy metal contents determined in the present study were basically consistent with those of the southern Gulf of China [13, 17, 27–29]. This comparison indicates that heavy metal content of the seawater of Jiaozhou Bay was the highest among all documented bays [30].

3.1.2. Main Factors Affecting Dissolved Heavy Metal Distributions in Seawater. According to the correlation analysis between the heavy metals in seawater and environmental factors (Table 5), significant correlations were determined between heavy metals (As, Hg, and Cu) and environmental factors (PO_4, Si, and DIN) ($R > 0.605$, $P < 0.05$, $N = 15$), indicating certain similar sources of the substances. In fact, the sources of heavy metals (As, Hg, and Cu) in seawater are indeed similar to those of PO_4, Si, and DIN, mainly being river water and domestic and industrial wastewater along the coast of Jiuzhen Bay. The distribution trend of heavy metals (As, Hg, and Cu) increased gradually from the mouth of the bay out to sea. The higher concentrations at the mouth were results from the changes in environmental factors such as salinity and redox factors. Specifically, the heavy metals adsorbed by suspended particles in the river water dissolved out, resulting in high contents of As, Hg, and Cu in the seawater at the mouth. This is consistent with the conclusions of Zhang et al. [31], in which study it was proposed that the content of heavy metals in the downstream of the Yellow River was lower than that at the estuary, and the content of dissolved heavy metals was closely related to the adsorption and desorption of heavy metals in suspended particles.

In the seawater of bays and estuaries, heavy metal content is affected by changes in environmental factors such as salinity, hydrodynamics, pH, redox, and biological effects [32, 33]. The investigation sea area is located at the mouth of

Table 3: Heavy metal contents in seawater layers of Jiuzhen Bay (μg/L).

Heavy metal type	Total average value (range)	Average value at the surface layer (range)	Average value at the bottom layer (range)
Cu	4.82 (3.37~6.33)	4.74 (3.37~5.88)	4.94 (4.05~6.33)
Zn	22.0 (8.9~123)	16.7 (11.5~29.2)	30.1 (8.9~123)
As	27.0 (20.3~31.5)	26.3 (20.3~29.8)	27.9 (25.0~31.5)
Cd	0.34 (0.24~0.50)	0.34 (0.24~0.50)	0.32 (0.29~0.35)
Hg	0.46 (0.26~0.72)	0.44 (0.26~0.72)	0.50 (0.39~0.67)
Pb	0.37 (0.25~0.54)	0.37 (0.25~0.45)	0.36 (0.25~0.54)

Jiuzhen bay, which is the mixing region of river water and seawater. Therefore, the environmental factors vary significantly, posing different degrees of impact on different heavy metals, which is the main reason for the poor correlation between heavy metals and environmental factors.

The maximum value of Pb content in surface seawater was located at station B1 of shallow water, which is consistent with the location of the high-value zone in the sediment, indicating that the concentration of Pb in seawater at station B1 was affected by the content of sediment. Upon changes of environmental conditions, the equilibrium between the overlying water and the sediment is broken, resulting in the migration of heavy metal pollutants from the sediment to the water body [12]. The high value area of Pb in bottom seawater was at the east side of the tidal channel, i.e., the Liu'ao Peninsula and the Liu'ao Port. The population on the Liu'ao Peninsula is mainly concentrated in Liu'ao Town. Large amount of sewage discharge from human domestic and industrial activities to the Jiuzhen Bay resulted in the high Pb content on the east side of the tidal channel. The maximum concentration of Zn detected at the C2 station in bottom seawater was also caused by the discharge of domestic and industrial sewage from Liu'ao Town.

The heavy metals in the seawater of the investigation area are mainly originated from the water of Luxi and Wujiang River, as well as the domestic and industrial wastewater along the coast of the Jiuzhen Bay. Moreover, the dissolution of heavy metals from sediments is another source of heavy metals in seawater.

3.1.3. Evaluation of Heavy Metal Pollution in Seawater. Values of the single-factor pollution indices of various heavy metals at each station are given in Table 6, and their respective ranges were Cu (0.67–1.27), Zn (0.45–6.13), As (1.02–1.58), Cd (0.24–0.50), Hg (5.29–14.33), and Pb (0.25–0.54). Typically, the single-factor pollution indices for both Hg and As in Jiuzhen Bay were greater than 1, indicating that both metals exceeded the Type I National Seawater Quality Standard at all stations. Cu and Zn exceeded the type I standard at some stations, at rates of 33% and 13%, respectively. Neither Cd or Pb exceeded the type I threshold. According to average values of single-factor pollution indices for heavy metals, their pollution degree was Hg > As > Zn > Cu > Pb > Cd.

3.2. Distribution Characteristics and Evaluation of Heavy Metal Pollution in Sediments

3.2.1. Distribution Characteristics of Heavy Metals in Sediments. Average heavy metal contents of sediments within Jiuzhen Bay are given in Table 7. Pb had highest values in sediments along the northern coast and in the northwest part of the mouth of the bay; they progressively declined eastward. A high value area of all five heavy metals (Cu, Zn, Cd, Hg, and As) occurred on the northeast side of Jiuzhen Bay. Heavy metal distributions in sediments are shown in Figure 3.

The heavy metal contents in sediments measured in this present study were compared with historical data and studies of other regions (Table 8). Compared with historical data [20], Pb contents have increased markedly, while other heavy metal contents have remained unchanged. In this paper, the heavy metal contents in sediments were lower than those of other marine areas and bays in China [10, 17, 28, 36, 37], except for Pb content, which was much higher than in all other locations.

3.2.2. Main Factors Affecting Heavy Metal Distributions in Sediments. According to our correlation analysis of heavy metals and environmental factors in the sediments (Table 9), a significant positive correlation was determined for Cu, Zn, Cd, Hg, and As ($R > 0.737$; $P < 0.05$, $N = 9$). This suggests these metals have the same mode of accumulation in surface sediments of Jiuzhen Bay. The main source of these heavy metals was land-based pollution. Regarding the effect of environmental factors, the correlation coefficients for total organic carbon (TOC), TP, total nitrogen (TN), and redox potential (Eh) with Cu, Zn, Cd, Hg, and As were all relatively high, showing strong correlations. The reproduction of plankton removes nutrients from fresh water inputs, forming a large amount of organic suspended matter, just like the natural large-scale ecological beds resulting from sewage treatment in Jiuzhen Bay [38]. The heavy metals combine with organic matter and remain suspended in water mixing zones water, before being precipitated. This may be the cause for the high value areas of all five heavy metals (Cu, Zn, Cd, Hg, and As) on both sides of the tidal channel, as well as the higher contents of heavy metals in sediments within the mouth area, compared with further offshore.

Based on a comparison of historical background values [20], the values of Pb in sediments were far higher than those of other heavy metals. In terms of their distributions, the correlations of Pb with other heavy metal elements were nonsignificant. For example, the Pb content at station B1 was tens of times more than those at other stations with serious pollution, indicating that increasing Pb content was related to pollution discharge from land areas on the west side of the bay.

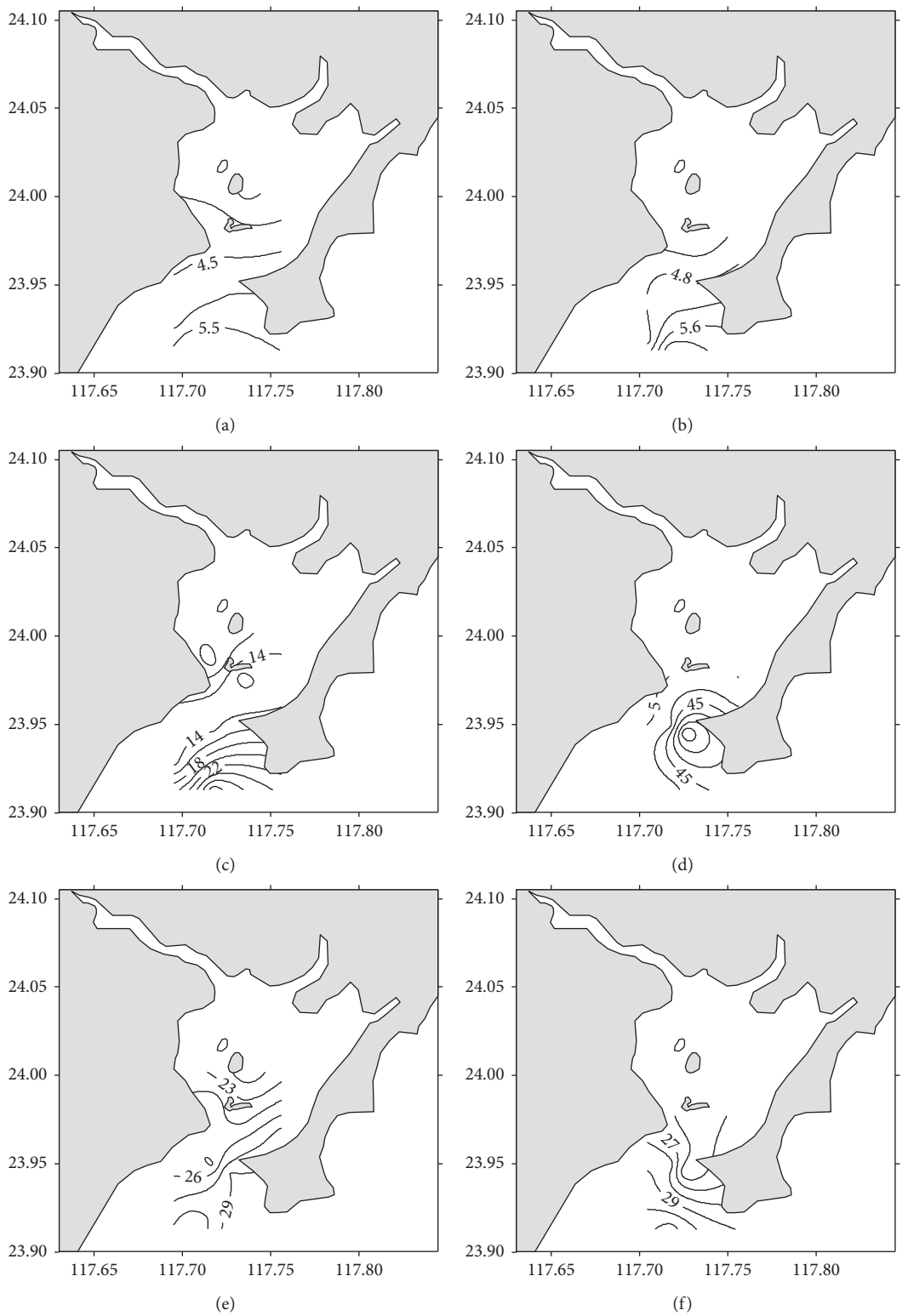

Figure 2: Continued.

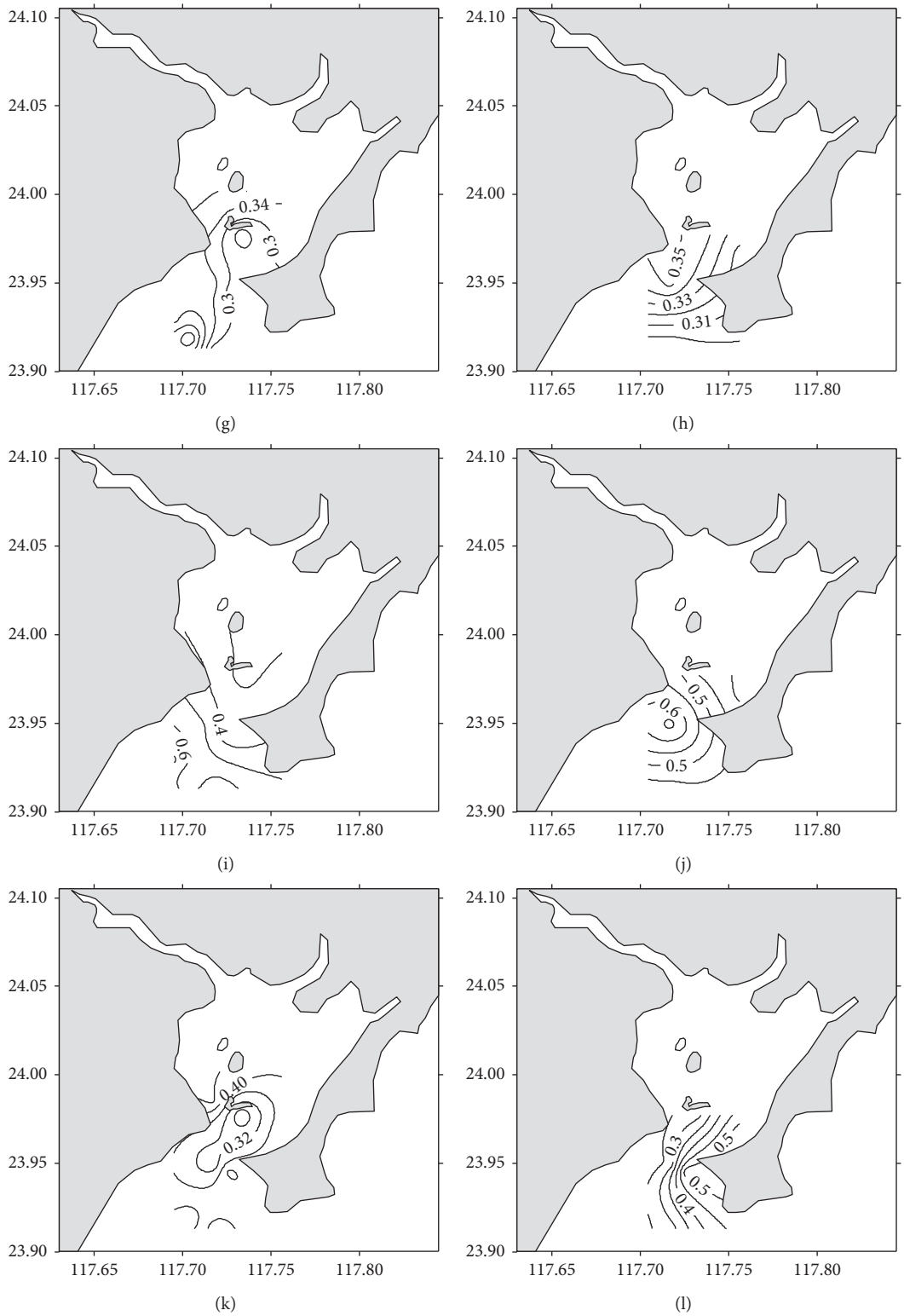

Figure 2: Distributions (surface layer, left panels; bottom layer, right panels) of various heavy metals in the seawater of Jiuzhen Bay (μg/L): (a) Cu Sur; (b) Cu Bot; (c) Zn Sur; (d) Zn Bot; (e) As Sur; (f) As bot; (g) Cd Sur; (h) Cd Bot; (i) Hg Sur; (j) Hg Bot; (k) Pb Sur; (l) Pb Bot.

The contents of Hg and As in the sediments at Futou Bay are higher than those at Jiuzhen Bay [36], related to the polluted discharge from Gulei Peninsula. Evaluation of the seawater and sediments in Jiuzhen Bay shows that Hg pollution was heavier than other heavy metals, suggesting that Futou Bay may be another source of Hg.

Table 4: Concentrations of heavy metals in seawater (μg/l) in the present study compared to published data for other locations in China.

Region	Cu	Pb	Zn	Cd	Hg	As	Reference
Dongshan Bay, China	1.21	1.66	11.1	0.032	—	—	[13]
Xiangshan Bay, China	4.5	2.23	16.8	0.14	0.061	2.6	[17]
East of Qinzhou Bay, China	0.63	—	8.4	428	0.0205	0.845	[27]
Maowei Sea, China	5.6	2.7	48.4	0.38	0.068	0.42	[28]
Bihe Bay, China	2.76	0.655	13.14	0.088	0.036	0.57	[29]
Jiaozhou Bay, China	2108.02	75.74	85.28	2.93	1.55	52.61	[30]
Data of history	0.40	0.33		0.028			[20]
Study area	4.82	0.37	22.0	0.34	0.46	27.0	

Table 5: Matrix chart of correlation coefficients among the heavy metals in the seawater.

	As	Hg	Cu	Pb	Cd	Zn	PO_4	DSi	DIN
As	1								
Hg	0.364	1							
Cu	0.812[a]	0.464	1						
Pb	−0.176	−0.040	−0.080	1					
Cd	−0.045	0.218	0.059	0.324	1				
Zn	−0.153	0.315	0.076	0.485	0.033	1			
PO_4	−0.755[a]	−0.734[a]	−0.605[b]	0.078	−0.129	−0.108	1		
Si	−0.834[a]	−0.634[b]	−0.689[a]	0.024	0.080	−0.187	0.918[a]	1	
DIN	−0.813[a]	−0.667[a]	−0.665[a]	−0.004	0.016	−0.194	0.943[a]	0.985[a]	1

[a]Correlation is significant at the 0.01 level. [b]Correlation is significant at the 0.05 level.

Table 6: Single-factor pollution indices for heavy metals in seawater at all stations of Jiuzhen Bay.

Station	Layer	Cu	Zn	As	Cd	Hg	Pb
A1	Sur	0.67	0.82	1.02	0.38	5.29	0.42
B1	Sur	0.87	0.93	1.27	0.36	7.52	0.45
B2	Sur	0.84	0.57	1.18	0.24	5.43	0.25
B2	Bot	0.81	0.54	1.25	0.35	9.01	0.29
B3	Sur	0.91	0.65	1.41	0.32	7.59	0.40
B3	Bot	0.94	0.45	1.35	0.32	7.71	0.54
C1	Sur	0.94	0.65	1.22	0.36	9.43	0.29
C1	Bot	1.02	0.79	1.43	0.35	13.31	0.27
C2	Sur	1.00	0.79	1.45	0.29	6.16	0.41
C2	Bot	0.97	6.13	1.26	0.34	11.95	0.53
E1	Sur	0.94	0.65	1.37	0.37	14.33	0.38
E2	Sur	1.18	0.98	1.49	0.50	10.07	0.43
E2	Bot	0.92	0.47	1.52	0.30	9.01	0.25
E3	Sur	1.17	1.46	1.44	0.29	13.83	0.34
E3	Bot	1.27	0.66	1.58	0.29	8.54	0.28
Total average		0.96	1.10	1.35	0.34	9.28	0.37

3.2.3. Ecological Risk Evaluation of Heavy Metal Pollution in Sediments. Evaluation results of potential ecological risks of heavy metals in sediments in the surface layer of Jiuzhen Bay are shown in Table 10. Ranges of the ecological risk index (E_r^i) for each heavy metal were Cu (0.54–10.66), Zn (0.17–2.43), As (2.44–5.91), Cd (3–25.97), Hg (5.8–139.5), and Pb (6.3–526.7), respectively. The E_r^i values of Cu, Zn, As, and Cd in sediments were less than 40 at all stations, representing a low degree of potential ecological risk. In contrast, the maximum E_r^i value for Pb in sediments was 526.7 (station B1), which indicates a very serious potential ecological risk. The E_r^i values of Pb at all other stations were less than 40, representing a low degree of potential ecological risk. The E_r^i values of Hg at three stations—A1, B3, and C2—were 83.8–139.5, indicating a relatively high degree of potential ecological risk. However, the E_r^i values of Hg at all other stations were less than 40, representing a low degree of potential ecological risk at other sites. According to the average E_r^i values of heavy metals, potential ecological risks related to single heavy metals were ranked: Pb > Hg > Cd > Cu > As > Zn.

Table 7: Heavy metal contents and background values in sediments of Jiuzhen Bay (μg/g dw).

Heavy metal type	Average value (range)	Background value	Reference
Cu	8.6 (1.1–21)	9.8	[20]
Zn	57 (9–134)	55	
Cd	0.062 (0.016–0.139)	0.056	
Pb	136 (11–946)	9	
As	6.3 (3.7–8.9)	15	[34]
Hg	0.028 (0.004–0.087)	0.025	[35]

The overall range of the potential ecological risk index (*RI*) was 18.9–556.1 in the study area, with a maximum value of 556.1 at station B1, indicating a relatively serious potential ecological risk. The *RI* values of stations A1 and B3 were 222.4 and 166.7, respectively, indicating a moderate potential ecological risk. The *RI* values of all other stations were less than 150, representing low to moderate potential ecological risks. According to average *RI* values of all stations, potential ecological risks linked to sediments at each station were ranked: B1 > A1 > B3 > C2 > B2 > C1 > E1 > E3 > E2.

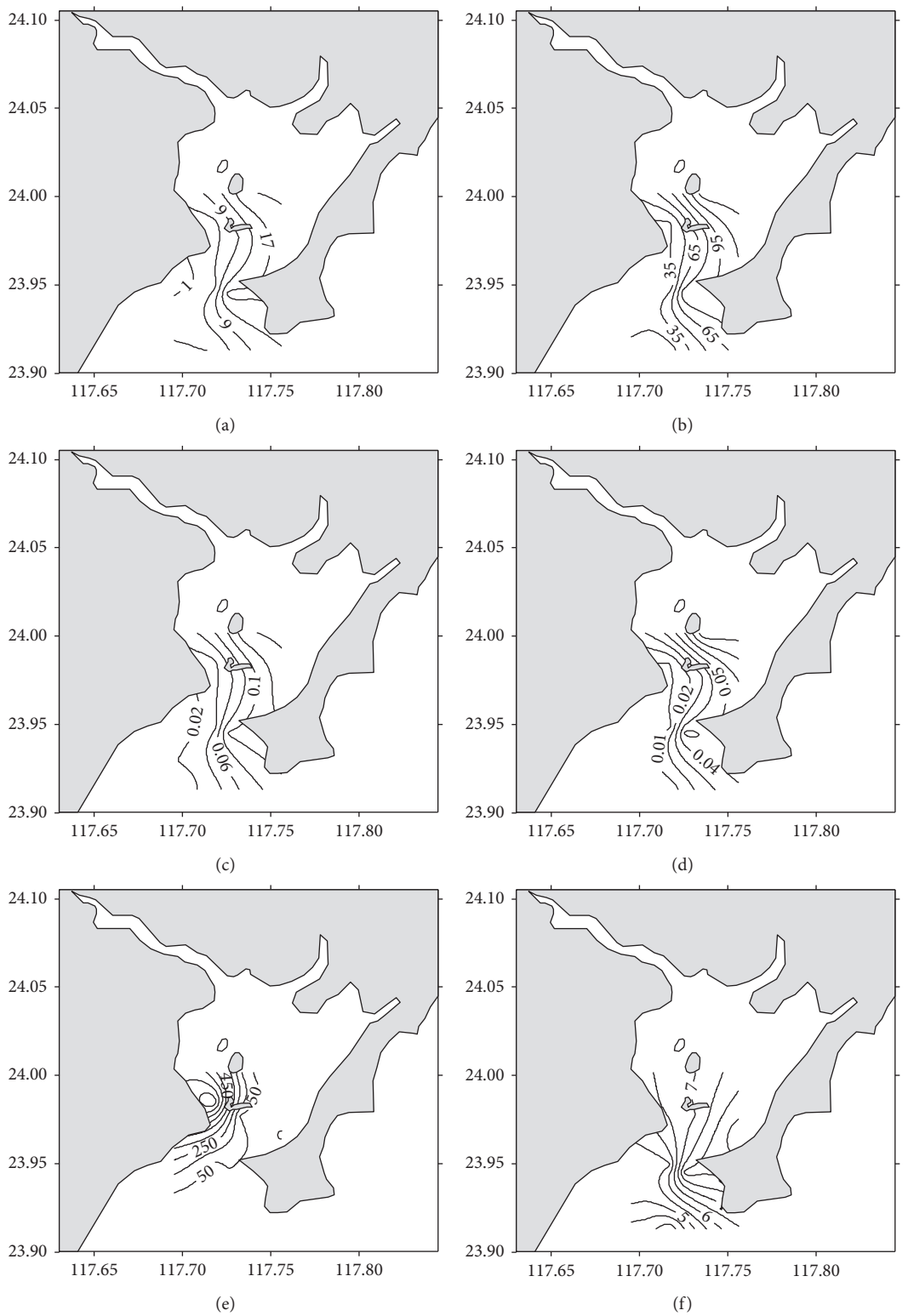

Figure 3: Distributions of various heavy metals in sediments of Jiuzhen Bay (μg/g dw): (a) Cu; (b) Zn; (c) Cd; (d) Hg; (e) Pb; (f) As.

Table 8: Concentrations of heavy metals in sediments (μg/g dw) in the present study compared to published data from other locations in China.

Region	Cu	Pb	Zn	Cd	Hg	As	Reference
Changjiang Subaqueous Delta	26.79	26.55	94.34	0.09			[10]
Zhejiang-Fujian coastal	33.98	37.69	129.26	0.08			
Xiangshan Bay, China	36.8	38.5	120.8	0.15	0.106	12.31	[17]
Maowei Sea, China	30.37	32.10	108.84	0.32	0.07	13.73	[28]
Futou Bay, China	3.54	14.2	25.8		0.079	6.1	[36]
Liaodong Bay, China	19.66	22.64	70.2	0.22	0.056	9.28	[37]
Data of history	9.8	9	55	0.056			[20]
Jiuzhen Bay, China	8.6	136	57	0.062	0.028	6.3	This study

Table 9: Matrix of correlation coefficients among heavy metals and environmental factors in sediments of Jiuzhen Bay.

	Hg	Cu	Pb	Zn	Cd	As	TOC	TP	TN	Eh
Hg	1									
Cu	0.970[a]	1								
Pb	−0.151	−0.158	1							
Zn	0.978[a]	0.983[a]	−0.129	1						
Cd	0.971[a]	0.988[a]	−0.155	0.982[a]	1					
As	0.737[b]	0.850[a]	0.155	0.828[a]	0.819[a]	1				
TOC	0.883[a]	0.921[a]	−0.163	0.909[a]	0.941[a]	0.814[a]	1			
TP	0.944[a]	0.980[a]	−0.160	0.945[a]	0.957[a]	0.811[a]	0.839[a]	1		
TN	0.924[a]	0.966[a]	−0.063	0.936[a]	0.937[a]	0.851[a]	0.804[a]	0.990[a]	1	
Eh	−0.877[a]	−0.914[a]	0.171	−0.944[a]	−0.923[a]	−0.858[a]	−0.858[a]	−0.863[a]	−0.874[a]	1

[a]Correlation is significant at the 0.01 level. [b]Correlation is significant at the 0.05 level. TOC, total organic carbon; TN, total nitrogen; TP, total phosphorus; Eh, redox potential.

3.3. Heavy Metal Contents in Living Organisms and Their Associated Ecological Risks

3.3.1. Heavy Metal Content Characteristics in Living Organisms. Average heavy metal contents of representative living organisms from the study area are shown in Table 11. Cu, Zn, and Cd contents were highly variable in different kinds of living organisms. Average Cu and Cd contents in oysters were 73.19 μg/g ww and 0.748 μg/g ww, respectively; these values were much higher than those in fish (0.23 μg/g ww and 0.001 μg/g ww). The Zn content was highest in oysters (234 μg/g ww), followed by those in shrimps (25.61 μg/g ww) and fish (5.47 μg/g ww). The content of Hg was highest in fish (0.043 μg/g ww) and lowest in clams (0.008 μg/g ww). The contents of Pb and As were highest in oysters, with average values of 0.361 μg/g ww and 3.14 μg/g ww, respectively. The lowest contents of Pb and As were detected in shrimps, with average values of 0.008 μg/g ww and 1.16 μg/g ww, respectively.

Enrichment degrees of most heavy metals in shellfish were higher than those in fish, as reported by many previous researchers [29, 39, 40]. In this study, the contents of five heavy metals (Cu, Zn, As, Cd, and Pb) in oysters were higher than those in all other living organisms. Two heavy metals (Cu and Zn) had high contents in shrimps, but these ranked second to their contents in oysters. The Hg contents in fish were higher than those in other living organisms.

3.3.2. Ecological Risk Evaluation of Heavy Metal Pollution in Living Organisms. Evaluation results of the single-factor pollution index (P_i) and comprehensive pollution index (P_{ij}) of heavy metals in living organisms are shown in Table 12. The evaluation index (P_i) ranges of various heavy metals were Cu (0.01–7.32), Zn (0.14–11.70), As (0.15–3.14), Cd (0–3.74), Hg (0.08–0.50), and Pb (0.03–3.61). The single-factor pollution index of heavy metals varied significantly in different species of living organisms. Although the heavy metal contents in fish and shrimps were all below the National Quality Standards, those in mollusks greatly exceeded the standards. Pb and As contents in clams were above the threshold values of their standards, while all heavy metals (except Hg) in oysters exceeded the standards. The ranking of the pollution indices of heavy metals in oysters was Zn > Cu > Cd > Pb > As > Hg.

The comprehensive pollution index (P_{ij}) of heavy metals in living organisms ranged from 0.13 to 9.00. Oysters displayed the highest comprehensive pollution index, being classified as heavily polluted. This was followed by clams, which were classified as lightly polluted. Heavy metal contents of fish and shrimps were not considered polluted.

3.3.3. Analysis of Enrichment of Different Heavy Metals in Living Organisms. According to the BCF and BSAF values of various organisms (Table 13), the rankings of enrichment coefficients of different heavy metals in seawater according to species were oysters: Cu > Zn > Cd > Pb > As > Hg, clams: Pb > Zn > Cu > Cd > As > Hg, fish: Pb > Zn > Hg > As > Cu > Cd, and shrimps: Cu > Zn > Pb > As > Hg > Cd. Likewise, the rankings of enrichment coefficients of different heavy metals in the sediments according to species were oysters: Cd > Cu > Zn > Hg > As > Pb, clams: Cd > As > Hg > Zn > Cu > Pb, fish: Hg > As > Zn > Cu > Cd > Pb, and shrimps:

Table 10: The ecological risk index (E_r^i) and potential ecological risk index (RI) values for different heavy metals in sediments at all stations within Jiuzhen Bay.

Station	E_{Cu}	E_{Zn}	E_{As}	E_{Cd}	E_{Hg}	E_{Pb}	RI
A1	10.66	2.43	4.73	25.97	139.5	39.1	222.4
B1	1.84	0.61	4.48	6.19	16.3	526.7	556.1
B2	4.77	1.19	4.69	13.41	39.4	18.9	82.3
B3	9.61	2.01	5.91	24.28	91.5	33.4	166.7
C1	1.20	0.40	3.61	4.22	10.2	11.9	31.6
C2	9.23	1.71	5.44	19.22	83.8	27.4	146.8
E1	1.16	0.64	3.39	3.75	9.3	9.4	27.6
E2	0.68	0.17	3.00	3.00	5.8	6.3	18.9
E3	0.54	0.24	2.44	5.53	6.1	6.6	21.5
Average	4.41	1.04	4.19	11.73	44.7	75.5	141.5

Table 11: Heavy metal contents in various living organisms in Jiuzhen Bay (μg/g ww).

Living organism	Cu	Zn	As	Cd	Hg	Pb	Reference
Oyster	73.19	234	3.14	0.748	0.025	0.361	Investigation data in this paper
Clam	1.49	10.77	2.41	0.031	0.008	0.189	
Shrimp	7.66	25.61	1.16	0.005	0.015	0.063	
Fish	0.23	5.47	2.40	0.001	0.043	0.097	
Bivalve mollusk	10	0.1	1.0	0.2	0.05	0.1	Marine biological quality (China) (GB18421-2001)
Shellfish	100	2.0	8.0	2.0	0.20	2.0	[24]
Fish	20	2.0	5.0	0.6	0.30	2.0	

Table 12: Values of the pollution index (P_i) and comprehensive pollution index (P_{ij}) for single-factor heavy metal pollution in various living organisms.

Living organism	P_{Cu}	P_{Zn}	P_{As}	P_{Cd}	P_{Hg}	P_{Pb}	AveP_i	P_{ij}
Oyster	7.32	11.70	3.14	3.74	0.50	3.61	5.00	9.00
Clam	0.15	0.54	2.41	0.16	0.16	1.89	0.88	1.82
Fish	0.01	0.14	0.48	—	0.14	0.05	0.14	0.35
Shrimp	0.08	0.17	0.15	—	0.08	0.03	0.08	0.13
Average value	1.89	3.14	1.54	0.97	0.22	1.40	1.53	2.82

Table 13: Bioconcentration factors (BCFs) and biota-sediment accumulation factors (BSAFs) of various living organisms.

Factor	Living organism	Cu	Zn	As	Cd	Hg	Pb
BCF	Oyster	15185	10636	116	2200	54	976
	Clam	309	490	89	91	17	511
	Fish	48	249	89	3	93	262
	Shrimp	1589	1164	43	15	33	170
BSAF	Oyster	8.47	4.08	0.50	12	0.90	<0.01
	Clam	0.17	0.19	0.38	0.50	0.29	
	Fish	0.03	0.10	0.38	0.02	1.54	
	Shrimp	0.89	0.45	0.18	0.08	0.54	

Cu > Hg > Zn > As > Cd > Pb. The ranking of heavy metal contents in living organisms was not consistent with that of seawater or sediments. This indicates that, at low concentrations, the enrichment of heavy metals is not only related to the concentrations of heavy metals in seawater and sediments but also to many other factors.

In oysters, clams, and shrimps, the enrichment coefficients of Cu, Zn, Cd, and Pb were higher than those of As and Hg. This is because Cu and Zn are essential elements of life; thus, they are actively absorbed by living organisms. Therefore, the ability of marine organisms to be enriched in Cu and Zn was much higher than for nonessential metal elements [41]. Notably, the excretion of Pb and Cd is very slow in most organisms. Because shellfish are filter feeders, and both Pb and Cd complexes in suspension and in the sediments were ingested by and enriched in shellfish [42], accounting for the high enrichment coefficients of Pb and Cd in oysters, clams, and shrimps.

According to Table 13, the enrichment coefficient of Hg was higher in fish than in shellfish. This is caused by the higher capacity of fish to absorb Hg through water and food intake, as well as physiological mechanisms that produce Hg enrichment within their bodies [43].

Studies have suggested that an enrichment coefficient greater than 1000 indicates a potential cumulative problem [25]. In the present study, an enrichment coefficient greater

than 1000 was found for Cu, Zn, and Cd in oysters and Cu and Zn in shrimps, indicating serious accumulation of Cu, Zn, and Cd by oysters and shrimps in Jiuzhen Bay. Although the enrichment coefficients of Pb, Hg, and As were lower than 1000, the pollution levels of Pb, Hg, and As in seawater and sediments were relatively high. Therefore, the ecological and human health risks related to Pb, Hg, and As in the marine organisms of Jiuzhen Bay cannot be neglected.

4. Conclusions

This study reported the contents, distributions, pollution levels, and ecological risks of heavy metals (Cu, Pb, Zn, Cd, Hg, and As) in seawater, sediments, and living organisms of Jiuzhen Bay. The seawater was mainly polluted by Hg and As, while heavy Pb and Hg pollution was detected in sediments at a few stations. The main sources of heavy metal pollution in the marine environments of Jiuzhen Bay are from surface runoff carried by the Luxi and Wujiang Rivers and coastal discharges from local industries. The enrichment coefficients of Cu, Zn, and Cd were high in oysters and clams. According to the comprehensive pollution index values, the heavy metal pollution in oysters and clams was classified as heavy and light pollution, respectively. The heavy metal contents in fish and shrimps did not reach polluted levels. Given the pollution of Pb, Hg, and As in seawater and sediments at some stations within Jiuzhen Bay, the potential risks of Pb, Hg, and As in living organisms to both the local ecology and human health deserve increased attention. To ensure the safety of aquaculture products in Jiuzhen Bay, the sources of heavy metal pollution should be strictly controlled, and the polluted areas should be treated to restore their ecological functions.

Data Availability

No data were used to support this study.

Disclosure

Xia Sun and Bao-Shi Li are the co-first authors.

Conflicts of Interest

The authors declare that they have no conflicts of interest.

Authors' Contributions

Xia Sun and Bao-Shi Li contributed equally.

Acknowledgments

This work was financially supported by the National Natural Science Foundation of China (Grant no. 41676074), the National Key Research and Development Program of China (no. 2018YFC140707600), and the Basic Scientific Fund for the National Public Research Institutes of China (Grant no. 2016Q04).

References

[1] P. Zhang, C. J. Jin, Z. F. Sun, G. H. Huang, and Z. L. She, "Assessment of acid enhancement schemes for electrokinetic remediation of Cd/Pb contaminated soil," *Water Air and Soil Pollution*, vol. 227, no. 6, p. 217, 2016.

[2] G. Hu, S. P. Bi, G. Xu, Y. Zhang, X. Mei, and A. C. Li, "Distribution and assessment of heavy metals off the Changjiang River mouth and adjacent area during the past century and the relationship of the heavy metals with anthropogenic activity," *Marine Pollution Bulletin*, vol. 96, no. 1-2, pp. 434–440, 2015.

[3] J. Lu, A. Li, and P. Huang, "Distribution, sources and contamination assessment of heavy metals in surface sediments of the South Yellow Sea and northern part of the East China Sea," *Marine Pollution Bulletin*, vol. 124, no. 1, pp. 470–479, 2017.

[4] L. Zhang, Z. Shi, J. Zhang, Z. Jiang, F. Wang, and X. Huang, "Spatial and seasonal characteristics of dissolved heavy metals in the east and west Guangdong coastal waters, South China," *Marine Pollution Bulletin*, vol. 95, no. 1, pp. 419–426, 2015.

[5] S. Yin, Y. Wu, W. Xu, Y. Li, Z. Shen, and C. Feng, "Contribution of the upper river, the estuarine region, and the adjacent sea to the heavy metal pollution in the Yangtze Estuary," *Chemosphere*, vol. 155, pp. 564–572, 2016.

[6] Q. Rao, Z. Sun, L. Tian, J. Li, W. Sun, and W. Sun, "Assessment of arsenic and heavy metal pollution and ecological risk in inshore sediments of the Yellow River Estuary, China," *Stochastic Environmental Research and Risk Assessment*, vol. 32, no. 10, pp. 2889–2902, 2018.

[7] Q. Cao, H. Wang, Y. Li et al., "The national distribution pattern and factors affecting heavy metals in sediments of water systems in China," *Soil and Sediment Contamination: An International Journal*, vol. 27, no. 2, pp. 79–97, 2018.

[8] Z. Sun, J. Li, T. He et al., "Spatial variation and toxicity assessment for heavy metals in sediments of intertidal zone in a typical subtropical estuary (Min River) of China," *Environmental Science and Pollution Research*, vol. 24, no. 29, pp. 23080–23095, 2017.

[9] J. Liang, J. Liu, G. Xu, and B. Chen, "Distribution and transport of heavy metals in surface sediments of the Zhejiang nearshore area, East China Sea: sedimentary environmental effects," *Marine Pollution Bulletin*, vol. 146, pp. 542–551, 2019.

[10] C. Wang, X. Zou, Z. Feng, Z. Hao, and J. Gao, "Distribution and transport of heavy metals in estuarine-inner shelf regions of the East China Sea," *Science of the Total Environment*, vol. 644, pp. 298–305, 2018.

[11] Y.-M. Chen, J.-b. Gao, Y.-Q. Yuan, J. Ma, and S. Yu, "Relationship between heavy metal contents and clay mineral properties in surface sediments: implications for metal pollution assessment," *Continental Shelf Research*, vol. 124, pp. 125–133, 2016.

[12] Y. N. Zhang, Q. He, J. M. Chen, C. Lin, and W. D. Ji, "Heavy metals process in water and pollution risk assessment in surface sediments of the ZhuJiang river estuary," *Acta Oceanologica Sinica*, vol. 35, no. 2, pp. 178–186, 2013, in Chinese.

[13] M. F. Yang, S. H. Zheng, Y. Y. Xi, and S. L. Zhong, "The horizontal distribution and affecting factors of dissolved heavy metals in seawater of DongShan bay, fujian Province of China," *Journal of Marine Sciences*, vol. 34, no. 2, pp. 75–82, 2016.

[14] M. M. Mazrouh and M. H. Mourad, "Biochemical composition and bioaccumulation of heavy metals in some seafood in the mediterranean coast of Egypt," *Egyptian Journal of Aquatic Biology and Fisheries*, vol. 23, no. 1, pp. 381–390, 2019.

[15] M. K. Ahmed, M. A. Baki, M. S. Islam et al., "Human health risk assessment of heavy metals in tropical fish and shellfish collected from the river Buriganga, Bangladesh," *Environmental Science and Pollution Research*, vol. 22, no. 20, pp. 15880–15890, 2015.

[16] S. Satapathy and C. R. Panda, "Toxic metal ion in seafood: meta-analysis of human carcinogenic and non-carcinogenic threat assessment, a geomedical study from Dhamra and Puri, Odisha," *Human and Ecological Risk Assessment: An International Journal*, vol. 23, no. 4, pp. 864–878, 2017.

[17] B. Zhao, X. Wang, H. Jin et al., "Spatiotemporal variation and potential risks of seven heavy metals in seawater, sediment, and seafood in Xiangshan Bay, China (2011-2016)," *Chemosphere*, vol. 212, pp. 1163–1171, 2018.

[18] R. Zhao, S. Yan, M. Liu et al., "Seafood consumption among Chinese coastal residents and health risk assessment of heavy metals in seafood," *Environmental Science and Pollution Research*, vol. 23, no. 16, pp. 16834–16844, 2016.

[19] J. L. Cheng, Y. N. Ma, T. T. Liu, and Q. Zhuo, "Accumulation and health risks of heavy metals in the seafood from China," *Journal of Hygiene Research*, vol. 46, no. 1, pp. 148–154, 2017.

[20] F. Chen, *Gulf Chronicles of China-Eighth Fascicle*, China Ocean Press, Beijing, China, 1993.

[21] L. Hakanson, "An ecological risk index for aquatic pollution control.a sedimentological approach," *Water Research*, vol. 14, no. 8, pp. 975–1001, 1980.

[22] W. X. Liu, Z. K. Luan, and H. X. Tang, "Environmental assessment on heavy metal pollution in the sediments of le an river with potential ecological risk index," *Acta Ecologica Sinica*, vol. 19, no. 2, pp. 206–211, 1999.

[23] N. X. Zhang, C. H. Cao, R. Z. Ren et al., "Heavy metals in the surface sediment of the dumping ground outside Jiaozhou bay and their potential ecological risk," *Environmental Science*, vol. 32, no. 5, pp. 1315–1320, 2011.

[24] W. D. Ji, *Monitoring and Evaluation Methods of Heavy Metal Pollution Elements in Offshore*, pp. 196-197, China Ocean Press, Beijing, China, 2015.

[25] N. Sun, W. X. Huang, and H. B. Yu, "Analysis and assessment of heavy metals accumulation feature of sediments and marine organisms from Zhanjiang Harbor," *Marine Environmental Science*, vol. 34, no. 5, pp. 669–672, 2015.

[26] M. Soto-Jiménez, F. Páez-Osuna, and F. Morales-Hernández, "Selected trace metals in oysters (Crassostrea iridescens) and sediments from the discharge zone of the submarine sewage outfall in Mazatlán Bay (southeast Gulf of California): chemical fractions and bioaccumulation factors," *Environmental Pollution*, vol. 114, no. 3, pp. 357–370, 2001.

[27] Y. H. Xu, R. Q. Liao, J. Su, and L. B. Gong, "The content and pollution evaluation of six heavy metals in surface water and plankton in the eastern area of Qinzhou bay," *Oceanologia et Limnologia Sinica*, vol. 48, no. 5, pp. 960–969, 2017.

[28] S. X. LI, S. q Wei, J. L. Lin, and D. B. Wang, "Pollution evaluation of heavy metals in sea water and surface sediments in maowei sea," *Journal of Jianghan University (Natural Science Edition)*, vol. 43, no. 5, pp. 471–476, 2015.

[29] Z. Zeng, C. L. Chen, S. Ke, Z. K. Zhao, and Q. Xie, "The characteristic and evaluation of heavy metal pollution in seawater and organisms of the Bohe Bay," *Ocean Development And Management*, vol. 8, pp. 24–28, 2019.

[30] T. T. Li, L. Wei, Y. L. Lv et al., "On distribution and pollution of heavy metals in water environment of Jiaozhou bay in Yellow sea," *Journal of Southwest China Normal University (Natural Science Edition)*, vol. 41, no. 6, pp. 60–66, 2016.

[31] X. L. Zhang, H. T. Chen, Q. Z. Yao, and X. X. Zhang, "The seasonal changes and flux of trace elements in the lower reaches of Yellow River," *Periodical of Ocean University of China*, vol. 43, no. 8, pp. 69–75, 2013.

[32] Y. Che, Q. He, and W.-Q. Lin, "The distributions of particulate heavy metals and its indication to the transfer of sediments in the Changjiang Estuary and Hangzhou Bay, China," *Marine Pollution Bulletin*, vol. 46, no. 1, pp. 123–131, 2003.

[33] R. P. Gambrell, J. B. Wiesepape, W. H. Patrick Jr., and M. C. Duff, "The effects of pH, redox, and salinity on metal release from a contaminated sediment," *Water, Air, and Soil Pollution*, vol. 57-58, no. 1, pp. 359–367, 1991.

[34] L. X. Zhang, S. Ren, and J. Cai, "Enrichment of heavy metals in the surface sediments from the three regions of random dumping in east China sea and assessment of their potential ecological risk," *Marine Science Bulletin*, vol. 24, no. 2, pp. 92–96, 2005.

[35] F. X. Guo, S. H. Lv, D. Q. Teng, T. Jiang, and Z. P. Jiao, "Distribution patterns and evaluation on potential ecological risk of heavy metals in surface sediments of the Yellow sea," *Journal of Anhui Agricultural Sciences*, vol. 39, no. 15, pp. 9212–9216, 2011.

[36] S. T. Chen, W. L. Wang, and Q. S. Li, "Assessment of environmental quality in seawater and sediment of Futou bay, fujia," *Environment and Sustainable Development*, vol. 3, pp. 156–158, 2017.

[37] J. Wang, S. Y. Ye, E. A. Laws, H. M. Yuan, X. G. Ding, and G. M. Zhao, "Surface sediment properties and heavy metal pollution assessment in the Shallow Sea Wetland of the Liaodong Bay, China," *Marine Pollution Bulletin*, vol. 120, no. 1-2, pp. 347–354, 2017.

[38] P. Zhang, G. Huang, C. An et al., "An integrated gravity-driven ecological bed for wastewater treatment in subtropical regions: Process design, performance analysis, and greenhouse gas emissions assessment," *Journal of Cleaner Production*, vol. 212, pp. 1143–1153, 2019.

[39] P. Bustamante, F. Caurant, S. W. Fowler, and P. Miramand, "Cephalopods as a vector for the transfer of cadmium to top marine predators in the north-east Atlantic ocean," *Science of the Total Environment*, vol. 220, no. 1, pp. 71–80, 1998.

[40] M. Cheggour, A. Chafik, N. S. Fisher, and S. Benbrahim, "Metal concentrations in sediments and clams in four Moroccan estuaries," *Marine Environmental Research*, vol. 59, no. 2, pp. 119–137, 2005.

[41] X. J. Zhang, S. Zhao, C. H. Feng, and H. R. Wang, "Distribution and accumulation factors of heavy metals in organisms in southern Bohai Bay," *Journal of Dalian Ocean University*, vol. 29, no. 3, pp. 267–271, 2014.

[42] W. P. Sun, J. M. Pan, X. Y. Liu, Y. X. Huang, and M. H. Zheng, "Study of the content of heavy metals in the mollusks from the near-shore of Zhejiang Province," *Journal of Marine Sciences*, vol. 28, no. 4, pp. 43–49, 2010.

[43] W. P. Sun, X. Y. Liu, J. M. Pan, and H. X. Weng, "Levels of heavy metals in commercial fish species from the near-shore of Zhejiang Province," *Journal of Zhejiang University (Science Edition)*, vol. 39, no. 3, pp. 338–344, 2012.

Hindawi
Journal of Chemistry
Volume 2019, Article ID 4506314, 28 pages
https://doi.org/10.1155/2019/4506314

Review Article

Risk Evaluation of Pyrolyzed Biochar from Multiple Wastes

Shem M. Ndirangu,[1] Yanyan Liu,[1] Kai Xu,[2] and Shaoxian Song[3]

[1]*School of Safety Science and Emergency Management, Wuhan University of Technology, Wuhan 430070, China*
[2]*Center for Material Research and Analysis, Wuhan University of Technology, Wuhan 430070, China*
[3]*School of Resources and Environmental Engineering, Wuhan University of Technology, Wuhan 430070, China*

Correspondence should be addressed to Yanyan Liu; wulengheiyin@whut.edu.cn

Received 13 August 2019; Accepted 16 November 2019; Published 16 December 2019

Guest Editor: Peng Zhang

This paper aims at demonstrating the significance of biochar risk evaluation and reviewing risk evaluation from the aspects of pyrolysis process, feedstock, and sources of hazards in biochar and their potential effects and the methods used in risk evaluation. Feedstock properties and the resultant biochar produced at different pyrolysis process influence their chemical, physical, and structural properties, which are vital in understanding the functionality of biochar. Biochar use has been linked to some risks in soil application such as biochar being toxic, facilitating GHGs emission, suppression of the effectiveness of pesticides, and effects on soil microbes. These potential risks originate from feedstock, contaminated feedstock, and pyrolysis conditions that favor the creation of characteristics and functional groups of this nature. These toxic compounds formed pose a threat to human health through the food chain. Determination of toxicity levels is a first step in the risk management of toxic biochar. Various sorption methods of biochar utilized low-cost adsorbents, engineered surface functional groups, and nZVI modified biochars. The mechanisms of organic compound removal was through sorption, enhanced sorption, modified biochar, postpyrolysis thermal air oxidation and that of PFRs degradation was through activation, photoactive functional groups, magnetization, and hydrothermal synthesis. Emissions of GHGs in soils amended with biochar emanated through physical and biotic mediated mechanisms. BCNs have a significance in reducing the health quotient indices for PTEs risk contamination by suppressing cancer risk arising from consumption of contaminated food. The degree of environmental risk assessment of HM pollution in biomass and biochars has been determined by using potential ecological risk index and RAC while organic contaminant degradation by EPFRs was considered when assessing the environmental roles of biochar in regulating the fate of contaminants removal. The magnitude of technologies' net benefit must be considered in relation to the associated risks.

1. Introduction

The endeavored activities a man is involved in generate unwanted material. Toxic waste management issues are of national concern in many countries because of the increased waste generation and lack of recycling, disposal, and handling capacity and facilities. Toxic waste has been utilized as biomass in pyrolysis processes to generate biochar for soil application and has resulted on spreading of toxic elements in the soil that ends up polluting the environment, abetting GHGs emission and suppression of the effectiveness of pesticides, and in the food chain affecting human health. Such potential risks arise from the feedstock, contaminated feedstock, and favorable pyrolysis environments that influence their creation. These toxic compounds formed pose a threat to the environment and human health as they end up in the food chain through toxic biochar soil application. Determination of toxicity levels of biomass for biochar use is an initial step in managing the risks of toxic biochar. Comparable developed countries have adopted systematic approaches to toxic waste identification and management, including scientific research in reducing, reusing, and recycling related to the economic level, and waste related policy with regulatory institutions, and the construction of facilities [1, 2] that has led to progressive sustainable development changes [3].

An increased number of studies have been paying attention to cost-effective and environmentally friendly

solutions on toxic waste management using pyrolysis for biochar production for environmental sustainability. Some of these wastes utilized as biomass (garbage or refuse, sludge from a waste treatment plant, discarded material resulting from industrial, commercial, mining, agricultural, and community activities) contain high toxic levels of contaminants such as heavy metals (HM), polycyclic aromatic hydrocarbons (PAH), polychlorinated biphenyl (PCB), inorganic pesticides, dioxins, and persistent organic pollutants (POPs) [4–6]. The composition and volume of waste generated and its pyrolysis treatment and disposal management methods for biochar determine the number of GHGs released into the air and PTE leaching. Without proper management and improvement of the pyrolysis and biochar techniques of waste management, the emissions of GHGs and toxic material are anticipated to rise. There have been some gaps in the production and use of biochar without evaluating the risks posed from the feedstock and pyrolysis process, undermining the sources of hazards and their potential effects to humans and the environment.

The nature of hazardous and solid waste materials for recycling is of great necessity to reduce any contamination to the environment. Many hazardous wastes can be recycled safely and effectively other than treatment and disposal, with benefits of reducing the consumption of raw materials and the volume of waste materials [7]. The materials used in the construction of landfill caps include low-permeability soils and geosynthetic products, which prevent permeability of water through the waste and highly porous soils that drain water [8]. To prevent toxic leaching, highly mobile waste and fluid pesticides cannot be directly landfilled without coagulation [9]. Stabilization method applies binding and filling materials (e.g., cement, lime, pozzolanas, thermoplastics, fly-ash, and silicate by-products) on hazardous waste leachable liquid and semisolid contaminants to physically modify and produce a stabilized solid and reduce the mobility of contaminants [8]. Stabilized wastes for landfill disposal may hinder other use of the environment and it is not effective in immobilizing organic contaminants [10].

Incineration is a high-temperature (870°C to 1200°C) destructive ex situ treatment of contaminated waste (including soil) fed into the incinerator, under controlled conditions of high temperature in the presence of oxygen, volatilizing and combusting the contaminants into innocuous substances [8], with an efficiency of up to 99.99% for PCBs and dioxins [11]. On the contrary, burning POPs (e.g., pesticides and PCBs) in incinerators have been linked with the spread of recent POPs (e.g., dioxins and furans) contaminating the immediate surrounding [12]. Additionally, industrial use standards and regulations of emission of gases have brought about the development of new systems where biomass is heated with controlled or no oxygen for efficient gasification or pyrolysis [13]. Very high temperatures and long residence time in the cement kiln offer an alternative to a high destruction efficiency of hazardous waste. The highly alkaline conditions in a cement kiln are ideal for decomposing chlorinated organic waste [8], with the destruction of compounds being more than 99% with no adverse effect on the quality of the exhaust gas [14]. High calorific value hazardous waste provide high energy resulting in energy saving. Improved kiln processes to pyrolysis, mitigate pollution, and increase the energy efficiency by producing biochar, gases, and liquids for the production of bioenergy and flaring the gases to reduce global warming [13].

Contaminants' mobility and bioavailability have augmented concerns due to soil contamination, food safety, arising health risks, and GHGs emission. Two major voluntary initiatives offer standardization programs to ensure sustainable biochar production and safety: International Biochar Initiative (IBI) offers standardized product definition and testing guidelines for biochar used in soil [15] and European Biochar Certification (EBC) gives a guideline for biochar production [16], and they have been developed by scientists to guide the public on adherence to high ethical standards of safety and appropriate use. The initiatives have some contaminant parameters where standard methodologies are used to examine and meet the minimum required standards for biochar application [17]. Schimmelpfennig and Glaser [18] established a minimum set of analytical properties and thresholds for biochar identification, suitable for soil amendment, and carbon sequestration. This helps in defining the desired stability properties of biochar for particular use. The application of biochar that immobilizes, stabilizes, and degrades contaminant elements with resultant safe residue offers a reassurance on the reduction of environmental risk. Figure 1 shows the remediation and evaluation of contaminated biochar. This paper aims at reviewing the risks posed on the utilization of biochar derived from multiple wastes and the necessary available mitigation and control measures. The significance of the biochar risk evaluation and reviewing the risk evaluation of biochar is demonstrated from the aspects of (1) pyrolysis process, (2) feedstock, (3) sources of hazards in biochar and their potential effects, and (4) the methods of risk evaluation. The irreversibility of applying biochar to soil necessitates an effective assessment of its stability for use.

2. Biochar

Biochar results from the break down of organic matter undergoing chemical decomposition to a stable form of carbon through pyrolysis in an oxygen-limited environment, usually at temperatures of 350°C–600°C [19]. Pyrolysis is the thermal degradation of biomass under pressure in the absence of reacting gases [8]. The highly recalcitrant aromatic nature of biochar can remain stable in soil for hundreds to thousands of years [20] reducing GHG emission and sequester carbon [21]. Synthetic gas (syngas) and pyrolysis liquor (bio-oil) are additional products of pyrolysis process that are source of renewable energy [22]. The resultant products and their chemical composition depend on the kind of feedstock used and the controlling rate of pyrolysis temperature. Pyrolysis is applicable to solid and organic materials that may undergo chemical decomposition in the presence of high temperature with contaminants. It is linked

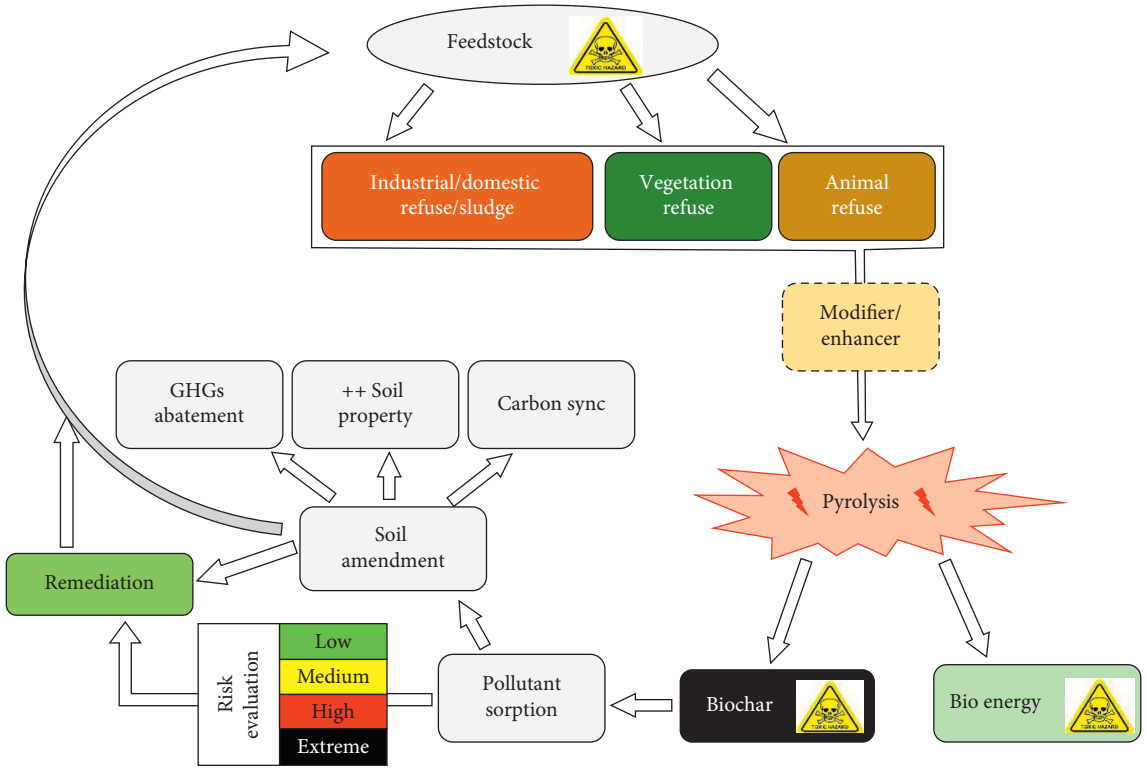

Figure 1: Feedstock recycling, pyrolysis, biochar, and remediation.

to thermal desorption through the conversion of energy of waste such as solid hazardous waste, mercury-contaminated soil, hospital waste, and coal [8]. This technology is not applicable for treatment of liquids and explosives materials with highly oxidizing nature under heat treatment and materials that cannot be decomposed by thermal treatment at 600°C [8]. A variety of feedstock and pyrolysis methods used significantly affect the results in biochar properties. Tables 1 and 2 show biochar functional group property changes from varied feedstock and pyrolysis temperature.

2.1. Properties of Biochar. The soil amendment of general properties of biochars irrespective of feedstock used or the pyrolysis method is the improvement in soil water holding capacity (WHC), cation-exchange capacity (CEC), soil carbon, soil nutrient, and crop productivity. These are often recorded in highly degraded and nutrient-poor soils due to ability to absorb and retain moisture longer in the soil [64–68]. Available nutrients are recycled through the critical role played by the biochar amendment, thus increasing crop productivity through improved indirect nutrient availability.

This is by means of pH change, CEC, and soil structure, resulting in improved fertilizer efficiency, decreased nutrient leaching, and some effects on nutrient availability [69]. Depending on pyrolysis conditions, biochar has a porous structure with carboxyl and hydroxyl functional groups effective in the adsorption of contaminants in soil and minimize the risk of contaminants entering the human food chain [70] with the longevity of soil biochar on application. These soil properties make biochar behave in a different way in different soil properties due to their varying adsorption behavior and biological activity [13, 71–74]. Other carbonaceous materials like biochar such as activated carbon have been used and exhibit varied performance for toxic compound absorption by prevention of leaching and secondary contamination [75].

2.2. Advantages and Disadvantages of Biochar. Biochar soil amendment for stressed agricultural soil improves soil structure and properties by increasing absorbency capacity and aeration of the soil [76, 77]. It also mitigates global warming, restores degraded lands, and balances the effect of water pollution by removing organic contaminants such as pesticides and dyes [78, 79]. Through this means, it has an affinity for adsorbing contaminants and keeping them away from plants [64]. Nutrient balancing created through biochar application with carbon sequestration in arable land is a way to alleviate GHG emission as some farmland has exhausted soil organic carbon (SOC) [64]. However, its application to fertile soils does not necessarily increase crop yield [64]. There are, however, some negatives effects of biochar with the use of contaminated feedstock for biochar. Table 1 shows some properties of biochar generated from biomass in the production of biochar with resultant toxic elements.

Since biochar production is from a range of feedstock sources, some contaminants can be present including PAHs, POPs, HMs, and organic compounds; therefore, there is an important consideration in the context of adding biochar to agricultural soils [80] due to negative effects on soil properties and function. These contaminants may also end up in the biochar depending on the pyrolysis conditions or the use of processing conditions that may favor their production [81]. High rates of biochar application in the soil can affect

Table 1: Biochar properties and hazards exhibited.

Biochar feedstock	Biochar properties measured (elemental composition)	Hazards exhibited	References
Bamboo	P, EC, H, Corg, Corg/N, Atomic H/Corg, ash, CEC, SA (BET), alkalinity	Cu, Zn	[23]
Municipal sewage sludge	pH, volatile matter, ash, fixed carbon, N, C, H, S, O, Cu, Cr, Zn	Cu, Cr, Zn	[24]
Pitch pine wood char and natural char	Helium solid density, surface area, electrical resistivity, H/C ratio	40 TCPL contaminant PAHs detected	[25]
Wheat straw	pH, SOC, N, bulk density	Increased CH_4 and CO_2 emission Decreased N_2O emission	[26]
Rice straw	Ash, C, H, N, O, H/C, O/C	Cu, Cd, Pb, Cr, Zn, Ni	[27]
Green waste compost and hardwood	pH, total organic carbon, water-soluble carbon, dissolved organic carbon, water-soluble nitrogen, and concentrations of dissolved total nitrogen	Pb, Zn, As, Cu Cd, PAH reduced	[28]
Paper mill sludge	pH, volatile matter, ash, fixed carbon, N, C, H, S, O, Cu, Cr, Zn	Cu, Cr, Zn	[24]
Sawdust	Ash, C, H, N, O, H/C, O/C	Cu, Cd, Pb, Cr, Zn, Ni	[27]
Wheat straw	pH, SOC, N, bulk density, surface area, ash content	CH_4 enhanced with more application N_2O emission reduced, CO_2 unchanged	[29]
Rice straw	P, EC, pH (H2O), C, N, H, Corg, Corg/N, Atomic H/Corg, ash, CEC, SA (BET), alkalinity	Cu, Pb and Zn	[23]
Wheat straw, poplar wood, and spruce wood	Ash content, C, N, H	9 US EPA PAHs identified	[30]
Slaughterhouse sludge	pH, volatile matter, ash, fixed carbon, N, C, H, S, O, Cu, Cr, Zn	Cu, Cr, Zn	[24]

micro-organism survival rates, including plants and animals, thus necessitating testing of biochars effects before the application on agricultural fields to avoid detrimental effects [82]. However, the negative implications and harmful effects on the ecological system due to the continued use of biochar have not been wholly understood [83]. There is need to identify suitable feedstock for the production of biochar from a range of biomass as provided for by European Biochar Certificate (EBC) in the positive list of biomass feedstock approved for use in producing biochar [84].

Production of biochar for soil application is an important means for establishing a long-term carbon sink with low-risk return of CO_2 to the atmosphere and the improvement in soil properties. Utilization of biochar for additional soil carbon has additional considerable potential to value addition beyond waste management and prevention of environmental contamination. The benefits improve soil nutrient availability and water holding capacity, hence improving degraded soils and promoting soil health. However, a range of contaminated feedstock sources should be avoided by utilizing suitable sources. These are key components in waste management and the development agricultural sustainability.

3. Effects of Pyrolysis Process and Feedstock on Biochar Properties

3.1. Effect of Pyrolysis on Biochar Properties. Laird et al. defined pyrolysis as a thermochemical process where high temperature transforms waste materials such as wood chips, crop residues, manures, and municipal wastes in the complete or near absence of oxygen into renewable energy products–biochar, bio-oil, and syngas [85]. Biochar is produced as a product or coproduct from several pyrolysis methods that include slow pyrolysis (SP), fast pyrolysis (FP), gasification, and flash pyrolysis [79, 83]. SP feedstock is combusted at temperatures between 350°C and 800°C, with the residence time varying from minutes to several hours, while in FP, the feedstock is combusted at temperatures between 425°C and 550°C, with the residence time being about 2 s [79]. In gasification, the feedstock is combusted in the presence of oxygen, and at times, the addition of steam or CO_2, at temperatures more than or equal to 800°C, with the residence time varying from a few seconds to some hours [79]. SP and FP biochars have different characteristics physically and chemically and hence different behavior in soil [71, 86]; therefore, application of partly pyrolyzed biomass heightens the immobilization of soil N needed by soil plants and animals [71]. A study FP left a labile unpyrolyzed biomass fraction that reduced pH and particle size and increased surface area from wheat straw-derived biochar, unlike SP biochar that pyrolyzed completely [87]. The residence time in SP biochars completely pyrolyzes resulting in less volatile C substrate, ultimately reducing N immobilization [87]. Table 2 illustrates functional group changes of biochar arising from varied feedstock and pyrolysis temperature.

Hydrochar is produced by hydrothermal carbonization of biomass treated with hot compressed water without

Table 2: Biochar functional group changes from varied feedstock and pyrolysis temperature.

Feedstock	Pyrolysis temp. (°C)	Heat rate (°C/min)	Yield (%)	pH	C (%)	H (%)	N (%)	O (%)	Ash (%)	H/C	O/C	C/N	(O + N)/C	Surface area (m^2/g)	Pore volume (cm^3/g)	Reference
Bamboo	600	—	—	9.81	—	—	—	—	—	0.33	—	165	—	63.9	0.035	[31]
Bamboo	750	—	—	9.5	860	14.9	4.5	—	11.9	0.21	—	186	—	907.4	—	[23]
Beech wood	400	—	—	8.4	87.7	2.98	0.6	6.1	2.6	—	—	—	—	65.47	—	[32]
Broiler litter	350	—	—	—	45.6	4	4.5	18.3	—	—	—	—	—	60	0	[33]
	700	—	—	—	46	1.42	2.82	7.4	—	—	—	—	—	94	0.018	
Corn cob	—	—	—	—	77.32	3.16	2.02	10.72	6.19	—	—	—	—	—	—	[34]
Corn straw	600	10	68.2	—	85.9	—	0.4	11.1	—	—	—	—	—	34	0.04	[35]
	800	10	72.8	—	79.4	—	0.25	10.1	—	—	—	—		61	0.036	
Cottonseed hull	200	—	83.4	—	51.9	6	0.6	40.5	3.1	—	—	—	—	—	—	[36]
	350	—	36.8	—	77	4.53	1.9	15.7	5.7	—	—	—	—	4.7	—	
	500	—	28.9	—	87.5	2.82	1.5	7.6	7.9	—	—	—	—	0	—	
	650	—	25.4	—	91	1.26	1.6	5.9	8.3	—	—	—	—	34	—	
	800	—	24.2	—	90	0.6	1.9	7	9.2	—	—	—	—	322	—	
Dairy manure	200	—	—	7.63	31.1	3.42	2.78	—	—	—	—	—	—	1.9	—	[37]
Dairy manure	350	—	—	9.98	25.2	1.67	2.22	—	—	—	—	—	—	5.61	—	
Eucalyptus salinga trees	450	5–10	—	8.64	67.4	—	0.52	—	—	—	—	—	—	191	57.2	[38]
	550	5–10	—	9.96	73.19	—	0.62	—	—	—	—	—	—	228.3	67.5	
Green waste	700	—	—	9.8	51.9	—	0.59	—	45.7	—	—	88	—	303	—	[39]
Hickory chips	600	20	—	—	84.7	1.83	0.3	11.3	—	—	—	—	—	256	—	[40]
Maize straw	350	—	—	7.9	58.9	3.36	1	21.3	—	0.685	—	—	0.286	6.71	—	[41]
	700	—	—	10.6	43.8	1.47	1.27	31.6	—	0.403	—	—	0.566	265	—	
Maize straw	400–450	—	—	9.8	59.16	4.69	0.98	—	—	—	—	—	—	53.03	—	[42]
Municipal solid waste	400	—	—	8	44.7	12.2	1.3	31.7	6.1	—	—	—	—	20.7	0.027	[43]
	500	—	—	8.5	59.5	9.1	1.4	20.8	9.2	—	—	—	—	29.1	0.039	
	600	—	—	9	70.1	8.4	1.3	13.7	6.2	—	—	—	—	29.8	0.038	
Municipal solid waste	300	—	69.63	—	78.76	8.49	1.85	10.91	—	1.29	0.1	—	—	—	—	[27]
MWTP sludge	300	5	80.44	6.55	11.19	1.83	1.72	—	—	—	—	—	—	36.84	—	[44]
	400	5	73.95	6.96	8.61	1.22	1.31	—	—	—	—	—	—	51.5	—	
	500	5	71.27	7.57	8.35	0.85	1.18	—	—	—	—	—	—	57.56	—	
	600	5	70.06	7.96	8.15	0.59	0.94	—	—	—	—	—	—	54.52	—	
	700	5	67.96	8.51	7.68	0.41	0.66	—	—	—	—	—	—	50.27	—	
MWTP sludge	300°C	—	68.65	7.02	21.16	2.3	3.35	8.22	63.97	1.3	0.29	0.14	—	—	—	[45]
	500°C	—	60.07	7.7	15.61	0.86	2.2	3.26	77.44	0.66	0.16	0.12	—	—	—	
	700°C	—	56.11	8.89	15.32	0.47	1.38	1.12	81.15	0.37	0.05	0.08	—	—	—	
MWWTP sludge (dewatered)	600	—	60.8	5.9	31.29	3.83	4.84	17.41	39.2	—	—	—	—	—	—	[46]
MWWTP sludge	300	20	70	—	36.87	—	5.81	—	41.09	—	—	6.35	—	180.57	20.17	[47]
	350	20	64	—	39.38	—	5.59	—	44.87	—	—	7.04	—	201.42	25.32	
MWWTP sludge	400	20	60	—	44.68	—	5.43	—	46.48	—	—	8.23	—	261.03	29.01	[47]
	450	20	54	—	45.68	—	4.88	—	48.06	—	—	9.37	—	250.01	28.51	
Oil mallee	550	—	—	8.4	70	—	0.81	—	8.6	0.48	0.13	—	—	—	—	[48]

Table 2: Continued.

Feedstock	Pyrolysis temp. (°C)	Heat rate (°C/min)	Yield (%)	pH	C (%)	H (%)	N (%)	O (%)	Ash (%)	H/C	O/C	C/N	(O + N)/C	Surface area (m^2/g)	Pore volume (cm^3/g)	Reference
Orange peel	150	—	82.4	—	50.6	6.2	1.75	41	0.5	—	—	—	—	22.8	0.023	[49]
	350	—	33	—	73.2	4.19	2.3	18.3	2	—	—	—	—	51	0.01	
	400	—	30	—	71.7	3.48	1.92	20.8	2.1	—	—	—	—	34	0.01	
	500	—	26.9	—	71.4	2.25	1.83	20.3	4.3	—	—	—	—	42.4	0.019	
	200	—	61.6	—	57.9	5.53	1.88	34.4	0.3	—	—	—	—	7.8	0.01	
	250	—	48.3	—	65.1	5.12	2.22	26.5	1.1	—	—	—	—	33.3	0.02	
	300	—	37.2	—	69.3	4.51	2.36	22.2	1.6	—	—	—	—	32.3	0.031	
	600	—	26.7	—	77.8	1.97	1.8	14.4	4.1	—	—	—	—	7.8	0.008	
	700	—	22.2	—	71.6	1.76	1.72	22.2	2.8	—	—	—	—	201	0.035	
Peanut shells	300	7	36.91	7.76	68.27	3.85	1.91	25.89	1.24	0.67	0.29	—	0.31	3.14	—	[50]
	700	7	21.89	10.57	83.76	1.75	1.14	13.34	8.91	0.25	0.12	—	0.13	448.2	0.2	
Pig manure	350	—	—	8.3	31.58	2.36	3.8	16.93	45.33	0.9	—	—	0.51	23.8	0.053	[51]
	700	—	—	9.5	25.16	1.12	2.05	4.83	66.84	0.53	—	—	0.21	32.6	0.035	
Pig manure	350	—	—	8.2	31.6	2.36	3.8	16.9	—	0.896	—	—	0.505	23.8	—	[41]
	700	—	—	10.6	25.2	1.12	2.05	4.83	—	0.533	—	—	0.213	32.6	—	
Pine needles	100	—	91.2	—	50.87	6.15	0.71	42.27	1.1	—	—	—	—	0.7	—	[52]
	200	—	75.3	—	57.1	5.71	0.88	36.31	0.9	—	—	—	—	6.2	—	
	250	—	56.1	—	61.24	5.54	0.86	32.36	1.2	—	—	—	—	9.5	—	
	300	—	48.6	—	68.87	4.31	1.08	25.74	1.9	—	—	—	—	19.9	—	
	400	—	30	—	77.85	2.95	1.16	18.04	2.3	—	—	—	—	112.4	0.044	
	500	—	26.1	—	81.67	2.26	1.11	14.96	2.8	—	—	—	—	236.4	0.095	
	600	—	20.4	—	85.36	1.85	0.98	11.81	2.8	—	—	—	—	206.7	0.076	
	700	—	14	—	86.51	1.28	1.13	11.08	2.2	—	—	—	—	490.8	0.186	
Pine sawdust	650	—	—	—	86.82	1.57	0.3		—	—	—	—	—	297.8	0.08	[53]
Pine wood	600	—	—	—	85.7	2.1	0.3	11.4	—	—	—	—	—	209.6	—	[54]
Pine wood sawdust	500	10	—	10.83	63.03	—	1.52	—	—	—	—	41.56	—	—	—	[55]
Poplar wood	400	8	32	9	67.3	4.42	0.78	—	3.5	—	—	—	—	3	—	[30]
	460	8	—	9.2	70	3.51	0.95	—	5.7	—	—	—	—	8.2	—	
	525	8	—	8.7	77.9	2.66	1.07	—	6.8	—	—	—	—	55.7	—	
Poultry litter	550	—	—	7.3	45	—	1.9	—	45.5	0.42	0.12	—	—	—	—	[48]
Residential sludge		—	—	—	30.24	1.29	3.13	0.01	64.17	—	—	—	—	—	—	[34]
Rice hull	500	—	—	10.2	205	—	2.6	—	—	—	—	—	—	—	—	[56]
Rice straw	600	—	—	10.2	—	—	—	—	—	0.61	—	55.9	—	97	0.041	[31]
Rice straw	300	—	44.12	—	73.14	7.51	2.46	16.9	—	1.23	0.17	—	—	—	—	[27]
Rice straw	500	—	—	10	508	17.2	16.6	—	42.7	0.44	—	28	—	36.7	—	[23]
Rice straw	350	—	—	7.8	44.5	2.69	1.64	22.1	—	0.725	—	—	0.404	9.01	—	[41]
	700	—	—	10.6	56.7	2.39	0.1	2.61	—	0.506	—	—	0.036	188	—	
Soybean stover	300	7	37.03	7.27	68.81	4.29	1.88	24.99	10.41	0.74	0.27	—	1.3	5.61	—	[50]
	700	7	21.59	11.32	81.98	1.27	1.3	15.45	17.18	0.19	0.14	—	0.16	420.3	0.19	
Spruce wood	400	8	36	6.9	63.5	5.48	1.02	—	1.9	—	—	—	—	1.8	—	[30]
	460	8	—	8.7	79.6	3.32	1.24	—	3	—	—	—	—	14.2	—	
	525	8	—	8.6	78.3	3.04	1.17	—	4.7	—	—	—	—	40.4	—	

Table 2: Continued.

Feedstock	Pyrolysis temp. (°C)	Heat rate (°C/min)	Yield (%)	pH	C (%)	H (%)	N (%)	O (%)	Ash (%)	H/C	O/C	C/N	(O + N)/C	Surface area (m^2/g)	Pore volume (cm^3/g)	Reference
Styrene butadiene rubber	200	10	93.5	9.2	74.7	6.38	—	3.92	15	0.085	0.052	—	0.052	—	—	[57]
	400	10	59.3	8.3	77.7	3.56	—	3.34	15.4	0.046	0.043	—	0.043	24.2	0.08	
	600	10	54.5	7.8	81.3	1.67	—	1.43	15.6	0.021	0.018	—	0.018	51.5	0.12	
	800	10	43	7.8	86	0.87	0.47	2.16	10.5	0.01	0.025	—	0.031	50	0.11	
Sugarcane crop harvest	550	—	—	—	66.28	2.15	0.9	—	—	—	—	—	—	27.9	0.038	[58]
Tire rubber	200	10	93.5	—	74.7	6.38	—	3.92	15	—	—	—	—	—	—	[57]
	400	10	59.3	—	77.7	3.56	—	3.34	15.4	—	—	—	—	24.2	0.08	
	600	10	54.5	—	81.3	1.67	—	1.43	15.6	—	—	—	—	51.5	0.12	
	800	10	43	—	86	0.87	0.47	2.16	10.5	—	—	—	—	50	0.11	
Walnut shell	500	—	31.7	—	69.42	3.85	1.54	25.07	—	—	—	—	—	94.509	0.054	[59]
	700	—	28.4	—	80.35	1.61	0.41	17.54	—	—	—	—	—	264.991	0.141	
	900	—	23.8	—	84.86	1.16	0.34	13.63	—	—	—	—	—	397.015	0.198	
Wheat chaff	550	—	—	8.9	58	—	2.8	—	16.2	0.53	0.15	—	—	—	—	[48]
Wheat straw	400	8	34	9.1	65.7	4.05	1.05	—	9.7	—	—	—	—	4.8	—	[30]
	460	8	—	8.7	72.4	3.15	1.07	—	12	—	—	—	—	2.8	—	
	525	8	—	9.2	74.4	2.83	1.04	—	12.7	—	—	—	—	14.2	—	
Wood (Chinese fir) sawdust	300	—	35.15	—	73.95	7.34	0.48	18.24	—	1.19	0.19	—	—	—	—	[27]
Wood biomass	300	5	67	—	62.75	4.25	0.3	30.44	2.2	0.807	0.364	—	0.368	109	—	[60]
	500	5	57	—	73.29	3.03	0.37	20.06	3.3	0.492	0.205	—	0.209	165	—	
	700	5	30	—	83.27	1.68	0.43	10.73	3.9	0.24	0.096	—	0.101	65	—	
WWTP sludge	500	—	—	7.18	27.8	—	2.34	—	—	—	—	—	—	5.57	0.015	[61]
WWTP sludge	450	5	46.3	8.6	21.3	—	3.17	—	—	—	—	—	—	—	—	[62]
WWTP sludge	550	10	13	7.47	5.5		1.1	—	—	—	—	—	—	24.73	—	[63]

drying [88]. The process of hydrochar production is eco-friendly with no hazardous chemical waste or by-products generation compared to dry pyrolysis [89]. The advantage is that hydrothermal process takes place at low temperatures (150°C to 350°C), and damp feedstock (moist animal manures, sewage sludge, and algae) can be used [90]. Moreover, hydrochar reduces alkali, alkaline Earth, and HM contents over biochar [88]. The disadvantage of hydrochar, however, is that it has generally a low surface area and poor microporosity [91], with a less C stability unlike biochar [64]. Temperature affects the resultant pyrolysis of biomass such that increasing pyrolysis temperature (450°C–700°C) decreases the particle size of biochar [13] and increases particle density and porosity [92]. The increasing temperature (300°C to 700°C) of urban sewage sludge biochar increased the resultant pH and electrical conductivity (EC) of biochar [92]. Low temperatures of 300°C produced biochar with high N and organic carbon (OC) but low carbon-to-nitrogen (C/N) ratio and total Na, K, and P contents [92]. In a poultry manure biochar, increased temperature of pyrolysis (300°C to 600°C) decreased yield, N, OC contents, and CEC but increased pH, ash content, OC stability, and the surface area [93]. The increase of pyrolysis temperature leads to the increase of surface area of biochar, which facilitates higher sorption.

The pyrolysis process with a varied feedstock composition, temperature, pressure, vapor residence time, moisture, and heat rate can be varied resulting in different quantities of syngas, biochar, and bio-oil product as well as their intrinsic properties. This means that maximizing biochar yields comes at the expense of the by-products. Novak et al. [94] opined that biochar production process can be customized to have specific characteristics matching select physicochemical problems of a particular degraded soil for the application of the biochar. Low pyrolysis temperature biochar (350°C) may contain large quantities of favorable nutrients with low sorptive capacities in comparison to high pyrolysis temperature (800°C) [95]. This arises because the C content and aromaticity of a biomass intensifies with the rise in temperature, whilst oxygen, hydrogen, and polarity reduce with an increase in micropores [52]. In a study, biochar produced at a higher temperature of 700°C was alkaline and applicable in neutralization of acidic soil and improved soil fertility and sequester C, while conversely, biochar produced at lower temperatures of 300°C was applicable for alkaline soils to correct the alkalinity problems [96]. To generate agricultural use biochar from poultry litter, pyrolysis at 300°C is suited unlike for C sequestration and other environmental applications [93].

3.2. Effects of Feedstock on Biochar Properties. A variety of feedstock is used in the preparation of biochar by pyrolysis method. Farmers and researchers are becoming more aware of the use of organic wastes and biomass as feedstock sources for pyrolysis; therefore, careful consideration has to be taken owing to the large effects of the feedstock on the resultant physicochemical properties of biochar. Most organic substances (crop and forestry residues, industrial by-products, animal manure, and sewage sludge) can be pyrolyzed [83] for the production of biochar. However, not all organic substances are suitable for producing biochar for agricultural purpose [83] due to the nature of the source and the conditions these biomass might have been exposed to. In addition, some pyrolysis conditions and feedstock source create biochar that cannot hold nutrients and are subject to microbial decay [97].

There are various potential feedstocks that are ideal with certain processing conditions for a desired maximum potential benefit in their end-use applications. Woody types with a high lignin content such as nutshells, residues from sawmills, and forest waste materials suit to capitalize on biochar yields [98] due to high quantities of lignin that is tough to break down in comparison to cellulose and hemicellulose [22]. Switch grass, a bioenergy crop, pyrolyzed in SP at 450°C–550°C, without oxygen, with more biomass, and vapor residence times, and in FP at 450°C–500°C, with little biomass and vapor residence time, generated syngas, bio-oil, and biochar [20, 86, 99]. A higher EC and CEC for crop residue biochar was observed in a study as compared to wood biochar [30], likened to corn cob biochar, wood biochar had higher CEC and greater pH neutralization in another study [100]. Furthermore, the variety of biomass and existing pyrolysis systems results in variable biochar produced [78]. Oxidized functional group, ash, and alkali (Na, K, Mg, and Ca) of feedstock affect biochar pH and EC; hence, their variability with pyrolysis conditions influences the resultant nutrient content accessible to plants on the application of biochar [83].

Biochar is also produced using animal wastes and food remains. Most manure is used in biogas production and the solid residue could be biomass in pyrolysis [22]. Plant nutrients therein, such as P, K, N, Mg, and Ca, maybe at a high level in the biochar. The use of plant product, nutrient-rich manure, and animal product for soil application biochar may decrease nutrient run-off and GHG emissions, such as CH_4 and N_2O [101]. The efficacy of rice straw char in a study was more than bamboo char in alleviating CH_4 and CO_2 emissions from paddy soils [21]. Amendment of biochars to soil enhanced the sorption of carbaryl pesticide due to chemical and biological degradation of the pesticide [41]. Pig manure char enhanced hydrolysis of carbaryl and atrazine in biochar at 700°C by decomposing the pesticide by 71.8% and 27.9% in 12 hours [51]. Some agricultural biomass are however not appropriate as biochar for agricultural application [80, 102]. Pyrolysis conditions and feedstock types can result in ineffective biochar in retaining nutrients and are prone to microbial decay [102]. Biochar derived from MSW and animal manure are rich in nutrients; however, they have been in limited use for agricultural soil due to safety concerns from toxic contamination of HM and organic pollutants such as PAHs dependent on their source. On the contrary, some sewage sludge biochars have low HM contents below risk levels and of low bioavailability levels to plants [96].

A variety of biomass is being employed in generating biochar at varied pyrolysis conditions, governing biochar properties. It is hence essential to categorize and rank suitable

feedstock for the production of biochar [83]. Varied properties of feedstock materials and the resultant biochar produced due to different production process influence their chemical, physical, and structural properties. Appropriate feedstock is a limitation since most available sources comprise residues from agricultural and forest biomass. The resultant properties of biochar are vital to appreciate functionality of biochar in the soil and potential to control GHG emission.

4. Hazards in Biochar

4.1. Sources of Hazards in Biochar. The use of biochar is linked to certain risks, such as biochar being possibly toxic, retaining HMs, and suppression of the effectiveness of pesticides and effects on soil microbes, in agricultural land [28, 103–105]. The biochar may potentially contain elements that may facilitate the emission of GHGs on their application to plant production. These potential risks are formed from feedstock, contaminated feedstock, and pyrolysis conditions favoring the creation of characteristics and functional groups of this nature. Table 3 shows identified concentration of toxic organic and inorganic compounds in biochars.

Biochar has received increasing attention concerning its ability to immobilize HMs and reduce their bioavailability in soil plants. However, it has also been attributed to being a source or an enhancer of HMs content. Among some of the HMs identified in a variety of biochar include iron (Fe), zinc (Zn), copper (Cu), manganese (Mn), lead (Pb), silver (Ag), cadmium (Cd), chromium (Cr), calcium (Ca), Mercury (Hg), Arsenic (As), and nickel (Ni). Biochar produced from organic waste such as sewage sludge has been associated with carrying numerous HMs [109]. Sludge such as municipal sewage, pulp and paper mill effluent, and slaughterhouse sludge have high potential of toxicity due to high contents of HMs such as Cu, Cr, Pb, Ni, Cd, and Zn [24, 106]. In a study, Cu and arsenic (As) HM contents were enhanced more than 30 times with the application of biochar and at the same time an increase in C and pH in the soil [28]. Organic elements of biochars with high carboxyl contents activate Cu taken by alkaline soil [33]. Similarly, an increase in As and Cu mobility was noted on biochar application contrary to the effect on Cd that was insignificant [110]. These HMs become toxic contaminants to the soil because of their bioaccumulation potential to micro- and macro-organisms. High concentrations of HMs in contaminated soils may cause continued risks to the environment affecting plants, animals, and human health.

Potential sources of hazardous compounds include PAHs, polychlorinated dibenzodioxins (PCDDs), polychlorinated dibenzofurans (PCDFs) [18], and toxins such as volatile organic compounds, xylenols, cresols, acrolein, and formaldehyde [56, 103, 111, 112]. PAHs have been identified to be detrimental to plants and microbial organisms [113, 114]. Some toxic PAHs formed during biochar synthesis through incomplete incineration are recalcitrant to some extent; nonetheless, an increase in synthesis temperature can affect PAH contents [64]. In a study, PAH levels increased with increasing pyrolysis temperatures in straw-based biochar unlike a reduction in wood-based biochar [30]. Numerous biochars produced from pitch pine wood has exhibited PAHs levels [25]. The toxic elements are frequently catalyzed by Fe and Cu and may be produced by the catalytic combination of dioxin structures from O2, C, and chloride (Cl) at temperatures of 300°C to 325°C including other reactions after combustion [103]. Table 3 shows some studies that have highlighted toxic organic contaminants (PAH) and heavy metals measured in the studied biochar material. These are potentially toxic substances that can result in accumulation of contaminants in the soils amended with biochar.

4.2. Potential Risks of Hazards in Biochar

4.2.1. Effects on Crop Production and Soil Quality. Proper application of biochar in the soil increases soil quality resulting in increased productivity; however, improper application might reduce crop productivity and deteriorate soil quality [64]. Studies conducted revealed the reduction of the grain yield of rice by 10% and 26% on application of biochar at 8 t and 16 $t \cdot ha^{-1}$, respectively, [115] and a reduction of ryegrass yield by 8% and 30% on application of biochar 100 t and 120 $t \cdot ha^{-1}$, respectively [116]. Yield reduction on increasing biochar application per hectare can be owed to immobilization of N caused by excessive C/N ratios [117], and hydrophobicity [111]. Moreover, application of biochar on heavy clayey soil can also cause waterlogging including harming acid-loving organisms [118]. The nutrients contained in biochar can increase its levels in the soil on application subject to biochar feedstock. Biochar is not as beneficial in soil with plenty of soil organic matter (SOM) as a result, the application may reduce plant growth [118].

Improper biochar type application to soils such as alkaline soil amended with high pH biochar might adversely affect soil quality [119]. Additionally, other biochars may also have a large quantity of ash containing salts causing salinity [64]. Sorption of pesticides by biochar has been shown to reduce pesticide remains in crop soil. 1% application of biochar to spring onions reduced the bioavailability of two pesticides applied in soil by less than 50% over 35 days' period [120]. This will, however, have direct implications in controlling pests due to the inefficiency of pesticides in the soils, which, in addition, may result in their increased application in the soil to control pests, hence endangering the crop harvest [121, 122]. This is an indication of the ability of biochar to immobilize plant nutrients and chemicals in the soil affecting economic pesticide application and quality of the harvest.

4.2.2. Effects on GHG Emission. The effect of biochar application into soil has been documented to either reducing or contributing to GHG emission through CO_2, CH_4, and N_2O. Studies have shown that biochar application enhances GHG emission. Biochar application pyrolyzed at 350°C–550°C from wheat straw at 40 $t \cdot ha^{-1}$, with and without N heightened the CH_4 emission by 34% and 41%, respectively [26], CO_2 emission by 12% [29] and 44.9% from municipal biowaste biochar in rice [123]. It was also reported that 24 t and

Table 3: Identified concentration of toxic organic and inorganic compounds in biochars.

Feedstock	Pyrolysis temp (°C)	Concentration of toxic elements	Reference
Green waste compost and hardwood	—	Cu, Zn, Pb, Cd, As, PAH	[28]
Pitch pine wood	450 to 1000	40 PAH	[25]
Paper mill sludge	200, 300, 400, 500, 600, and 700	Cu, Zn, Pb, Cd, Ni, Cr	[106]
Beech wood	400	Cu, Zn, Ni, B, 18 PAH	[32]
Municipal solid waste	400, 500, and 600	Cu, Zn, Pb, Cd, Ni, Cr	[43]
WWTP sewage sludge	500	Cu, Zn, Pb, Cd, As, co, Mn	[61]
Rice hull	500	Cu, Zn, Pb, Cd	[56]
Wheat straw, poplar wood and spruce wood	400, 460, and 525	16 PAH	[30]
MWWTP dewatered sewage sludge	600	Cu, Zn, Pb, Cd, Ni, Cr	[46]
Municipal solid waste, rice straw and wood (Chinese fir) sawdust	300	Cu, Zn, Pb, Cd, Ni, Cr	[27]
WWTP sludge	550	Cu, Zn, Pb, Cd, Ni, Cr	[63]
MSS, paper mill sludge and slaughterhouse sludge	550 and 750	Cu, Zn, Cr	[24]
WWTP sewage sludge	500	16 PAH	[107]
MWWTP digested sludge	350, 500, 650, 800, and 900	Cu, Zn, Pb, Cd, Ni, Cr, Mn	[108]
Rice straw and bamboo	550 and 750	Cu, Zn, Pb	[23]

MSS, municipal sewage sludge; MWWTP, municipal wastewater treatment plant; WWTP, wastewater treatment plant.

48 $t \cdot ha^{-1}$ of biochar applied from pyrolysis (500°C) of wheat straw increased the emission of N_2O by 150% and 190%, respectively [124].

Soils amended with biochar at high rate derived from bamboo and rice straw pyrolyzed at 600°C reduced CH_4 emissions from the paddy soil by 51.1% and 91.2%, respectively, in comparison to paddy soil without biochar, while more CO_2 was dissolved in the water under alkaline condition reducing CO_2 emission from the paddy soil at all rates of biochar application evaluated [21]. There was no significant effect on CH_4 uptake from forest soil and grassland soils applied with pine sawdust-derived biochar produced at 550°C with and without steam activation, but cumulative N_2O emission significantly reduced by 27.5% and 31.5% in forest soil and 14.8% and 11.7% in the grassland soil, respectively, while cumulative CO_2 emission from the forest soil by 16.4%, but not from the grassland soil as compared to the control soil without biochar [125]. Increased soil organic matter through biochar application has positive impacts on soil physical properties, indirectly contributing to climate change mitigation by decreasing the quantity of N fertilizer required for crop production.

4.2.3. Effects on Human Health. Biochar in its dust form poses danger to humans during application in agricultural farms. Biochar generated from rice husk at high temperatures above 550°C contains toxic crystalline substance [126] including silica, that poses risk to human health [127]. When inhaled during biochar production, movement, and application process, it affects the respiratory system. There is a need for care during top dressing with biochar, and care should be taken to prevent erosion by wind and water and to manage health risks from biochar dust. Hence, such biochar producers must ensure quality control on the use by employing appropriate health and safety precautions during handling and application to soil [126]. Human health is additionally affected by the use of intoxicated biochar as a soil applicant, as indicated in Figure 2. Toxic elements and organic compounds pose a prominent risk to human health, leading to organ failure, due to their highly toxic carcinogenic substances in their compounds [128]. These toxic compounds become a threat to human health through the consumption of food through plants.

5. Risk Evaluation of Hazards in Biochar

Several evaluation methods have been utilized in various studies on the concentration of HMs, organic compounds, and the alleviation of GHGs. They include sorbent of extractable HMs, immobilization, stabilization of HMs, and metalloids concentration. Several mechanisms have been described occurring on the surface of the biochar among them: electrostatic attraction of metal cations with mineral; cation exchange of metal ions with mineral ions; interaction of metals ions with functional groups of biochars; and precipitation of HMs. The properties of the soil are important factors to consider in the immobilization and bioavailability of HMs, and hence, regulating to determine the right condition using various biochars would be important. There are a number of ways to evaluate the risk parameters of biochar depending on the content of evaluation.

5.1. Toxicity Characteristics of Leaching Procedure (TCLP). TCPL determines if waste meets the environmental protection toxicity definition levels of hazardous waste. The TCLP is designed to determine the mobility of both organic and inorganic analytes present in liquid, solid, and multiphasic wastes with capability to analyze and test for 40 contaminants of maximum concentration for toxicity characteristic [129]. If a sample of tested waste fails one or more of these contaminant compounds, then it is considered to have a hazardous waste characteristic. It is important to have in mind that a characteristic waste with any of the 40 contaminant material may still be considered as hazardous waste even if there is an exemption that applies [129]. Leaching behavior of HMs and organic and inorganic

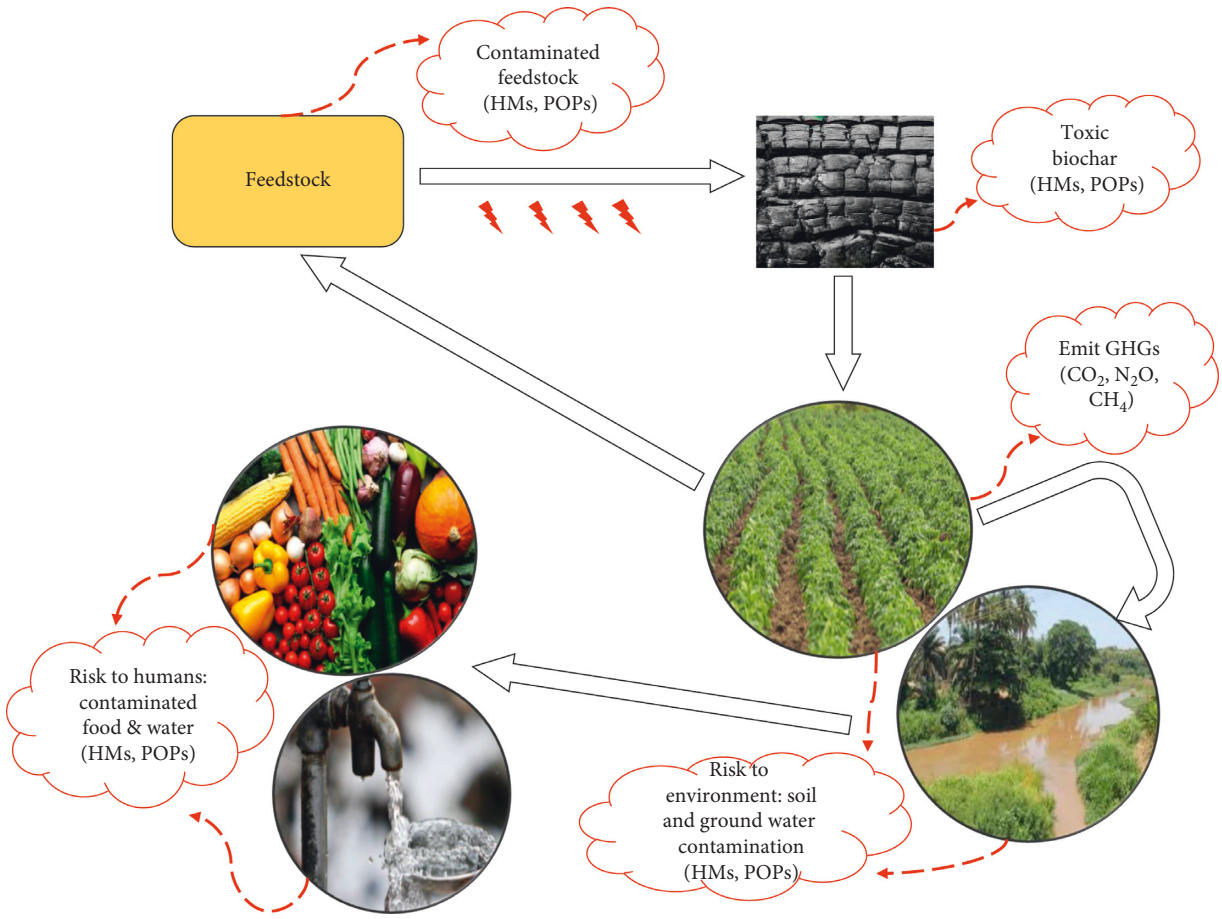

Figure 2: Risk of contaminant reaching environment and food chain.

analytes can be analyzed using the toxicity characteristic leaching procedures defined by the US EPA TCLP procedure [129].

5.2. Heavy Metal Concentration. HMs are a group of metals and metalloids with relatively high densities and are toxic at low-level concentrations occurring naturally or artificially. The release of these metals into the environment both naturally and anthropogenically can cause serious pollution through leaching of HMs into water resources and soil. Table 4 shows identified heavy metals and their reported effect in biochar application. The controlling factor to recycle and dispose contaminated waste is the accumulation and bioavailability of toxic elements. HMs, unlike organic pollutants, are non-biodegradable with a tendency to accumulate in living organisms such as plants and animals. The reuse of waste becomes possible with the removal of contaminants or immobilized/stabilized wastes present in order to allow recycle into raw material. Devi and Saroha [106], in their experiment to determine the risk analysis of bioavailability and eco-toxicity of HMs in biochar, used sequential extraction procedure to determine HM concentration in biomass and biochar using the following equation [106, 135]:

$$\text{HM concentration (mg|kg)} = \frac{[\text{HM concentration (mg|L)} \times \text{total volume makeup (mL)}]}{\text{weight of solid sample (g)}}. \quad (1)$$

The toxicity of HMs depends on the total and bioavailable concentrations. Copyrolysis of pig manure and rice straw considerably reduced in the biochar the extractable concentrations of bioavailable Cu and considerably reduced the concentration of interchangeable and carbonate-associated Zn as compared to pig manure biochar at the same temperatures [136]. The dilution effect reduced the total and bioavailable Cu and Zn concentration associated with the minerals, surface area, and surface functional groups of biochar that are believed to reduce the release of HMs by

Table 4: Heavy metals identified and risk effect in biochar application.

Feedstock	Pyrolysis temp (°C)	Hazard-GHGs exhibited	Risk effect	Reference
MSS, slaughterhouse sludge, and paper mill sludge	550, 750	Cu, Cr, and Zn	Pyrolysis affected toxicity by reducing Cu and Zn in sludge. 750°C favored migration and transformation of HMs. HM environment risks decreased. Dewatered sludge was highly toxic before pyrolysis.	[24]
Bagasse	600	Cr(VI), Cr_{total}	Cr(VI) and Cr_{total} immobilization efficiency was 100% and 92.9%. Remediation reduced the phytotoxicity of Cr. Leachable Fe and was favorable for plant growth.	[130]
Broiler litter	350, 700	Cu(II), Cd(II), Ni(II)	High carboxyl mobilized Cu(II) retained by alkaline soil. Base treatment of 350°C char improved the immobilization of all heavy metals. Total sulfur released in soluble form in soil amended char.	[33]
Residential sewage sludge and corn cob	—	As, Cd, Cu, Pb, Hg, Mo, Ni, Se, Zn, Cr	Pb, Ni, Cu, Zn, Cr largely retained in the biochar carbonization. Hg, As, Cd, and Se fairly released during carbonization. Carbonizer biochar never adsorbed much volatile HMs. Biochar unsuitable for land application.	[34]
Peanut straw (PS), soybean straw (SS) and canola straw CS)	400	Cu(II)	The adsorption increased with increase in pH. The adsorption order of char: PS > SS > CS. Cu(II) adsorption greater than commercial activated carbon.	[131]
Dairy manure	200, 350	Cu, Zn, Cd	Biochar at 350°C more effective in sorbing all three metals. Both biochars had highest affinity for Cu, then Zn and Cd. Mineral in biochar influenced biochar's high sorption capacity.	[37]
Pine wood	600	As, Pb	Modified biochars sorbed higher As(V),Pb(II) than unmodified Birnessite enhanced biochar had highest sorption enhancement due to strong As(V) and Pb(II) affinity.	[132]
Peanut shell and Chinese medicine material residue	300–600	Pb	Pb^{2+} adsorbed on biochars. Biochars (>500°C) and Pb^{2+} sorption complexation reduced. Pb2+-π interaction was enhanced.	[133]
Pine wood and natural hematite	600	As	Stronger magnetic property of aqueous As by modified biochar. Magnetized biochar can be used in As contaminant removal.	[54]
MWTP sewage sludge	300, 500, and 700	Cu, Zn, Cr, Ni, Pb, and Cd	HTP and pyrolysis immobilizes HMs. High-temperature reduced the HMs ecological risk. Higher temperature HTP process transforms bioavailable fraction HMs to more stable fractions. Potential environmental risk of the HMs in sludge transformed from high-risk to low-risk, or even no-risk.	[45]

Table 4: Continued.

Feedstock	Pyrolysis temp (°C)	Hazard-GHGs exhibited	Risk effect	Reference
Paper mill sludge	270 to 720	As(V) and Cd(II)	Equilibrium uptakes of As(V) and Cd(II) were 22.8 anf 41.6 mg/g. Decreased As(V), Cd(II), Ni(II) ions adsorption increased PO_4^{-3} concentration. Regeneration demonstrated through NaOH or HCl desorption.	[134]
Pine wood sawdust	500	Cd, Cr, Pb, Ni	BCNs cutback health hazards of PTEs. Reduced bioavailability and uptake of PTEs by wheat plants. The hazard indices (HIs) for PTEs in all treatments were <1. The cancer risks for Cd, Cr, and Ni higher in all treatments. BCNs addition suppressed cancer risk compared to control.	[55]

HTP, hydrothermal pretreatment.

chemical extraction reagent [136–139]. Similarly, this was observed in the copyrolysis of sewage sludge with rice straw/husks, with the addition of rice straw [140, 141].

Various sorption methods have been examined on HMs using a variety of biochars, including surface precipitation, functional groups, coprecipitation, and π-π interaction [63, 131, 133, 142]. Sorption of Pb using sludge-derived biochar in the determination of acid mine drainage treatment containing metals efficiently removes Pb^{2+}, the reason being that Pb sorption primarily involved the coordination with organic hydroxyl and carboxyl functional groups, as well as the coprecipitation with the release of Ca^{2+} and Mg^{2+} [63]. Adsorption of Cu^{2+} by three crop straws biochars indicated that adsorption involved carboxyl and hydroxyl groups, with canola straw having more adsorption of Cu^{2+} compared to the other two biochars [131]. The relationship between Pb^{2+} adsorption and physicochemical properties of peanut shell and material from Chinese medicine-derived biochars indicated that functional groups complexation, Pb^{2+}-π interaction, and minerals precipitation jointly contributed to Pb^{2+} adsorption [133]. Two biochars in the sorption of Pb^{2+}, Cu^{2+}, Ni^{2+}, and Cd^{2+} from aqueous solutions indicated effectiveness in removing the four HMs mainly through surface precipitation mechanism [142].

Broiler litter biochar (350°C and 700°C) enhanced HM immobilization (CdII, CuII, NiII, and PbII), and cation exchange was outweighed by the coordination of π-π electrons of carbon and precipitation [33]. HM anions stabilizers (Al2O3, CaCO3, FeCl3, and NaOH) on biochar with varied pyrolysis temperature have been experimented on. Slow pyrolysis hickory wood (600°C) with the modification of NaOH considerably improved biochar's surface area, cation-exchange capacity, and thermal stability showed higher sorption of HMs (Pb^{2+}, Cu^{2+}, Ni^{2+}, Cd^{2+}, and Zn^{2+}) but preferentially removed Pb^{2+} and Cu^{2+} out of the mixed metal solution adsorption capacity as compared to pristine biochar [40].

Low-cost adsorbents including synthesizing biochar with Fe and Ca has been used in the removal of As and Cr from aqueous solutions. Organic municipal solid wastes, sewage sludge, rice husk and sandy-loam soil biochars (300°C) in the adsorption of As(V) and Cr(III and VI) from aqueous solutions managed to remove more Cr(III) and less As(V) and Cr(VI) due to high Fe_2O_3 content [143]. Independently, sewage sludge biochar removed 89% of Cr(VI) and 53% of As(V) due to enhanced metal adsorption via precipitation, unlike sandy-loam soil biochar that most effectively removed As(V) but could not retain metal anions unlike biochars [143]. Further investigations using rice husk biochar (300°C) impregnated with Ca and organic municipal solid wastes and rice husk biochars (300°C) impregnated with Fe for the removal of As(V) and Cr(VI), revealed that the enhanced biochars demonstrated low Cr(VI) removal rates. However, there was high As(V) removal capacity compared to the non-impregnated biochars due to metal precipitation and electrostatic interactions [144]. Pyrolyzed magnetic biochar (hematite mineral and pine wood biomass) at 600°C revealed a cheap source and unlike the unmodified biochar, the hematite-modified biochar not only had strong magnetic property but also the superior capability to remove As, due to sorption sites created through electrostatic interactions with Fe [54].

Engineering surface functional groups of biochar has been crucial in the advancement of high-performance adsorbents of HM and organic contaminants and cocontamination. Cd pollution in soil and water resources is a serious threat due to its release in the smelting of iron, lead, and copper ores. Modification of biochars using Bentonite (Bt), Fe and Mn oxides, and nanoscale zero-valent iron have been utilized in the removal of As and Cr. Due to the poor adsorption capacity of pure nanometals caused by agglomeration in aqueous solution, modified nanometals have demonstrated high-capacity adsorption. Bt-coated rosin biochar pyrolyzed at 400°C revealed fast and high Cr(VI) adsorption capacity with removal effectiveness of 95% within a minute under both acidic and basic conditions due to the dispersion of nanoparticles through the biochar network [145]. Fe-impregnated biochar indicated more sorption of aqueous As compared to pristine biochar, and

further investigation suggested that As sorption was mainly controlled by the chemisorption mechanism [146]. Pyrolysis of paper mill sludge produced with Fe/Ca-rich engineered biochar showed a decrease in adsorption of As(V) and Cd(II) with an increase in PO43− concentration and Ni(II) ion, respectively, and NaOH or HCl desorption renewed the absorption [134]. Biochar modified with sodium alginate using Ca(II)-impregnated biomass resulted in the removal of high Pb(II) capacity compared to most adsorbents due to anti-interference caused by functional groups and minerals of the biochar [147].

Nanoscale zero-valent iron (nZVI) biochars for the remediation of Cr-contaminated soil exhibited immobilization of Cr(VI) and reduced the phytotoxicity of Cr and the leachable Fe favorable for plant growth [130]. Modified biochar produced with acid, base, and oxidation treatment that supported zero-valent iron nanoparticles improved the removal of Cr(VI) using acid treated biochar, owing to the large surface area, low surface negative charge, and low pH [148]. Magnesium oxide nanoparticles stabilized on N-doped biochar synthesized by fast pyrolysis (400–600°C) resulted in a high Pb adsorption capacity in short equilibrium time (<10 min) and a large material through the system including removal of Cd^{2+} and tetracycline [149]. Modified biochar through activation has demonstrated great sorption efficiency of HMs.

The degree of environmental risk assessment of HM pollution in biomass and biochars has been determined by using potential ecological risk index and risk assessment code. Potential ecological risk index (RI) is used to assess the degree of potential risk of HM pollution in biomass and resultant biochar. The following ecological risk index equation were proposed and used [106, 150].

$$\begin{aligned} \mathrm{Cf} &= \frac{\mathrm{Ci}}{\mathrm{Cn}}, \\ \mathrm{Er} &= \mathrm{Tr} \times \mathrm{Cf}, \\ \mathrm{RI} &= \sum \mathrm{Er}. \end{aligned} \tag{2}$$

Cf, the contaminant factor of a HM, is the sum ratio of the HM concentrations extracted from the sequential extraction to the concentration of the HM in the residual fraction [151]. This value is inversely proportional to the leaching potential of the HM; Ci is the mobile fraction and Cn is stable fraction of the HMs; Er is the potential ecological index for individual HM; Tr is the toxic factor of the individual HM; and RI is the potential ecological risk index and it is obtained by multiplying the contamination factor (Cf) of the HM with the toxic factor (Tr) of the HM. The Tr values for individual metal can be obtained from Hakanson, [150, 152]. The potential ecological risk index (RI) of biomass and resultant biochar is obtained by adding the potential ecological index (Er) of each HM present in the solid [106].

Risk assessment code (RAC) evaluates HM toxicity in the environment including assessment of potential risk of HM in biomass and resultant biochar [24, 46]. RAC is based on the percentage of directly bioavailable exchangeable metal and carbonate-associated fractions of the total HM, and the value is obtained from the total amount divided by the total concentration of available HM multiplied by one hundred percent [46].

$$\mathrm{RAC} = \frac{\text{total amount of available heavy metal}}{\text{total concentrations of available HM}} \times 100\%. \tag{3}$$

5.3. Organic Chemical (POPs) Concentration. Biochar from a variety of biomass and waste products has been utilized and investigated in the elimination of organic substances through various mechanisms. The porosity of biochar develops more with the increase in relative high pyrolysis temperature and the lack of activation process limits pollutant removal efficiency, including other value-added applications [35]. Table 5 shows some reported effects of biochar utilization on detected organic pollutants. The mechanisms of removal by biochar through adsorption include hydrogen-bond, π-π electron donor-acceptor interaction, pore-filling, and hydrophobic effect for organic compounds [50, 51, 57, 159]. Single- and bisolute sorption of organic compounds (1,3-dichlorbenzene (DCB), 1,3-dinitrobenzene (DNB), and 2,4-dichlorophenol (DCP)) on ground tire rubber char (200°C–800°C) in a study showed that the organic compound surface area, aromaticity, and hydrophobicity increase greatly with pyrolytic temperature [57]. The adsorption was attributed to pep electron donor-acceptor interaction, H-bonding, and partition [57]. Soybean stover and peanut shell biochars (300°C and 700°C) removed organic compounds from water through adsorption dependent on the biochar's properties and its efficiency comparable to that of activated carbon due to increased hydrophobicity, surface area, and decrease in polarity [50]. Pig manure biochar adsorbed pesticide (carbaryl and atrazine) with enhanced hydrolysis due to high pH through hydrophobic effect, pore-filling, and π-π electron donor-acceptor interactions [51]. The sorption behavior of organic pollutants on biochars (300°C and 700°C) determined from orange peel, pine needle, and sugarcane bagasse feedstock resulted in biochar (300°C) displaying high sorption due to high adsorption fraction on the surface and pore-filling mechanisms [159].

Biochar with enhanced sorption capacity or selectivity for pollutant removal through activation, magnetization [60, 154], and hydrothermal synthesis has been researched on. Recently, N-doped porous carbons have demonstrated better performance in adsorption [35, 53, 60], catalysis, and capacitors relative to pure carbons [35]. Lian et al., [35] reported a high adsorption capacity for cationic and anionic organic compound dyes, better than many other reported adsorbents using N-doped biochar (600°C–800°C) from crop straws as raw material. Pyrolysis at 800°C had the highest anionic and cationic adsorption that was attributed to electrostatic attraction, π-π electron donor-accepter interaction, Lewis acid-base interaction, and microporous

Table 5: Organic contaminant potential and effect of biochar amendment.

Feedstock	Pyrolysis temp (°C)	Detected organic pollutants	Effect	Reference
Hardwood	450°C–500°C	10 PAH	Enhanced seedling growth. Greatest capacity to neutralize allelochemicals present in corn residues.	[153]
Corn	500°C 732°C	5 PAH 15 PAH	Enhanced seedling growth.	
Switch grass	850°C 845°C	17 PAH 19 PAH	Suppressed seedling growth.	
Coconut, pine nut and walnut shells	500°C	Carbamazepine and tetracycline	Fe_3O_4 enhancement exhibited fast and high sorption for carbamazepine and tetracycline. Ball milling is effective for degradation of adsorbed carbamazepine and tetracycline on the adsorbents.	[154]
Pig manure	350 and 700°C	Carbaryl and atrazine	The pesticides were adsorbed by the biochars. Hydrolyze faster on elevated pH with biochar 700°C. Carbaryl and atrazine decomposed by 71.8% and 27.9%.	[51]
Pine wood, corn stalks, peanut shells, rice straw, and wheat straw	200, 350, 500, and 700°C,	p-Nitrophenol, p-aminophenol	PNP degraded through the direct contact with EPFRs. Biochars degrade PNP in soil and natural water. EPFR-promoted degradation for 5 biochars and PNP.	[155]
Cottonwood	600°C	Methylene blue and phosphate	Excellent adsorption abilities for the contaminants.	[156]
Birchwood and Norway spruce wood	380°C–430°C	Glyphosate, diuron	Duron adsorption enhanced by biochar in soils. Glyphosate adsorption decreased in sandy soil. Ageing of soil-biochar mixtures decreased adsorption of both herbicides.	[157]
Lignin and cellulose	500°C	p-Nitrophenol	PNP decay was only modestly suppressed (12–30%). Lignin char more reactive than cellulose char. The Fe impurity in lignin played no role.	[158]
Pig manure, rice and wheat straw	350 and 700°C	Carbaryl	Enhanced chemical hydrolysis of carbaryl at high temp. Promoted biodegradation at low temp. high temp reduced biodegradation of carbaryl.	[41]

EPFRs, environmentally persistent free radicals, PNP, p-Nitrophenol.

structure formed in the biochar [35]. Active sites on biochar-graphene and wood biochar (300°C, 500°C, 700°C) in the adsorption of phthalic acid esters (PAEs) organic compounds resulted in biochar-graphene exhibiting higher adsorption capacity for contaminants remediation due to the pore-diffusion mechanism, π-π electron donor-acceptor interaction, and hydrophobicity [60].

Modification of biochar with metal ions has shown sorption capacity of organic pollutants by means of creating active sites. Shan et al., [154] prepared magnetic biochar and activated carbon with Fe_3O_4 by ball milling for removal of pharmaceutical compounds by adsorption and mechanochemical degradation. The hybrid adsorbents exhibited high removal through degrading and were easily separated magnetically and the sequential quartz sand milling improved the mechanochemical degradation of pharmaceutical compounds on biochar [154]. The formation of magnetic Fe_3O_4 on pine sawdust biochar (650°C) via oxidative hydrolysis of $FeCl_2$ to remove organic compound sulfamethoxazole solution ended up in favorable adsorption of the organic compound onto biochar through exothermic adsorption and physisorption due to hydrophobic interaction [53]. 20% optimized MgO-impregnated porous

biochar from sugarcane harvest residue prepared using adsorption pyrolysis method (550°C) from swine wastewater exhibited maximum adsorption capabilities for phosphate, ammonium, and organic substances from nutrient-rich livestock wastewaters [58].

Postpyrolysis thermal air oxidation of biochar has enhanced the sorption of organic compounds [160] and water-extractable substances that are toxic to aquatic plants and animals [161]. Investigation of the effects of thermal air oxidation on corn cob biochar after pyrolysis (300°C–700°C) showed that well-carbonized biochar was made at 600°C and 700°C with increased surface area, porosity, and adsorption, 120 times that of neutral organic substances [160]. The effects of thermal air oxidation of wood and pecan shell biochar had adsorptive properties towards organic compounds, with up to 100-fold of enhanced adsorption by means of enlarged surface area and nanopores [161].

Modified biochar is also an effective degradation method of organic pollutants through PFRs. Degradation can completely remove organic toxins from the environment as compared with sorption method. Persistent free radicals (PFRs) in biochar has indicated tremendous ability to activate persulfate/hydrogen peroxide/oxygen for the degradation of organic contaminants. The outcomes provide a method of manipulating the transformation of PFRs of contaminants in the biochar for the development of activator persulfate-based towards remediation of contaminated soils. Pine needles, wheat, and maize straw biochars effectively activated H_2O_2 for PFRs degradation to produce hydroxyl radical that degraded the organic compound [162]. Hydroxyl radical generation from biochar suspensions in the presence of oxygen degraded the organic compound diethyl phthalate (DEP) [163]. Metals (Fe^{3+}, Cu^{2+}, Ni^{2+}, and Zn^{2+}) and phenolic compound loaded on biomass increased the concentrations of PFRs in biochar and changed the type of PFRs formed to persulfate, indicating that the manipulation of the number of metals and phenolic compounds in biomass is an effective method to control PFRs in biochar [164]. Additionally, PCBs contaminants efficiently degraded with the catalytic ability of biochar to persulfate activation [164].

Fallen-leaves and wood chips hydrochar enhanced sulfadimidine organic chemical degradation due to abundant photoactive surface oxygenated functional groups in daylight irradiation than in the dark compared to fallen-leaves and wood chips pyrochar that generated reactive oxygen in the dark due to PFRs present [165]. Photogeneration of reactive oxygen species from pine needles and wheat straws biochar degraded and partially mineralized diethyl phthalate organic pollutant under UV and simulated solar lights [166]. Similarly, environmental persistent free radicals (EPFR) in the presence of different types of biochars promoted degradation of organic compounds (p-nitrophenol and p-aminophenol) and not even coating of biochar with natural organic matter inhibited p-nitrophenol degradation, suggesting the organic compound degradation capability of biochars in soil and natural water [155]. With such promising effects to degrade organic compounds with biochar, it is of importance to take caution on pesticide remediation process and the intended use of pesticide to bring a balance.

5.4. GHGs Emission. GHG effect is the heat-trapping process by GHGs within the surface-troposphere system. N_2O, CO_2, and CH_4 are potent GHGs. Taking CO_2 as a reference point with a global warming potential (GWP) of 1, N_2O, and CH_4 are estimated to have a GWP of 28–36 and 265–298 times that of CO_2, respectively [167]. Emission of the main long-standing atmospheric GHGs, N_2O, CO_2, and CH_4, increases global warming and consequently the necessity to mitigate them from the environment [168]. On average, CH_4 absorbs more energy than CO_2 and CH_4 and N_2O remain in the atmosphere more than a decade while CO_2 remains in the atmosphere for thousands of years [167]. Agricultural activities influence global warming as a result of the considerable discharge of GHGs, notwithstanding it being the major sink of CO_2 during photosynthesis [169, 170]. Biochar has a primary key function of carbon sequestration, and its stability in the soil can affect its efficiency. The stability and resistance to microbial degradation of carbon in biochar is the basis as a sequestration technique, due to its steadiness in severe weather conditions and resilience to the effects of chemicals [171]. The priming effect of biochar, however, reduces with the rise in pyrolysis temperature.

Biochar and its application to soil are mostly known for the effect of increasing the soil carbon among other nutrients through the pyrolysis process as carbon is sequestered more than its release in the atmosphere. Despite this, some application of biochar may increase the release of CO_2, suggesting signs of decay. In a study, CO_2 in soil increased with biochar application rate; however, it diminished within 6 days of the incubation [172]. The use of biochars derived from different types of biomass has enabled the maximum utilization of biochar in the pursuit of global climate change mitigation. Varied biochar application amount and time have enabled the investigation of GHGs, with results indicating the effectiveness to sequester carbon [72, 99] with a low degradation rate and long-term stability in soil [173]. CO_2 is the principal GHG and the consistent rise in its release is the main cause of global warming. There are some controversies regarding the role of biochar on CO_2 release [174]. Pyrolysis temperature during biochar preparation determines the CO_2 emission from soil. Application of biochars to soils in stabilization of soil organic matter is influenced by the soil type, and high-temperature biochar produced is suitable for long-term soil-C sequestration while low-temperature biochar is suitable in the increase of soil fertility due to mineralization [175].

The longer reaction time of over 12 months soil incubation mineralized biochar and the mean residence times for the biochars projected between 44 years and 610 years [38]. The mean residence time may, however, vary under different environmental and soil conditions, an indication that the biochar stabilized by variable charge minerals at high temperatures [38]. A 5-year laboratory experiment on the stability of 11 biochars (400°C and 550°C) observed that 0.5% and 8.9% of the biochar C was mineralized over 5 years

with C in manure-based biochars mineralizing faster than that in plant-based at 400°C than at 550°C biochars [176]. The estimated mean residence time of C in the 11 biochars varied between 90 years and 1600 years; however, it is likely to be higher under field conditions with lower moisture and temperatures or nutrient availability constraints [176]. High hydrothermal temperature, longer reaction residence time, and biomass of higher-lignin content with larger particle size produced biochar with higher stability [38, 176–179]. The effect of peak temperature, particle size, and pressure on the potential stability of slow pyrolysis (800°C) vine shoots biochar activated with aluminum oxide observed that particle size under higher peak temperatures conditions was the most influential as large particles lead to an increase in the fixed-carbon yield, percentage of aromatic carbon, and pH, hence a more stable biochar [179].

Designer biochars with enhanced capacity for carbon sequestration and stability using beneficial minerals have been used in copyrolyzing feedstock resulting in biochar enriched with minerals, adding to soil fertility. Pyrolyzed rice straw with kaolin, calcite, and calcium dihydrogen phosphate minerals to biochar enhanced the stability of biochar [178]. Yak dung and attapulgite clay mixed to produce biochars at 50/50 ratio clay to dung in Tibet resulted in low-cost high pasture yields and grass nutrition quality [180]. Higher pyrolysis temperature with the addition of clay proportions resulted in higher concentration of stable carbon, surface area and porosity, surface mineral concentration, and electrochemical capacitance, contrary to the lower temperature that resulted in higher concentration of total C and N, C/O and N functional groups, and magnetic moment [180].

Carbon sequestration potential of chicken manure-derived biochars impregnated with mineral salts ($CaCl_2$, $MgCl_2$, and $FeCl_3$) prior to pyrolysis affected biochar nutrient composition and dynamics and increased C sequestration potential [181]. The bioavailability of enriched Cu and Zn in the biochars significantly reduced, and the biochar treated with Fe mineral salt samples had the least C loss during pyrolysis and chemical oxidation and the greatest chemical and biological stability compared to pristine biochars [181]. Soils having high minerals favor long-term stability of biochar. The interaction between soil minerals ($FeCl_3$, $AlCl_3$, $CaCl_2$, and kaolinite) to investigate biochar stability and the long-term stability for comprehensive assessment of carbon sequestration efficiency demonstrated that the minerals attached tightly to biochar (surface or inner pores) and organometallic complexes (Fe-O-C) were generated with all the 4 minerals, enhancing the oxidation resistance of biochar surface by decreasing the bond of C-O, C=O, and COOH [182]. Through chemical oxidation with kaolinite, the stability of biochar increased by reducing the biodegradable C loss of total biochar, hence beneficial long-term carbon sequestration in the environment [183].

The incorporation of metals (Mg, Al, Fe, Ni, Ca, and Na) enhanced the CO_2 adsorption onto the metalized walnut shell biochars and N_2 heat treatment, with Mg-biochar and Na-biochar being highest and lowest adsorbers due to physisorption [59]. Additionally, Mg-biochar indicated a great stability of cycles of adsorption-desorption with no loss of capture capacity, easy regeneration, and fast desorption kinetic, an indication of a superior capture performance towards CO_2 over N_2, O_2, and CH_4 [59]. Sewage sludge use with the addition of $Ca(OH)_2$ to improve carbon stability in biochar indicated an increase in dissolved organic carbon content, carbon retention, and improved the surface area and alkalinity of the biochar due to the formation of $CaCO_3$ and an increase in carbon-containing functional groups [44]. Cottonwood biochar treated with metal ions (aluminum hydroxide, magnesium hydroxide, and iron oxide), pyrolyzed at 600°C, indicated that at room temperature and atmospheric pressure, biochar optimization with metal ions enhanced CO_2 adsorption ability, with aluminum hydroxide-biochar composite capturing more CO_2 than other metal composites [184]. This was attributed by surface adsorption mechanisms causing surface bonding from carbon surface and metal oxyhydroxide particles [184].

Methane has more global warming potential than CO_2 with paddy fields being among the sources of its global release [26, 169]. The method of biochar application to agricultural soil as a mitigation measure for CH_4 and N_2O emissions has been studied. N_2O emissions had a significant increase with rice plant and rice-straw-derived biochar amendment under ambient CO_2 concentration and air temperature, while N_2O emissions were suppressed under simultaneous elevated CO_2 concentration and air temperature, with and without biochar amendment, thus weakening the biochar [185]. Reduced mineral N concentrations and increased dissolved organic carbon concentrations could inhibit N_2O emission at simultaneously elevated CO_2 concentration and air temperature [185].

Anaerobic incubation of paddy soil for 14 days with rice straw biochar showed that abundance of denitrifying bacteria was reduced with biochar amendments, contributing to the decreased N_2O emissions while increased abundance of iron-reducing bacteria, competed with methanogens to produce CH_4, thereby leading to lower increase in CH_4 emission [186]. It was concluded in this study that biochar amendments with high pH and surface area were effective in mitigating the emission of N_2O and CH_4 from paddy soil [186]. N_2O, CO_2, and CH_4 were monitored twice a week for 1.5 months after adding biochar that resulted in high CH_4 uptake, but no significant differences were found in CO_2 and N_2O emissions [187]. Adding rice straw-derived biochar in a paddy soil reduced CH_4 emission under ambient and elevated temperature and CO_2, attributed to the decreased microbial activity along with the increased CH_4 oxidation activity [188]. Soilborne emissions are predominantly the major sources of N_2O in the air [32] caused mainly by nitrogen transformation microbes in the soil through nitrification and denitrification. Suppression of N_2O becomes an important climate change mitigation, varying with biomass source and pyrolysis environment. The high GWP of N_2O makes it an important GHG; hence, progressive reduction of its emission from paddy fields is of importance. The alternating wet and dry conditions of rice paddies make it a major source of N_2O emissions [170].

It has been observed that the use of biochar in the mitigation of N_2O emission escalates CO_2 emission. An incubation study with 4 contrasting soils and oil mallee, wheat chaff, and poultry litter biochars resulted in Tenosol soil having the highest mitigation of N_2O in that biochar limited the availability of NO^{3-} with the resultant rise in N_2O including liming and increased microbial respiration [48]. Biochar used in an experiment to mitigate CO_2 and N_2O from agricultural soils suppressed N_2O at moderate levels without earthworms, and CO_2 and N_2O emissions in the presence of earthworms increased, which was influenced by biochar type and application rates [189]. It was concluded that normal agricultural conditions suppress N_2O under high biochar application and heightens CO_2 emissions [189]. Biochar amendment can affect bacteria composition of N_2O-reducing functional microbial traits in soil [39]. Biochar enhancement in the growth of organisms involved in N cycling and flux of N_2O in the soil showed that biochar acts as a transitory store of nitrogen in the soil, moderating N cycling dynamics, thereby reducing N losses to leaching and gas fluxes [190]. Additionally, biochar influenced bacterial N cycling by either promoting the denitrification, N_2O to N_2, or possibly producing NH^{4+}, adsorbed to biochar and alter soil N dynamics [190].

Emission of GHGs (CO_2, CH_4, and N_2O) in soils amended with biochar was through physical and biotic mediated mechanisms and corrected with soils and biochar properties. Table 6 indicates some effects of feedstock on GHG reduction. The use of various biomass for biochar, different soil types, enhancement with beneficial minerals and salts, and increasing the soil incubation time has brought various results suitable in the pursuit of global climate change mitigating with some arising contradiction attributed to the different soils and biochar properties used. Continuous research on the effects of biochar type on soils, microbial community on HM concentration, GHGs, and organic contaminants should continue.

5.5. Health Risk. Soil pollution generates serious effects endangering the natural environment, agricultural sustainability in food safety, and the health of those who consume the food. Biomass intended to be used for the production of biochar may contain contaminants that pose a risk to the environmental and health of humans, plants, and animals. In a soil pollution survey in China cropland, HM contaminants (Zn, Se, and Cd) were identified and reported to be affecting subsistence-diet farmers in rice grain, raising health concerns [194, 195]. Cd health risk through food exposure from consumption of rice has been a concern originating from contaminated acidic rice paddies irrigated with wastewater from municipal sewage and mining tailing as well as chemical fertilization in South China [194, 196, 197]. Biochar brought about a profound implication among those using it as an agricultural field applicant. The effect of biochar amendment on rice in a Cd contaminated paddy field reduced Cd plant uptake in a 2 year monitoring by 16.8%, 37.1%, and 45.0% in 2009 and by 42.7%, 39.9%, and 61.9% in 2010, while the total plant Cd uptake was found to decrease by 28.1%, 45.7%, and 54.2% in 2009 and by 14.4%, 35.9%, and 45.9% in 2010, with biochar amendment at 10t, 20t, and 40 t/ha, respectively [196]. Biochar amendment in combination with low Cd cultivars may offer a basic option to reduce Cd levels in rice as well as to reduce GHGs emissions in rice agriculture in contaminated paddies [196].

PTEs discharge to the soil environment through increased anthropogenic activities is a global threat and plants grown in PAH-contaminated soils or water can become contaminated [153]. PAHs detected in the aqueous extracts are believed to be partly responsible for the reduction in corn seedling growth with repeated leaching of biochars eliminating the negative effects on the seedling growth [153]. These PTEs can have harmful and chronic-persistent health effects on exposed populations through food consumption grown on contaminated soils. Efforts to investigate the transformation mechanism and accumulation behavior of PTEs in soil plant system and their adverse health effects have been focused extensively. However, limited studies address biochar nanosheets (BCNs) as a potential soil amendment to reduced humans' health risks through dietary intake of food-crop grown on PTE-contaminated soil [55]. BCNs synthesized from pine wood sawdust used as soil amendment to reduce potential risks of PTEs through consumption of food grown in PTE-contaminated (Cd, Cr, Ni, and Pb) soils showed some cutback on health hazards of PTEs through reduced bioavailability and phyto-accumulation and their daily intake via consumption of wheat compared to both conventional organic amendments (COAs) and control [55]. The risk assessment outcomes for the hazard indices (HIs) were <1 for PTEs in all treatments with the BCNs addition significantly ($P \leq 0.05$) reduced risk level, when compared to control. BCNs addition significantly suppressed cancer risk for Cd, Cr, and Ni over a lifetime of exposure compared to control [55].

Consumption of rice contaminated with PTEs is a major pathway for human exposure to PTEs as revealed in China's so called "Cancer Villages"; hence, sewage sludge biochar was applied to suppress PTE (As, Cd, Co, Cu, Mn, Pb, and Zn) phyto-availability in soil to reduce PTE levels in rice grown in mining-impacted paddy soils [61]. Risk assessment indicated that 10% biochar ($P \leq 0.05$) decreased the daily intake, associated with the consumption of rice by 68, 42, 55, 29, 43, 38, and 22% PTEs, respectively [61]. Health quotient (HQ) indices for PTEs (except for As, Cu, and Mn) were <1, indicating a suppression of health risk pointing to the incremental lifetime cancer (ILTR) value for iAs (AsIII + AsV) associated with the consumption of rice significantly reducing ($P \leq 0.01$) by 66% [61]. Biochar application can enhance phthalic acid ester adsorption in soils, which is a priority pollutant, endocrine-disrupting compounds, and its accumulation in the human body causes potential mutagenic health threats [198]. The immobilizing ability of enhanced biochar is useful to consider when designing phthalic acid ester immobilizer for the reduction of phthalic acid ester bioavailability [51]. The presence of contaminants such as HMs and organic compounds in biochar for soil application presents undesirable agricultural and human health risks

Table 6: GHG abatement potential and effect of biochar amendment.

Feedstock	Pyrolysis temp (°C)	GHGs	Effect	Reference
Wheat straw	350–550	CH_4, CO_2, N_2O	Maize yield was increased. Increased crop productivity, soil properties. N_2O emission was decreased. Biochar increased the total CO_2 emission. Increased CH_4.Total GWP of CH_4 and N_2O decreased.	[29, 191]
Maize straw	400–450	CO_2	Insignificant CO_2 emissions Lowered CO_2 emissions and higher dry matter.	[42]
Rice straw	500	N_2O	Increased N_2O without char. N_2O reduction via denitrification with char. Reduced mineral N with and without biochar.	[185]
Biosolids	—	CH_4, N_2O	Decreased N_2O by 84% but increased CO_2 emission. Changed soil pH and increased soil aeration.	[192]
Oil mallee, wheat chaff and poultry litter	550	N_2O	Oil mallee biochar reduced more N_2O. Insignificant reduction of N_2O in poultry litter biochar. Biochars reduced overall N_2O emissions in Tenosol.	[48]
Bamboo	600	N_2O	Biochar lowered NO^{2-}-N concentrations Lowered total N_2O from pig manure compost. Less N_2O producing and more N_2O-consuming bacteria present.	[193]
Rice straw and bamboo	600	CH_4	Rice straw char more efficient in reducing CH_4 emission than bamboo char. Rice straw char decrease CH_4 emission by 47.30%–86.43%. Decreased methanogenic activity with rice straw char. Rice yield increased.	[31]

GWP–global warming potential.

with its continuous use. Testing for the presence of toxic content should be a priority component of biochar quality assessment due to the particular concern of the hydrophobic, recalcitrant, persistent, potentially carcinogenic, mutagenic, and phytotoxic properties [153].

6. Environmental Implications

In order to evaluate the environmental implications of biochar application, the heterogeneous properties need to be understood. Application of biochar to soils creates an irreversible condition of its removal; hence, cautious consideration on the use of waste is needed on its production and assessment of effects on the environment and agricultural use. Identified of potential sources of hazards can be prevented at the initial stage of the biochar production process by isolating and prohibiting contaminated feedstock/biomass, including regulating the pyrolysis environment that may favor their production to avoid detrimental resultant biochar. Physical and chemical properties of biochar such as composition and particle and pore size distribution are largely controlled by feedstock type and pyrolysis conditions, hence the necessity to determine its behavior to plants, outcome to the environment, suitability to soil improvement application, and contaminant removal. Other properties of biochar, such as CEC, pH, and functional groups, also vary. This enables the introduction of a necessary control measure to assess and monitor the production quality of biochar suitable for particular uses such as land-use type, climate change, soil type property improvement, and soil contaminants.

There are numerous biomass wastes such as plant and animal residue, sewage sludge, and MSW with beneficial use as optional feedstock sources. Minimization of agricultural waste and reuse of manmade biomass for biochar has brought positive contamination remediation and mitigation effects to the environment. However, some feedstock may contain toxicants (HMs, organic compounds) and biological (pathogens) threats to human health and the environment with the uncontrolled application. The concentration of metal elements, including essential elements, may lead to DNA and cell membrane damage [199], including oxidative stress [200]. The potential to alter these threats through controlled feedstock, pyrolysis conditions, modified biochar, activation materials, metal oxide nanoparticles on N-doped, and zero-valent iron nanoparticles offers substantial environmental advantage through nonavailability of metal ions, immobilization, and stabilization of harmful ions, cations, and compounds. The eco-toxicity of HM in sludge has been shown to decrease significantly after pyrolysis or liquefaction processes resulting in a decrease in the environmental risk of biochar utilization [24, 106]. Regulating the type of feedstock

used controls undesired detrimental properties from the initial.

Thermal air oxidation on post-pyrolysis has been shown to affect bioavailability of organic substances. Thermal air oxidation of biochar at high-heat thermal temperatures open pores, introducing hydrogen bonds for ionizable compounds to enhance the adsorption of organic substances affecting bioavailability to plants, soil, and water [160, 161]. Hydrochar as compared to pyrochar had more organic pollutant degradation due to higher photochemical reactive oxygen generation ability, an indication of a viable environmental remediation tool under solar light irradiation [165]. Photo generation of reactive oxygen species in biochar further reveals that biochar particles can partake in the photo-transformation of contaminants in the natural environment for the degradation of organic contaminants in wastewater [166]. Organic contaminant degradation by EPFRs can be a process considered when assessing the environmental roles of biochar and other carbonaceous materials regulating the fate of contaminants removal [155]. Multilayer surface sorption, pore-filling, and thermodynamic of low-temperature biochar are suitable for remediating environmental organic molecules pollutants, hence a basis for designing biochars multifunctional sorbents of pollutants [159]. Manipulation of metal and organic concentrations in biomass significantly changed the concentrations factors of PFRs in biochar which was an alternative activator of persulfate for the degradation of contaminants, a strategy for the reuse of hyperaccumulator biomass in the phytoremediation of HM from soil. Hydrogen peroxide and persulfate oxidants can be replaced with pyrolyzed hyperaccumulator biomass to make catalytic oxidant decomposition for organic pollutant degradation and contaminated soil remediation [164].

Carbon sequestration has been proposed from varied feedstock, with some addition of minerals, applied to diverse soil and plant environment, each with different results; hence, the total environmental recalcitrance is a function of both the properties of the biochar generated and soil environment to which it is applied [201]. The reduction of CH_4 production with the use of biochar in paddy soil under the elevated temperature and CO_2 condition is relevant to the prediction of global warming environment and points the essence of biochar in assisting with slowing down the greenhouse effect [188]. Biochar has been shown to promote changes in bacterial families; hence, advanced research to measure temporal changes and metabolism of specific bacteria in the soil can be considered beneficial, more importantly in mitigation of GHGs fluctuation [190]. The MgO-impregnated livestock wastewater biochar facilitates resource conservation, nutrient cycling, and sustainable development of the environment through removal of phosphate and ammonium, availing a source of nutrient-rich fertilizer product for agricultural soil application and reduces agricultural waste disposal as it lessens CO_2 emission [58].

The effective use of biochar as a carbon sequestration strategy requires quality assessment with regards to environmental recalcitrance during the sourcing of feedstock and biochar preparation and before and after application to soil. There are a number of characterization procedures used involving cost and time of analysis associated resulting in unreasonable to the wide-range application [177]. To this understanding, there is not a well-known current framework conducting quality assurance/quality control checks in pre- and postapplication assessment of biochar carbon sequestration. A framework for assessing biochar carbon sequestration ought to describe the environmental effect on degradation, which includes temperature, moisture, mineralogy, and organic matter of soils [201–205]. The development of R50-based model accounts for variability in appropriate environmental situations and predict intermittent biochar carbon loss and recalcitrance likelihood over time. The model can be incorporated with an economic model to assess the long-term tradeoffs of a specific R50 biochar application to soil compared to other alternatives [177]. The R50 index-based methodological framework assesses the environmental recalcitrance including carbon sequestration potential of biochars applicable to the preapplication screening of modified carbons into Class A ($R50 \geq 0.70$), Class B ($0.50 \leq R50 < 0.70$), or Class C ($R50 < 0.50$) recalcitrance/carbon sequestration classes [177]. By coupling R50 with biochar properties, it can be screened to find the "optimum" biochar for practice applications with additional targeted benefits for soil improvement [206].

Biochar for soil amendment can be produced depending on the conditional needs of the soil to enhance soil properties and reduce the threats of contaminants from pollution and overuse of soil nutrients and organic compounds on the environment. The remediation effect of biochar to remove the contaminants and make the soil contaminant free and nutritious will ensure the normal growth of various crops. Usage of biochar in the right way, appropriate biochar, and dose in a particular soil are necessary. Screening of effective biochars as engineered sorbents has been proposed with the use of peanut shell and Chinese medicine material-derived biochars to remove or immobilize Pb^{2+} in polluted water and soil [132]. Pyrolysis of some biomass can be a source of secondary pollution of HMs. A single chemical extraction procedure does not reveal the total bioavailable HMs in the biochars, and therefore, to assess the potential risk and long-term stability of the biochars, the chemical speciation of HMs in the biochars need to be examined and assessed. Sequential extraction procedures have been successfully used to determine the extractable total and bioavailable HMs in manure [136–139]. This enhances the utilization of suitable engineering production, and risk assessment approaches to ensure potential hazards are eluded. It is necessary to keep abreast with up-to-date research and engage the expertise on the current production technologies to control possible hazards.

Biochar use as an alternative adsorbent to remediate contaminants could be advantageous and cheap compared to activated carbon since less energy is required with low-cost and readily available pre- or postactivation materials. Modified biochar with magnet (hematite) and NaOH are cheap sources to enhance biochar properties and create friendly environmental substitute adsorbent in the removal

of As contaminant using external magnet, and HMs (Pb^{2+}, Cd^{2+}, Cu^{2+}, Zn^{2+}, Ni^{2+}) [40, 54]. Magnesium oxide nanoparticles on N-doped biochar is suitable for Pb adsorption and the removal of Cd^{2+} and tetracycline in various environment obstructions (pH, natural organic matter, and metal ions), thus its suitability in the treatment of wastewater, natural water resources, and drinking water [149]. Similarly, modified and efficient zero-valent iron nanoparticles methods are cost effective. Bt-coated rosin with Fe_2O_3 can be efficiently used for Cr(VI) removal in water resources in varied pH range or even during leakage [145, 148]. The resultant Cr(III)/Fe(III) hydroxides produced in the biochar are insoluble and can easily be removed to eliminate secondary pollution [148]. The release of scrap tire chars in the environment is also a cost-effective sorbent in the treatment of organic contaminated (DCB, DNB, and DCP) wastewater if properly managed and would exhibit distinct effects on the fate and transport of organic contaminants due to hydrophobicity, polarity, and H-bonding acceptor/donor properties [57].

Toxic compounds that are related with thermal treatment products and feared for soil amendments should be controlled for biochar use. PAH can be produced during the pyrolysis process and is controlled by substrate composition and temperature, which play an important role in its formation, and it is adsorbed onto biochar surfaces [153]. Consideration can be made on the flexibility of minimizing the production of contaminated biochar and maximizing production of syngas and bio-oil, co-products of pyrolysis. The health quotient (HQ) is often used for assessing potential risks and adverse health effects resulting from the ingestion of pollutants, with food chain being a major pathway for human exposure [61]. High-capacity accumulation of PTEs in rice and its high level of consumption are the main source of exposure with dietary consumption exposure being 3–11 times higher than that in vegetables, with rice consumption contributing >75% of the PTE intake for a population of a village near the abandoned mine [61].

An assessment of biochar production suitability for use as a soil additive or production of energy, without environmental and production risks, requires a comprehensive analysis of biomass. The variety of biochar properties, with a range of nutrients and acceptable contaminant levels, suggests soil application suitability for growth of plants for consumption and forestry. Certification schemes operated by governing bodies need to administer a robust set of standards to ensure the sustainable use of biomass resources by identifying suitable biomass and analyze test procedures for industry standard. Minimum risks of measured quantity levels that do not pose a significant risk have been recommended. Standards given by IBI and EBC provide a starting point guidance to consider possible risks that can be tested, measured, monitored, and controlled. A continuous and essential quality assessment and monitoring methodology can demonstrate effective control of hazards in biochar. Effective risk evaluation, management, and sustainability guidelines, with scientific research being a driving factor, will cause biochar to be an indispensable tool for environmental management.

7. Conclusion

It is important to have in mind the characteristics of waste being considered as biomass. The degree of biochar net benefit must supersede the related risks. The toxicity of HMs depends on the total and bioavailable concentrations. Various sorption methods of biochar utilized, among them low-cost adsorbents, engineered surface functional groups, and nZVI modified biochars, have been examined on HMs using a variety of biochars, which involved surface precipitation, functional groups, coprecipitation, and π-π interaction. The chemisorption mechanism involved the coordination with organic hydroxyl and carboxyl functional groups, functional group complexation, minerals precipitation, electrostatic interactions, and the dispersion of nanoparticles through the biochar network. The mechanisms of organic compound removal through sorption and enhanced sorption was through activation, magnetization, and hydrothermal synthesis. These involved hydrogen-bond, π-π electron donor-acceptor interaction, pore-filling, pep electron donor-acceptor interaction, hydrophobicity, H-bonding, partition, polarity, high surface adsorption fraction, electrostatic attraction, Lewis acid-base interaction, and microporous structure and pore-diffusion mechanism. Modified biochar with metal ions involved magnetic separation through exothermic adsorption and physisorption due to hydrophobic interaction. Postpyrolysis thermal air oxidation had adsorptive properties through increased surface area, porosity, and adsorption. Degradation through Persistent free radicals (PFRs) activated persulfate/hydrogen peroxide/oxygen due to abundant photoactive surface oxygenated functional groups. Emissions of GHGs in soils amended with biochar emanate through physical and biotic mediated mechanisms, which are lessened with enhanced soils and biochar properties. High-temperature biochar produced is suitable for long-term soil-C sequestration. High hydrothermal temperature, longer reaction residence time, and biomass of higher-lignin content with larger particle size produced biochar with higher stability. Designer biochar with the addition of beneficial minerals enhanced capacity for carbon sequestration and long-term stability attributed by surface adsorption mechanisms. Biochar and BCNs have a significance in reducing the health quotient indices for PTEs risk contamination by suppressed cancer risk arising from consumption of food contaminated with PTEs, pointing to a reduction in the incremental lifetime cancer (ILTC) value.

The immobilizing ability of enhanced biochar has been successfully used to reduce bioavailability of pollutants with mutagenic health threats. The degree of environmental risk assessment of HM pollution in biomass and biochars has been determined by using potential ecological risk index and RAC in assessing the degree of potential risk of HM pollution in biomass and resultant biochar. Organic contaminant degradation by EPFRs can be a process considered when assessing the environmental roles of biochar and other carbonaceous materials regulating the fate of contaminants removal. Identified potential sources of hazards can be prevented at the initial stage of the biochar production

process by isolating and prohibiting contaminated feedstock/biomass, including regulating the pyrolysis environment that may favor their production to avoid detrimental resultant biochar. The potential to alter these threats through controlled feedstock, pyrolysis conditions, biochar, and modified biochar offers substantial environmental advantage through nonavailability of PTE. Hazards posed by the use of biochar necessitate it to be at a manageable level such that the resulting risks are considered acceptable. Challenges and disparity of laboratory pot experiments outcomes under optimum operating conditions and the recommendations given by researchers on biochar applications need to translate into pilot scale and to commercial level under normal environmental conditions. Effective implementation of risk control in biochar production, management, and sustainability mechanisms, driven by up-to-date research and acceptable social standards and policy will advance safe utilization of biochar as a soil applicant, to control contaminants and in GHG management.

Conflicts of Interest

The authors declare that they have no significant competing financial, professional, or personal interests that might have influenced the performance or presentation of the work described in this manuscript.

Acknowledgments

This study was supported by National Natural Science Foundation of China (51504174) and Open Research Foundation of Center of Material Research and Measurement of Wuhan University of Technology (2018KFJJ12).

References

[1] L. Wei, L. Sha, and H. Guan, "Research on the sorting reclaim system of municipal solid waste based on the concept of "cradle to cradle"," in *Proceedings of the Tenth International Conference on Waste Management and Technology (ICWMT)*, pp. 482–490, Mianyang, China, 2016.

[2] B. Zhou, C. Sun, and H. Yi, "Solid waste disposal in Chinese cities: an evaluation of local performance," *Sustainability*, vol. 9, no. 12, p. 2234, 2017.

[3] A. Pires, G. Martinho, and N.-B. Chang, "Solid waste management in European countries: a review of systems analysis techniques," *Journal of Environmental Management*, vol. 92, no. 4, pp. 1033–1050, 2011.

[4] A. M. Camps, S. Surinder, and L. Jens, "Environmental benefits and risks of biochar application to soil," *Agriculture, Ecosystems & Environment*, vol. 191, pp. 1–4, 2014.

[5] EPA, *Criteria for the Definition of Solid Waste and Solid and Hazardous Waste Exclusions*, United States Environmental Protection Agency (EPA), Washington, DC, USA, 2018.

[6] Q. Huang, L. Wang, B. Xi, and B. Zhou, "The current situation of solid waste management in China," *Journal of Material Cycles and Waste Management*, vol. 8, no. 1, pp. 63–69, 2006.

[7] EPA, *EPA's Cradle-To-Grave Hazardous Waste Management Program*, United States Environmental Protection Agency (EPA), Washington, DC, USA, 2017.

[8] A. Lodolo, E. V. Gonzalez, and S. Miertus, "Overview of remediation technologies for persistent toxic substances," in *International Centre for Science and High Technology, ICS-UNIDO Workshop on Contamination of Food and Agro products*, Trieste, Italy, 2000.

[9] USEPA, *Persistent, Bio Accumulative, and Toxic (PBT) Chemicals Initiative*, Office of Pollution Prevention and Toxics, Washington, DC, USA, 1999.

[10] ICS-UNIDO, UNECE, *Compendium of Soil Clean-Up Technologies and Soil Remediation Companies*, New York, NY, USA, 2nd edition, 2000.

[11] OHM, *Trial Burn Report for the Baird & McGuire Superfund Site*, OHM, Remediation Service, Orlando, FL, USA, 1995.

[12] P. Costner, *Technical Criteria for the Destruction of Stockpiled POPs*, Third Meeting of the Intersessional Group Intergovernmental Forum on Chemical Safety, Yokohama, Japan, 1998.

[13] A. Downie, A. Crosky, and P. Munroe, *Physical Properties of Biochar*, Earthscan, London, UK, 2009.

[14] C. Benestad, "Incineration of hazardous waste in cement kilns," *Waste Management & Research*, vol. 7, no. 1, pp. 351–361, 1989.

[15] IBI, "Standardized product definition and product testing guidelines for biochar that is used in soil," *International Biochar Initiative (IBI)*, 2012.

[16] EBC, *Guidelines for Biochar Production: European Biochar Certificate*, European Biochar Certificate (EBC) Foundation, Arbaz, Switzerland, 2012.

[17] EBC, *Comparison of European Biochar Certificate Version 4.8 and IBI Biochar Standards Version 2.0*, European Biochar Certificate (EBC) Foundation, Arbaz, Switzerland, 2014.

[18] S. Schimmelpfennig and B. Glaser, "One step forward toward characterization: some important material properties to distinguish biochars," *Journal of Environment Quality*, vol. 41, no. 4, pp. 1001–1013, 2012.

[19] B. Singh and M. D. Raven, *X-ray Diffraction Analysis of Biochar. , Biochar: A Guide to Analytical Methods*, p. 245, CRC Press, Taylor and Francis group, Boca Raton, FL, USA, 2017.

[20] S. Sohi, "Biochar, climate change and soil: a review to guide future research," CSIRO Land and Water Science Report, vol. 5, pp. 17–31, 2009.

[21] Y. Liu, M. Yang, Y. Wu, H. Wang, Y. Chen, and W. Wu, "Reducing CH_4 and CO_2 emissions from waterlogged paddy soil with biochar," *Journal of Soils and Sediments*, vol. 11, no. 6, pp. 930–939, 2011.

[22] J. Sparkes and P. Stoutjesdijk, *Biochar: Implications for Agricultural Productivity*, Australian Bureau of Agricultural and Resource Economics and Sciences, Government of Australia, Canberra, Australia, 2011.

[23] K. Lu, X. Yang, J. Shen et al., "Effect of bamboo and rice straw biochars on the bioavailability of Cd, Cu, Pb and Zn to Sedum plumbizincicola," *Agriculture, Ecosystems & Environment*, vol. 191, pp. 124–132, 2014.

[24] J. Shao, X. Yuan, L. Leng et al., "The comparison of the migration and transformation behavior of heavy metals during pyrolysis and liquefaction of municipal sewage sludge, paper mill sludge, and slaughterhouse sludge," *Bioresource Technology*, vol. 198, pp. 16–22, 2015.

[25] R. A. Brown, A. K. Kercher, T. H. Nguyen, D. C. Nagle, and W. P. Ball, "Production and characterization of synthetic wood chars for use as surrogates for natural sorbents," *Organic Geochemistry*, vol. 37, no. 3, pp. 321–333, 2006.

[26] A. Zhang, L. Cui, G. Pan et al., "Effect of biochar amendment on yield and methane and nitrous oxide emissions from a rice paddy from Tai Lake plain, China," *Agriculture, Ecosystems & Environment*, vol. 139, no. 4, pp. 469–475, 2010.

[27] L. Leng, S. Leng, J. Chen et al., "The migration and transformation behavior of heavy metals during co-liquefaction of municipal sewage sludge and lignocellulosic biomass," *Bioresource Technology*, vol. 259, pp. 156–163, 2018.

[28] L. Beesley, E. Moreno-Jiménez, and J. L. Gomez-Eyles, "Effects of biochar and greenwaste compost amendments on mobility, bioavailability and toxicity of inorganic and organic contaminants in a multi-element polluted soil," *Environmental Pollution*, vol. 158, no. 6, pp. 2282–2287, 2010.

[29] A. Zhang, Y. Liu, G. Pan et al., "Effect of biochar amendment on maize yield and greenhouse gas emissions from a soil organic carbon poor calcareous loamy soil from Central China Plain," *Plant and Soil*, vol. 351, no. 1-2, pp. 263–275, 2012.

[30] S. Kloss, F. Zehetner, A. Dellantonio et al., "Characterization of slow pyrolysis biochars: effects of feedstocks and pyrolysis temperature on biochar properties," *Journal of Environment Quality*, vol. 41, no. 4, pp. 990–1000, 2012.

[31] D. Dong, M. Yang, C. Wang et al., "Responses of methane emissions and rice yield to applications of biochar and straw in a paddy field," *Journal of Soils and Sediments*, vol. 13, no. 8, pp. 1450–1460, 2013.

[32] N. Hagemann, J. Harter, R. Kaldamukova et al., "Does soil aging affect the N_2O mitigation potential of biochar? a combined microcosm and field study," *GCB Bioenergy*, vol. 9, no. 5, pp. 953–964, 2017.

[33] M. Uchimiya, I. M. Lima, K. T. Klasson, and L. H. Wartelle, "Contaminant immobilization and nutrient release by biochar soil amendment: roles of natural organic matter," *Chemosphere*, vol. 80, no. 8, pp. 935–940, 2010.

[34] S. V. Wesenbeeck, W. Prins, F. Ronsse, and M. J. Antal, "Sewage sludge carbonization for biochar applications. Fate of heavy metals," *Energy & Fuels*, vol. 28, pp. 5318–5326, 2014.

[35] F. Lian, G. Cui, Z. Liu, L. Duo, G. Zhang, and B. Xing, "One-step synthesis of a novel N-doped microporous biochar derived from crop straws with high dye adsorption capacity," *Journal of Environmental Management*, vol. 176, pp. 61–68, 2016.

[36] M. Uchimiya, L. H. Wartelle, K. T. Klasson, C. A. Fortier, and I. M. Lima, "Influence of pyrolysis temperature on biochar property and function as a heavy metal sorbent in soil," *Journal of Agricultural and Food Chemistry*, vol. 59, no. 6, pp. 2501–2510, 2011.

[37] X. Xu, X. Cao, L. Zhao, H. Wang, H. Yu, and B. Gao, "Removal of Cu, Zn, and Cd from aqueous solutions by the dairy manure-derived biochar," *Environmental Science and Pollution Research*, vol. 20, no. 1, pp. 358–368, 2013.

[38] Y. Fang, B. Singh, B. P. Singh, and E. Krull, "Biochar carbon stability in four contrasting soils," *European Journal of Soil Science*, vol. 65, no. 1, pp. 60–71, 2014.

[39] J. Harter, P. Weigold, M. El-Hadidi, D. H. Huson, A. Kappler, and S. Behrens, "Soil biochar amendment shapes the composition of N_2O-reducing microbial communities," *Science of the Total Environment*, vol. 562, pp. 379–390, 2016.

[40] Z. Ding, X. Hu, Y. Wan, S. Wang, and B. Gao, "Removal of lead, copper, cadmium, zinc, and nickel from aqueous solutions by alkali-modified biochar: batch and column tests," *Journal of Industrial and Engineering Chemistry*, vol. 33, pp. 239–245, 2016.

[41] X. Ren, P. Zhang, L. Zhao, and H. Sun, "Sorption and degradation of carbaryl in soils amended with biochars: influence of biochar type and content," *Environmental Science and Pollution Research*, vol. 23, no. 3, pp. 2724–2734, 2016.

[42] Y. Shen, L. Zhu, H. Cheng, S. Yue, and S. Li, "Effects of biochar application on CO_2 emissions from a cultivated soil under semiarid climate conditions in Northwest China," *Sustainability*, vol. 9, no. 8, p. 1482, 2017.

[43] H. Jin, S. Capareda, Z. Chang, J. Gao, Y. Xu, and J. Zhang, "Biochar pyrolytically produced from municipal solid wastes for aqueous As(V) removal: adsorption property and its improvement with KOH activation," *Bioresource Technology*, vol. 169, pp. 622–629, 2014.

[44] N. Ren, Y. Tang, and M. Li, "Mineral additive enhanced carbon retention and stabilization in sewage sludge-derived biochar," *Process Safety and Environmental Protection*, vol. 115, pp. 70–78, 2018.

[45] X. Wang, Q. Chi, X. Liu, and Y. Wang, "Influence of pyrolysis temperature on characteristics and environmental risk of heavy metals in pyrolyzed biochar made from hydrothermally treated sewage sludge," *Chemosphere*, vol. 216, pp. 698–706, 2019.

[46] L. Leng, X. Yuan, H. Huang, H. Jiang, X. Chen, and G. Zeng, "The migration and transformation behavior of heavy metals during the liquefaction process of sewage sludge," *Bioresource Technology*, vol. 167, pp. 144–150, 2014.

[47] X. Liu, Y. Wang, C. Gui et al., "Chemical forms and risk assessment of heavy metals in sludge-biochar produced by microwave-induced low temperature pyrolysis," *RSC Advances*, vol. 6, no. 104, pp. 101960–101967, 2016.

[48] L. Van Zwieten, B. P. Singh, S. W. L. Kimber et al., "An incubation study investigating the mechanisms that impact N_2O flux from soil following biochar application," *Agriculture, Ecosystems & Environment*, vol. 191, pp. 53–62, 2014.

[49] B. Chen and Z. Chen, "Sorption of naphthalene and 1-naphthol by biochars of orange peels with different pyrolytic temperatures," *Chemosphere*, vol. 76, no. 1, pp. 127–133, 2009.

[50] M. Ahmad, S. S. Lee, X. Dou et al., "Effects of pyrolysis temperature on soybean stover- and peanut shell-derived biochar properties and TCE adsorption in water," *Bioresource Technology*, vol. 118, pp. 536–544, 2012.

[51] P. Zhang, H. Sun, L. Yu, and T. Sun, "Adsorption and catalytic hydrolysis of carbaryl and atrazine on pig manure-derived biochars: impact of structural properties of biochars," *Journal of Hazardous Materials*, vol. 244-245, pp. 217–224, 2013.

[52] B. Chen, D. Zhou, L. Zhu, and X. Shen, "Sorption characteristics and mechanisms of organic contaminant to carbonaceous biosorbents in aqueous solution," *Science in China Series B: Chemistry*, vol. 51, no. 5, pp. 464–472, 2008.

[53] F. Reguyal, A. K. Sarmah, and W. Gao, "Synthesis of magnetic biochar from pine sawdust via oxidative hydrolysis of $FeCl_2$ for the removal sulfamethoxazole from aqueous solution," *Journal of Hazardous Materials*, vol. 321, pp. 868–878, 2017.

[54] S. Wang, B. Gao, A. R. Zimmerman et al., "Removal of arsenic by magnetic biochar prepared from pinewood and natural hematite," *Bioresource Technology*, vol. 175, pp. 391–395, 2015b.

[55] B. Yousaf, G. Liu, Q. Abbas et al., "Comparative effects of biochar-nanosheets and conventional organic-amendments on health risks abatement of potentially toxic elements via consumption of wheat grown on industrially contaminated-soil," *Chemosphere*, vol. 192, pp. 161–170, 2018.

[56] H.-S. Kim, K.-R. Kim, H.-J. Kim et al., "Effect of biochar on heavy metal immobilization and uptake by lettuce (*Lactuca sativa* L.) in agricultural soil," *Environmental Earth Sciences*, vol. 74, no. 2, pp. 1249–1259, 2015.

[57] F. Lian, F. Huang, W. Chen, B. Xing, and L. Zhu, "Sorption of apolar and polar organic contaminants by waste tire rubber and its chars in single- and bi-solute systems," *Environmental Pollution*, vol. 159, no. 4, pp. 850–857, 2011.

[58] R. Li, J. J. Wang, B. Zhou et al., "Simultaneous capture removal of phosphate, ammonium and organic substances by MgO impregnated biochar and its potential use in swine wastewater treatment," *Journal of Cleaner Production*, vol. 147, pp. 96–107, 2017.

[59] P. Lahijani, M. Mohammadi, and A. R. Mohamed, "Metal incorporated biochar as a potential adsorbent for high capacity CO_2 capture at ambient condition," *Journal of CO_2 Utilization*, vol. 26, pp. 281–293, 2018.

[60] G. Abdul, X. Zhu, and B. Chen, "Structural characteristics of biochar-graphene nanosheet composites and their adsorption performance for phthalic acid esters," *Chemical Engineering Journal*, vol. 319, pp. 9–20, 2017.

[61] S. Khan, B. J. Reid, G. Li, and Y.-G. Zhu, "Application of biochar to soil reduces cancer risk via rice consumption: a case study in Miaoqian village, Longyan, China," *Environment International*, vol. 68, pp. 154–161, 2014.

[62] T. Liu, B. Liu, and W. Zhang, "Nutrients and heavy metals in biochar produced by sewage sludge pyrolysis: its application in soil amendment," *Polish Journal of Environmental Studies*, vol. 23, pp. 271–275, 2014.

[63] H. Lu, W. Zhang, Y. Yang, X. Huang, S. Wang, and R. Qiu, "Relative distribution of Pb^{2+} sorption mechanisms by sludge-derived biochar," *Water Research*, vol. 46, no. 3, pp. 854–862, 2012.

[64] M. Hussain, M. Farooq, A. Nawaz et al., "Biochar for crop production: potential benefits and risks," *Journal of Soils and Sediments*, vol. 17, no. 3, pp. 685–716, 2016.

[65] R. Lal, "Black and buried carbons' impacts on soil quality and ecosystem services," *Soil and Tillage Research*, vol. 99, no. 1, pp. 1–3, 2008.

[66] J. Lehmann and S. Joseph, *Biochar for Environmental Management: An Introduction*, Earthscan from Routledge, London, UK, 2nd edition, 2015.

[67] J. Lehmann, J. Skjemstad, S. Sohi et al., "Australian climate-carbon cycle feedback reduced by soil black carbon," *Nature Geoscience*, vol. 1, no. 12, pp. 832–835, 2008.

[68] S. P. Sohi, E. Krull, E. Lopez-Capel, and R. Bol, "A review of biochar and its use and function in soil," *Advances in Agronomy*, vol. 105, pp. 47–82, 2010.

[69] H. Scott, "Biochar: an improver of nutrient and soil water availability-what is the evidence?" *CAB Reviews: Perspectives in Agriculture, Veterinary Science, Nutrition and Natural Resources*, vol. 9, 2014.

[70] M. Uchimiya, D. I. Bannon, and L. H. Wartelle, "Retention of heavy metals by carboxyl functional groups of biochars in small arms range soil," *Journal of Agricultural and Food Chemistry*, vol. 60, no. 7, pp. 1798–1809, 2012.

[71] C. E. Brewer, K. Schmidt-Rohr, J. A. Satrio, and R. C. Brown, "Characterization of biochar from fast pyrolysis and gasification systems," *Environmental Progress & Sustainable Energy*, vol. 28, no. 3, pp. 386–396, 2009.

[72] B. Fungo, D. Guerena, M. Thiongo, J. Lehmann, H. Neufeldt, and K. Kalbitz, "N_2O and CH_4 emission from soil amended with steam-activated biochar," *Journal of Plant Nutrition and Soil Science*, vol. 177, no. 1, pp. 34–38, 2014.

[73] S. E. Kolb, K. J. Fermanich, and M. E. Dornbush, "Effect of charcoal quantity on microbial biomass and activity in temperate soils," *Soil Science Society of America Journal*, vol. 73, no. 4, pp. 1173–1181, 2009.

[74] Y. Kuzyakov, I. Subbotina, H. Chen, I. Bogomolova, and X. Xu, "Black carbon decomposition and incorporation into soil microbial biomass estimated by 14C labeling," *Soil Biology and Biochemistry*, vol. 41, no. 2, pp. 210–219, 2009.

[75] J. Chen, W. Hong, T. Huang, L. Zhang, W. Li, and Y. Wang, "Activated carbon fiber for heterogeneous activation of persulfate: implication for the decolorization of azo dye," *Environmental Science and Pollution Research*, vol. 23, no. 18, pp. 18564–18574, 2016.

[76] B. Glaser, J. Lehmann, and W. Zech, "Ameliorating physical and chemical properties of highly weathered soils in the tropics with charcoal - a review," *Biology and Fertility of Soils*, vol. 35, no. 4, pp. 219–230, 2002.

[77] J. Lehmann, J. Pereira da Silva Jr., C. Steiner, T. Nehls, W. Zech, and B. Glaser, "Nutrient availability and leaching in an archaeological Anthrosol and a Ferralsol of the Central Amazon basin: fertilizer, manure and charcoal amendments," *Plant and Soil*, vol. 249, no. 2, pp. 343–357, 2003.

[78] C. J. Barrow, "Biochar: potential for countering land degradation and for improving agriculture," *Applied Geography*, vol. 34, pp. 21–28, 2012.

[79] M. Inyang and E. Dickenson, "The potential role of biochar in the removal of organic and microbial contaminants from potable and reuse water: a review," *Chemosphere*, vol. 134, pp. 232–240, 2015.

[80] J. Lehmann, J. Gaunt, and M. Rondon, "Bio-char sequestration in terrestrial ecosystems—a review," in *Mitigation and Adaptation Strategies for Global Change*, vol. 11, pp. 395–419, Springer, Berlin, Germany, 2006.

[81] F. G. A. Verheijen, S. Jeffery, A. C. Bastos, M. van der Velde, and I. Diafas, *Biochar Application to Soils-A Critical Scientific Review of Effects on Soil Properties, Processes and Functions*, p. 149, Institute for Environment and Sustainability, Luxembourg, 2009.

[82] F. D. Conti, C. Gardi, G. Visioli, and C. Menta, "Environmental risks of biochar in soils: ecotoxicological effects on plants and microarthropos," in *Topical Scientific Workshop on Soil Risk Assessment*, E. F. S. Authority, Ed., European Chemicals Agency (ECHA), Helsinki, Finland, 2015.

[83] S. Kuppusamy, P. Thavamani, M. Megharaj, K. Venkateswarlu, and R. Naidu, "Agronomic and remedial benefits and risks of applying biochar to soil: current knowledge and future research directions," *Environment International*, vol. 87, pp. 1–12, 2016.

[84] EBC, "Positive list of biomasse feedstock approved for use in producing biochar," in *European Biochar Certificate (EBC) Foundation*, Feedstock, Ed., European Biochar Foundation, Groningen, Holland, 1st edition, 2013.

[85] D. A. Laird, R. C. Brown, J. E. Amonette, and J. Lehmann, "Review of the pyrolysis platform for coproducing bio-oil and biochar," *Biofuels, Bioproducts and Biorefining*, vol. 3, no. 5, pp. 547–562, 2009.

[86] R. A. Brown, "Biochar production technology," in *Biochar for Environmental Management: Science and Technology*, J. Lehmann and S. Joseph, Eds., pp. 127–146, Earthscan, London, UK, 2009.

[87] S. Bruun, S. Clauson-Kaas, L. Bobuľská, and I. K. Thomsen, "Carbon dioxide emissions from biochar in soil: role of clay, microorganisms and carbonates," *European Journal of Soil Science*, vol. 65, no. 1, pp. 52–59, 2014.

[88] H. S. Kambo and A. Dutta, "A comparative review of biochar and hydrochar in terms of production, physico-chemical properties and applications," *Renewable and Sustainable Energy Reviews*, vol. 45, pp. 359–378, 2015.

[89] N. K. Niazi, B. Murtaza, I. Bibi et al., "Removal and recovery of metals by biosorbents and biochars derived from biowastes," *Environmental Materials and Waste*, pp. 149–177, 2016.

[90] Y. Xue, B. Gao, Y. Yao et al., "Hydrogen peroxide modification enhances the ability of biochar (hydrochar) produced from hydrothermal carbonization of peanut hull to remove aqueous heavy metals: batch and column tests," *Chemical Engineering Journal*, vol. 200–202, pp. 673–680, 2012.

[91] W. Hao, E. Björkman, M. Lilliestråle, and N. Hedin, "Activated carbons prepared from hydrothermally carbonized waste biomass used as adsorbents for CO_2," *Applied Energy*, vol. 112, pp. 526–532, 2013.

[92] Z. Khanmohammadi, M. Afyuni, and M. R. Mosaddeghi, "Effect of pyrolysis temperature on chemical and physical properties of sewage sludge biochar," *Waste Management & Research*, vol. 33, no. 3, pp. 275–283, 2015.

[93] W. Song and M. Guo, "Quality variations of poultry litter biochar generated at different pyrolysis temperatures," *Journal of Analytical and Applied Pyrolysis*, vol. 94, pp. 138–145, 2012.

[94] J. M. Novak, W. J. Busscher, D. L. Laird, M. Ahmedna, D. W. Watts, and M. A. S. Niandou, "Impact of biochar amendment on fertility of a southeastern coastal plain soil," *Soil Science*, vol. 174, no. 2, pp. 105–112, 2009.

[95] M. J. Gundale and T. H. DeLuca, "Temperature and source material influence ecological attributes of ponderosa pine and Douglas-fir charcoal," *Forest Ecology and Management*, vol. 231, no. 1–3, pp. 86–93, 2006.

[96] M. K. Hossain, V. Strezov, K. Y. Chan, A. Ziolkowski, and P. F. Nelson, "Influence of pyrolysis temperature on production and nutrient properties of wastewater sludge biochar," *Journal of Environmental Management*, vol. 92, no. 1, pp. 223–228, 2011.

[97] U. Ogbonnaya and K. Semple, "Impact of biochar on organic contaminants in soil: a tool for mitigating risk?" *Agronomy*, vol. 3, no. 2, pp. 349–375, 2013.

[98] A. Demirbas, "Effects of temperature and particle size on bio-char yield from pyrolysis of agricultural residues," *Journal of Analytical and Applied Pyrolysis*, vol. 72, no. 2, pp. 243–248, 2004.

[99] K. G. Roberts, B. A. Gloy, S. Joseph, N. R. Scott, and J. Lehmann, "Life cycle assessment of biochar systems: estimating the energetic, economic, and climate change potential," *Environmental Science & Technology*, vol. 44, no. 2, pp. 827–833, 2010.

[100] C. Gerard, D. W. Rutherford, H. P. H. Arp, D. R. Peter, C. N. Kelly, and C. E. Rostad, "Sorption of pure N_2O to biochars and other organic and inorganic materials under anhydrous conditions," *Environmental Science & Technology*, vol. 47, pp. 7704–7712, 2013.

[101] B. J. He, Y. Zhang, T. L. Funk, G. L. Riskowski, and Y. Yin, "Thermochemical conversion of swine manure: an alternative process for waste treatment and renewable energy production," *Transactions of the Asae*, vol. 43, pp. 1827–1833, 2000.

[102] M. P. McHenry, "Agricultural bio-char production, renewable energy generation and farm carbon sequestration in Western Australia: certainty, uncertainty and risk," *Agriculture, Ecosystems & Environment*, vol. 129, no. 1–3, pp. 1–7, 2009.

[103] H. K. Chagger, A. Kendall, A. Mcdonald, M. Pourkashanian, and A. Williams, "Formation of dioxins and other semi-volatile organic compounds in biomass combustion," *Applied Energy*, vol. 60, no. 2, pp. 101–114, 1998.

[104] A. M. Liesch, S. L. Weyers, J. W. Gaskin, and K. C. Das, "Impact of two different biochars on earthworm growth and survival," *Annals of Environmental Science*, vol. 4, 2010.

[105] X.-B. Yang, G.-G. Ying, P.-A. Peng et al., "Influence of biochars on plant uptake and dissipation of two pesticides in an agricultural soil," *Journal of Agricultural and Food Chemistry*, vol. 58, no. 13, pp. 7915–7921, 2010.

[106] P. Devi and A. K. Saroha, "Risk analysis of pyrolyzed biochar made from paper mill effluent treatment plant sludge for bioavailability and eco-toxicity of heavy metals," *Bioresource Technology*, vol. 162, pp. 308–315, 2014.

[107] S. Khan, N. Wang, B. J. Reid, A. Freddo, and C. Cai, "Reduced bioaccumulation of PAHs by *Lactuca satuva* L. grown in contaminated soil amended with sewage sludge and sewage sludge derived biochar," *Environmental Pollution*, vol. 175, pp. 64–68, 2013.

[108] T. Liu, Z. Liu, Q. Zheng et al., "Effect of hydrothermal carbonization on migration and environmental risk of heavy metals in sewage sludge during pyrolysis," *Bioresource Technology*, vol. 247, pp. 282–290, 2018.

[109] A. Hospido, T. Moreira, M. Martín, M. Rigola, and G. Feijoo, "Environmental evaluation of different treatment processes for sludge from urban wastewater treatments: anaerobic digestion versus thermal processes (10 pp)," *The International Journal of Life Cycle Assessment*, vol. 10, no. 5, pp. 336–345, 2005.

[110] L. Beesley and N. Dickinson, "Carbon and trace element fluxes in the pore water of an urban soil following greenwaste compost, woody and biochar amendments, inoculated with the earthworm *Lumbricus terrestris*," *Soil Biology and Biochemistry*, vol. 43, no. 1, pp. 188–196, 2011.

[111] T. McClellan, G. Uehara, J. Deenik, and M. Antal, "Effects of flashed carbonized macadamia nutshell charcoal on plant growth and soil chemical properties," in *Proceedings of the SSA, ASA, CSSA*, International Annual Meetings, New Orleans, LA, USA, November 2007, http://a-c-s.confex.com/recording/crops/2007am/pdf/free/4db77adf5df9fff0d3caf5cafe28f496/paper35834_1.pdf.

[112] J. Thies and M. C. Rillig, "Characteristics of biochar: biological properties," in *Biochar for Environmental Management: Science and Technology*, J. Lehmann and S. Joseph, Eds., pp. 85–105, Earthscan, London, UK, 2009.

[113] M. Ogawa, "Symbiosis of people and nature in the tropics," *Farming Japan*, vol. 28, pp. 10–34, 1994.

[114] O. Zackrisson, M.-C. Nilsson, and D. A. Wardle, "Key ecological function of charcoal from wildfire in the boreal forest," *Oikos*, vol. 77, no. 1, pp. 10–19, 1996.

[115] A. Hidetoshi, S. Benjamink, S. Haefelem et al., "Biochar amendment techniques for upland rice production in Northern Laos : 1. Soil physical properties, leaf SPAD and grain yield," *Field Crops Research*, vol. 111, pp. 81–84, 2009.

[116] S. Baronti, G. Alberti, G. Delle Vedove et al., "The biochar option to improve plant yields: first results from some field and pot experiments in Italy," *Italian Journal of Agronomy*, vol. 5, no. 1, pp. 3–12, 2010.

[117] M. A. Rondon, J. Lehmann, J. Ramírez, and M. Hurtado, "Biological nitrogen fixation by common beans (*Phaseolus*

vulgaris L.) increases with bio-char additions," *Biology and Fertility of Soils*, vol. 43, no. 6, pp. 699–708, 2007.

[118] L. Chalker-Scott, *Biochar: A Home Gardener's Primer*, Washington State University Puyallup Research and Extension Center, Puyallup, WA, USA, 2014.

[119] R. D. Hottle, Impact of biochar on plant productivity andsoil properties under a maize soybean rotation on an Alfisolin Central Ohio Dissertations & Theses-Gradworks, 2013.

[120] X.-Y. Yu, G.-G. Ying, and R. S. Kookana, "Reduced plant uptake of pesticides with biochar additions to soil," *Chemosphere*, vol. 76, no. 5, pp. 665–671, 2009.

[121] R. S. Kookana, "The role of biochar in modifying the environmental fate, bioavailability, and efficacy of pesticides in soils: a review," *Soil Research*, vol. 48, no. 7, pp. 627–637, 2010.

[122] K. A. Spokas, "Review of the stability of biochar in soils: predictability of O : C molar ratios," *Carbon Management*, vol. 1, no. 2, pp. 289–303, 2010.

[123] R. Bian, Z. Zhang, A. Zhang et al., "Effect of municipal biowaste biochar on greenhouse gas emissions and metal bioaccumulation in a slightly acidic clay rice paddy," *Bio Resources*, vol. 9, pp. 685–703, 2013.

[124] J. Liu, J. Shen, Y. Li et al., "Effects of biochar amendment on the net greenhouse gas emission and greenhouse gas intensity in a Chinese double rice cropping system," *European Journal of Soil Biology*, vol. 65, pp. 30–39, 2014.

[125] P. Pokharel, J.-H. Kwak, Y. S. Ok, and S. X. Chang, "Pine sawdust biochar reduces GHG emission by decreasing microbial and enzyme activities in forest and grassland soils in a laboratory experiment," *Science of the Total Environment*, vol. 625, pp. 1247–1256, 2018.

[126] J. Lehmann and S. Joseph, *Biochar for Environmental Management: Science and Technology*, Earthscan, London, UK, 2009.

[127] H. Paul, *Biochar Knowledge Gaps Commentary*, EcoNexus, Oxford, UK, https://www.econexus.info/publication/biochar-knowledge-gaps.

[128] X. Peng, Y. Deng, Y. Peng, and K. Yue, "Effects of biochar addition on toxic element concentrations in plants: a meta-analysis," *Science of the Total Environment*, vol. 616-617, pp. 970–977, 2018.

[129] EHSO, "The TCLP:Toxicity Characteristic Leaching Procedure, Hazardous Waste Fact Sheet. TCLP: Toxicity Characteristic Leaching Procedure and Characteristic Hazardous Wastes," Environment, Health and Safety Online (EHSO), Atlanta, GA, USA, 2016.

[130] H. Su, Z. Fang, P. E. Tsang, J. Fang, and D. Zhao, "Stabilisation of nanoscale zero-valent iron with biochar for enhanced transport and in-situ remediation of hexavalent chromium in soil," *Environmental Pollution*, vol. 214, pp. 94–100, 2016.

[131] X.-j. Tong, J.-y. Li, J.-h. Yuan, and R.-k. Xu, "Adsorption of Cu(II) by biochars generated from three crop straws," *Chemical Engineering Journal*, vol. 172, no. 2-3, pp. 828–834, 2011.

[132] S. Wang, B. Gao, Y. Li et al., "Manganese oxide-modified biochars: preparation, characterization, and sorption of arsenate and lead," *Bioresource Technology*, vol. 181, pp. 13–17, 2015.

[133] Z. Wang, G. Liu, H. Zheng et al., "Investigating the mechanisms of biochar's removal of lead from solution," *Bioresource Technology*, vol. 177, pp. 308–317, 2015.

[134] K. Yoon, D.-W. Cho, D. C. W. Tsang, N. Bolan, J. Rinklebe, and H. Song, "Fabrication of engineered biochar from paper mill sludge and its application into removal of arsenic and cadmium in acidic water," *Bioresource Technology*, vol. 246, pp. 69–75, 2017.

[135] R. Pöykiö, H. Nurmesniemi, T. Kuokkanen, and P. Perämäki, "The use of a sequential leaching procedure for assessing the heavy metal leachability in lime waste from the lime kiln at a caustizicing process of a pulp mill," *Chemosphere*, vol. 65, no. 11, pp. 2122–2129, 2006.

[136] J. Meng, S. Liang, M. Tao, X. Liu, P. C. Brookes, and J. Xu, "Chemical speciation and risk assessment of Cu and Zn in biochars derived from co-pyrolysis of pig manure with rice straw," *Chemosphere*, vol. 200, pp. 344–350, 2018.

[137] Z. Dai, P. C. Brookes, Y. He, and J. Xu, "Increased agronomic and environmental value provided by biochars with varied physiochemical properties derived from swine manure blended with rice straw," *Journal of Agricultural and Food Chemistry*, vol. 62, no. 44, pp. 10623–10631, 2014.

[138] J. Meng, X. Feng, Z. Dai, X. Liu, J. Wu, and J. Xu, "Adsorption characteristics of Cu(II) from aqueous solution onto biochar derived from swine manure," *Environmental Science and Pollution Research*, vol. 21, no. 11, pp. 7035–7046, 2014.

[139] T. Wang, Y. Xue, M. Zhou et al., "Comparative study on the mobility and speciation of heavy metals in ashes from co-combustion of sewage sludge/dredged sludge and rice husk," *Chemosphere*, vol. 169, pp. 162–170, 2017.

[140] H.-j. Huang, T. Yang, F.-y. Lai, and G.-q. Wu, "Co-pyrolysis of sewage sludge and sawdust/rice straw for the production of biochar," *Journal of Analytical and Applied Pyrolysis*, vol. 125, pp. 61–68, 2017.

[141] J. Jin, M. Wang, Y. Cao et al., "Cumulative effects of bamboo sawdust addition on pyrolysis of sewage sludge: biochar properties and environmental risk from metals," *Bioresource Technology*, vol. 228, pp. 218–226, 2017.

[142] M. Inyang, B. Gao, Y. Yao et al., "Removal of heavy metals from aqueous solution by biochars derived from anaerobically digested biomass," *Bioresource Technology*, vol. 110, pp. 50–56, 2012.

[143] E. Agrafioti, D. Kalderis, and E. Diamadopoulos, "Arsenic and chromium removal from water using biochars derived from rice husk, organic solid wastes and sewage sludge," *Journal of Environmental Management*, vol. 133, pp. 309–314, 2014.

[144] E. Agrafioti, D. Kalderis, and E. Diamadopoulos, "Ca and Fe modified biochars as adsorbents of arsenic and chromium in aqueous solutions," *Journal of Environmental Management*, vol. 146, pp. 444–450, 2014.

[145] Z.-H. Ruan, J.-H. Wu, J.-F. Huang et al., "Facile preparation of rosin-based biochar coated bentonite for supporting α-Fe_2O_3 nanoparticles and its application for Cr(VI) adsorption," *Journal of Materials Chemistry A*, vol. 3, no. 8, pp. 4595–4603, 2015.

[146] X. Hu, Z. Ding, A. R. Zimmerman, S. Wang, and B. Gao, "Batch and column sorption of arsenic onto iron-impregnated biochar synthesized through hydrolysis," *Water Research*, vol. 68, pp. 206–216, 2015.

[147] J. Deng, X. Li, Y. Liu et al., "Alginate-modified biochar derived from Ca(II)-impregnated biomass: excellent anti-interference ability for Pb(II) removal," *Ecotoxicology and Environmental Safety*, vol. 165, pp. 211–218, 2018.

[148] H. Dong, J. Deng, Y. Xie et al., "Stabilization of nanoscale zero-valent iron (nZVI) with modified biochar for Cr(VI) removal from aqueous solution," *Journal of Hazardous Materials*, vol. 332, pp. 79–86, 2017.

[149] L.-L. Ling, W.-J. Liu, S. Zhang, and H. Jiang, "Magnesium oxide embedded nitrogen self-doped biochar composites: fast and high-efficiency adsorption of heavy metals in an aqueous solution," *Environmental Science & Technology*, vol. 51, no. 17, pp. 10081–10089, 2017.

[150] L. Hakanson, "An ecological risk index for aquatic pollution control.a sedimentological approach," *Water Research*, vol. 14, no. 8, pp. 975–1001, 1980.

[151] M. K. Jamali, T. G. Kazi, H. I. Afridi, M. B. Arain, N. Jalbani, and A. R. Memon, "Speciation of heavy metals in untreated domestic wastewater sludge by time saving BCR sequential extraction method," *Journal of Environmental Science and Health, Part A*, vol. 42, no. 5, pp. 649–659, 2007.

[152] M. Chabukdhara and A. K. Nema, "Heavy metals in water, sediments, and aquatic macrophytes: river Hindon, India," *Journal of Hazardous, Toxic, and Radioactive Waste*, vol. 16, pp. 273–281, 2011.

[153] N. Rogovska, D. Laird, R. M. Cruse, S. Trabue, and E. Heaton, "Germination tests for assessing biochar quality," *Journal of Environment Quality*, vol. 41, no. 4, pp. 1014–1022, 2012.

[154] D. Shan, S. Deng, T. Zhao et al., "Preparation of ultrafine magnetic biochar and activated carbon for pharmaceutical adsorption and subsequent degradation by ball milling," *Journal of Hazardous Materials*, vol. 305, pp. 156–163, 2016.

[155] J. Yang, B. Pan, H. Li et al., "Degradation ofp-nitrophenol on biochars: role of persistent free radicals," *Environmental Science & Technology*, vol. 50, no. 2, pp. 694–700, 2015.

[156] M. Zhang and B. Gao, "Removal of arsenic, methylene blue, and phosphate by biochar/AlOOH nanocomposite," *Chemical Engineering Journal*, vol. 226, pp. 286–292, 2013.

[157] A. Zhelezova, H. Cederlund, and J. Stenström, "Effect of biochar amendment and ageing on adsorption and degradation of two herbicides," *Water Air & Soil Pollution*, vol. 228, p. 216, 2017.

[158] J. Yang, J. J. Pignatello, B. Pan, and B. Xing, "Degradation ofp-nitrophenol by lignin and cellulose chars: H2O2-mediated reaction and direct reaction with the char," *Environmental Science & Technology*, vol. 51, no. 16, pp. 8972–8980, 2017.

[159] Z. Chen, B. Chen, D. Zhou, and W. Chen, "Bisolute sorption and thermodynamic behavior of organic pollutants to biomass-derived biochars at two pyrolytic temperatures," *Environmental Science & Technology*, vol. 46, no. 22, pp. 12476–12483, 2012.

[160] F. Xiao, A. H. Bedane, J. X. Zhao, M. D. Mann, and J. J. Pignatello, "Thermal air oxidation changes surface and adsorptive properties of black carbon (char/biochar)," *Science of the Total Environment*, vol. 618, pp. 276–283, 2018.

[161] F. Xiao and J. J. Pignatello, "Effects of post-pyrolysis air oxidation of biomass chars on adsorption of neutral and ionizable compounds," *Environmental Science & Technology*, vol. 50, no. 12, pp. 6276–6283, 2016.

[162] G. Fang, J. Gao, C. Liu, D. D. Dionysiou, Y. Wang, and D. Zhou, "Key role of persistent free radicals in hydrogen peroxide activation by biochar: implications to organic contaminant degradation," *Environmental Science & Technology*, vol. 48, no. 3, pp. 1902–1910, 2014.

[163] G. Fang, C. Zhu, D. D. Dionysiou, J. Gao, and D. Zhou, "Mechanism of hydroxyl radical generation from biochar suspensions: implications to diethyl phthalate degradation," *Bioresource Technology*, vol. 176, pp. 210–217, 2015.

[164] G. Fang, C. Liu, J. Gao, D. D. Dionysiou, and D. Zhou, "Manipulation of persistent free radicals in biochar to activate persulfate for contaminant degradation," *Environmental Science & Technology*, vol. 49, no. 9, pp. 5645–5653, 2015.

[165] N. Chen, Y. Huang, X. Hou, Z. Ai, and L. Zhang, "Photochemistry of hydrochar: reactive oxygen species generation and sulfadimidine degradation," *Environmental Science & Technology*, vol. 51, no. 19, pp. 11278–11287, 2017.

[166] G. Fang, C. Liu, Y. Wang, D. D. Dionysiou, and D. Zhou, "Photogeneration of reactive oxygen species from biochar suspension for diethyl phthalate degradation," *Applied Catalysis B: Environmental*, vol. 214, pp. 34–45, 2017.

[167] EPA, *Understanding Global Warming Potentials Greenhouse Gas Emissions*, EPA, Washington, DC, USA, 2017.

[168] Z. Ming and S. O. Yong, "Biochar soil amendment for sustainable agriculture with carbon and contaminant sequestration," *Carbon Management*, vol. 5, pp. 255–257, 2014.

[169] P. R. Forster, P. Artaxo, T. Berntsen et al., "Changes in atmospheric constituents and in radiative forcing," in *Climate Change 2007: The Physical Science Basis. Contribution of Working Group I to the Fourth Assessment Report of the Intergovernmental Panel on Climate Change*, S. Q. D. Solomon, M. Manning, Z. Chen et al., Eds., pp. 129–234, Cambridge University, Cambridge, UK, 2007.

[170] J. Verhoeven, B. Arheimer, C. Yin, and M. Hefting, "Regional and global concerns over wetlands and water quality," *Trends in Ecology & Evolution*, vol. 21, no. 2, pp. 96–103, 2006.

[171] M. P. W. Schneider, J. Lehmann, and M. W. I. Schmidt, "Charcoal quality does not change over a century in a tropical agro-ecosystem," *Soil Biology and Biochemistry*, vol. 43, no. 9, pp. 1992–1994, 2011.

[172] J. L. Smith, H. P. Collins, and V. L. Bailey, "The effect of young biochar on soil respiration," *Soil Biology and Biochemistry*, vol. 42, no. 12, pp. 2345–2347, 2010.

[173] A. R. Zimmerman, "Abiotic and microbial oxidation of laboratory-produced black carbon (biochar)," *Environmental Science & Technology*, vol. 44, no. 4, pp. 1295–1301, 2010.

[174] M. L. Cayuela, M. A. Sánchezmonedero, A. Roig, K. Hanley, A. Enders, and J. Lehmann, "Biochar and denitrification in soils: when, how much and why does biochar reduce N_2O emissions?" *Scientific Reports*, vol. 3, no. 1, p. 1732, 2013.

[175] M. F. Qayyum, D. Steffens, H. P. Reisenauer, and S. Schubert, "Kinetics of carbon mineralization of biochars compared with wheat straw in three soils," *Journal of Environment Quality*, vol. 41, no. 4, pp. 1210–1220, 2012.

[176] B. P. Singh, A. L. Cowie, and R. J. Smernik, "Biochar carbon stability in a clayey soil as a function of feedstock and pyrolysis temperature," *Environmental Science & Technology*, vol. 46, no. 21, pp. 11770–11778, 2012.

[177] O. R. Harvey, L.-J. Kuo, A. R. Zimmerman, P. Louchouarn, J. E. Amonette, and B. E. Herbert, "An index-based approach to assessing recalcitrance and soil carbon sequestration potential of engineered black carbons (biochars)," *Environmental Science & Technology*, vol. 46, no. 3, pp. 1415–1421, 2012.

[178] F. Li, X. Cao, L. Zhao, J. Wang, and Z. Ding, "Effects of mineral additives on biochar formation: carbon retention, stability, and properties," *Environmental Science & Technology*, vol. 48, no. 19, pp. 11211–11217, 2014.

[179] J. J. Manyà, M. A. Ortigosa, S. Laguarta, and J. A. Manso, "Experimental study on the effect of pyrolysis pressure, peak temperature, and particle size on the potential stability of vine shoots-derived biochar," *Fuel*, vol. 133, pp. 163–172, 2014.

[180] M. K. Rafiq, S. D. Joseph, F. Li et al., "Pyrolysis of attapulgite clay blended with yak dung enhances pasture growth and soil health: characterization and initial field trials," *Science of the Total Environment*, vol. 607-608, pp. 184–194, 2017.

[181] R. Xiao, J. J. Wang, L. A. Gaston et al., "Biochar produced from mineral salt-impregnated chicken manure: fertility properties and potential for carbon sequestration," *Waste Management*, vol. 78, pp. 802–810, 2018b.

[182] F. Yang, L. Zhao, B. Gao, X. Xu, and X. Cao, "The interfacial behavior between biochar and soil minerals and its effect on biochar stability," *Environmental Science & Technology*, vol. 50, no. 5, pp. 2264–2271, 2016.

[183] F. Yang, Z. Xu, L. Yu et al., "Kaolinite enhances the stability of the dissolvable and undissolvable fractions of biochar via different mechanisms," *Environmental Science & Technology*, vol. 52, no. 15, pp. 8321–8329, 2018.

[184] A. E. Creamer, B. Gao, and S. Wang, "Carbon dioxide capture using various metal oxyhydroxide-biochar composites," *Chemical Engineering Journal*, vol. 283, pp. 826–832, 2016.

[185] X. Sun, X. Han, F. Ping et al., "Effect of rice-straw biochar on nitrous oxide emissions from paddy soils under elevated CO_2 and temperature," *Science of the Total Environment*, vol. 628-629, pp. 1009–1016, 2018.

[186] N. Wang, Z.-Z. Chang, X.-M. Xue et al., "Biochar decreases nitrogen oxide and enhances methane emissions via altering microbial community composition of anaerobic paddy soil," *Science of the Total Environment*, vol. 581-582, pp. 689–696, 2017.

[187] K. Karhu, T. Mattila, I. Bergström, and K. Regina, "Biochar addition to agricultural soil increased CH_4 uptake and water holding capacity - results from a short-term pilot field study," *Agriculture, Ecosystems & Environment*, vol. 140, no. 1-2, pp. 309–313, 2011.

[188] X. Han, X. Sun, C. Wang et al., "Mitigating methane emission from paddy soil with rice-straw biochar amendment under projected climate change," *Scientific Reports*, vol. 6, p. 24731, 2016.

[189] N. Namoi, D. Pelster, T. S. Rosenstock et al., "Earthworms regulate ability of biochar to mitigate CO_2 and N_2O emissions from a tropical soil," *Applied Soil Ecology*, vol. 140, pp. 57–67, 2019.

[190] C. R. Anderson, L. M. Condron, T. J. Clough et al., "Biochar induced soil microbial community change: implications for biogeochemical cycling of carbon, nitrogen and phosphorus," *Pedobiologia*, vol. 54, no. 5-6, pp. 309–320, 2011.

[191] A. Zhang, R. Bian, G. Pan et al., "Effects of biochar amendment on soil quality, crop yield and greenhouse gas emission in a Chinese rice paddy: a field study of 2 consecutive rice growing cycles," *Field Crops Research*, vol. 127, pp. 153–160, 2012.

[192] L. V. Zwieten, S. Kimber, S. Morris et al., "Influence of biochars on flux of N_2O and CO_2 from Ferrosol," *Soft Computing*, vol. 48, pp. 1043–1046, 2010.

[193] C. Wang, H. Lu, D. Dong et al., "Insight into the effects of biochar on manure composting: evidence supporting the relationship between N_2O emission and denitrifying community," *Environmental Science & Technology*, vol. 47, no. 13, pp. 7341–7349, 2013.

[194] Y. Teng, S. Ni, J. Wang, R. Zuo, and J. Yang, "A geochemical survey of trace elements in agricultural and non-agricultural topsoil in Dexing area, China," *Journal of Geochemical Exploration*, vol. 104, no. 3, pp. 118–127, 2010.

[195] L. Y. Zhang, L. Li, and G. Pan, "Variation of Cd, Zn and Se contents of polished rice and the potential health risk for subsistence-diet farmers from typical areas of South China," *Huan Jing Ke Xue*, vol. 30, pp. 2792–2797, 2009.

[196] L. Cui, L. Li, A. Zhang, G. Pan, D. Bao, and A. Chang, "Biochar amendment greatly reduces rice Cd uptake in a contaminated paddy soil: a two-year field experiment," *BioResources*, vol. 6, pp. 2605–2618, 2011.

[197] D. Qin, M.-X. Chen, Z. Rong et al., "Cd toxicity and accumulation in rice plants vary with soil nitrogen status and their genotypic difference can be partly attributed to nitrogen uptake capacity," *Rice Science*, vol. 16, pp. 283–291, 2009.

[198] L. He, G. Gielen, N. S. Bolan et al., "Contamination and remediation of phthalic acid esters in agricultural soils in China: a review," *Agronomy for Sustainable Development*, vol. 35, no. 2, pp. 519–534, 2015.

[199] A. V. Kachur, C. J. Koch, and J. E. Biaglow, "Mechanism of copper-catalyzed oxidation of glutathione," *Free Radical Research*, vol. 28, no. 3, pp. 259–269, 1998.

[200] P. B. Tchounwou, C. G. Yedjou, A. K. Patlolla, and D. J. Sutton, "Heavy metal toxicity and the environment," *Experientia Supplementum*, vol. 101, pp. 133–164, 2012.

[201] S. D. Joseph, M. Camps-Arbestain, Y. Lin et al., "An investigation into the reactions of biochar in soil," *Soil Research*, vol. 48, no. 7, pp. 501–515, 2010.

[202] C. H. Cheng, J. Lehmann, J. E. Thies, and S. D. Burton, "Stability of black carbon in soils across a climatic gradient," *Journal of Geophysical Research: Biogeosciences*, vol. 113, 2008.

[203] B. T. Nguyen and J. Lehmann, "Black carbon decomposition under varying water regimes," *Organic Geochemistry*, vol. 40, no. 8, pp. 846–853, 2009.

[204] B. T. Nguyen, J. Lehmann, W. C. Hockaday, S. Joseph, and C. A. Masiello, "Temperature sensitivity of black carbon decomposition and oxidation," *Environmental Science & Technology*, vol. 44, no. 9, pp. 3324–3331, 2010.

[205] A. R. Zimmerman, B. Gao, and M.-Y. Ahn, "Positive and negative carbon mineralization priming effects among a variety of biochar-amended soils," *Soil Biology and Biochemistry*, vol. 43, no. 6, pp. 1169–1179, 2011.

[206] J. Lehmann, "Bio-energy in the black," *Frontiers in Ecology and the Environment*, vol. 5, no. 7, pp. 381–387, 2007.

Hindawi
Journal of Chemistry
Volume 2019, Article ID 2428505, 10 pages
https://doi.org/10.1155/2019/2428505

Research Article

Adsorption of Bisphenol A on Peanut Shell Biochars: The Effects of Surfactants

Fang Wang[1], **Qiang Zeng**[1], **Wenting Su**[1], **Min Zhang**[1], **Lei Hou**[2] and **Zhong-Liang Wang**[1]

[1]*Tianjin Key Laboratory of Water Resources and Environment, Tianjin Normal University, Tianjin 300387, China*
[2]*College of Ecology and Environment, Southwest Forestry University, Kunming 650224, China*

Correspondence should be addressed to Lei Hou; leihou@swfu.edu.cn

Received 17 June 2019; Accepted 30 August 2019; Published 16 December 2019

Guest Editor: Peng Zhang

Bisphenol A (BPA) is a typical endocrine-disrupting chemical. The removal of BPA has raised much concerns in recent years. This paper examined the adsorption behavior of BPA to biochars and the different effects of cationic, anionic, and nonionic surfactants. The results indicated that peanut shell biochars prepared at 300°C (BC300), 500°C (BC500), and 700°C (BC700) showed strong adsorption affinity for BPA, and the adsorption affinity of biochars increased with the increase of pyrolysis temperature. The range of log K_d values was 2.83~3.71, 2.91~4.57, and 3.24~5.50 for BC300, BC500, and BC700, respectively. Both the type of surfactants and the properties of biochars could affect the adsorption behavior of BPA. Cetyltrimethyl ammonium bromide (CTAB) showed negligible effect on the adsorption of BPA on BC300, and the inhibition effect of CTAB was stronger with the increase of biochar pyrolysis temperature. Tween 20 and sodium dodecyl benzene sulfonate (SDBS) showed stronger inhibition effect than CTAB, especially on BC300. This is likely because the inhibition effect caused by competition of CTAB may be counterbalanced by the enhancement caused by the partitioning effect by adsorbed CTAB and the bridge effect between the $-NH_4^+$ group of CTAB and the phenol group on BPA/O-functional groups of biochars, whereas Tween 20 and SDBS do not have this bridge effect advantage. This study could provide insightful information for the application of biochars in removal of BPA.

1. Introduction

Bisphenol A (BPA) is one of the most common endocrine-disrupting chemicals, which is widely applied to produce plastics, resins, and other materials [1]. It could mimic or block the biological activity of natural hormones in the endocrine systems of wildlife and humans and may interfere with the transport and metabolic processes of natural hormones and threaten the health of wildlife and human even at trace levels (ng/L) [2, 3]. In recent years, BPA has been frequently detected in air, soil, sediments, water bodies, and food, and the concentration could reach as high as several milligram per liter [1, 4–6]. Therefore, it is of great importance to find an efficient method for BPA removal.

Biochar, which is a kind of carbon-rich, porous, and low-cost product formed by pyrolysis of biomass [7–9], has been reported to be an excellent adsorbent in wastewater treatment, especially for hydrophobic organic pollutants [10]. Previous studies found that biochars showed strong adsorption affinities to BPA [11–13]. For example, Wu et al. [11] have reported that wood, walnut, and apricot shell biochars all showed strong adsorption affinity to BPA. Choi et al. [12] showed that the maximum adsorption capacity of BPA to alfalfa biochar prepared at 650°C was as high as 38 mg/g. Kim et al. [13] reported that the adsorptive capacity of BPA to biochars is even stronger than that to powdered activated carbon. The adsorption behavior of biochars could be affected by aqueous chemistry conditions once they were applied in wastewater treatment [14, 15]. Surfactants, which are widely used in the daily life of humans, such as personal care products, textiles, pesticide formulations, pharmaceuticals, and household cleaning detergents [16], could be released into the environment and coexist with the organic contaminants. However, the influences of surfactants on the adsorption behavior of the organic contaminants to biochars were not fully investigated yet [17–19].

It is noted that there are many different types of surfactants, such as anionic surfactants, cationic surfactants, and nonionic surfactants. Therefore, they could have different effects on the adsorption behavior of organic contaminants due to their different chargeability and functional groups. For example, Zhang et al. [20] reported that high concentration of cationic surfactant, cetyltrimethyl ammonium bromide (CTAB), could enhance the adsorption of phenanthrene on black carbon, whereas high concentration of anionic surfactant, sodium dodecyl benzene sulfonate (SDBS), inhibited the adsorption of phenanthrene. This is likely because the phenanthrene molecular could be adsorbed on the hemimicelles or cosmids formed by CTAB which was adsorbed on black carbon and the adsorption was enhanced, whereas the presence of SDBS in the solution could increase the solubility of phenanthrene and inhibited the adsorption. On the contrary, Oleszczuk and Xing [21] reported that SDBS could enhance the dispersibility of the multiwalled carbon nanotubes, which led to the increase of oxytetracycline adsorption sites and strong enhancement of adsorption affinity to multiwalled carbon nanotubes, whereas the presence of TX100 and CTAB decreased the adsorption of oxytetracycline by multiwalled carbon nanotubes significantly. These studies indicated that the effects of surfactants on adsorption behavior were not only in relation to the types of the surfactants but also in relation to the properties of adsorbents. Up to now, there are few studies focused on the effects of different types of surfactants on the adsorption of BPA on biochars. Thus, it is of great importance to explore the effects of surfactants on the adsorption behavior of BPA to biochars and compare the differences between the different types of surfactants.

In this paper, the adsorption behavior of BPA to peanut shell biochars was examined, and the effects of different types of surfactants were also evaluated. CTAB, SDBS, and Tween 20 were selected as the model cationic, anionic, and nonionic surfactants, respectively. Physicochemical properties of peanut shell biochars under different pyrolysis temperatures were characterized. The adsorption affinities of BPA to the peanut shell biochars in absence and presence of the surfactants were examined by batch experiment. The controlling mechanisms were also discussed.

2. Materials and Methods

2.1. Chemicals. BPA was purchased from Sigma-Aldrich (Shanghai, China). The physicochemical properties are shown in Table 1. The three types of surfactants, CTAB, SDBS, and Tween 20, were all purchased from Sinopharm Chemical Reagent Co., Ltd. (Shanghai, China). Their critical micelle concentrations and molecular structures are summarized in Table 2. Methanol was purchased from Kangkede Technology Co., Ltd. (Tianjin, China). Disodium hydrogen phosphate (Na_2HPO_4) and sodium dihydrogen phosphate (NaH_2PO_4) were obtained from Guangfu Technology Development Co. Ltd. (Tianjin, China).

Table 1: Selected physicochemical properties of BPA.

Adsorbate	Molecular structure[a]	C_{sat} (mg/L)	Log K_{OW}	pK_a
Bisphenol A[a]	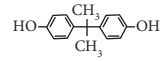	380	2.2	9.6

[a]From Pan et al. [22].

2.2. Biochar Preparation. Peanut shells were collected from Linyi (Shandong, China). Biochars were prepared as follows [25]. First, peanut shells were rinsed with distilled water. After air-drying, they were cut into small pieces and placed in a ceramic pot. The samples were then heated in a muffle furnace at 300, 500, and 700 °C for 2 h. Finally, the samples were grinded, and the biochar powders which passed through a 0.147 mm sieve were referred as BC300, BC500, and BC700, respectively.

2.3. Characterization of Biochars. Surface elemental compositions of the biochars were determined with X-ray photoelectron spectroscopy (XPS) (PHI 5000, VersaProbe, Japan). Fourier-transform infrared (FTIR) transmission spectra were obtained using a 110 Bruker Tensor 27 apparatus (Bruker Optics Inc., Germany), with a biochar to KBr ratio of 1 : 100. The morphological structures of the biochars were observed by both the scanning electron microscopy (SEM, S-3400N II, Hitachi, Japan) and transmission electron microscopy (TEM, JEM-2100, JEOL, Japan). The surface areas of the biochars were calculated using the multipoint Brunauer–Emmett–Teller method. The micropore volume and diameter were determined using the Horvath–Kawazoe method. The pH of point of zero charge (pH_{PZC}) of biochar was determined using the method reported by Dastgheib et al. [26].

2.4. Adsorption Experiments. The adsorption isotherm experiment of BPA on biochar was carried out by the batch experiment [12]. First, 10 mg of biochars was added to a glass vial, and then 20 mL of buffer solution (10 mM Na_2HPO_4-NaH_2PO_4, pH = 6.0) was spiked to the vial. When adsorption isotherm experiment in presence of surfactants was conducted, the surfactant solutions were added as the background solution and the surfactant concentration was set as 40 mg/L. Subsequently, certain amounts of BPA stock solution were added to the vials to make the initial concentration in the range of 0.44 to 28 mg/L. The volume of stock solution added to vials was kept below 0.1% to minimize the cosolvent effect. Then, the vials were tumbled at 3 rpm at room temperature for 14 days until the adsorption equilibrium was reached, and the concentrations of BPA in the supernatants were measured.

To test the effect of the concentration of surfactant, the concentrations of surfactant were set as 0.05, 0.1, 0.3, 0.5, and 0.8 CMC of each surfactant. The initial concentration of BPA was 4.5 mg/L. All the adsorption isotherm experiments were

Table 2: Molecular weight (MW), critical micelle concentration (CMC), and molecular structure of the surfactants.

Surfactant	MW (g/mol)	CMC (mg/L)	Molecular structure
Sodium dodecyl benzene sulfonate (SDBS)[a]	348.48	490	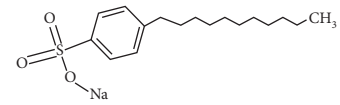
Cetyltrimethyl ammonium bromide (CTAB)[a]	1228	340	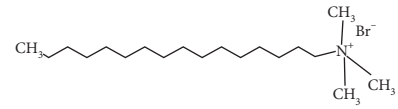
Tween 20, $n = \sim 20$[b]	1226	70	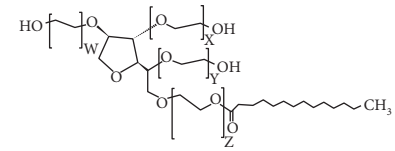

[a]From Han et al. [23]. [b]From Bak et al. [24].

run in duplicate, and the surfactant concentration effect experiments were run in triplicate.

2.5. Analytical Methods. The concentration of BPA was measured by a high-performance liquid chromatograph equipped with a 4.6 mm × 250 mm Eclipse Plus C18 column. The mobile phase was 70 : 30 (v/v) of methanol and deionized water with 1% acetic acid, and the flow rate was 1 mL/min. It was detected with a fluorescence detector at an excitation wavelength of 220 nm and an emission wavelength of 350 nm. No peaks were detected in the spectra for potential degraded/transformed products of the test compounds. All data were analyzed using Graph Pad Prism 6.

2.6. Statistical Analysis. One-way analysis of variance (ANOVA) with Duncan or Dunnett's T3 test was applied to test the significant differences of BPA solubility in presence and absence of surfactants and the effects of surfactant concentrations on the adsorption of BPA on BC300. Differences were considered significant at $p < 0.05$. All the statistical analyses were carried out using SPSS software (version 19.0, SPSS Inc., Chicago, USA).

3. Results and Discussion

3.1. Characterization of Biochars. The morphology properties of biochars can be described by SEM (Figure 1) and TEM images (Figure 2). It can be easily seen that the pore diameter of BC300 was 25.4 nm, which was significantly larger than that of BC500 and BC700, whereas the pore volume of BC300 was the smallest (Table 3). This was likely because during the pyrolysis of the biomass (i.e., peanut shell), it decomposed and a large number of fiber chain structures were destroyed [27]. Some substances under their volatilization temperature would deposit on the surface of the biochar and form an irregular block stack [27]. With the increase of pyrolysis temperature, the residual biomass was gradually decomposed, and the removal of volatile materials resulted in the increased pore volume [27–29].

The surface elemental compositions of biochars are summarized in Table 3. It was shown that with the increase of the pyrolysis temperature, the C content increased while N and O content decreased. Furthermore, (O + N)/C decreased from 0.29 to 0.23, which indicated the polarity of biochar decreased with the increasing pyrolysis temperature [28]. To further explore the changes in functional groups on the surface of different biochar samples, FTIR spectra are presented in Figure 3. The peaks around 3392, 1594, 1370, and 1030 cm^{-1} wavenumbers indicated the stretching vibration of O-H [30], double bond stretching vibration of C=O [31, 32], bending vibration of O-H [33], and stretching vibration of alkyl C-O [34] in the functional groups of biochars, respectively. The intensities of all these aforementioned peaks decreased with the increasing pyrolysis temperature. The content of each functional group was calculated based on XPS spectra. As shown in Figure 4 and Table 3, the content of C-C/C=C gradually increased with the increasing pyrolysis temperature, while that of oxygen-containing functional groups (e.g., C-O, C=O and COOH) decreased. This trend was consistent with the results of FTIR characterization. This is likely because with the increase of the pyrolysis temperature, the low degree of graphitized amorphous carbon could be converted to high degree of graphitized aromatic carbon via dehydration, decarboxylation, and decarbonylation effects [10, 32, 33, 35]. The loss of polar functional groups on the surface of biochar samples also resulted in the increase of pH_{PZC} value from 7.34 to 10.2 (Table 3) [36].

3.2. Adsorption of Bisphenol A by Biochar. The adsorption isotherms of BPA to BC300, BC500, and BC700 are shown in Figure 5. The adsorption data were fitted with the Freundlich sorption model: $q = K_F \cdot C_W^n$, where q (mg/kg) and

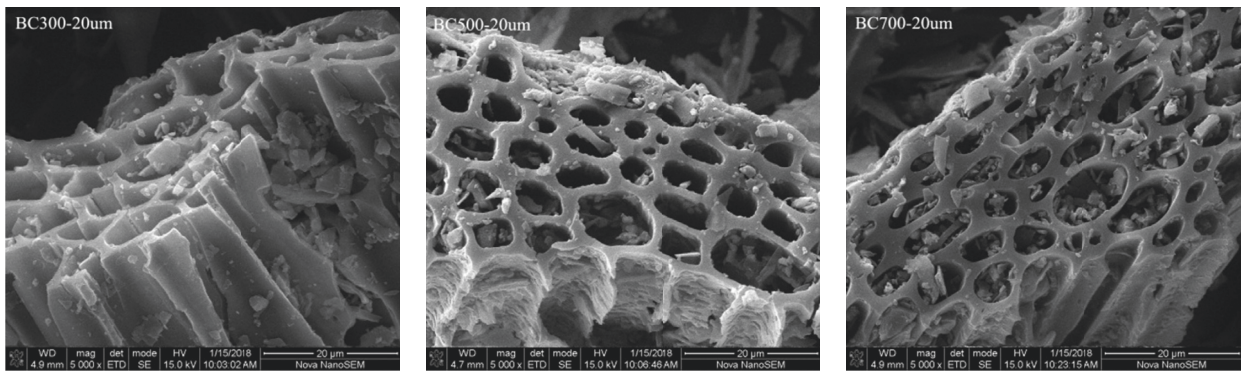

Figure 1: Scanning electron microscopy (SEM) images of BC300, BC500, and BC700.

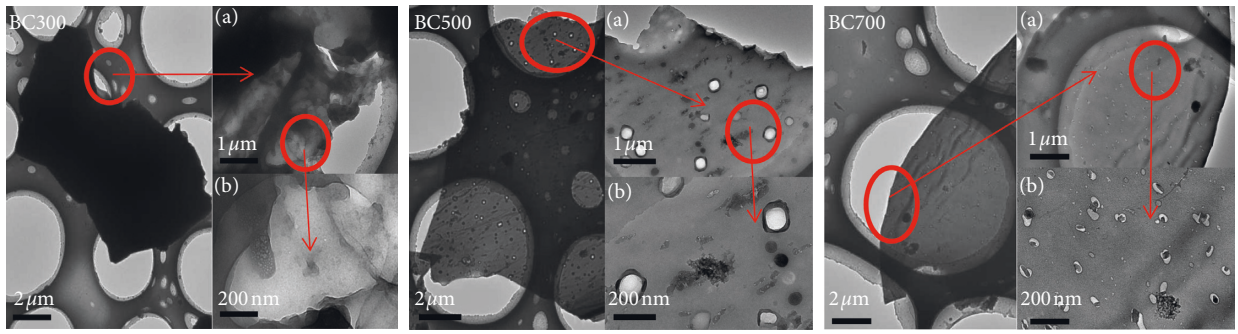

Figure 2: Transmission electron microscopy (TEM) images of BC300, BC500, and BC700 at different dimensions.

Table 3: Selected physicochemical properties of BC300, BC500, and BC700.

	C (wt%)[a]				Total C (wt.%)[a]	Total O (wt.%)[a]	Total N (wt.%)[a]	(O + N)/C ratio[a]	Specific surface area[b] ($m^2 \cdot g^{-1}$)	Pore volume[c] ($cm^3 \cdot g^{-1}$)	Pore diameter[c] (nm)	pH_{pzc}[d]
	C-C/C=C	C-O	C=O	COOH								
BC300	54.38	29.41	11.55	4.660	70.82	18.14	2.550	0.292	0.890	0.0058	25.4	7.34
BC500	68.68	16.23	10.80	4.300	73.33	16.56	2.250	0.256	58	0.053	3.66	9.93
BC700	74.00	11.66	10.32	4.030	75.02	14.81	2.150	0.226	376	0.23	2.32	10.2

[a]Analyzed using X-ray photoelectron spectroscopy. [b]Specific surface area measured using the Brunauer–Emmett–Teller (BET) method. [c]Volume of micropores (smaller than 20 Å in diameter) was determined using the Horvath–Kawazoe method. [d]Determined by a modified pH-drift method.

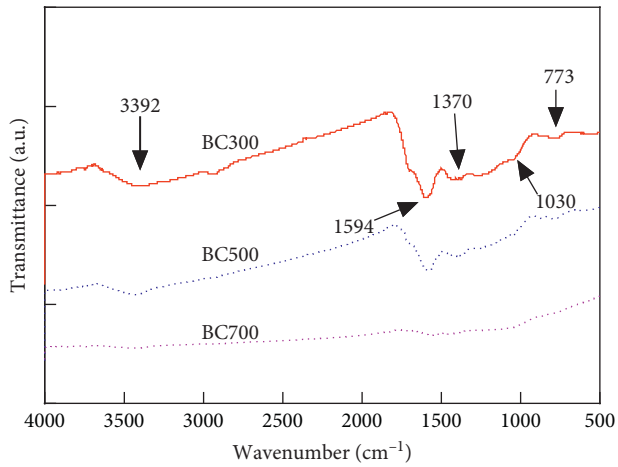

Figure 3: Fourier-transform infrared (FTIR) transmission spectra of BC300, BC500, and BC700.

C_W (mg/L) are the equilibrium concentrations of an adsorbate on the BCs and in the solution, respectively; K_F (mg^{1-n} L^n/kg) is the Freundlich affinity coefficient and n (unitless) is the Freundlich linearity index [37]. The n value could reflect the state of the energy distribution of the adsorption site [38, 39], and the heterogeneity of the adsorption sites increased with the decrease of n value [40]. The fitted Freundlich model parameters and the ranges of log K_d are summarized in Table 4, where K_d ($K_d = q/C_w$) is the adsorption coefficient [41]. In general, the Freundlich model fitted the adsorption data well.

As shown in Table 4, the values of n decreased from 0.48 to 0.22 with the increase of pyrolysis temperature. This is because the condensed aromatic domain of biochars and the heterogeneity of the adsorption sites increased with the increase of pyrolysis temperature [42]. The log K_d value of BC300 was in a range of 2.83~3.71, which was much lower than that of BC500 (2.91~4.57) and BC700 (3.24~5.50).

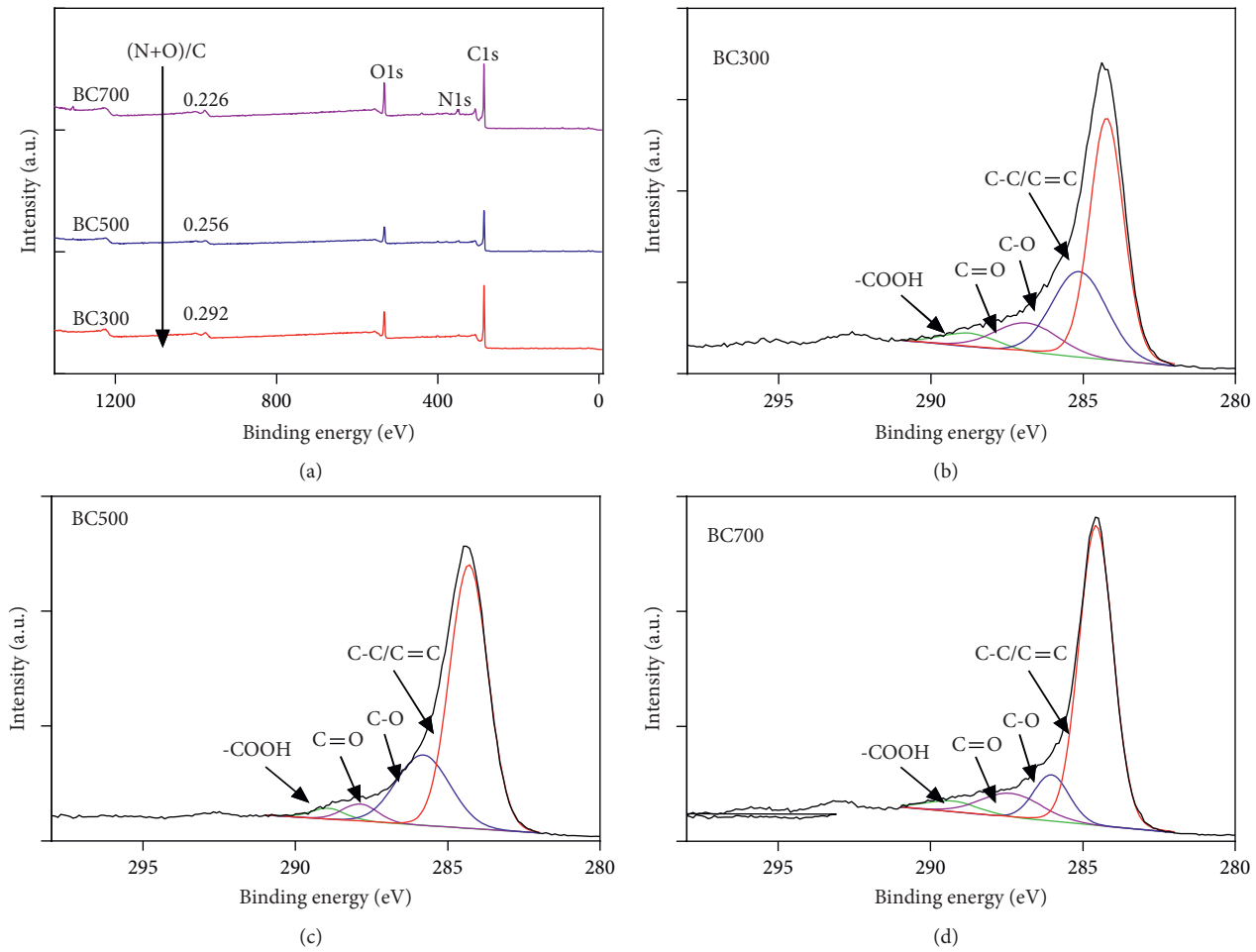

Figure 4: X-ray photoelectron spectroscopy (XPS) spectra and the C1s spectra of BC300, BC500, and BC700.

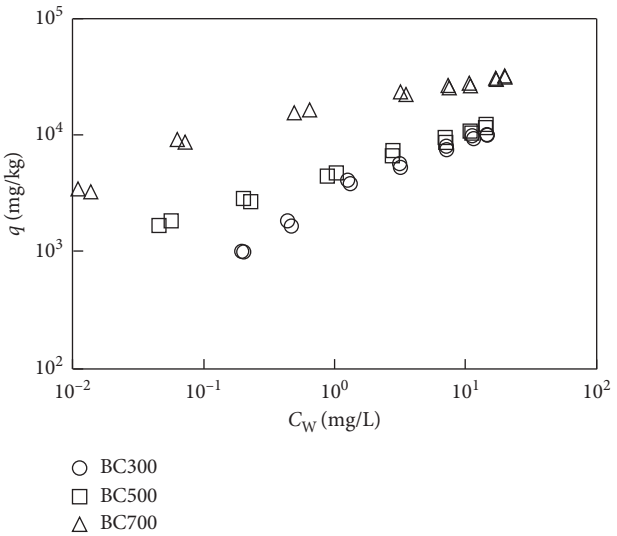

Figure 5: Adsorption isotherms of BPA to BC300, BC500, and BC700.

This result was comparable with the previous studies [11–13]. This also indicated that the adsorption affinity of biochars to BPA was following the order as BC700 > BC500 > BC300. One of the important reasons is that the increased pyrolysis temperature resulted in the enlarged pore volume and increased surface areas of biochar and provided more adsorption sites for BPA. On the other hand, the hydrophobicity of the biochar increased with the increase of pyrolysis temperature. Previous studies have reported that hydrophobic interaction is the main adsorption mechanism for the hydrophobic organic contaminants to biochars [27]. Therefore, the hydrophobic interaction between biochar and BPA was also enhanced. Thirdly, the amount of aromatic benzene ring of the biochar increased with the increase of pyrolysis temperature and made the biochars become a stronger π-electron acceptor. BPA could act as a strong a π-electron donor. Thus, the π-π electron donor/acceptor (EDA) interaction between biochar and BPA was enhanced. Chen et al. [27] also reported that π-π EDA interaction was one of the important factors that could affect the adsorption of BPA, which was consistent with our conclusion. It is noted that with the increase concentration of BPA, the adsorption affinity on the biochar under low pyrolysis temperature was closer to that on the biochar under high pyrolysis temperature. This is likely because biochars derived under low pyrolysis temperature contained more O-functional groups, and the H-bonding effect between the –OH group of BPA and the O-functional

Table 4: Summary of adsorption parameters (Freundlich model coefficients (K_F and n) and distribution coefficients (K_d)) obtained from adsorption results.

Adsorbent	Background	K_F (mmol^{1-n}L^n/kg)[a]	n[a]	R^2	Log K_d (L/kg)
BC300	None	3100 ± 170	0.45 ± 0.02	0.984	2.83–3.71
	CTAB	2200 ± 110	0.57 ± 0.02	0.993	2.75–3.68
	SDBS	1200 ± 88	0.35 ± 0.03	0.938	2.30–3.33
	Tween 20	1000 ± 70	0.43 ± 0.03	0.967	2.31–3.21
BC500	None	4700 ± 140	0.34 ± 0.01	0.992	2.91–4.57
	CTAB	3400 ± 230	0.54 ± 0.03	0.985	2.93–3.57
	SDBS	1800 ± 90	0.42 ± 0.02	0.980	2.57–3.49
	Tween 20	1700 ± 90	0.31 ± 0.02	0.960	2.42–3.55
BC700	None	16000 ± 520	0.22 ± 0.01	0.980	3.24–5.50
	CTAB	3200 ± 290	0.44 ± 0.04	0.965	3.77–4.49
	SDBS	4400 ± 280	0.33 ± 0.03	0.960	2.72–4.28
	Tween 20	5700 ± 240	0.31 ± 0.02	0.981	2.83–4.58

[a]Values after ± sign indicate relative standard deviation.

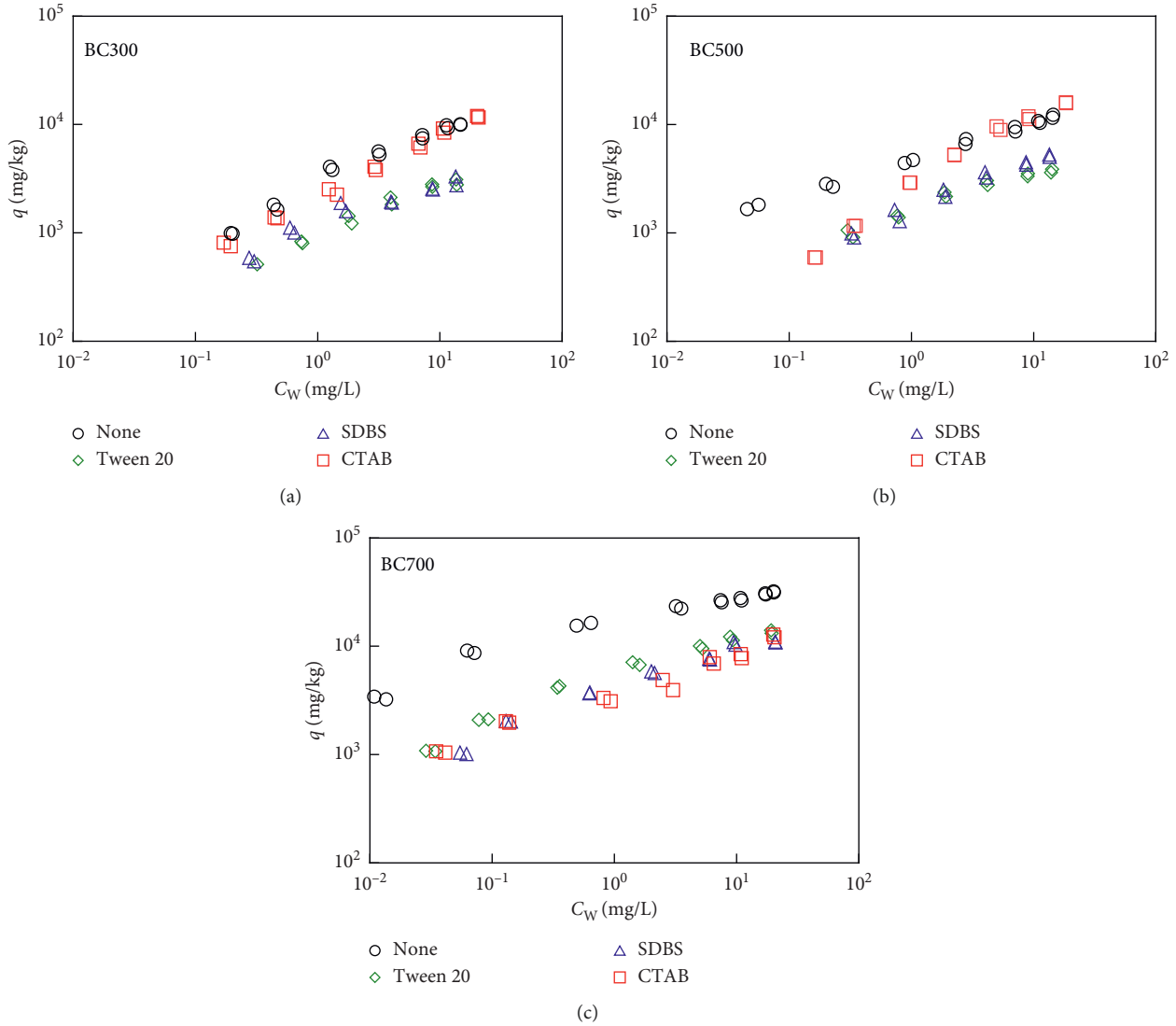

Figure 6: Adsorption isotherms of BPA to BC300, BC500, and BC700 in absence and presence of the surfactants.

groups on biochars was stronger [43]. With the increased concentration of BPA, the H-bonding effect was more obvious. Thus, although the hydrophobicity effect and π-π EDA interaction were weak on biochars derived under low pyrolysis temperature, the relatively stronger H-bonding, especially at higher BPA concentration, could offset part of the

hydrophobicity effect and π-π EDA interaction effect. Thus, H-bonding is another important mechanism that controls the adsorption behavior.

3.3. Adsorption of Bisphenol A by Biochar in presence of the Surfactants. The adsorption isotherms of BPA in presence of the surfactants are shown in Figure 6, and the fitted Freundlich model parameters are summarized in Table 4. The three different types of surfactants all showed inhibition effect on the adsorption of BPA. However, the extents of the inhibition varied, which may be in relation to the types of surfactants and the properties of biochars.

Previous studies have reported that the surfactants could be adsorbed on biochars via the hydrophobic effect, electrostatic attraction, cation exchange, π-π interaction, pore-filling effect, etc. [23, 44]. Thus, they could occupy the adsorption sites of the organic contaminants or block the pores that the organic contaminants may enter in [37]. On the other hand, the adsorbed surfactants on biochars could form hemimicelles or admicelles, which could also offer absorption (partitioning) sites for the organic contaminants [45]. Next, the surfactants could increase the solubility of organic contaminants [20]. Thus, the effects of the surfactants on the adsorption of organic contaminants depend on the contribution of each mechanism. To further explore the mechanisms that surfactants affect the adsorption behavior of BPA on biochars, the adsorption coefficient ($\log K_d$) of BPA in absence and presence of the surfactants at different equilibrium concentrations of BPA was calculated based on the Freundlich model (Table 5).

As shown in Figure 6, the adsorption isotherms of BPA on BC300 in presence of CTAB almost overlapped with that in absence of the surfactant. The $\log K_d$ varied less than 1.4% when the equilibrium concentration of BPA was 10 mg/L compared with that in absence of the surfactant on BC300, whereas it decreased 14.5% on BC700 (Table 5). Zhang et al. [20] reported that the solubilization effect could be an important reason that resulted in the inhibition effect in presence of surfactants. However, in our study, the experimental concentration of CTAB was 40 mg/L, which was much lower than the critical micelle concentration (CMC) of CTAB (340 mg/L). Thus, it has little effect on the solubility of BPA (Figure 7). Therefore, the solubility enhancement effect could be negligible. As shown in Table 2, the cationic CTAB molecules have a long hydrophobic chain and a positively charged "head" ($-NH_4^+$); thus, it could be adsorbed on the hydrophobic surface of biochars via the hydrophobic effect and the negatively charged O-functional groups via electrostatic attraction. As discussed earlier, these adsorption sites on the surface of biochars were also available for BPA. Thus, the adsorption sites for BPA would decrease in presence of CTAB, and the micropores of biochars that BPA could go in may be blocked. On the other hand, the partitioning of BPA to hemimicelles that adsorbed CTAB formed on BC300 could enhance the adsorption of BPA. Another important mechanism is that the $-NH_4^+$ group of CTAB could interact with the phenol group of BPA via Lewis acid-base interaction [37]. Thus, CTAB could serve as a cation bridge between the BPA and biochars and enhance the adsorption. Therefore, the adsorption isotherms of BPA in presence of CTAB almost overlapped with that in absence of surfactants probably due to the counterbalance between the inhibition effect caused by competition and the enhancement effect caused by the partitioning and the bridging effect by adsorbed CTAB.

It is noted that the inhibition effect of CTAB decreased with the increase of BPA concentration. For example, the adsorption coefficient ($\log K_d$) of BPA decreased 6.8% on BC300 at $C_W = 0.1$ mg/L compared with that in absence of CTAB, whereas it decreased 1.3% at $C_W = 10$ mg/L. At low concentration of BPA, the BPA molecules were prone to be adsorbed on the high adsorption energy sites, such as micropores. With the increase of the concentration of BPA, they started to be adsorbed on other adsorption sites with relatively low adsorption energy, such as the hemimicelles formed on biochars and NH_4^+ group of CTAB. Thus, the inhibition effect was weakened.

Tween 20 and SDBS showed similar inhibition effect on the BPA adsorption, which were different from CTAB, especially on BC300 (Figure 6). The $\log K_d$ values of BPA in

Table 5: The adsorption coefficients ($\log (K_d)$) calculated based on Freundlich model in absence and presence of the surfactants at different equilibrium concentrations of BPA.

Adsorbent	Background	Log K_d (L/kg)	
		$C_W = 0.1$ mg/L	$C_W = 10$ mg/L
BC300	None	4.05	2.94
	CTAB	3.77	2.90
	SDBS	3.75	2.44
	Tween 20	3.59	2.44
BC500	None	4.33	3.02
	CTAB	3.99	3.07
	SDBS	3.82	2.68
	Tween 20	3.91	2.55
BC700	None	4.99	3.44
	CTAB	4.07	2.94
	SDBS	4.31	2.97
	Tween 20	4.44	3.07

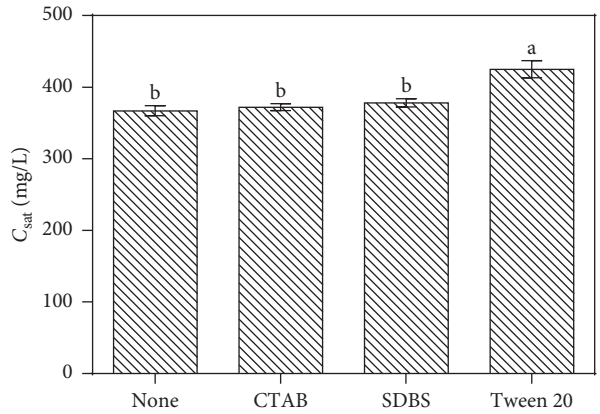

Figure 7: Solubility of BPA in absence and presence of the surfactants. The bars indicate the standard error of triplicates, and different letters indicate significant difference ($p < 0.05$).

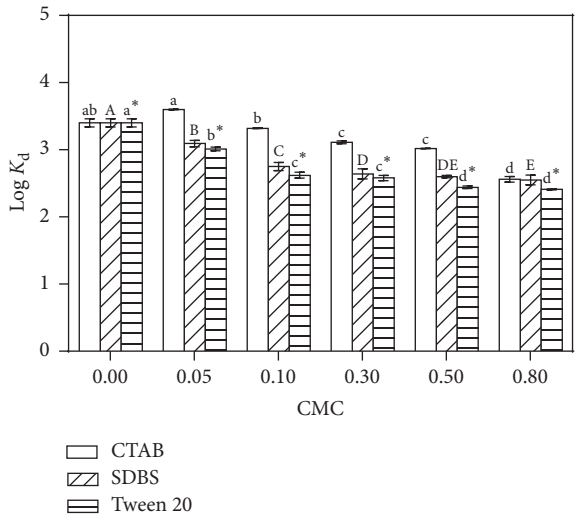

Figure 8: Effects of the surfactants on adsorption of BPA on BC300 under different surfactant concentrations. The bars indicate the standard error of triplicates, and different letters indicate significant difference ($p < 0.05$).

presence of SDBS and Tween 20 were 2.44, which was much lower than that in presence of CTAB (2.90). One of the important reasons is that Tween 20 and SDBS do not have the advantage of the bridging effect which is caused by the $-NH_4^+$ group of CTAB. Secondly, as shown in Figure 7, the solubility of BPA was increased by 15% in presence of Tween 20; thus, the BPA molecule was prone to dissolve in the surfactant solutions rather than being adsorbed on biochars [37]. On the other hand, Tween 20 could be adsorbed on the biochars via hydrophobic interaction due to its long hydrophobic chains structure, and the adsorption kinetics of Tween 20 was reported to be faster than that of BPA [46, 47]. Therefore, the molecules of Tween 20 could preferentially occupy the adsorption sites. Tween 20 could twine around the surface of biochars or block the entrances of micropores [46], and the available adsorption sites decreased. Thus, it inhibited the adsorption of BPA. Although SDBS was negatively charged and showed less adsorption on biochar surface [37], the hemimicelles or admicelles formed on biochar surface also decreased. According to the adsorption results, we speculated that the enhancement caused by the partitioning effect by adsorbed SDBS could not counterbalance the inhibition effect caused by competition effect. Thus, the inhibition effect was also strong in presence of SDBS.

With the increase of pyrolysis temperature, the extent of inhibition effect, which is indicated by the decreased percent of adsorption coefficient ($\log K_d$) (Table 5), was stronger in presence of CTAB, especially at low concentration of BPA. In presence of SDBS and Tween 20, the decreased percent of adsorption coefficient decreased less than that in presence of CTAB at low concentration of BPA, and it showed even a little increase at high concentration of BPA. This is likely because the pore diameter of biochars decreased with the increase of pyrolysis temperature. The adsorbed surfactant molecules could block more micropores on biochars produced at high pyrolysis temperature, and the inhibition effect of CTAB was stronger with the increase of pyrolysis temperature at low concentration of BPA. However, this may be not the main mechanism because of the different effects on CTAB and SDBS/Tween 20. With the increase of pyrolysis temperature, the O-functional groups of biochars decreased, and the zeta potential also decreased. Thus, the electronic attraction between CTAB and biochar decreased, and the adsorption of CTAB on biochars weakened. The enhancement caused by the partitioning effect by adsorbed CTAB and the bridging effect could not counterbalance the competition effect; thus, the inhibition effect became stronger.

To further identify the mechanisms controlling the effects of the surfactants, we examined the values of $\log K_d$ of BPA on BC300 under different surfactant concentrations (Figure 8). For SDBS and Tween 20, it showed similar trend that with the increase of the surfactant concentration, the inhibition effect was enhanced significantly ($p < 0.05$). This may be because with the increase of the surfactant concentration, the solubility enhancement effect also increased which may decrease the adsorption of BPA on biochars. Zhang et al. [20] also reported that the increase of SDBS concentration could result in decrease of phenanthrene adsorption on black carbon because of the solubility enhancement. However, CTAB showed a slight increase of BPA adsorption on biochars at lower concentration (0.05 CMC) ($p > 0.05$) and then decreased significantly ($p < 0.05$). This is likely because the partitioning effect and the bridging effect caused by adsorbed CTAB might be the main mechanisms at low concentration of CTAB.

4. Conclusion

The pyrolysis temperature could affect the physical and chemical properties of peanut shell biochar, and the adsorption affinity of BPA would be stronger on the biochars produced at higher temperature due to the larger surface area and pore volume, higher hydrophobicity, and aromaticity. The main mechanisms of adsorption of BPA on peanut shell biochars were hydrophobic effect, π-π EDA interaction, and H-bonding. The presence of surfactants could affect the adsorption behavior of BPA to biochars. The cationic, anionic, and nonionic surfactants all showed inhibition effect on the adsorption of BPA. The adsorption affinities of BPA in presence of CTAB were similar with those in absence of surfactants to BC300 probably due to the counterbalance between the inhibition effect caused by competition and enhancement caused by the partitioning and bridging effect by adsorbed CTAB, and the inhibition effect of CTAB was stronger with the increase of pyrolysis temperature. However, Tween 20 and SDBS do not have the advantage of the bridging effect which is caused by the $-NH_4^+$ group of CTAB. Thus, Tween 20 and SDBS showed stronger inhibition effect than CTAB, especially on BC300. This study revealed the mechanisms controlling the adsorption behavior of BPA to biochars. It is of great importance for the application of the biochar in wastewater treatment. However, further studies (in particular, the

desorption behavior in presence of surfactants) are needed to fully understand the mechanism of the adsorption process of BPA to biochars.

Data Availability

The data used to support the findings of this study are available from the corresponding author upon request.

Conflicts of Interest

The authors declare that there are no conflicts of interest regarding the publication of this paper.

Acknowledgments

This study was supported by the National Natural Science Foundation of China (grant nos. 21707101 and 21607120), Science and Technology Development Foundation of Tianjin Municipal Education Commission of China (grant no. JW1715), the Opening Foundation of Ministry of Education Key Laboratory of Pollution Processes and Environmental Criteria (grant no. 2017-06), the Doctoral Fund of Tianjin Normal University (grant no. 52XB1403), and the Innovation Team Training Plan of the Tianjin Education Committee (TD13-5073).

References

[1] Y. H. Ou, Y. J. Chang, F. Y. Lin, M. L. Chang, C. Y. Yang, and Y. H. Shih, "Competitive sorption of bisphenol A and phenol in soils and the contribution of black carbon," *Ecological Engineering*, vol. 92, pp. 270–276, 2016.

[2] A. Tomza-Marciniak, P. Stepkowska, J. Kuba, and B. Pilarczyk, "Effect of bisphenol A on reproductive processes: a review of in vitro, in vivo and epidemiological studies," *Journal of Applied Toxicology*, vol. 38, no. 1, pp. 51–80, 2018.

[3] K. Anongporn, P. Wachirasek, C. Nipon, and W. Orawan, "Damaging effects of bisphenol A on the kidney and the protection by melatonin: emerging evidences from in vivo and in vitro studies," *Oxidative Medicine and Cellular Longevity*, vol. 2018, Article ID 3082438, 15 pages, 2018.

[4] S. Flint, T. Markle, S. Thompson, and E. Wallace, "Bisphenol A exposure, effects, and policy: a wildlife perspective," *Journal of Environmental Management*, vol. 104, no. 16, pp. 19–34, 2012.

[5] Y. Q. Huang, C. K. C. Wong, J. S. Zheng et al., "Bisphenol A (BPA) in China: a review of sources, environmental levels, and potential human health impacts," *Environment International*, vol. 42, pp. 91–99, 2012.

[6] T. Yamamoto, A. Yasuhara, H. Shiraishi, and O. Nakasugi, "Bisphenol A in hazardous waste landfill leachates," *Chemosphere*, vol. 42, no. 4, pp. 415–418, 2001.

[7] L. Lu and B. Chen, "Enhanced bisphenol A removal from stormwater in biochar-amended biofilters: combined with batch sorption and fixed-bed column studies," *Environmental Pollution*, vol. 243, pp. 1539–1549, 2018.

[8] P. Zhang, H. Sun, L. Yu, and T. Sun, "Adsorption and catalytic hydrolysis of carbaryl and atrazine on pig manure-derived biochars: impact of structural properties of biochars," *Journal of Hazardous Materials*, vol. 244-245, pp. 217–224, 2013.

[9] P. Zhang, G. Huang, C. An et al., "An integrated gravity-driven ecological bed for wastewater treatment in subtropical regions: process design, performance analysis, and greenhouse gas emissions assessment," *Journal of Cleaner Production*, vol. 212, pp. 1143–1153, 2019.

[10] A. Ghaffar, S. Ghosh, F. Li et al., "Effect of biochar aging on surface characteristics and adsorption behavior of dialkyl phthalates," *Environmental Pollution*, vol. 206, pp. 502–509, 2015.

[11] Z. Wu, X. Wei, Y. Xue, X. He, and X. Yang, "Removal effect of atrazine in co-solution with bisphenol A or humic acid by different activated carbons," *Materials*, vol. 11, no. 12, p. 2558, 2018.

[12] Y. K. Choi and E. Kan, "Effects of pyrolysis temperature on the physicochemical properties of alfalfa-derived biochar for the adsorption of bisphenol A and sulfamethoxazole in water," *Chemosphere*, vol. 218, pp. 741–748, 2019.

[13] E. Kim, C. Jung, J. Han et al., "Sorptive removal of selected emerging contaminants using biochar in aqueous solution," *Journal of Industrial and Engineering Chemistry*, vol. 36, pp. 364–371, 2016.

[14] J. Chen, D. Zhu, and C. Sun, "Effect of heavy metals on the sorption of hydrophobic organic compounds to wood charcoal," *Environmental Science and Technology*, vol. 41, no. 7, pp. 2536–2541, 2007.

[15] B. Sun, F. Lian, Q. Bao, Z. Liu, Z. Song, and L. Zhu, "Impact of low molecular weight organic acids (lmwoas) on biochar micropores and sorption properties for sulfamethoxazole," *Environmental Pollution*, vol. 214, pp. 142–148, 2016.

[16] G.-G. Ying, "Fate, behavior and effects of surfactants and their degradation products in the environment," *Environment International*, vol. 32, no. 3, pp. 417–431, 2006.

[17] W. Que, L. Jiang, C. Wang et al., "Influence of sodium dodecyl sulfate coating on adsorption of methylene blue by biochar from aqueous solution," *Journal of Environmental Sciences*, vol. 70, no. 8, pp. 166–174, 2018.

[18] X. Mi, G. Li, W. Zhu, and L. Liu, "Enhanced adsorption of orange II using cationic surfactant modified biochar pyrolyzed from cornstalk," *Journal of Chemistry*, vol. 2016, Article ID 8457030, 7 pages, 2016.

[19] D. Han, X. T. Liu, G. X. Zhang, K. Sun, and Y. Jiao, "Effects of cationic surfactant on pentachlorophenol sorption by sediment activecarbon and biochar," *Fresenius Environmental Bulletin*, vol. 22, no. 4B, pp. 1280–1286, 2013.

[20] J. Zhang and M. He, "Effect of surfactants on sorption and desorption of phenanthrene onto black carbon," *Water Environment Research*, vol. 83, no. 1, pp. 15–22, 2011.

[21] P. Oleszczuk and B. Xing, "Influence of anionic, cationic and nonionic surfactants on adsorption and desorption of oxytetracycline by ultrasonically treated and non-treated multiwalled carbon nanotubes," *Chemosphere*, vol. 85, no. 8, pp. 1312–1317, 2011.

[22] B. Pan, D. Lin, H. Mashayekhi, and B. Xing, "Adsorption and hysteresis of bisphenol A and 17α-ethinyl estradiol on carbon nanomaterials," *Environmental Science and Technology*, vol. 43, no. 2, pp. 5480–5485, 2008.

[23] Z. Han, F. Zhang, D. Lin, and B. Xing, "Clay minerals affect the stability of surfactant-facilitated carbon nanotube suspensions," *Environmental Science and Technology*, vol. 42, no. 18, pp. 6869–6875, 2008.

[24] A. Bak and W. Podgórska, "Interfacial and surface tensions of toluene/water and air/water systems with nonionic surfactants Tween 20 and Tween 80," *Colloids and Surfaces A: Physicochemical Engineering Aspects*, vol. 504, pp. 414–425, 2016.

[25] J. Li, N. Liang, X. Jin et al., "The role of ash content on bisphenol A sorption to biochars derived from different agricultural wastes," *Chemosphere*, vol. 171, pp. 66–73, 2017.

[26] S. A. Dastgheib, T. Karanfil, and W. Cheng, "Tailoring activated carbons for enhanced removal of natural organic matter from natural waters," *Carbon*, vol. 42, no. 3, pp. 547–557, 2004.

[27] J. Chen, D. Zhang, H. Zhang, S. Ghosh, and B. Pan, "Fast and slow adsorption of carbamazepine on biochar as affected by carbon structure and mineral composition," *Science of the Total Environment*, vol. 579, pp. 598–605, 2016.

[28] Z. Chen, B. Chen, and C. T. Chiou, "Fast and slow rates of naphtalene sorption to biochars produced at different temperatures," *Environmental Science and Technology*, vol. 46, no. 20, pp. 11104–11111, 2012.

[29] H. Zheng, Z. Wang, J. Zhao, S. Herbert, and B. Xing, "Sorption of antibiotic sulfamethoxazole varies with biochars produced at different temperatures," *Environmental Pollution*, vol. 181, pp. 60–67, 2013.

[30] Y. Fu, N. Zhang, Y. Shen, X. Ge, and M. Chen, "Micro-mesoporous carbons from original and pelletized rice husk via one-step catalytic pyrolysis," *Bioresource Technology*, vol. 269, pp. 67–73, 2018.

[31] G. Chu, J. Zhao, F. Chen et al., "Physi-chemical and sorption properties of biochars prepared from peanut shell using thermal pyrolysis and microwave irradiation," *Environmental Pollution*, vol. 227, pp. 372–379, 2017.

[32] M. Ahmad, S. S. Lee, X. Dou et al., "Effects of pyrolysis temperature on soybean stover- and peanut shell-derived biochar properties and TCE adsorption in water," *Bioresource Technology*, vol. 118, pp. 536–544, 2012.

[33] M. Keiluweit, P. S. Nico, M. G. Johnson, and M. Kleber, "Dynamic molecular structure of plant biomass-derived black carbon (biochar)," *Environmental Science and Technology*, vol. 44, no. 4, pp. 1247–1253, 2010.

[34] M. Lawrinenko, D. Jing, C. Banik, and D. A. Laird, "Aluminum and iron biomass pretreatment impacts on biochar anion exchange capacity," *Carbon*, vol. 118, pp. 422–430, 2017.

[35] Z. Chang, L. Tian, M. Wu, X. Dong, J. Peng, and B. Pan, "Molecular markers of benzene polycarboxylic acids in describing biochar physiochemical properties and sorption characteristics," *Environmental Pollution*, vol. 237, pp. 541–548, 2018.

[36] L. Ye, J. Zhang, J. Zhao, Z. Luo, S. Tu, and Y. Yin, "Properties of biochar obtained from pyrolysis of bamboo shoot shell," *Journal of Analytical and Applied Pyrolysis*, vol. 114, pp. 172–178, 2015.

[37] F. Wang, Z. Jia, W. Su, Y. Shang, and Z.-L. Wang, "Adsorption of phenanthrene and 1-naphthol to graphene oxide and L-ascorbic-acid-reduced graphene oxide: effects of pH and surfactants," *Environmental Science and Pollution Research*, vol. 26, no. 11, pp. 11062–11073, 2019.

[38] N. Xu, B. Zhang, G. Tan, J. Li, and H. Wang, "Influence of biochar on sorption, leaching and dissipation of bisphenol A and 17α-ethynylestradiol in soil," *Environmental Science: Processes and Impacts*, vol. 17, no. 10, pp. 1722–1730, 2015.

[39] M. Wu, B. Pan, D. Zhang et al., "The sorption of organic contaminants on biochars derived from sediments with high organic carbon content," *Chemosphere*, vol. 90, no. 2, pp. 782–788, 2013.

[40] H. Li, C. Wei, D. Zhang, and B. Pan, "Adsorption of bisphenol A on dispersed carbon nanotubes: role of different dispersing agents," *Science of the Total Environment*, vol. 655, pp. 807–813, 2019.

[41] C. Jung, J. Park, K. H. Lim et al., "Adsorption of selected endocrine disrupting compounds and pharmaceuticals on activated biochars," *Journal of Hazardous Materials*, vol. 263, pp. 702–710, 2013.

[42] K. Sun, K. Ro, M. Guo, J. Novak, H. Mashayekhi, and B. Xing, "Sorption of bisphenol A, 17α-ethinyl estradiol and phenanthrene on thermally and hydrothermally produced biochars," *Bioresource Technology*, vol. 102, no. 10, pp. 5757–5763, 2011.

[43] P. Wu, Z. Cai, H. Jin, and Y. Tang, "Adsorption mechanisms of five bisphenol analogues on pvc microplastics," *Science of the Total Environment*, vol. 650, pp. 671–678, 2019.

[44] Q. Wang, Y. Han, Y. Wang, Y. Qin, and Z.-X. Guo, "Effect of surfactant structure on the stability of carbon nanotubes in aqueous solution," *The Journal of Physical Chemistry B*, vol. 112, no. 24, pp. 7227–7233, 2008.

[45] K. Yang, Q. Jing, W. Wu, L. Zhu, and B. Xing, "Adsorption and conformation of a cationic surfactant on single-walled carbon nanotubes and their influence on naphthalene sorption," *Environmental Science and Technology*, vol. 44, no. 2, pp. 681–687, 2010.

[46] C. K. Ahn, S. H. Woo, and J. M. Park, "Enhanced sorption of phenanthrene on activated carbon in surfactant solution," *Carbon*, vol. 46, no. 11, pp. 1401–1410, 2008.

[47] C. K. Ahn, Y. M. Kim, S. H. Woo, and J. M. Park, "Selective adsorption of phenanthrene dissolved in surfactant solution using activated carbon," *Chemosphere*, vol. 69, no. 11, pp. 1681–1688, 2007.

Hindawi
Journal of Chemistry
Volume 2019, Article ID 4932837, 10 pages
https://doi.org/10.1155/2019/4932837

Research Article

Adsorption Characteristics and Transport Behavior of Cr(VI) in Shallow Aquifers Surrounding a Chromium Ore Processing Residue (COPR) Dumpsite

Yu Liu,[1,2] **Yin Li**,[2] **Yucheng Hu**,[2] **Khan M. G. Mostofa**,[1] **Siliang Li**,[1] **and Zhenying Liu**[3]

[1]*Institute of Surface-Earth System Science, Tianjin University, Weijin Road 92, Tianjin 300072, China*
[2]*Tianjin Hydraulic Science Research Institute, Youyi Road 60, Tianjin 300061, China*
[3]*School of Environmental Science and Safety Engineering, Tianjin University of Technology, Tianjin 300191, China*

Correspondence should be addressed to Yu Liu; liuyu2017@tju.edu.cn

Received 26 August 2019; Accepted 3 October 2019; Published 3 November 2019

Guest Editor: Yifeng Zhang

This study explored the stratigraphic distribution and soil/shallow aquifer characteristics surrounding a chromium ore processing residue (COPR) dumpsite at a former chemical factory in China. Total Cr levels in top soils (5–10 cm) nearby the COPR dumpsite were in the range of 8571.4–10711.4 mg/kg. Shallow aquifers (1–6 m) nearby the COPR dumpsite showed a maximum total Cr level of 9756.7 mg/kg. The concentrations of Cr(VI) in groundwater nearby the COPR dumpsite were 766.9–1347.5 mg/L. These results display that the top soils, shallow aquifers, and groundwater of the study site are severely polluted by Cr(VI). Then, three aquifers (silt, clay, and silty clay), respectively, collected from the depth of 1.4–2.4 m, 2.4–4.8 m, and 4.8–11.00 m were first used to evaluate the adsorption characteristics and transport behavior of Cr(VI) in shallow aquifers by both batch and column experiments. The adsorption of Cr(VI) on tested aquifers was well described by pseudo-second-order equation and Freundlich model. The adsorption capacities of Cr(VI) on three aquifers followed the order: clay > silty clay > silt. The kinetics proved that Cr(VI) is not easily adsorbed by the aquifer mediums but transports with groundwater. Thermodynamics indicated that Cr(VI) adsorption on tested aquifers was feasible, spontaneous, and endothermic. Cr(VI) adsorption on tested aquifers decreased with increasing pH. Furthermore, the transport of Cr(VI) in adsorption columns followed the sequence of clay < silty clay < silt. Desorption column experiments infer that the Cr(VI) adsorbed on aquifers will desorb and release into groundwater in the case of rainwater leaching. Therefore, a proper treatment of the COPR and a comprehensive management of soils are vital to prevent groundwater pollution.

1. Introduction

Chromium (Cr) is widely used in various chemical industries, such as electroplating, steelmaking, metallurgy, leather tanning, pigment manufacturing, wood preservative, and textile dyeing [1]. Hexavalent chromium (Cr(VI)) and trivalent chromium (Cr(III)) are the most stable species of Cr in the environment [2]. Cr(III) is relatively stable and has low solubility and mobility in soils and aquifers [3]. On the contrary, Cr(VI) is a strong oxidant and highly mobile, thereby causing Cr(VI) more environmentally available than Cr(III) [4]. Cr(VI) exposure could cause skin irritation, respiratory cancer, and kidney damage [5]. The contamination of soils and groundwater with Cr(VI) has posed a chronic public health and environmental threat due to its high solubility, mobility, toxicity, and mutagenic and carcinogenic properties [6]. The drinking water standard for total Cr of US EPA is 100 μg/L [7]. The permitted concentration of Cr(VI) in drinking water based on the World Health Organization (WHO) guideline is 0.05 mg/L [8].

Chromium ore processing residue (COPR), because of its high content of dissolvable Cr(VI), is one of the most hazardous solid wastes [9]. The continuous Cr(VI) leaching from COPR could cause severe pollution to its surrounding environment, including groundwater [6, 10]. It was reported that only 100 million tons of COPR were treated in China

from 2005 to 2010, yet 300 million tons of COPR still harm the environment [11]. Former Tianjin Tongsheng Chemical Factory started to produce chromate in 1958, which was one of the pioneer chemical factories in China. Even though the factory was shut down in 1998, more than 400 kilotons of COPR were piled up in the open air (just covered by black cloth) in the southwest corner of the factory till 2012. According to our site investigation during 2014 and 2015, there was still significant COPR stored in the factory which has not been properly disposed. Given the large quantity of COPR being placed in the open air for several decades, the continuous Cr(VI) leaching by rain endangers the public health of local residents. It is therefore vital to investigate the distribution, adsorption, and transport of Cr(VI) in surrounding soils and aquifers nearby the COPR dumpsite. However, to the best of our knowledge, no study has been reported in that regards.

Heavy metals in soils may undergo several processes: adsorption/desorption, precipitation/dissolution, oxidation/reduction, plant uptake, microbial conversion, and transport through the soil profile [12]. Although these processes can occur simultaneously, adsorption was the most dominating process controlling existence of metals in soils [12]. Many studies reported about metal adsorption in soil, but fewer studies combine adsorption batch experiments with adsorption/desorption column experiments to investigate the adsorption characteristics and transport behavior of heavy metal in soil and its risk to groundwater. Although many studies were about the Cr(VI) adsorption in soils, previous research studies focused on the adsorption of Cr(VI) in top soils (e.g., 0–6 cm depth [13] and 0–20 cm depth [14–17]), only limited studies reported the adsorption of Cr(VI) in aquifers [18, 19]. However, the adsorption and desorption of Cr(VI) by aquifer mediums are different from the top soils, which are affected by their different geochemical characteristics. In addition, compared with batch experiments of adsorption, only limited studies applied column experiments [14, 16, 17] and 3D sandbox [11] to investigate the transport behavior of Cr(VI) in soils. Desorption experiments were also not carried out in aforementioned column experiments [14, 16, 17]. And rarely works have used real shallow aquifers to fill up columns or sandboxes to investigate the transport behavior of Cr(VI) in aquifers.

In this work, we measured the concentrations of Cr(VI) in top soils (5–10 cm), shallow aquifers and groundwater nearby the COPR dumpsite and explored the stratigraphic distribution and soil characteristics of the study site. Then, three kinds of aquifers were first used to evaluate the adsorption characteristics and transport behavior of Cr(VI) in shallow aquifers by both batch and column experiments. The objectives of the present work were to (1) evaluate the concentrations of Cr(VI) in top soils, shallow aquifers, and groundwater nearby the COPR dumpsite, (2) investigate the adsorption characteristics of Cr(VI) in different aquifers and gain insight into the adsorption mechanism of Cr(VI) in these aquifers, and (3) reveal the adsorption-desorption behaviors of Cr(VI) in aquifers by dynamic column studies. The results of our study can be used to predict the fate and transport behavior of Cr(VI) in polluted soils and aquifers, which will also be helpful to value the risk of contaminant migration and to establish effective remediation plans for contaminated soils.

2. Materials and Methods

2.1. Study Site and Sampling. Geological and hydrogeochemical investigations were carried out near the COPR dumpsite (see Supplementary Material Figure S1) of the former Tianjin Tongsheng Chemical Factory, Tianjin, China. The COPR dumpsite lies at latitude 39°14′21.4″N and longitude 117°06′28.3″E. The topography is alluvial and coastal plain. Eleven sampling sites at different distances from the COPR dumpsite were set to carry out drilling sampling. Schematic of sampling sites is shown in Figure 1. Geographical locations of the drilling sampling sites (Table S1), photographs of core drilling and groundwater sampling (Figure S2), and other detailed information of sampling are all described in the Supplementary Material.

2.2. Stratigraphic Distribution and Soil Characteristics. Based on the Standard for Engineering Classification of Soil (GB/T 50145-2007) [20] and Technical Specification for Division of Subsoil Sequence in Tianjin (DB/T29-191-2009) [21], soils and aquifers within 20 m depth of the study site are divided into 5 layers according to the formation time. From top to bottom, the 5 layers are composed of the artificial fill layer (Qml): the new alluvium (Q_4^{3N}al), the Holocene upper-group lagoon-facies sedimentary layer (Q_4^3 l + h), the Holocene middle-group marine-facies sedimentary layer (Q_4^2m), and the Holocene lower-group continental-facies alluvium (Q_4^1al). The vertical distribution of local geological formations is shown in Table S2. The detailed information of soil and aquifers characteristics is described in the Supplementary Material.

The aquifers used in this study included silt, clay, and silty clay, which were respectively collected from the depth of 1.4–2.4 m, 2.4–4.8 m, and 4.8–11.00 m. At this point, it should be noted that the depth of the groundwater fluctuates between 0.7 m and 1.4 m in our study site. Hence, it is more appropriate to address the silt, clay, and silty clay used in this study as "aquifers" rather than "soils." Therefore, the term "aquifers" will be used in this text to denote silt, clay, and silty clay.

2.3. Experiments. The experiments include batch study and column study. A schematic diagram of the column setup is depicted in Figure S3. The packing status of columns and operating conditions for the adsorption/desorption column experiments are mentioned in Table S3. Also, detailed information of experiments is described in the Supplementary Material.

3. Results and Discussion

3.1. High Concentration of Cr(VI) in Top Soils, Shallow Aquifers, and Groundwater. Drillcore samples were analyzed to determine the stratigraphic distribution and soil

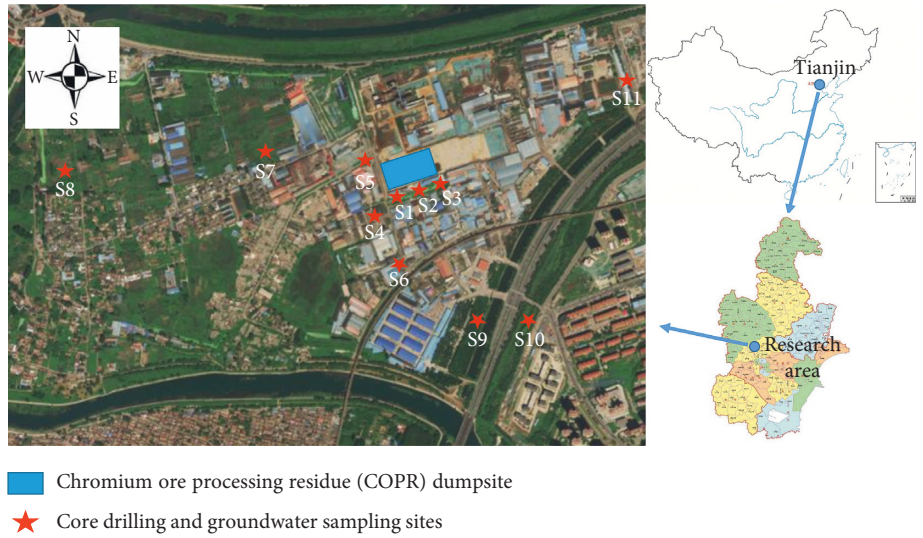

Figure 1: Schematic of sampling sites near the chromium ore processing residue (COPR) dumpsite.

characteristics of the study site. The aquifers (silt, clay, and silty clay) used in this study were collected from the depth of 1.4–2.4 m, 2.4–4.8 m, and 4.8–11.0 m, respectively. Also, the detailed stratigraphic distribution has been discussed in Materials and Methods section. The physicochemical properties of different aquifers are shown in Table S4. The concentrations of total Cr in top soils (5–10 cm) and shallow aquifers (1–6 m) of 11 drilling sampling sites are, respectively, shown in Figures S4 and S5. The concentrations of total Cr in top soils (5–10 cm) nearby the COPR dumpsite (sampling sites S1–S3) were in the range of 8571.4–10711.4 mg/kg. Shallow aquifers (1–6 m) nearby the COPR dumpsite also present high levels of total Cr. Most samples of shallow aquifers (1–6 m) at sampling sites of S1–S6 show high concentrations of total Cr, which were much higher than the Environmental Quality Standard for Soils (250 mg/kg) (GB 15618-2018) [22]. The maximum total Cr level (9756.7 mg/kg) appears at the depth of 1 m at sampling site S2, which was 160 times higher than the background value of Chinese soils (61 mg/kg) [23]. The concentrations of total Cr decrease with increasing depth at most of the sampling sites. Moreover, the concentrations of total Cr at sampling sites of S1–S5 were much higher than those at S6–S11, showing that the shallow aquifers nearer the COPR dumpsite are more severely polluted. The concentrations of Cr(VI) and total Cr of groundwater in 11 monitoring wells are shown in Table S5. The Cr(VI) concentrations of groundwater (monitoring wells S1–S3) nearby the COPR dumpsite range from 766.9 to 1347.5 mg/L, which significantly exceeded the V grade value (0.1 mg/L) of Quality Standard for Groundwater (GB/T 14848-2017) [24] and drinking water standard (0.05 mg/L) of WHO guideline [8]. The pH values of groundwater range from 7.5 to 8.2, which were alkalescent. These results suggest that the top soils (5–10 cm), shallow aquifers (1–6 m), and groundwater nearby the COPR dumpsite are severely contaminated and should get great concern.

3.2. Adsorption Characteristics

3.2.1. Adsorption Kinetics. The adsorption kinetics experiments were studied at pH 7-8, 288 K, and an initial Cr(VI) concentration of 1.0 mg/L. The adsorption kinetics of Cr(VI) in three kinds of aquifers are shown in Figure 2(a). The Cr(VI) adsorption was fast in the first 120 min and then increased slightly until reaching the equilibrium at 240 min. The adsorption capacities of Cr(VI) at the equilibrium time were 1.22, 0.94, and 0.81 mg/kg for clay, silty clay, and silt, respectively. The maximum adsorption rates of Cr(VI) in clay, silty clay, and silt were only 11.9%, 9.3%, and 7.9%, respectively. It demonstrates that Cr(VI) is not easily adsorbed by the aquifer mediums but transports with groundwater, causing long-distance pollution.

To better understand the adsorption kinetics, the pseudo-first-order (PFO) (equation (1)) and pseudo-second-order (PSO) (equation (2)) kinetic models [25] and Elovich equation (equation (3)) [26] were applied to investigate the adsorption kinetics process. Meanwhile, the intraparticle diffusion model (IPD) (equation (4)) [25] was further tested to analyze the diffusion mechanism of the adsorption.

$$\log(Q_e - Q_t) = \log(Q_e) - \frac{k_1}{2.303}t, \quad (1)$$

$$\frac{t}{Q_t} = \frac{1}{k_2 Q_e^2} + \frac{1}{Q_e}t, \quad (2)$$

$$Q_t = \beta \ln(\alpha\beta) + \beta \ln t, \quad (3)$$

$$Q_t = a + k_i t^{1/2}, \quad (4)$$

where Q_t (mg/g) and Q_e (mg/g) are the amounts of Cr(VI) adsorbed at time t (min) and at equilibrium, respectively, and k_1 (min^{-1}), k_2 (g/mg·min), k_i ($\text{mg/g·min}^{1/2}$), α (mg/g·min), and β (g/mg) are the rate constants of PFO, PSO, IPD, and Elovich equation, respectively.

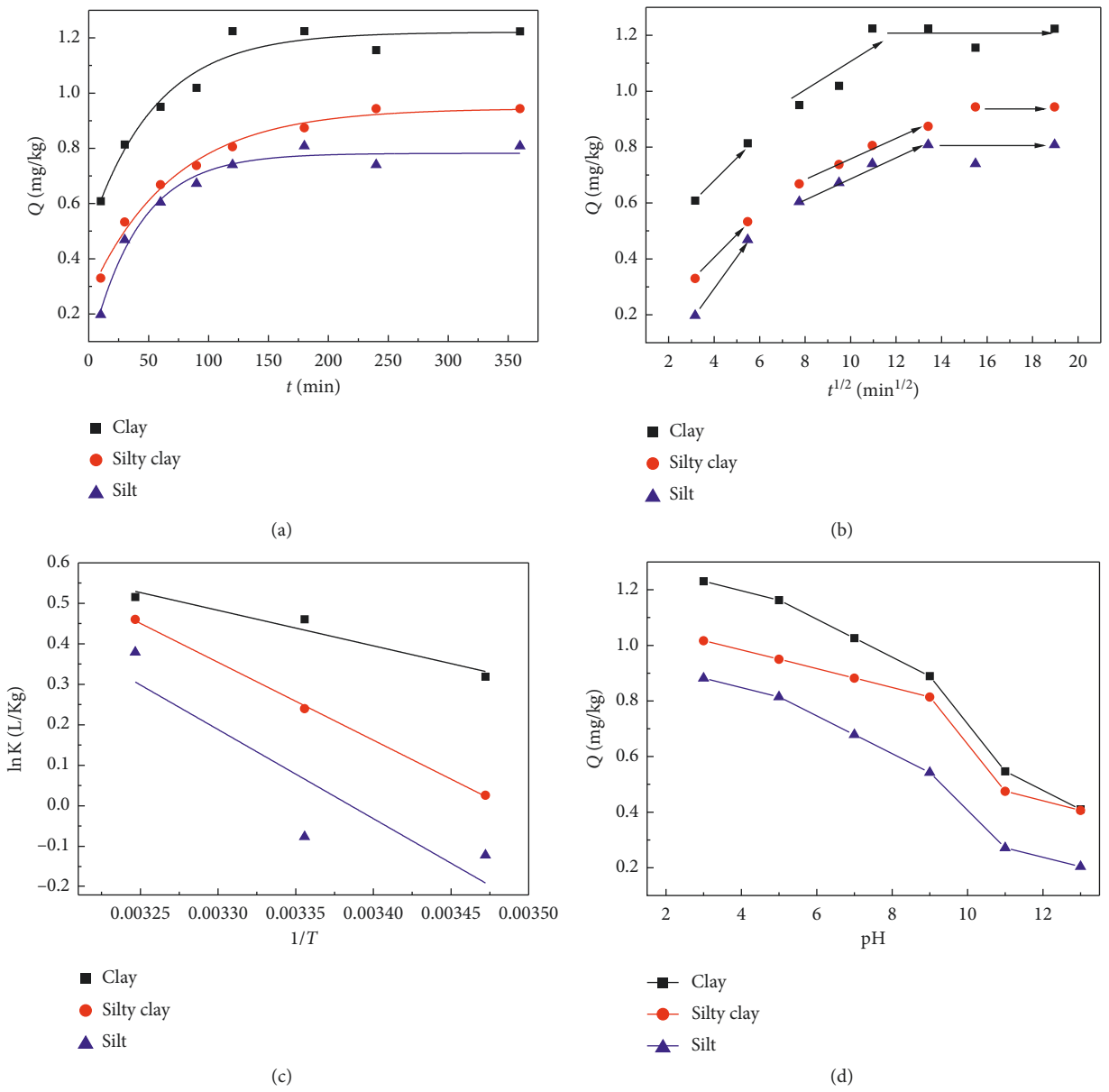

Figure 2: (a) Adsorption equilibration curves of Cr(VI) adsorption by clay, silty clay, and silt. Cr(VI) solution 1.0 mg/L, aquifers 0.1 g/mL, pH 7-8, and 288 K. (b) Intraparticle diffusion kinetics for adsorption of Cr(VI) by clay, silty clay, and silt. Cr(VI) solution 1.0 mg/L, aquifers 0.1 g/mL, pH 7-8, and 288 K. (c) Typical plots of ln K versus $1/T$ for adsorption of Cr(VI) by clay, silty clay, and silt. (d) Effect of pH on Cr(VI) adsorption by clay, silty clay, and silt. Cr(VI) solution 1.0 mg/L, aquifers 0.1 g/mL, and 288 K.

The values of different model constants are given in Table 1. The values of correlation coefficient (R^2) for the PFO kinetic model were quite low. It indicates that the adsorption of Cr(VI) onto aquifers does not follow the PFO kinetic. The values of correlation coefficient (R^2) for the PSO kinetic model were the highest. Also, the adsorption capacities calculated by the PSO kinetic model were 1.27, 1.02, and 0.87 mg/kg for clay, silty clay, and silt, respectively, which were most close to the experimental results. It indicates that the PSO model (see Supplementary Material Figure S6) was most suitable for describing the adsorption kinetics of Cr(VI) in three tested aquifers. The well-fitting PSO model suggests that the adsorption of Cr(VI) onto aquifers is highly controlled by chemisorption. Electronic forces occur between anion groups of Cr(VI) and cation groups of aquifers by sharing or exchange of electrons [27]. Similar results reported in earlier studies also showed that the PSO kinetic model was most suitable for Cr(VI) adsorption [26, 28, 29]. The experimental data also had a good fit of Elovich equation (R^2 values of 0.912–0.990). This implies a multilayer adsorption which predominates Cr(VI) adsorption in aquifers, and every layer shows various activation energy for chemisorption [30].

In addition, to better understand the adsorption mechanism, it is necessary to determine the rate-limiting step. Figure 2(b) shows that the plots are not good linear over

Table 1: Constants and coefficients of kinetic models.

Aquifers	Pseudo-first-order kinetics $\log(Q_e - Q_t) = \log(Q_e) - (k_1/2.303)t$			Pseudo-second-order kinetics $t/Q_t = (1/k_2Q_e^2) + (1/Q_e)t$			Elovich model $Q_t = \beta \ln(\alpha\beta) + \beta \ln t$			Intraparticle diffusion model $Q_t = a + k_i t^{1/2}$		
	k_1 (min^{-1})	Q_e (mg/g)	R^2	k_2 (g/mg·min)	Q_e (mg/g)	R^2	α (mg/g·min)	β (g/mg)	R^2	a	k_i (mg/g·$min^{1/2}$)	R^2
Clay	0.0215	0.83	0.455	0.1382	1.27	0.996	16.49	0.1845	0.912	0.6252	0.0380	0.775
Silty clay	0.0281	1.49	0.828	0.0376	1.02	0.998	3.575	0.1815	0.990	0.3231	0.0384	0.889
Silt	0.0276	0.82	0.617	0.0246	0.87	0.995	2.679	0.1713	0.930	0.2652	0.0334	0.753

the whole time range. It suggests more than one mechanism involved in the adsorption process [31]. Figure 2(b) shows that the IPD model fitting plots are constituted by three straight lines. The first steeper line was controlled by external surface adsorption (film diffusion); the second step with less steep was controlled by intraparticle diffusion; and the equilibrium stage was due to pore diffusion [32]. These results suggest that the adsorption mechanisms of Cr(VI) in aquifers were complex and affected by film diffusion, intraparticle diffusion, and pore diffusion. Similar findings were reported about the Cr(VI) adsorption by microporous activated carbon [33] and graphene/SiO_2@polypyrrole nanocomposites [25].

3.2.2. Adsorption Isotherm. Adsorption isotherm experiments were conducted with different initial Cr(VI) concentrations under controlled conditions of pH 7-8 and temperature 288 K, 298 K, and 308 K.

As seen in Figure 3, the adsorption capacities increased steadily with increasing initial Cr(VI) concentrations. Such a trend can be explained that the greater the quantity of Cr(VI) in the solution the higher the driving force for mass transfer to the surface of aquifers [34]. Figure 3 also shows that the adsorption of Cr(VI) in clay, silty clay, and silt all increased with increasing temperature, which implies that the adsorption process is endothermic in nature. Moreover, Figure 3 also shows that the Cr(VI) adsorption capacities of three tested aquifers varied distinctly due to their different physicochemical properties. The adsorption capacities of Cr(VI) in the three aquifers followed the order: clay > silty clay > silt.

Langmuir and Freundlich equations are the most common models in earlier studies [25, 35, 36] to describe adsorption isotherms. The Langmuir equation (equation (5)) and Freundlich equation (equation (6)) are as follows:

$$\frac{C}{Q} = \frac{1}{K_L q_m} + \frac{C}{q_m}, \tag{5}$$

$$\lg Q = \lg K_F + n \lg C, \tag{6}$$

where Q (mg/kg) is the amount of Cr(VI) adsorbed by the aquifers, C (mg/L) is the equilibrium concentration of Cr(VI), q_m (mg/kg) is the maximum adsorption capacity, K_L (L/kg) represents the Langmuir constant related to the bonding force of adsorption, K_F (L/kg) is the Freundlich adsorption equilibrium constant representing the adsorption capacity, and n is the Freundlich constant indicative of adsorption intensity.

Isotherm parameters of above described models for Cr(VI) adsorption in different aquifers at different temperatures are listed in Table 2. According to the coefficients of determination (R^2), Cr(VI) adsorption data of all tested aquifers were simultaneously better fitted by Freundlich model (Table 2). The Freundlich isotherm reflects the adsorption process occurs in a heterogeneous surface with interaction between adsorbed ions [37]. These results imply that Cr(VI) adsorption in this study was a heterogeneous multilayered adsorption [38]. Given that K_F reflects the adsorption capacity of aquifers for Cr(VI), the order of adsorption capacities was clay > silty clay > silt. As shown in Table 2, values of n were smaller than 1.0 at all temperatures, indicating that Cr(VI) is not favorably adsorbed by clay, silty clay, and silt [26]. Furthermore, the low values of K_F (Table 2) indicate that Cr(VI) is probably highly mobile in the aquifers [39]. These results suggest that Cr(VI) may transfer easily in these aquifers and cause severe pollution to the surrounding groundwater.

3.2.3. Adsorption Thermodynamics. To further clarify the adsorption mechanisms, adsorption experiments of Cr(VI) by different aquifers were carried out at 288, 298, and 308 K. The results demonstrated that the adsorption of Cr(VI) in clay, silty clay, and silt all increased with the increasing temperature (see Supplementary Material Figure S7), which is consistent with the result of the above adsorption isotherms.

The thermodynamic parameters were calculated by using the following equations:

$$\begin{aligned} \Delta G^\theta &= \Delta H^\theta - T\Delta S^\theta, \\ \Delta G^\theta &= -RT \ln K, \\ \ln K &= \frac{\Delta S^\theta}{R} - \frac{\Delta H^\theta}{RT}, \end{aligned} \tag{7}$$

where T (Kelvin) is the absolute temperature, ΔG^θ (kJ/mol) is the standard Gibbs free energy, ΔH^θ (kJ/mol) is the standard enthalpy change, ΔS^θ (J/mol·K) is the standard entropy change, and R is the gas constant (8.314 J/mol·K).

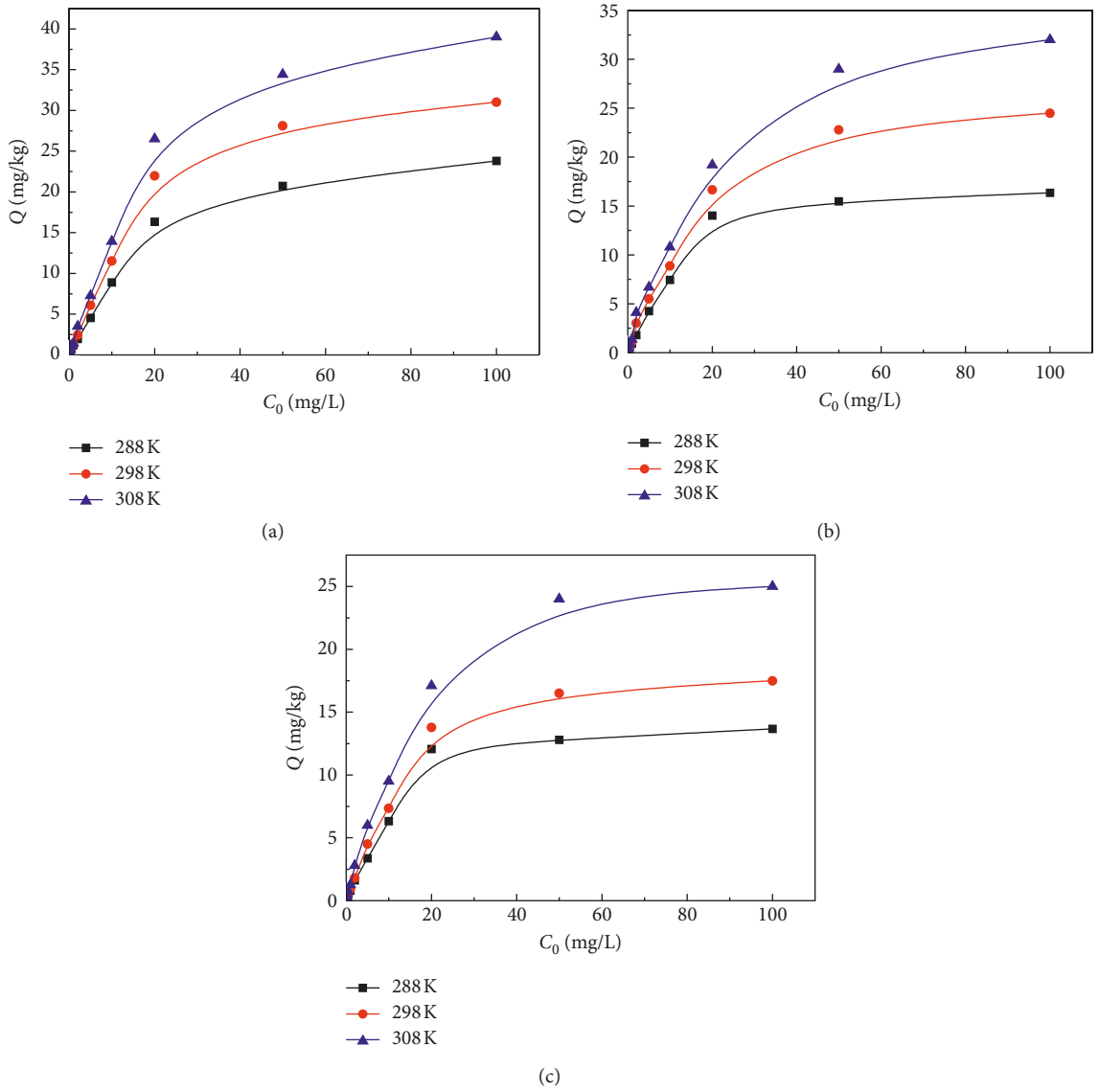

Figure 3: Adsorption isotherm curves of Cr(VI) adsorption in clay (a), silty clay (b), and silt (c).

Table 2: Isotherm parameters for adsorption of Cr(VI) in different aquifers at different temperatures.

Aquifers	Temperature (K)	Langmuir model $(C/Q) = (1/K_L q_m) + (C/q_m)$			Freundlich model $\lg Q = \lg K_F + n\lg C$		
		K_L (L/kg)	q_m (mg/kg)	R^2	K_F (L/kg)	n	R^2
Clay	288	0.057	28.33	0.907	1.438	0.751	0.991
	298	0.052	40.00	0.892	1.830	0.776	0.988
	308	0.052	49.26	0.887	2.230	0.784	0.986
Silty clay	288	0.070	20.45	0.939	1.199	0.749	0.987
	298	0.057	30.86	0.942	1.523	0.775	0.9891
	308	0.055	39.37	0.934	1.865	0.783	0.986
Silt	288	0.071	16.89	0.939	1.002	0.749	0.987
	298	0.061	22.47	0.946	1.154	0.774	0.9891
	308	0.056	32.68	0.956	1.573	0.778	0.986

ΔH^θ and ΔS^θ were computed from the slopes and intercepts of the linear regression of ln K versus $1/T$.

Thermodynamic parameters (ΔG^θ, ΔH^θ, and ΔS^θ) are present in Table 3.

Negative values of ΔG^θ (Table 3) indicate that the Cr(VI) adsorption in three tested aquifers is thermodynamically feasible and spontaneous within the temperature range 288–308 K [40]. ΔG^θ decreases with the increase in

Table 3: Thermodynamic parameters for Cr(VI) adsorption in different aquifers.

Aquifers	Temperature (K)	ΔG^{θ} (kJ/mol)	ΔH^{θ} (kJ/mol)	ΔS^{θ} (J/mol·K)
Clay	288	−0.79	7.30	28.08
	298	−1.07		
	308	−1.35		
Silty clay	288	−0.05	16.00	55.73
	298	−0.60		
	308	−1.16		
Silt	288	−0.02	18.38	62.39
	298	−0.22		
	308	−0.84		

temperature, reflecting an endothermic adsorption process. Moreover, the more negative value of ΔG^{θ} for clay indicates that more energetically favorable adsorption occurs in clay than that in silty clay and silt [41]. This phenomenon could also be explained by the higher contents of clay particles with smaller size (implies much more specific surface area), the higher average porosity (means more micropores available) [42], and the more organic matter content [43, 44] of clay than that of silty clay and silt as described in Table S4 (see Supplementary Material).

The positive enthalpy change (ΔH^{θ} ranges from 7.30 to 18.38 kJ/mol) suggests an entropy-driven process [45], which further confirms an endothermic adsorption process as observed in the aforementioned adsorption isotherms. The values of ΔH^{θ} are all less than 40 kJ/mol, suggesting a physisorption of Cr(VI) onto clay, silty clay, and silt [46]. Combined with the adsorption kinetics in earlier section, physisorption and chemisorption play important roles together in adsorption of Cr(VI) onto clay, silty clay, and silt. The values of ΔS^{θ} are positive, indicating an increased randomness at the solid-solution interface [47]. Besides, the values of ΔS^{θ} follow the sequence of clay < silty clay < silt, suggesting that the degree of randomness increases from clay to silt.

3.2.4. Effect of pH. As well known, pH plays important roles in the adsorption behavior. So, the influence of the solution pH on the Cr(VI) adsorption by three tested aquifers was investigated at 288 K and an initial Cr(VI) concentration of 1.0 mg/L. As shown in Figure 2(d), adsorption of Cr(VI) is strongly dependent on the pH; the adsorption amount of Cr(VI) in aquifers decreased with the increasing pH. The results are consistent with previous studies [17, 25, 42, 48], showing lower pH which provides more advantage for Cr(VI) adsorption. There are two main reasons for this phenomenon. Firstly, at low pH condition, large number of H^+ ions neutralize the negatively charged hydroxyl group (-OH) on the adsorbent surface, thereby reducing hindrance to the diffusion of Cr(VI) ions [25]. On the contrary, at higher pH values, the abundance of OH^- ions causes increased hindrance to diffusion of Cr(VI) ions. Secondly, the predominant form of $HCrO_4^-$ shifts to CrO_4^{2-} as pH increases [49]. $HCrO_4^-$ ion needs only one active site, whereas CrO_4^{2-} needs two active sites due to its two negative charges, thus causing a decrease of Cr(VI) adsorption as pH increases [50].

3.3. Adsorption/Desorption Columns of Cr(VI) Transport in Aquifers. In the present work, adsorption column experiments were carried out to model the contaminant transport process. In addition, the desorption column experiments were applied to model the rainwater washing the contaminant from the upper layers of soils and aquifers to subsequent depths. The breakthrough curves showed the performance of fixed-bed column. The point on the S-shaped curve at which the effluent concentration (C_t) reaches its maximum allowable value is referred as the breakthrough point [51]. The breakthrough point time and the shape of the breakthrough curve are important characteristics to determine the dynamic response of adsorption columns [52, 53].

Three breakthrough curves of adsorption columns with different aquifers are displayed in Figure 4(a). As seen from Figure 4(a), the curves all look like "S" shaped, but the slopes of the breakthrough curves change with varying aquifers. The breakthrough curves of silty clay and silt are steeper than that of clay, which may be explained on the mass transfer fundamentals [53]. A slower transport of Cr(VI) in clay could be caused by a decrease in mass transfer coefficient or diffusion coefficient [54, 55]. Moreover, this result also supported the aforementioned adsorption kinetics study. As illustrated in Table S4 (see Supplementary Material), more clay particles (means more adsorbent surface area) and more organic matter content in clay column provided more binding sites with Cr(VI), indicating a relatively slow transfer process. Also, the organic matter in the aquifers may have reduced some Cr(VI) into Cr(III), greatly reducing the transport of Cr(VI) through the aquifers [16, 56, 57]. Considering that the porosity of the packed column (Table S3) is higher than the actual porosity of study site (Table S4), it could be inferred that the seepage velocity of Cr(VI) in the actual aquifers is slower.

On the other hand, the breakthrough curves of desorption columns are shown in Figure 4(b). The results showed that the concentrations of Cr(VI) in three kinds of columns of aquifers all decreased with time (Figure 4(b)). It demonstrated that the Cr(VI) adsorbed on aquifers will desorb and release into groundwater day by day in the case of rainwater leaching, causing groundwater recontamination. Meanwhile, the curve slopes of silty clay and silt columns were steeper than that of clay column, and the breakthrough curve of clay showed a strong trailing phenomenon. It suggests that the desorption process of clay

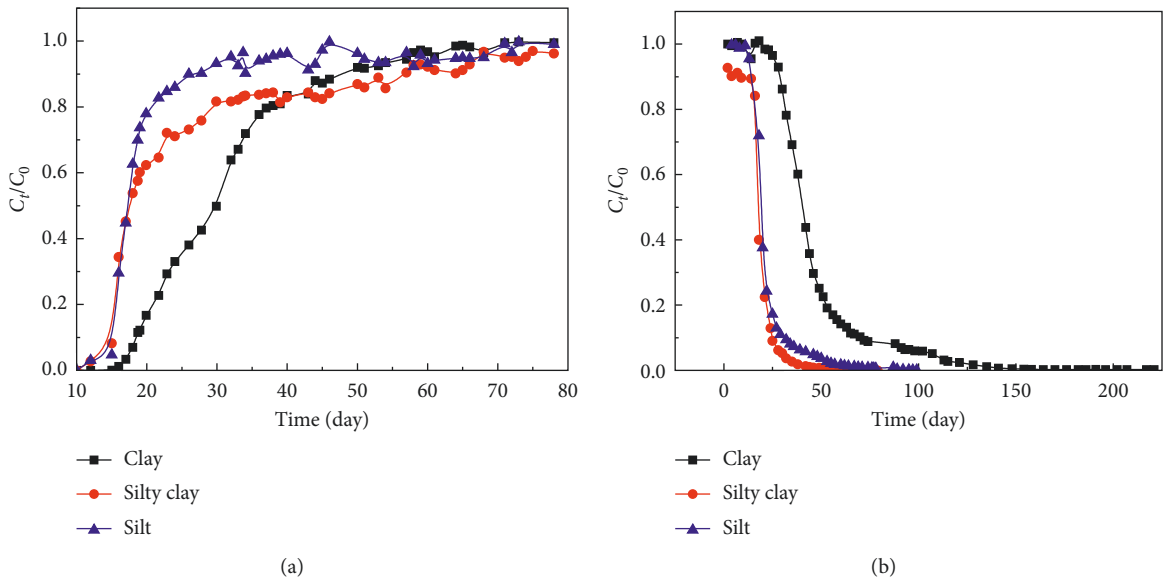

Figure 4: Breakthrough curves of adsorption columns (a) and desorption columns (b).

column is much slower than that of silty clay and silt columns. This result is also consistent with aforementioned results of adsorption isotherms.

Finally, according to the result of adsorption and desorption column experiments, the COPR leachate will continuously transport into aquifers and groundwater therefore causing severe pollution. At the same time, the chromium adsorbed on the aquifers will desorb and release into groundwater under the action of rainwater leaching, causing a recontamination of groundwater. Therefore, the COPR dumpsite is urgent to be properly treated. Also, comprehensive management of soils must be attached importance to prevent any further pollution of groundwater.

4. Conclusions

The results from this study are summarized as follows:

(1) The top soils (5–10 cm), shallow aquifers, and groundwater nearby the chromium ore processing residue (COPR) dumpsite are severely polluted by Cr(VI).

(2) The adsorption of Cr(VI) in aquifers was well described by pseudo-second-order kinetics equations and Freundlich model. The kinetic results proved that Cr(VI) is not easily adsorbed by aquifer mediums but transports with groundwater, causing long-distance pollution. The adsorption capacities of Cr(VI) in three tested aquifers followed the order: clay > silty clay > silt. Cr(VI) adsorption capacities in three tested aquifers decreased with increasing pH.

(3) Different thermodynamic parameters such as ΔG^{θ}, ΔH^{θ}, and ΔS^{θ} showed that the adsorption of Cr(VI) onto tested aquifers was feasible, spontaneous, and endothermic in nature. Adsorption kinetic and thermodynamic results imply that physisorption and chemisorption play important roles together in the Cr(VI) adsorption onto clay, silty clay, and silt.

(4) Breakthrough curves of adsorption columns with different aquifers showed that the transport of Cr(VI) followed the sequence of clay < silty clay < silt.

(5) Desorption column experiments infer that the Cr(VI) adsorbed on aquifers will desorb and release into groundwater in the case of rainwater leaching, causing groundwater recontamination.

Data Availability

The data used to support the findings of this study are available from the corresponding author upon request.

Conflicts of Interest

The authors declare no conflicts of interest.

Acknowledgments

This work was supported by the Science and Technology Project of Tianjin Water Bureau (no. KY2014-03). The authors also gratefully acknowledge the support from the National Science Foundation of China (no. 41807386).

Supplementary Materials

The detailed information of sampling, soil characteristics, and experiments are described in the Supplementary Material. Photos of chromium ore processing residue (COPR) dumpsite in the former Tianjin Tongsheng Chemical Factory in 2012 (Figure S1). Photos of core drilling and groundwater sampling (Figure S2). Schematic of adsorption column packed with aquifers (Figure S3). The concentrations of total

Cr in top soils (5–10 cm) of 11 sampling sites (Figure S4). The concentrations of total Cr in aquifers at different depths of 1–6 m of 11 sampling sites (Figure S5). Pseudo-second-order kinetics for adsorption of Cr(VI) onto clay, silty clay, and silt. Cr(VI) solution 1.0 mg/L, aquifers 0.1 g/mL, pH 7-8, and 288 K (Figure S6). Effect of temperature on Cr(VI) adsorption by clay, silty clay, and silt. Cr(VI) solution 1.0 mg/L, aquifers 0.1 g/mL, and pH 7-8 (Figure S7). Geographical locations of the drilling sampling sites (Table S1).Vertical distribution of local geological formations (Table S2). Packing status of columns and operating condition for the adsorption/desorption column study (Table S3). The physicochemical properties of different aquifers (Table S4). The concentration of Cr(VI) and total Cr of groundwater in monitoring wells of 11 sampling sites (Table S5). (*Supplementary Materials*)

References

[1] B. A. Marinho, R. O. Cristóvão, R. Djellabi et al., "Strategies to reduce mass and photons transfer limitations in heterogeneous photocatalytic processes: hexavalent chromium reduction studies," *Journal of Environmental Management*, vol. 217, pp. 555–564, 2018.

[2] L. Zhong and J. Yang, "Reduction of Cr(VI) by malic acid in aqueous Fe-rich soil suspensions," *Chemosphere*, vol. 86, no. 10, pp. 973–978, 2012.

[3] L. J. D. Moreira, E. B. Da Silva, M. P. F. Fontes, X. Liu, and L. Q. Ma, "Speciation, bioaccessibility and potential risk of chromium in Amazon forest soils," *Environmental Pollution*, vol. 239, pp. 384–391, 2018.

[4] H. Lyu, H. Zhao, J. Tang et al., "Immobilization of hexavalent chromium in contaminated soils using biochar supported nanoscale iron sulfide composite," *Chemosphere*, vol. 194, pp. 360–369, 2018.

[5] J. Johnson, L. Schewel, and T. E. Graedel, "The contemporary anthropogenic chromium cycle," *Environmental Science & Technology*, vol. 40, no. 22, pp. 7060–7069, 2006.

[6] C. V. Coller-Myburgh, L. V. Rensburg, and M. Maboeta, "Utilizing earthworm and microbial assays to assess the ecotoxicity of chromium mine wastes," *Applied Soil Ecology*, vol. 83, pp. 258–265, 2014.

[7] USEPA, *Edition of the Drinking Water Standards and Health Advisories*, Office of Water, U.S. Environmental Protection Agency, Washington, DC, USA, 2012.

[8] R. A. Fallahzadeh, R. Khosravi, B. Dehdashti et al., "Spatial distribution variation and probabilistic risk assessment of exposure to chromium in ground water supplies; a case study in the east of Iran," *Food and Chemical Toxicology*, vol. 115, pp. 260–266, 2018.

[9] J. S. Geelhoed, J. C. L. Meeussen, M. J. Roe et al., "Chromium remediation or release? Effect of iron(II) sulfate addition on chromium(VI) leaching from columns of chromite ore processing residue," *Environmental Science & Technology*, vol. 37, no. 14, pp. 3206–3213, 2003.

[10] H. S. Shi and L. L. Kan, "Study on the properties of chromium residue-cement matrices (CRCM) and the influences of superplasticizers on chromium(VI)-immobilising capability of cement matrices," *Journal of Hazardous Materials*, vol. 162, no. 2-3, pp. 913–919, 2009.

[11] X. Zhao, P. A. Sobecky, L. Zhao, P. Crawford, and M. Li, "Chromium(VI) transport and fate in unsaturated zone and aquifer: 3D Sandbox results," *Journal of Hazardous Materials*, vol. 306, pp. 203–209, 2016.

[12] T. Sherene, "Mobility and transport of heavy metals in polluted soil environment," *Biological Forum-An International Journal*, vol. 2, no. 2, pp. 112–121, 2010.

[13] C.-H. Weng, C. P. Huang, and P. F. Sanders, "Transport of Cr(VI) in soils contaminated with chromite ore processing residue (COPR)," *Practice Periodical of Hazardous, Toxic, and Radioactive Waste Management*, vol. 6, no. 1, pp. 6–13, 2002.

[14] A. A. Khan, M. Muthukrishnan, and B. K. Guha, "Sorption and transport modeling of hexavalent chromium on soil media," *Journal of Hazardous Materials*, vol. 174, no. 1–3, pp. 444–454, 2010.

[15] J. Jiang, R. Xu, Y. Wang, and A. Zhao, "The mechanism of chromate sorption by three variable charge soils," *Chemosphere*, vol. 71, no. 8, pp. 1469–1475, 2008.

[16] P. M. Jardine, S. E. Fendorf, M. A. Mayes, I. L. Larsen, S. C. Brooks, and W. B. Bailey, "Fate and transport of hexavalent chromium in undisturbed heterogeneous soil," *Environmental Science & Technology*, vol. 33, no. 17, pp. 2939–2944, 1999.

[17] D. M. Dong, X. M. Zhao, X. Y. Hua, J. Liu, and G. Ming, "Investigation of the potential mobility of Pb, Cd and Cr(VI) from moderately contaminated farmland soil to groundwater in Northeast, China," *Journal of Hazardous Materials*, vol. 162, no. 2-3, pp. 1261–1268, 2009.

[18] D. B. Kent, J. A. Davis, L. C. D. Anderson, and B. A. Rea, "Transport of chromium and selenium in a pristine sand and gravel aquifer: role of adsorption processes," *Water Resources Research*, vol. 31, no. 4, pp. 1041–1050, 1995.

[19] D. B. Kent, J. A. Davis, L. C. D. Anderson, B. A. Rea, and T. D. Waite, "Transport of chromium and seleniumin the suboxicz one of a shallow aquifer: influence of redox and adsorption reactions," *Water Resources Research*, vol. 30, no. 4, pp. 1099–1114, 1994.

[20] China MC, *Standard for Engineering Classification of Soil*, Ministry of Construction of China, Beijing, China, 2007, in Chinese.

[21] TCMC, *Technical Specification for Division of Subsoil Sequence in Tianjin*, Tianjin Construction Management Committee, Tianjin, China, 2009, in Chinese.

[22] China MEE, "Environmental quality standard for soils," Ministry of Ecology and Environmental of China, Beijing, China, 2018, in Chinese.

[23] X. Liu, J. Jiang, Y. Yan et al., "Distribution and risk assessment of metals in water, sediments, and wild fish from Jinjiang River in Chengdu, China," *Chemosphere*, vol. 196, pp. 45–52, 2018.

[24] China MEE, "Quality standard for groundwater," Ministry of Ecology and Environmental of China, Beijing, China, 2017, in Chinese.

[25] W. Fang, X. Jiang, H. Luo, and J. Geng, "Synthesis of graphene/SiO_2@polypyrrole nanocomposites and their application for Cr(VI) removal in aqueous solution," *Chemosphere*, vol. 197, pp. 594–602, 2018.

[26] K. L. Tan and B. H. Hameed, "Insight into the adsorption kinetics models for the removal of contaminants from aqueous solutions," *Journal of the Taiwan Institute of Chemical Engineers*, vol. 74, pp. 25–48, 2017.

[27] J.-H. Park, J. J. Wang, R. Xiao et al., "Mercury adsorption in the Mississippi River deltaic plain freshwater marsh soil of Louisiana Gulf coastal wetlands," *Chemosphere*, vol. 195, pp. 455–462, 2018.

[28] N. Li, F. Fu, J. Lu, Z. Ding, B. Tang, and J. Pang, "Facile preparation of magnetic mesoporous $MnFe_2O_4$@SiO_2-CTAB composites for Cr(VI) adsorption and reduction," *Environmental Pollution*, vol. 220, pp. 1376–1385, 2017.

[29] S. Mallick, S. S. Dash, and K. M. Parida, "Adsorption of hexavalent chromium on manganese nodule leached residue obtained from NH_3-SO_2 leaching," *Journal of Colloid and Interface Science*, vol. 297, no. 2, pp. 419–425, 2006.

[30] M. Omidvar Borna, M. Pirsaheb, M. Vosoughi Niri et al., "Batch and column studies for the adsorption of chromium(VI) on low-cost Hibiscus Cannabinus kenaf, a green adsorbent," *Journal of the Taiwan Institute of Chemical Engineers*, vol. 68, pp. 80–89, 2016.

[31] A. Kumar and H. M. Jena, "Adsorption of Cr(VI) from aqueous phase by high surface area activated carbon prepared by chemical activation with $ZnCl_2$," *Process Safety and Environmental Protection*, vol. 109, pp. 63–71, 2017.

[32] W. Zhang, S. Zhang, J. Wang et al., "Hybrid functionalized chitosan-Al_2O_3@SiO_2 composite for enhanced Cr(VI) adsorption," *Chemosphere*, vol. 203, pp. 188–198, 2018.

[33] R. Gottipati and S. Mishra, "Preparation of microporous activated carbon from *Aegle Marmelos* fruit shell and its application in removal of chromium(VI) from aqueous phase," *Journal of Industrial and Engineering Chemistry*, vol. 36, pp. 355–363, 2016.

[34] A. Iriel, S. P. Bruneel, N. Schenone, and A. F. Cirelli, "The removal of fluoride from aqueous solution by a lateritic soil adsorption: kinetic and equilibrium studies," *Ecotoxicology and Environmental Safety*, vol. 149, pp. 166–172, 2018.

[35] J. O. Vinhal, K. K. Nege, M. R. Lage, J. W. M. Carneiro, C. F. Lima, and R. J. Cassella, "Adsorption of of the herbicides diquat and difenzoquat on polyurethane foam: kinetic, equilibrium and computational studies," *Ecotoxicology and Environmental Safety*, vol. 145, pp. 597–604, 2017.

[36] L. A. Holmes, A. Turner, and R. C. Thompson, "Adsorption of trace metals to plastic resin pellets in the marine environment," *Environmental Pollution*, vol. 160, pp. 42–48, 2012.

[37] A. El Nemr, A. Khaled, O. Abdelwahab, and A. El-Sikaily, "Treatment of wastewater containing toxic chromium using new activated carbon developed from date palm seed," *Journal of Hazardous Materials*, vol. 152, no. 1, pp. 263–275, 2008.

[38] B. Fuentes, M. de la Luz Mora, R. Bol, F. San Martin, E. Pérez, and P. Cartes, "Sorption of inositol hexaphosphate on desert soils," *Geoderma*, vol. 232–234, pp. 573–580, 2014.

[39] K. M. Doretto and S. Rath, "Sorption of sulfadiazine on Brazilian soils," *Chemosphere*, vol. 90, no. 6, pp. 2027–2034, 2013.

[40] M. Jain, V. K. Garg, and K. Kadirvelu, "Adsorption of hexavalent chromium from aqueous medium onto carbonaceous adsorbents prepared from waste biomass," *Journal of Environmental Management*, vol. 91, no. 4, pp. 949–957, 2010.

[41] X. Guo, C. Yang, Z. Dang, Q. Zhang, Y. Li, and Q. Meng, "Sorption thermodynamics and kinetics properties of tylosin and sulfamethazine on goethite," *Chemical Engineering Journal*, vol. 223, pp. 59–67, 2013.

[42] Z. A. Zakaria, M. Suratman, N. Mohammed, and W. Azlina Ahmad, "Chromium(VI) removal from aqueous solution by untreated rubber wood sawdust," *Desalination*, vol. 244, no. 1–3, pp. 109–121, 2009.

[43] X. Zhang, J. Tong, B. X. Hu, and W. Wei, "Adsorption and desorption for dynamics transport of hexavalent chromium (Cr(VI)) in soil column," *Environmental Science and Pollution Research*, vol. 25, no. 1, pp. 459–468, 2018.

[44] D. A. Brose and B. R. James, "Hexavalent chromium reduction by tartaric acid and isopropyl alcohol in mid-atlantic soils and the role of Mn(III, IV)(hydr)oxides," *Environmental Science & Technology*, vol. 47, no. 22, pp. 12985–12991, 2013.

[45] J. Yang, M. Yu, and W. Chen, "Adsorption of hexavalent chromium from aqueous solution by activated carbon prepared from longan seed: kinetics, equilibrium and thermodynamics," *Journal of Industrial and Engineering Chemistry*, vol. 21, pp. 414–422, 2015.

[46] M. Kara, H. Yuzer, E. Sabah, and M. S. Celik, "Adsorption of cobalt from aqueous solutions onto sepiolite," *Water Research*, vol. 37, no. 1, pp. 224–232, 2003.

[47] J. Maszkowska, M. Wagil, K. Mioduszewska, J. Kumirska, P. Stepnowski, and A. Białk-Bielińska, "Thermodynamic studies for adsorption of ionizable pharmaceuticals onto soil," *Chemosphere*, vol. 111, pp. 568–574, 2014.

[48] S. R. Chowdhury and E. K. Yanful, "Arsenic and chromium removal by mixed magnetite-maghemite nanoparticles and the effect of phosphate on removal," *Journal of Environmental Management*, vol. 91, no. 11, pp. 2238–2247, 2010.

[49] T. Shanthi and V. M. Selvarajan, "Removal of Cr(VI) and Cu(II) ions from aqueous solution by carbon prepared from henna leaves," *Journal of Chemistry*, vol. 2013, Article ID 304970, 6 pages, 2013.

[50] J. Yang, M. Yu, and T. Qiu, "Adsorption thermodynamics and kinetics of Cr(VI) on KIP210 resin," *Journal of Industrial and Engineering Chemistry*, vol. 20, no. 2, pp. 480–486, 2014.

[51] S. Kundu, S. S. Kavalakatt, A. Pal, S. K. Ghosh, M. Mandal, and T. Pal, "Removal of arsenic using hardened paste of Portland cement: batch adsorption and column study," *Water Research*, vol. 38, no. 17, pp. 3780–3790, 2004.

[52] R. P. Han, Y. Wang, X. Zhao et al., "Adsorption of methylene blue by phoenix tree leaf powder in a fixed-bed column: experiments and prediction of breakthrough curves," *Desalination*, vol. 245, no. 1–3, pp. 284–297, 2009.

[53] A. A. Ahmad and B. H. Hameed, "Fixed-bed adsorption of reactive azo dye onto granular activated carbon prepared from waste," *Journal of Hazardous Materials*, vol. 175, no. 1–3, pp. 298–303, 2010.

[54] M. T. Uddin, M. Rukanuzzaman, M. M. R. Khan, and I. Akhtarul, "Adsorption of methylene blue from aqueous solution by jackfruit (*Artocarpus heteropyllus*) leaf powder: a fixed-bed column study," *Journal of Environmental Management*, vol. 90, no. 11, pp. 3443–3450, 2009.

[55] N. Chen, Z. Y. Zhang, C. P. Feng, L. Miao, C. Rongzhi, and N. Sugiura, "Investigations on the batch and fixed-bed column performance of fluoride adsorption by Kanuma mud," *Desalination*, vol. 268, no. 1–3, pp. 76–82, 2011.

[56] J. L. Gardea-Torresday, K. J. Tiemann, V. Armendariz et al., "Characterization of Cr(VI) binding and reduction to Cr(III) by the agricultural byproducts of *Avena monida* (Oat) biomass," *Journal of Hazardous Materials*, vol. 80, no. 1–3, pp. 175–188, 2000.

[57] N.-H. Hsu, S.-L. Wang, Y.-C. Lin, G. D. Sheng, and J.-F. Lee, "Reduction of Cr(VI) by crop-residue-derived black carbon," *Environmental Science & Technology*, vol. 43, no. 23, pp. 8801–8806, 2009.